

**ACCELERATED SKELETAL DEVELOPMENT IN
RECEPTOR ACTIVITY MODIFYING PROTEIN 3 KNOCK-OUT MICE AND
NOVEL INSIGHTS INTO CALCITONIN RECEPTOR IN PRIMARY OSTEOLASTS.**

SURUCHI UTTAM JYOTI PACHARNE

Thesis submitted for the degree of Doctor of Philosophy (Ph. D)

Mellanby Centre for Bone Research

Academic Unit of Bone Biology

University of Sheffield

March 2014

A word of thanks

I am overwhelmed by the feeling that one of most incredible journeys of my life has come to an end. I find myself at a loss of words to express my gratitude to the extraordinary people who have selflessly guided me and supported me to become what I am today.

I could have not asked for anyone but you as my mentor Tim. Thank you so much for respecting me and believing in me. You've always brought the best in me without changing me. It was always what you would of thought of me, defined my work and decisions. All the hard work that I have put in was because the thought of letting you down as a mentor, was just unthinkable. You've taught me how to be honest, ethical and independent. You've not only taught me how to be a good scientist, but also a good person, and someday I wish to be like you. From the bottom of my heart, thank you so much for everything Tim!

Gareth, thank you so much for being the 'go to guy'. If it was not for you I wouldn't have developed my critical thinking. It takes immense patience to be 'you'. I will always cherish those times when I used to come up to you with a hypothesis. You were always so enthusiastic. Again, from the deepest corner of my heart thank you.

I am really fortunate to have you as my personal tutor Ilaria. I never walked out of your office not feeling reassured. You have always looked out for me and have believed in me. Again letting you down is never an option and it is my promise that I will always live up to your expectations. I have seen scientists like you, Tim and Peter Croucher striving to provide students like me a platform to make our mark. I cannot thank you all for all the opportunities that you have given me to develop as a scientist. Thank you so much for being the people who fight to making things right.

Orla, thank you for all the professional and personal support. Thank you, Gillian Griffiths for all the help. I look up to you all with nothing but utmost respect and gratitude.

Mumma, Pappa , Subdi and Sandy my PhD and whatever I do in my life is dedicated to you guys. I am truly blessed to have you all watching over me and making sure I sleep soundly at night. *"Mumma, pappu I am so sorry me ghar sodle pun me aj tumhala delela promise purna kela"*. Thank you so much for giving me everything, the unconditional love, trust, respect and the gift of education. You guys made me what I am. I love you and I will always be your 'kuttta' who will do anything to just make her mumma and pappu smile. Subdi, although you are younger than me, you have always been like an elder brother watching over my shoulder and protecting me. I have nothing but gratitude and respect for you. I am so proud of you, thank you so much for being my strength. Sandy, I don't know where to begin or what to say! You are most wonderful thing that has happened to me. You are my inner peace. Things you have done for me, that too so easily, are beyond my understanding of how selfless and strong a person can be. All I can say is that I am forever indebted to you. Thank you so much for being real Sandy!

Defne, thank you for lifting up my spirit, whenever I was feeling low. You are my best friend and an inspiration, thank you! Thank you Khushi, Rishabh, Shishira, Dipalimami, Pappumama, Varshamami, Kiran mama, Sunitamami, Deepakmama, Frudo, Gummy and apt 31 gang, you all rock and I am so lucky to have you guys in my life! Ajji, Ajji, Ajoba and Bhau, thank you for your blessings. Krishna aunty, Kishan uncle, Abba aunty and Sanjay uncle thank you so much for always making me feel so blessed. Ravala, Bhoomika Manali, Siddhu, Sheena and now Urmi and Timir thank you so much for being a part of my happiness. Also thanks to Manish bhaiya, Neetu didi, and baby Shimmer for being there for me.

Without the love and support of each and every one of you, I would not be who I am today. I would like to express my sincere, heartfelt gratitude to you all. Thank you!

Acknowledgements

Firstly I would like to thank the University of Sheffield for the prestigious honour bestowed upon me by granting me the Faculty Prize Studentship. Sincere thanks to Prof. Tim Skerry and Dr. Gareth Richards for supervising me throughout this project.

This work would not be possible without the support and guidance of many people. Thanks to Dr Kathleen Caron, University of North Carolina, USA for providing the RAMP3 KO mice. Thanks to Matt Cardwell, Jane Cardwell, William Sean and all the members of the Sheffield Biological services, for all the help with the maintenance of the transgenic breeding lines. Thanks to Dr Susana Martinez-Bautista and Dr Peter Grabowski for all the help with primary cultures and for providing the RAW 264 cDNA. Thanks to Dr Ning Wang for performing the ovariectomy procedures. Thanks to Orla Gallagher Darren Laith and Millie Gelder for processing the samples for histology. Thanks to Dr Sandeep Rajan for all the help with the Western blotting optimisation. Thanks to Zahra Faraahi for the help with beta-catenin antibodies.

Lastly I would like to thank all my colleagues in the Mellanby Centre for Bone research, University of Sheffield for all the help and support. I am sincerely grateful for giving me the opportunity of being a part of a world class research group.

This work has been presented at the following conferences

- "Role of receptor activity modifying proteins (RAMPs) in skeleton. ECTS 2013, Lisbon, Portugal. (May 2013)
- "Role of receptor activity modifying proteins (RAMPs) in skeletal regulation in skeletal regulation", 3rd annual meeting Mellanby centre for Bone research, The Ridge conference centre, Sheffield, UK (June 2012)
- "Role of receptor activity modifying proteins (RAMPs) in skeletal regulation in skeletal regulation" Mellanby centre for Bone research (internal seminar) University of Sheffield, UK. (Feb 2012)
- "Regulation of age-related degeneration of musculoskeletal system by Receptor activity modifying proteins- RAMPs", Centre for Integrated Research into Musculoskeletal Ageing (CIMA) Launch meeting, Foresight Centre, University of Liverpool. (16-17th July 2012)
- "Role of Adrenomedullin and Amylin in skeletal regulation" School research day, University of Sheffield, UK.(2012)
- "Advanced skeletal phenotype on RAMP3 knockout." at the 3rd Joint meeting of the Bone Research Society (BRS) and the British Orthopaedic Research Society (BORS), Cambridge, UK. (June 2011)
- "Role of Adrenomedullin and Amylin in skeletal regulation" at the School research day, University of Sheffield, UK. (June 2011)
- "Role of Adrenomedullin and Amylin in skeletal regulation", Mellanby centre for Bone research, internal seminar, University of Sheffield, UK. (March 2011)
- Presentation for an external panel interview for the award of the MRC ARUK for the Centre for Integrated Research into Musculoskeletal Ageing (CIMA) "Regulation of age-related degeneration of musculoskeletal system by Receptor activity modifying proteins – RAMPs", Academy of Medical Sciences, 41 Portland Place, London - Awarded (Oct 2011)
- "Role of Adrenomedullin and Amylin in skeletal regulation" at the 4th International Workshop on Advances in the Molecular Pharmacology & Therapeutics of Bone Diseases, St Catherine's College, Oxford, UK. (2010)
- "Role of Adrenomedullin and Amylin in skeletal regulation" at the at the 2nd Annual meeting , Mellanby centre for Bone Research, The Ridge conference centre, Sheffield, UK. (2010)

Publication

- Mahita Kadmiel, Kimberly Fritz-Six, Suruchi Pacharne, Gareth O. Richards, Manyu Li, Tim M. Skerry and Kathleen M. Caron, **2011**, Haploinsufficiency of Receptor Activity-Modifying Protein-2 (Ramp2) Causes Reduced Fertility, Hyperprolactinemia, Skeletal Abnormalities, and Endocrine Dysfunction in Mice, *Molecular Endocrinology* vol. 25 no. 7 1244-1253.

Abstract

Receptor activity modifying proteins (RAMPs 1, 2 and 3) a family of single transmembrane accessory proteins, which were discovered for predominantly regulating ligand selectivity and trafficking of G-protein coupled receptors (GPCRs) for the Calcitonin (CT) family of peptides. Calcitonin family of peptides mainly include: Calcitonin (CT), Calcitonin gene related peptide (CGRP), Adrenomedullin (AM) and Amylin (AMY). Functional receptors to these peptides comprise RAMP heterodimers with either Calcitonin receptor (CTR) or Calcitonin like receptor (CLR). Over the last few years, these three isoforms of human RAMPs have been identified to form heterodimers with several other GPCRs.

Given the expanding number RAMP-GPCR interactions being identified every year, it is important to understand the role of individual RAMP isoform in both normal and pathological conditions. Since the CT family of peptides are recognized hypocalcaemic peptides that have been studied extensively for developing therapies for low bone mass skeletal disorders, we intended to investigate the role of RAMPs in regulating bone mass. Our pilot study suggested that not RAMP1 but RAMP2 and RAMP3 play an important role in regulating skeletal development. The current work aims to investigate the phenotypic consequence of globally silencing RAMP3 expression in 129/SvEv mice on the skeletal development.

Using microCT, dynamic histomorphometry and histology we have demonstrated that RAMP3 KO 129/SvEv mice have anabolic acceleration in skeletal development at an early age that provides protection against age-dependent bone loss. Furthermore, using qPCR and western blotting we have shown that the expression of individual RAMP regulates osteoblasts differentiation and that in response to the stimulation of PTH, AM and AMY, the expression of RAMPs in RAMP3 KO primary osteoblasts is significantly different to that in WT primary osteoblasts. We have also determined a variant of CTR that responds to AMY stimulation in primary osteoblasts. Additionally our study provides novel insights into role of RAMP3 in regulating the Wnt/ β -catenin pathway in primary osteoblasts.

This study provides evidence of RAMP3 being an anabolic regulator of skeletal development. Whether this is due to its roles in regulating functions of the CT family of peptides; AM and AMY, or through exerting its effects on other osteotropic hormone receptors that interact with RAMP3 is not yet elucidated. Nevertheless the modulation of RAMP3 function may offer opportunities for anabolic therapies for treating low mass skeletal disorders.

Contents

List of Figures	11
List of Tables.....	13
Abbreviations	14
Chapter 1: Introduction	17
1.1 Bone.....	19
1.1.1 Structure of bone	19
1.1.2 Bone formation	20
1.1.3 Bone cells	21
1.1.3.i Osteoblasts.....	21
1.1.3.ii Osteocytes.....	25
1.1.3.iii Osteoclasts	26
1.1.4 Bone remodelling.....	27
1.2 Osteoporosis	30
1.2.1 Diagnosis and current therapies.....	31
1.2.1.i Bisphosphonates	32
1.2.1.ii Strontium renelate.....	32
1.2.1.iii Selective oestrogen receptor modulator (SERM)	32
1.2.1.iv Recombinant PTH and anti-RANKL therapy - Teriparatide and Denosumab.....	32
1.3 Calcitonin family of peptides.....	34
1.3.1 Calcitonin (CT).....	34
1.3.2 Calcitonin gene related peptide (CGRP)	36
1.3.3 Amylin (AMY).....	38
1.3.4 Adrenomedullin (AM).....	41
1.4 Receptors of the CT family of peptides.....	44
1.4.1 Calcitonin receptor (CTR) and Calcitonin like receptor (CLR).....	44
1.4.2 Receptor Activity Modifying Proteins (RAMPs)	46
1.5 Importance of investigating receptors for CT family of peptides.....	51
1.6 Hypothesis, aim and objectives	54

Chapter 2: Accelerated skeletal development in RAMP3 KO mice	55
2.1 Introduction	56
2.2 Methods and materials	58
2.2.1 Animals.....	58
2.2.2 Genotyping.....	60
2.2.2.i Genomic DNA extraction.....	60
2.2.2.ii PCR for genotyping.....	60
2.2.3 Animal housing and humane culling.....	61
2.2.4 Age groups.....	61
2.2.5 Treatments.....	61
2.2.5.i Dual Calcein labelling treatment.....	61
2.2.6 Specimen preparation.....	62
2.2.7 Alcian Blue / Alzarin Red staining.....	63
2.2.8 Weights,Tail lengths and whole bone lengths.....	64
2.2.9 Micro Computed Tomography (MicroCT) Analysis	66
2.2.9.i Specimen processing.....	66
2.2.9.ii MicroCT scanning	66
2.2.9.iii Reconstruction	66
2.2.9.iv Region of Interests (ROIs) for analysis	67
2.2.9.v Morphometric measures.....	71
2.2.10 Results	71
2.2.10.i Quantitative results	71
2.2.10.ii Qualitative results: 3D rendering.....	71
2.2.11 Dynamic histomorphometry: Dual Calcein labelling	73
2.2.12 Histology: H and E staining and TRAP stained sections	74
2.2.12.i Specimen processing	74
2.2.12.ii Haematoxylin and Eosin (H&E)	74
2.2.12.iii Virtual analysis	74
2.2.12.iv Osteoblast and osteoclast numbers	76
2.2.12.v Growth plate analysis	77
2.3 Results	79
2.3.1 Five day old pups	79

2.3.1.i Whole body weight.....	79
2.3.1.ii MicroCT analysis whole femur and tibia	82
2.3.1.iii Three dimension model rendering	84
2.3.1.iv Skeletal staining	85
2.3.2 Four week old mice	86
2.3.2.i Whole body weight	86
2.3.2.ii MicroCT analysis and three dimensional skeletal models.....	87
2.3.2.ii.a Whole femur	87
2.3.2.ii.b Whole tibia-fibula	89
2.3.2.ii.c Femur cortical bone	90
2.3.2.ii.d Tibia cortical bone.....	92
2.3.2.ii.e Femur trabecular bone	94
2.3.2.ii.f Tibia trabecular bone	97
2.3.2.ii.g Caudal vertebra	100
2.3.2.ii.h Three dimension skeletal models of 4 week old mice	102
2.3.3 Eight week old mice	104
2.3.3.i Whole body weight	104
2.3.3.ii MicroCT analysis	105
2.3.3.ii.a Whole femur and tibia	105
2.3.3.ii.b Femur cortical bone	107
2.3.3.ii.c Tibia cortical bone.....	109
2.3.3.ii.d Femur trabecular bone	111
2.3.3.ii.e Tibia trabecular bone	114
2.3.3.ii.f Three dimension skeletal models	117
2.3.3.iii Dynamic histomorphometry	118
2.3.3.iv Histology.....	121
2.3.3.iv.a Trabecular analysis	122
2.3.3.v Osteoblasts and osteoclasts quantification	124
2.3.3.v.a Medial endocortical osteoblast and osteoclast quantification	124
2.3.3.v.b Lateral endocortical osteoblast and osteoclast quantification.....	126
2.3.3.v.c Trabecular osteoblast and osteoclast quantification.....	128
2.3.3.vi Growth plate analysis.....	130
2.3.3.vi.a Growth plate measurements.....	131

2.4 Discussion	133
2.4.1 Technical limitations.....	133
2.4.1.i Animals.....	133
2.4.1.ii MicroCT analysis.....	133
2.4.1.iii Histology.....	134
2.4.2 Silencing RAMP3 gene results in an advanced skeletal phenotype.....	134
Chapter 3: Skeletal response of RAMP3 KO mice to ovariectomy	138
3.1 Introduction	139
3.2 Methods and materials	142
3.2.1 Ovariectomy.....	142
3.3 Results	144
3.3.1 Weight of Uterus.....	144
3.3.2 Whole body weights.....	145
3.3.3 MicroCT analysis.....	146
3.3.3.i Whole femur and tibia bone volume.....	146
3.3.3.ii Femur cortical bone.....	147
3.3.3.iii Tibia cortical bone.....	148
3.3.3.iv Femur trabecular bone.....	149
3.3.3.v Tibia trabecular bone.....	151
3.3.4 Three dimension skeletal models.....	153
3.4 Discussion	154
Chapter 4: Characteristics of primary osteoblasts from RAMP3 KO mice .156	
4.1 Introduction	157
4.2 Methods and materials	160
4.2.1 Primary osteoblast cultures.....	160
4.2.2 Mineralizing fibroblast-colony-forming assays.....	161
4.2.2.i Alkaline phosphatase staining.....	161
4.2.2.ii Mineralisation assay.....	161
4.2.2.iii Collagen staining.....	162

4.2.2.iv CFU staining.....	162
4.2.2.v Image analysis.....	163
4.3 Results	164
4.3.1 Alkaline phosphatase (ALP) activity	164
4.3.2 Mineralisation assay	166
4.3.3 Collagen assay.....	168
4.3.4 Colony forming units assay.....	170
4.4 Discussion.....	172

Chapter 5: Expression of RAMP1, 2 and 3 mRNA in differentiating primary osteoblasts.....	175
5.1 Introduction.....	176
5.2 Methods and materials	178
5.2.1 Sample preparation.....	178
5.2.1.i Total RNA from differentiating primary osteoblasts.....	178
5.2.1.ii Controls	178
5.2.1.iii DNase treatment.....	178
5.2.1.iv Reverse transcription to generate cDNA	179
5.2.2 End point PCR	180
5.2.3 Real time PCR	181
5.2.3.i Gene of Interest.....	181
5.2.3.ii Reference gene	182
5.2.3.iii qPCR reaction mix (for all reference genes and genes of interest)	183
5.2.3.iv Thermocycler conditions in Real Time PCR machine.....	183
5.2.3.v “CT value”	183
5.2.3.vi Calculating relative expression of a gene of Interest	184
5.2.3.vii Graphical representation and statistical analysis	185
5.3 Results	186
5.3.1 End point PCR to detect RAMP cDNA expression in primary osteoblasts	186
5.3.1.i RAMP1.....	186
5.3.1.ii RAMP2	187
5.3.1.iii RAMP3	188

5.3.2 Quantitative PCR.....	189
5.3.2.i Reference gene identification using geNorm™ kit.....	189
5.3.2.i.a geNorm M value	192
5.3.2.i.b geNorm V value.....	194
5.3.2.ii Genes of interest	195
5.3.2.ii.a RAMP1	195
5.3.2.ii.b RAMP2	197
5.3.2.ii.c RAMP3	199
5.4 Discussion.....	201
Chapter 6: Expression of RAMPs in response to stimulation.....	204
6.1 Introduction.....	205
6.1.1 Effect of Parathyroid hormone (PTH), Adrenomedullin (AM) & Amylin (AMY) stimulation ..	205
6.1.2 The Wnt/ β -catenin and RAMP3 association.....	206
6.2 Methods	207
6.2.1 Stimulation of primary osteoblast cultures.....	207
6.2.1.i Experimental set-up for RAMP2 and RAMP3 expression.....	207
6.2.1.ii Experimental set-up for total β -catenin expression	207
6.2.1.iii Experimental set-up for phosphorylated β -catenin expression	207
6.2.1.iv Experimental set-up for endogenous phosphorylated β -catenin expression	208
6.2.1.v Experimental set-up for phospho- β -catenin expression on Wnt3A stimulation	208
6.2.2 Protein expression analysis	209
6.2.2.i Total cell lysate protein from differentiating primary osteoblasts.....	209
6.2.2.ii Total brain lysate protein-positive control	209
6.2.2.iii Sodium Dodecyl Sulphate-Polyacrylamide Gel Electrophoresis (SDS-PAGE).....	209
6.2.2.iv Protein sample preparation for SDS – PAGE.....	210
6.2.2.v Western Blotting	210
6.2.2.vi Immuno-blotting.....	210
6.2.2.vii Quantification of protein expression	212
6.2.3 Statistical analysis	212
6.3 Results	213
6.3.1 Parathyroid hormone (PTH), Adrenomedullin (AM) and Amylin (AMY) stimulation.....	213

6.3.1.i RAMP3 expression on PTH,AM and AMY stimulation.....	213
6.3.1.ii RAMP2 expression in RAMP3 KO and WT 129/SvEv primary osteoblasts.....	215
6.3.2 Wnt/ β -catenin pathway in RAMP3 KO primary osteoblasts.....	218
6.3.2.i Total β -catenin expression in WT & RAMP3 KO 129/SvEv primary osteoblasts..	218
6.3.2.ii Phosphorylated β -catenin expression in WT and RAMP3 KO 129/SvEv primary osteoblasts on Wnt3A stimulation.....	220
6.3.2.iii Effect of DKK1 stimulation on endogenous phosphorylated β -catenin expression in WT and RAMP3 KO 129/SvEv primary osteoblasts.....	222
6.3.2.iv Effect of DKK1 and Wnt3A stimulation on phosphorylated β -catenin expression in WT and RAMP3 KO 129/SvEv primary osteoblast	225
6.4 Discussion.....	228
Chapter 7: Expression of CTR in differentiating primary osteoblasts	232
7.1 Introduction.....	233
7.2 Methods and materials	237
7.2.1: Protein sample preparation.....	237
7.2.1.i Total cell lysate protein from differentiating primary osteoblasts	237
7.2.1.ii Total cell lysate protein from basal and AMY stimulated primary osteoblasts.....	237
7.2.1.iii Total brain lysate protein a positive control.....	237
7.2.2 Western Blotting for CTR.....	238
7.2.3 RNA sample preparation.....	238
7.2.3.i Total RNA from differentiating primary osteoblasts	238
7.2.3.ii Total RNA from mouse brain – positive control.....	238
7.2.4 Reverse transcription to generate cDNA	239
7.2.5 End-point PCR.....	239
7.2.6 Determining expression and sequence of CTR cDNA in calvarial, primary osteoblasts	240
7.2.7 Sequencing and <i>in-silico</i> analysis of osteoblast CTR cDNA	242
7.3 Results	243
7.3.1 PCR using overlapping primer pairs	243
7.3.2 Sequencing	244
7.3.3 Generating full length osteoblast CTR cDNA sequence <i>in-silico</i> from short overlapping PCR fragments and predicting protein sequence	244

7.3.4 PCR for full length CTR.....	248
7.3.5 Predicting osteoblast CTR variant protein sequence.....	249
7.3.6 CTR protein expression in differentiating primary osteoblast lysates	251
7.3.7: Expression of CTR in WT and RAMP3KO primary osteoblasts in response to PTH, AM and AMY stimulation	253
7.4 Discussion.....	254
Chapter 8: Discussion.....	258
8.1 Summary and discussion.....	259
8.1.1 RAMP3 KO mice have an age dependent anabolic skeletal phenotype	259
8.1.2 RAMP2 protein compensates for RAMP3 protein in an event of stimulation.....	260
8.1.3 RAMP2 and RAMP3, differences and preferences	262
8.1.4 Calcitonin receptor in osteoblasts	263
8.2. Technical limitations	264
8.3 Future work.....	265
8.4 Conclusion	266
Chapter 9: Appendix	267
9.1 Appendix	268
9.1.1 Chapter 2: Accelerated skeletal development in RAMP3 KO mice	268
9.1.2 Chapter 3: Skeletal response of RAMP3KO mice to ovariectomy	269
9.1.2.i Statistical analysis of microCT analysis of baseline, sham and OVX WT and RAMP3 KO mice.....	269
9.1.3 Chapter 4: Characterising RAMP3 KO primary osteoblasts	274
9.1.3.i Primary Osteoblast culture buffers and solutions.....	274
9.1.4 Chapter 5: Expression of RAMPs in differentiating primary osteoblasts.....	274
9.1.4.i CT and Delta CT values of RAMP1, 2 and 3 in WT and RAMP3 osteoblasts.....	274
9.1.5. Chapter 6: Expression of RAMPs in response to stimulation.....	276
9.1.5.i Western Blotting Reagents	276
9.1.6 Chapter 7: Expression of CTR in differentiating primary osteoblasts	278

9.1.6.i Sequencing results: Sequences of the amplicons of all individual overlapping primer pairs.....	278
9.1.6.ii NCBI BLAST results	280
9.1.6.ii.a NCBI BLAST2n result for osteoblast CTR cDNA and full length CTR variant	280
9.1.6.ii.b NCBI BLAST result for osteoblast CTR cDNA sequence	282
Bibliography	286

List of Figures

Figure 1.1: Schematic of the endochondral ossification process	20
Figure 1.2: Osteoblasts lining the cortical bone surface	21
Figure 1.3: Schematic representation of complex osteoblast endocrinology.....	24
Figure 1.4: Osteocytes embedded in the bone matrix	25
Figure 1.5: Schematic showing differentiation of osteoblast and osteocyte	25
Figure 1.6: Multinucleated osteoclasts on trabecular bone surface	26
Figure 1.7: Schematic showing differentiation of osteoclast.....	26
Figure 1.8: Schematic showing interactions between osteoblast-osteoclast in bone remodelling.....	28
Figure 1.9: Electron micrograph images of normal and osteoporotic bone.....	30
Figure 1.10: Therapeutic approaches used to treat osteoporosis	31
Figure 1.11: Schematic representation of structure of Calcitonin	34
Figure 1.12: Schematic representation of structure of Calcitonin gene related peptide	36
Figure 1.13: Schematic showing alternate splicing of CALC 1 gene.....	37
Figure 1.14: Schematic representation of structure of Amylin	38
Figure 1.15: Schematic representation of structure of Adrenomedullin.....	41
Figure 1.16: Image showing distended yolk sac and hydrops fetalis in AM KO mice embryos	43
Figure 1.17: Predicted structure of CLR.....	45
Figure 1.18: Proposed structure of RAMP1	46
Figure 1.19: Interactions of RAMPs with CTR and CLR – generation of functional receptors	48
Figure 1.20: Schematic showing mRNA expression of RAMPs in different tissues	49
Figure 1.21: Images of RAMP2 KO mice showing signs of hydrops fetalis	50
Figure 1.22: Schematic showing anabolic effect of CT family of peptides on bone	51
Figure 1.23: Results published by Hoff et al 2002 showing advanced bone phenotype	52
Figure 1.24: MicroCT images of femurs of WT and RAMP transgenic animals.....	52
Figure 2.1: Schematic showing generation of WT 129/SvEv mice from RAMP transgenic mice.....	59
Figure 2.2i: Representative image showing measurement region of mouse tail	64
Figure 2.2ii: Representative image showing whole bone measurements in postnatal day 5 mice ..	65
Figure 2.3: Summary of physical markers used for determining region of interest.....	68
Figure 2.4: Representative image showing analysis of tibial region of interest in microCT	69
Figure 2.5: Representative image showing analysis of femoral region of interest in microCT	70
Figure 2.6: Screen-shot showing rendering of a femur model in Voxler software	72

Figure 2.7: Image showing method to measure dual Calcein labels.....	73
Figure 2.8: Figure showing quantification criteria using Image-Scope software.....	75
Figure 2.9 Figure showing analysis of endocortical and trabecular cell measurements.....	76
Figure 2.10: Figure showing analysis of growth plate	77
Figure 2.11 to Figure 2.47: Results of Chapter 2.....	79-132
Figure 2.48: Schematic representation of lateral endocortical bone in WT and R3 KO mice	135
Figure 3.1 to Figure 3.10: Results of Chapter 3.....	144-153
Figure 4.1: Schematic showing markers expressed during osteoblast differentiation.....	158
Figure 4.2 summary of image analysis protocol for a stained well	163
Figure 4.3 to Figure 4.6: Results of Chapter 4.....	165-171
Figure 4.7: Schematic showing activity of ALP in WT and RAMP 3 KO osteoblasts	173
Figure 5.1: Example of a qPCR amplification plot (for RAMP 3).....	184
Figure 5.2 to Figure 5.12: Results of Chapter 5	186-200
Figure 6.1 to Figure 6.9: Results of Chapter 6	214-227
Figure 6.10: Schematic for hypothesized compensatory mechanisms between RAMP 2 & 3	229
Figure 7.1: Figure summarizing the receptors expressed on bone cells.....	235
Figure 7.2: Schematic showing experimental design for sequencing CTR cDNA.....	234
Figure 7.3 to Figure 7.9: Results of Chapter 7.....	243-253
Figure 7.10: Three-dimensional ribbon models of CTR variants.....	254
Figure 7.11: Schematic showing regulation of osteoclast and osteoblast differentiation by CTR....	256
Figure 8.1: Schematic depicting competitive hetero-dimerization between RAMP 2&3 with CLR..	261

List of Tables

Table 2.1: Genotyping primer sequences for WT and RAMP 3 mice.....	61
Table 2.2: Resolutions and threshold levels used for 3D reconstructions.....	67
Table 2.3: Summary table of physical markers used for identifying region of interest.....	68
Table 2.4 to Table 2.23: Results of Chapter 2.....	82-131
Table 4.1 to Table 4.4: Results of Chapter 4.....	164-170
Table 5.1: RAMP 1, 2 & 3 primer sequences for end point PCR.....	180
Table 5.2: Custom double dye primer sequences for RAMP 1, 2 and 3.....	181
Table 5.3 to Table 5.5: Results of Chapter 5.....	195-199
Table 6.1: Antibodies used in Western blotting.....	211
Table 7.1: Primer sequences for full length mouse osteoblast CTR sequence.....	241
Table 7.2 to Table 7.3: Results of Chapter 7.....	246-247
Table 7.4: Expression of CTR in brain, osteoblasts and osteoclasts.....	255
Table 9.1 and Table 9.2: Appendix tables.....	269-278

Abbreviations

3D	Three dimensional
aa	Amino acid
ACTH	Adrenocorticotropic hormone
ALP	Alkaline phosphatase
AM	Adrenomedullin
AMY	Amylin
AP-1	Activator protein-1
AP-2	Activator protein-2
AR	Androgen receptor
ATPase	Adenosine Triphosphatase
BMD	Bone Mineral Density
BMPs	Bone Morphogenic Protein
BMU	Bone Multicellular Units
BV	Bone Volume
BV/TV	Bone Volume / Tissue Volume ration
CALC-1	Calcitonin-1 gene
CALCR	Calcitonin gene receptor
CI	Confidence interval
cAMP	Cyclic adenosine monophosphate
cDNA	complimentary DNA
CaSR	Calcium sensing receptor
CFUs	Colony forming units
CGRP	Calcitonin gene related peptide
CLR	Calcitonin receptor like receptor
CRE	cAMP-regulated enhancer
CSF-1	Colony Stimulating Factor
CT	Calcitonin
CTR	Calcitonin receptor
Cys	Cysteine
DAP	Diabetes-Associated Peptide
DPD	Deoxypyridinoline

DEXA	Dual energy x-ray absorptiometry
EDTA	Ethylenediaminetetraacetic acid
Erk2/3	Extracellular signal regulated pathway2/3
FGF	Fibroblast Growth Factor
FGFR	FGF Receptor
Fmol	Femto molar
FSH	Follicle-stimulating hormone
GPCR	G-protein coupled receptor
GTPase	Guanosine Triphosphatase
H & E	Hematoxylin and Eosin
Het	Heterozygous
HR	Heart rate
HSCs	Hematopoietic Stem Cells
IAPP	Islet amyloid polypeptide
IC 1/2/3	Intracellular Loop 1/2/3
IGF-1	Insulin-like growth factor 1
IL-6	Interleukin 6
kDa	Kilo dalton
kbp	Kilo base pair
KO	Knock-out
LH	Lutenizing hormone
LPS	Lipopolysaccharide
microCT	Micro-computer tomography
MAPK	Mitogen-activated protein kinase
M-CSF	Macrophage Colony Stimulating Factor
MiTf	Microphthalmia-associated Transcription factor
ml	Milli litre
MSCs	Mesenchymal Stem Cells
NHERF-1	Na ⁺ /H ⁺ exchanger regulatory factor-1
NICE	National Institute for health and Clinical Excellence
Nf-kB	Nuclear factor kappa B
NSF	N-ethylmaleimide Sensitive Factor
NS/ns	Non-significant

NO	Nitric oxide
NOS	Nitric oxide synthase
OPG	Osteoprotogerin
OVX	Ovariectomy/ovariectomised
PAMP	Proadrenomedullin N-terminal 20 peptide
PBS	Phosphate buffer saline
PCR	Polymerase chain reaction
PCAP	Pituitary Adenylate Cyclase-Activating Peptide
PDGF	Platelet Derived Growth Factor
PND5	Post natal day 5
PKA/C	Protein Kinase A or C
PLC	Phospholipase C
PRF	Prolactin releasing factor
PRIF	Prolactin Release Inhibitory Factor
PTH	Parathyroid hormone
PTHR1/2	PTH Receptor 1/2
qPCR	Quantitative PCR
RT-PCR	Real time PCR
RAMP1/2/3	Receptor activity modifying protein 1/ 2/ 3
RDC1	Rhodopsin-like receptors
ROI	Region of interest
SEM	Standard error of the means
SERM	Selective oestrogen receptor modulator
TbN	Trabecular Number
TbSp	Trabecular Separation
TbTh	Trabecular Thickness
TGF	Transforming Growth Factor
TNF α :	Tumor necrosis factor α
TRAcP/TRAP	Tartrate Resistant Acid Phosphatase
TSH	Thyroid Stimulating Hormone
VPAC1:	Pituitary adenylate cyclase-activating peptide 1
VIP:	Vasointestinal peptide
WT:	Wild type

Chapter 1: Introduction

Low bone mass skeletal disorders like Osteoporosis are amongst the major health concerns worldwide. It is estimated that about 3 million people suffer from osteoporosis in the U.K that account for about 0.3 million fractures every year with a mortality rate as high as 10-20% due to frequent fractures (Lewiecki 2004) (National Health Service (NHS)). Majority of the skeletal disorders arise from an imbalance in bone remodeling resulting in an increased bone resorption and reduced bone formation. Therapeutic approaches for treating skeletal disorders, therefore, are aimed towards restoring this balance in bone remodeling. Most of the current therapies such as bisphosphonates are anti-catabolic. However given that the patients affected by skeletal disorders are over the age of 60 and have reduced bone formation, it is important to develop anabolic therapeutic targets for treating these disorders.

Calcitonin (CT) family of peptides are known hypocalcaemic hormones hence receptors for these peptides are amongst the potential therapeutic targets for treating skeletal disorders. Receptors for calcitonin family of peptides comprise G-protein couple receptors (GPCRs) - Calcitonin Receptor (CTR) and Calcitonin-like Receptor (CLR). For most of the CT peptides, a functional receptor arises from the hetero-dimerization of either of these GPCRs with an accessory protein called the Receptor Activity Modifying Protein (RAMP). To date three isoforms of RAMPs; 1, 2 and 3, have been identified in human. Murine knock-out (KO) studies for the GPCRs – CTR and CLR, aimed at ablating the hypocalcaemic effect of the CT peptides unexpectedly revealed high bone-mass skeletal phenotypes.

In our pilot study we determined the skeletal phenotype of individual RAMP knockout model. We observed that alteration in RAMP2 and RAMP3 but not RAMP1 influenced the skeletal phenotype. RAMP2 heterozygous mice at 8 weeks of age had increased cortical porosity, reduced cortical thickness and increased marrow cavity along with increased inter vertebral distance in the spine (Kadmiel et al 2011). RAMP3 knockout mice had increased cortical thickness and bone volume compared to the wild types, at the age of 8 weeks. However this data was obtained from very few numbers (n= 3 each genotype).

This dissertation presents an investigation of the potential role of Receptor Activity Modifying Protein3 (RAMP3) in treating skeletal disorders. We focus on characterizing the skeletal phenotype and the primary osteoblast cultures derived from RAMP3 KO mice. We further investigate the effects of hypocalcaemic peptide stimulation on the primary osteoblasts in order to determine whether RAMP3 is a potential anabolic therapeutic target for treating skeletal disorders.

1.1 Bone

Bone is a dynamic tissue that undergoes constant remodelling. In humans, 206 bones form the “skeleton” which predominantly provides the bipedal structure, support and movement to the human body. This mechanical structure of the bone provides grace, flexibility and posture that make human-beings superior to other organisms. The skeleton also protects vital organs such as heart, brain and lungs, acts as a reservoir for essential minerals including calcium and phosphate, growth factors and fat, and also acts as a site for generating the cellular components of blood – haematopoiesis. Solid bone is composed of predominantly an inorganic component, ‘hydroxylapatite’ a hydrated calcium phosphate $\text{Ca}_{10}(\text{PO}_4)_6(\text{OH})_2$, which accounts for 70% of dry weight of the composite bone, linked to the organic component predominantly the protein ‘collagen’, although there are many smaller non-collagenous organic molecules in bone matrix including glycoaminoglycans, proteoglycans, and growth factors (Iozzo 1998, Mohan & Baylink 1991, Vejlens 1971, Wendel et al 1998). Depending on the orientation of the collagen fibres, bone can be either compact or spongy/cancellous.

1.1.1 Structure of bone: In 1678, Leeuwenhoek first observed the microscopic canal system and cells in the bone. It was then realised that bone is not a homogenous solid structure. Leeuwenhoek’s observations were later extensively studied and characterised by Havers in his monogram “Osteologia Nova,” in 1691, cited by Enlow in 1962 (Enlow 1962). The canal system was later termed as the ‘Haversian system’ and the cells were named osteocytes.

The compact bone is called cortical and spongy bone is called trabecular bone. The cortical bone surrounds the trabecular bone at in the metaphyseal and epiphyseal regions and has a lamellar structure that is made up of inter-connected vascular and neuronal canals. The proportion of cortical to trabecular bone varies between each type of bone. Bone is arranged in concentric circles around the canals with embedded bone cells – osteocytes which communicate with each other through the canaliculi. Each canal and the concentric bone containing embedded osteocytes forms an ‘osteon’ (Enlow 1962).

Three main cell types – the osteoblasts, osteocytes and osteoclasts, regulate bone formation and maintenance. Osteoblasts and osteocytes are mono-nucleated cells that arise from differentiation of the progenitor mesenchymal stem cells, whereas osteoclasts are multinucleated differentiated haematopoietic stem cells.

1.1.2 Bone formation: The process of bone formation is called ossification. There are two types of ossification: intramembranous and endochondral. In flat bones such as the mandible and the calvaria, the mesenchymal stem cells undergo differentiation and form mature osteoblasts (Ducy et al 2000). In other bones, bone formation takes place through endochondral ossification. It is the process in which the cartilage undergoes vascular invasion and mineralisation. The dead chondrocytes in the cartilage are then replaced by the osteoblasts (Horton & Machado 1988) (Fig 1.1 below).

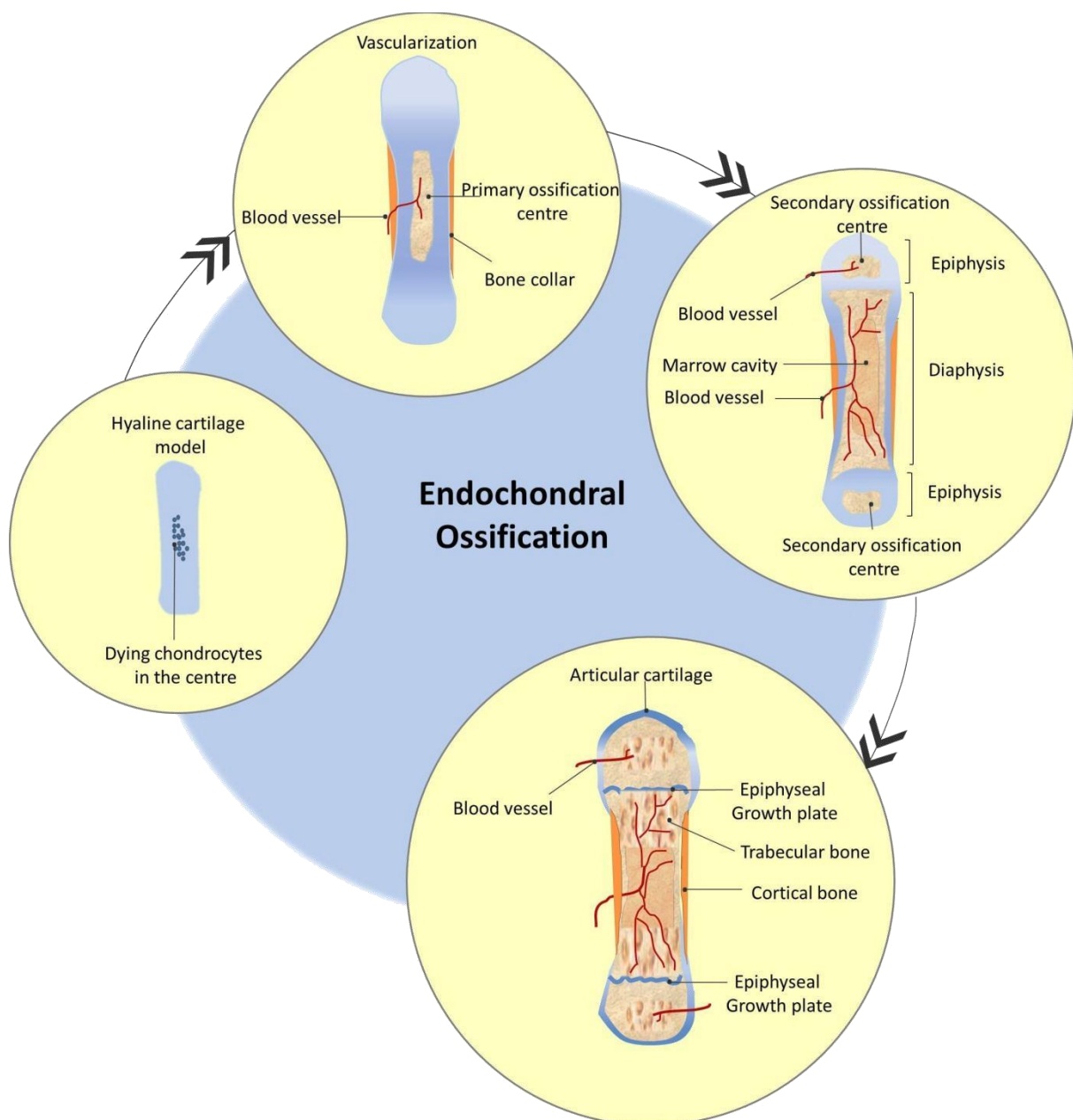


Fig 1.1: Schematic representation of endochondral ossification where the cartilage is vascularised and then mineralised to form bone. Image adapted from the image of endochondral ossification published by Benjamin Cummings, Pearson Education, Inc.

1.1.3 Bone cells:

1.1.3.i Osteoblasts

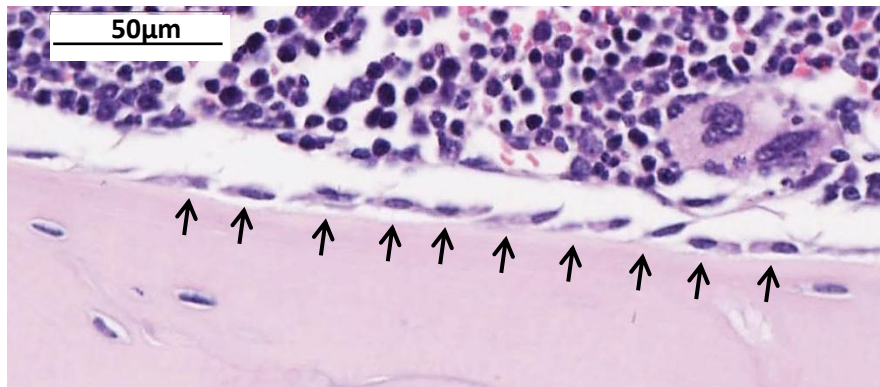


Fig 1.2: Osteoblasts lining the cortical bone surface (black arrows) seen in tibia.

Osteoblasts are the 'bone forming' cells that differentiate from mesenchymal stem cells. A high concentration of alkaline phosphatase in the cell membrane is a characteristic feature of osteoblasts. A number of transcription factors are involved in osteoblast differentiation. First, Runx2 commits the mesenchymal stem cells to differentiate into pre-osteoblasts instead of chondrocytes or adipocytes. Then Runx2, β -catenin, and Osterix direct the differentiation of the pre-osteoblasts to form mature osteoblasts (Day et al 2005, Ducky et al 1997, Komori 2006). Growth factors including fibroblast growth factor (FGF), bone morphometric proteins (BMPs) and Wnt regulate osteoblast differentiation (Chen et al 1997a, Levasseur 2001, Mayahara et al 1993). Differentiation of osteoblasts from progenitor mesenchymal stem cells is summarised in Figure 1.5 (Bonewald 2011). Osteoblasts also produce Osteoprotegerin (OPG) that inhibits osteoclasts formation and cytokines like colony stimulating factor1 (CSF-1) and RANK ligand which when cleaved activates osteoclastogenesis (Taichman & Emerson 1994, Udagawa et al 1990, Yasuda et al 1998).

Mature and progenitor osteoblasts express several integrins, adhesion molecules and receptors for oestrogen, parathyroid hormone, prostaglandins, vitamin D and various cytokines (Calvi et al 2001, Eriksen et al 1988, Hakeda et al 1985, Sooy et al 2005). Despite being a bone cell, the differentiation, proliferation and regulation of osteoblasts is dictated by growth factors and hormones released by various organs. It is hence important to review the regulation of osteoblasts by organs other than bones; although, a complete comprehension of regulation of all the

hormones that regulate osteoblasts is beyond the scope of this project. In this section we shall briefly review the complexity of osteoblast endocrinology.

Insulin like growth factor (IGF) and fibroblast growth factor (FGF) both regulate the proliferation of progenitor osteoblast cells and osteoblast differentiation through the IGF receptor (IGFR) and FGF receptor (FGFR) (Chen et al 2012, Marie 2003). Wnt, Transforming Growth Factor-beta ($TGF\beta$) and Bone Morphogenetic Proteins (BMPs) activate Lrp5/6 and Fzd receptor complex, TGF receptor and BMP receptors (BMPR) respectively to regulate the differentiation of mesenchymal stem cells to mature osteoblasts (Redlich & Smolen 2012). The Wnt - Fizzled pathway regulates osteoblast differentiation through the activation of cytoplasmic β -catenin whereas TGF and BMPs stimulation results in transcriptional activation of runt-related transcription factor 2 (RUNX2) through SMAD proteins (Redlich & Smolen 2012).

One of the most important hormonal osteoblast regulation is through the 'calcium homeostasis' pathway. Increased serum calcium levels, results in secretion of calcitonin by the 'C- cells' of the thyroid gland. Increased serum calcitonin results increases the incorporation serum calcium into mineralised bone by activating osteoblasts. Calcitonin also inhibits osteoclast activity of mobilization of bone and calcium. When the serum calcium levels drop, parathyroid glands secrete the parathyroid hormone (PTH) which increases the osteoclast mediated bone resorption that releases calcium in the blood, hence regulating serum calcium levels (Copp & Cheney 1962).

Osteoblasts express PTH receptor 1 (PTHR1) on their cell surface and intermittent PTH stimulation induces bone formation. Sex hormones, oestrogen and testosterone blocks PTH mediated osteoclast differentiation by affecting the hematopoietic blasts cells and by affecting osteoblasts. Oestrogen and testosterone stimulate osteoblasts by activating the Oestrogen receptors α and β ($ER\alpha/\beta$) and androgen receptor (AR) respectively. The activation of ER and AR blocks the cAMP signalling of PTHR1 receptor that is in turn responsible for the activation of osteoclast differentiation (Kaji et al 1996). Activation of ER and AR also induces osteoblast differentiation in progenitor osteoblasts and downstream Src/Shc/ERK signally in mature osteoblasts that has an anti-apoptotic effect on the cells (Kung 2003). Oestrogen stimulation also reduces the secretion of interleukin 6 (IL-6) that promotes osteoclast activity.

Another hormone that plays an important role in regulating osteoblast function is Insulin. Insulin secreted by the Beta-cells of the pancreas activates the insulin receptor (IR) expressed by osteoblasts and induces the production of osteocalcin which in turn increases the production of

insulin. Insulin also down regulates the production of osteoprotegerin (OPG), a decoy RANKL receptor (Karsenty & Ferron 2012). Insulin also promotes the production of Leptin in fat cells in the adipose tissue. Leptin activates the leptin receptor (LepR) present on the serotonin producing neurons of the raphe nuclei in the brainstem which results in activation of the sympathetic tonus (Paz-Filho et al 2012). This in turn activates the beta2 adrenergic receptor on the osteoblasts (ADRB2) which increases the expression of Enterococcal surface protein (Esp) which down regulates osteocalcin mediated insulin production (Paz-Filho et al 2012). Several other hormones and cytokines not mentioned in this review regulate osteoblast activity.

Figure 1.3 overleaf, summarises the complexity of osteoblast endocrinology and different receptors through which various organs regulate osteoblasts.

1.1.3.ii Osteocytes:

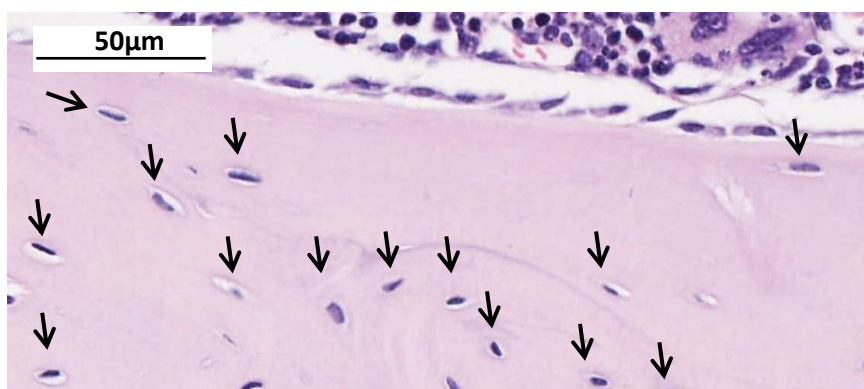


Fig 1.4: Osteocytes embedded in the bone matrix (black arrows) seen in tibia cortical bone.

Osteocytes are the most abundant cell type in the bone. These mono-nucleated cells with extended cytoplasmic processes are decedents of the mesenchymal stem cells resulting from osteoblast differentiation (Manolagas 2000, Marotti et al 1976) (see Fig 1.5(Bonewald 2011)). Osteocytes are generated from a subpopulation of osteoblasts that get trapped in the matrix in pockets called the osteocytic lacunae (Baud 1968), (Fig 1.4) (Franz-Odendaal et al 2006). Once the osteocytes are embedded in the matrix, they rapidly develop long dendritic extensions (Baud 1968). The location of the osteocytes allows them to regulate bone remodelling in response to mechanical forces and thus act as mechanoreceptors of the bone (Ajubi et al 1999). Osteocytes also maintain the bone matrix by regulating calcium concentrations. There is evidence that the osteocyte cytoplasmic calcium concentration is about 1.5mM whereas the calcium concentration in the extra cellular matrix is a much lower of about 0.5mM (Baud 1968, Knothe Tate et al 2004). This suggests a continuous flow of calcium ions out of the cells and into the bone matrix (Knothe Tate et al 2004).

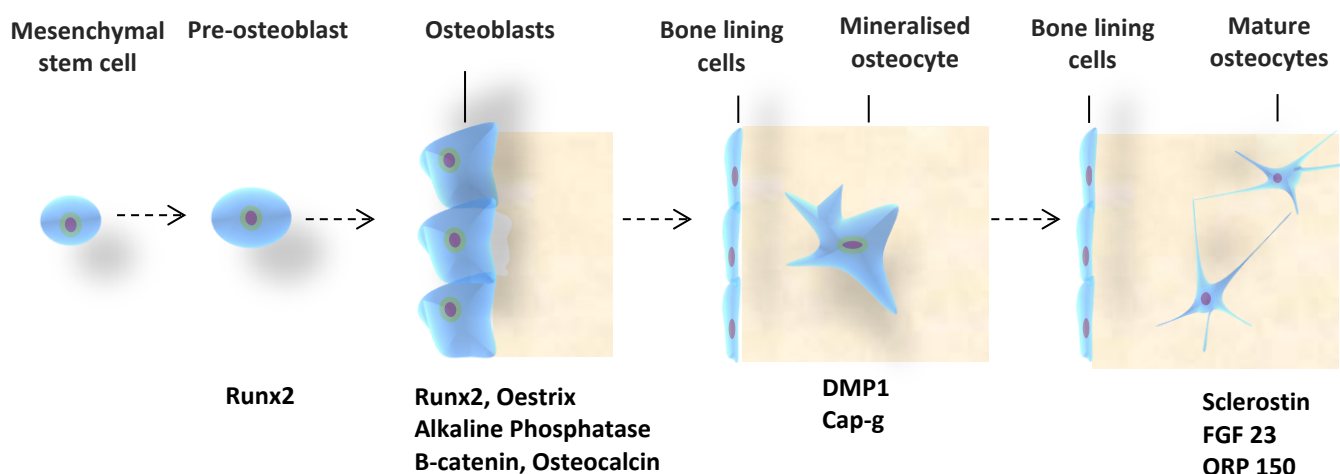


Fig 1.5: Osteoblast and osteocyte differentiation from mesenchymal stem cells and the various transcription factors involved in the process. Image adapted from (Bonewald 2011)

1.1.3.iii Osteoclasts:

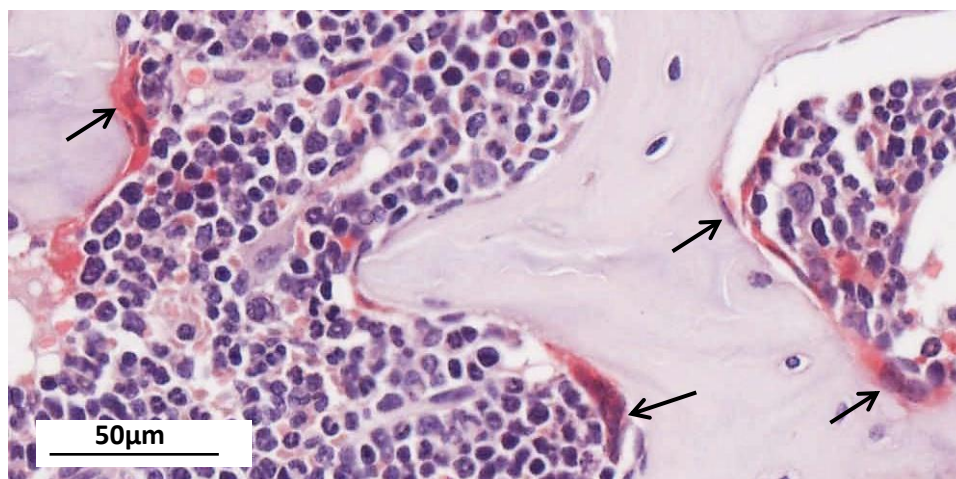


Fig 1.6: Tartrate resistant acid phosphatase positive, multinucleated osteoclasts stained red (black arrows) seen on trabecular bone surface of tibia section.

Osteoclasts are the bone resorbing multinucleated cells that descend from haematopoietic stem cells (Fig 1.6). Osteoclasts are generated from asynchronous fusion of precursor mono-nucleated cells and may have 4 -20 nuclei. Osteoclast differentiation depends on RANK receptor activation from the RANKL produced by osteoblasts. Macrophage colony stimulation factor (M-CSF) which is essential for proliferation of monocytes is also essential for RANK formation (Yasuda et al 1998). Hence the key regulators of osteoclast differentiation include the cytokines: RANKL and M-CSF (Teti et al 1989, Udagawa et al 1990). The transcription factors that regulate osteoclast differentiation include NF- κ B, c-Fos, MiTf and PU-1 (Franzoso et al 1997, Grigoriadis et al 1994, Hertwig 1942, Tondravi et al 1997). Osteoclast differentiation is summarised in Figure 1.7 below.

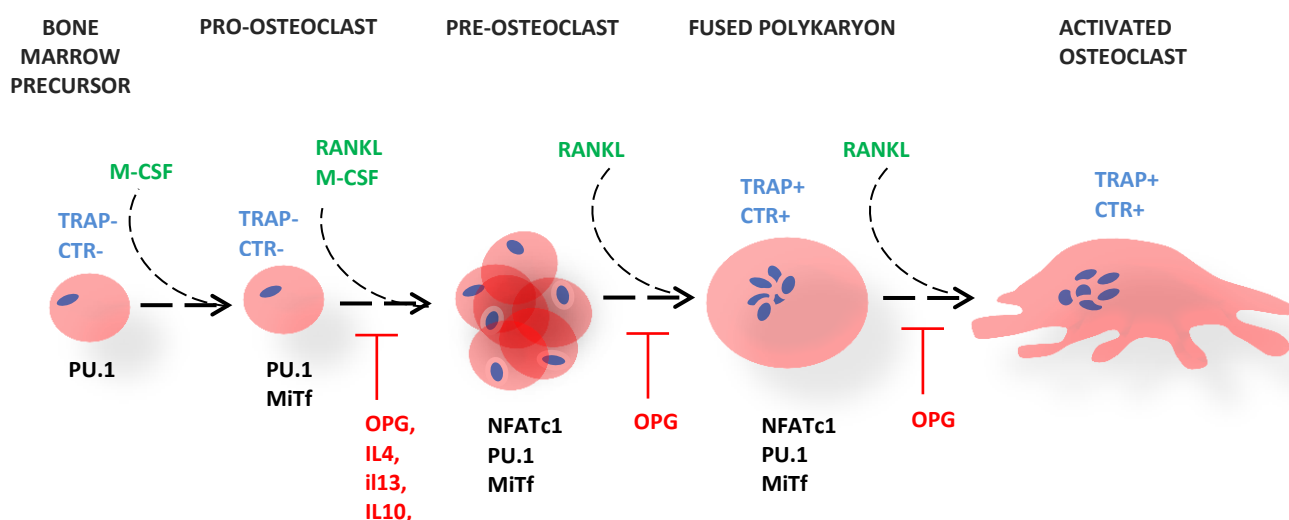


Fig 1.7: Schematic representation of osteoclast differentiation from hematopoietic stem cells and the various transcription factors involved. Image adapted from (Boyle et al 2003, Wendel et al 1998)

Osteoclasts have abundant Golgi complex and mitochondria. The cytoplasm of an osteoclast has a foamy appearance due to the presence of large vacuoles. The transport vesicles within osteoclasts are filled with cathepsin K and tartrate resistant acid phosphatase (TRAcP) that are characteristic to these cells. The basolateral cell membrane expresses Na^+ and K^+ ATPase, Na^+/H^+ and $\text{HCO}_3^-/\text{Cl}^-$ exchangers and receptors such as RANK, OPG receptor, M-CSF receptor and Calcitonin receptor (CTR) (Nakagawa et al 1998, Teti et al 1989, Udagawa et al 1990). The bicarbonate exchangers expressed on the basolateral membrane remove excess bicarbonate from the cytoplasm to maintain intracellular pH (Hall and Chambers 1989).

Osteoclasts form Howship's lacunae by resorbing the underlying bone matrix. The bone resorbing activity of osteoclasts depends on the stretch of plasma membrane that forms the zone of contact with the bone which is called the "ruffled border". Around this zone of contact, actin in the cell cytoskeleton generates a sealing zone (Gothlin & Ericsson 1976). The ruffled border is rich in integrins, and Calcium channels (C1C7) that regulate adhesion and mobility of the cell, and produces ATPase that helps in resorbing the underlying bone (Blair et al 1989). The ruffled border also releases acids, metalloproteinases and cathepsins that degrade the bone matrix (Nesbitt & Horton 1997). The degradation products are removed via transcytosis (Väänänen et al 2000).

1.1.4 Bone remodelling:

An adult skeleton is constantly broken down by osteoclasts and replaced by new bone formed by osteoblasts. This tightly regulated lifelong process is called bone remodelling. In humans, a bone remodelling cycle lasts for about 120 days (20 days resorption, 100 days bone formation) (Vignery & Baron 1980). Bone remodelling can either occur at the growth plate during skeletal development or occur as a part of the bone turnover process, where mature bone is replaced by new bone as a part of skeletal maintenance.

The remodelling process is always initiated by recruitment and activation of osteoclasts. The recruitment and differentiation of osteoclasts is mediated by osteoblasts by releasing M-CSF and RANKL cytokines. Osteoclasts release enzymes to breakdown the underlying bone matrix. The resorption pits generated by the osteoclasts release local factors such as osteocalcin, calcium, hydroxyproline which then recruit osteoblasts and inhibit osteoclast-mediated resorption. Osteoclasts also release insulin like growth factors (IGFs) that inhibit their own activity and enhance osteoblast activity (Mackie 2003). This is known as the early resorptive phase. On

completion of resorption of the bone, the osteoclasts leave the resorption site and osteoblasts migrate into the resorption site (reversal phase) and produce new bone (formative phase). A sub population of the osteoblasts get mineralised and embedded in the new bone matrix forming osteocytes, and others form the bone lining of the completely mineralised (Franz-Odendaal et al 2006, Manolagas 2000). It is important that the initiation and termination of both resorption and formation of bone occurs properly. This mechanism is called coupling (Parfitt et al 1987). Once the formation of the new osteon is completed, the bone goes into the quiescent phase. Bone remodelling occurs in small regions called the bone multicellular units (BMUs), and each BMU is different from the other (Frost 1991, Hill 1998, Parfitt et al 1987). It is therefore evident that the bone microenvironment regulates the cell activation sequence. The interaction between osteoblast and osteoclast at the resorption site is summarised in Figure 1.8 below (Stein 1999).

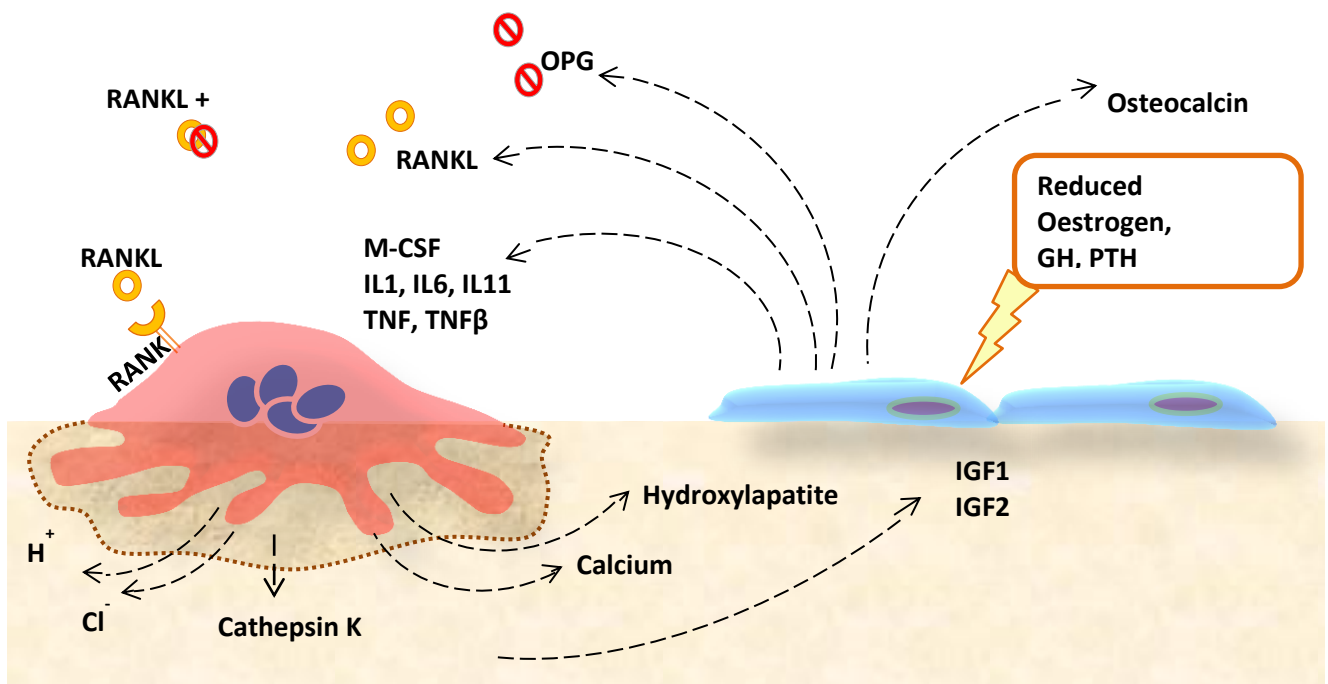


Fig 1.8: Schematic representation of the interactions between osteoclast (red) and osteoblasts (blue) at the bone resorption site whilst bone remodelling. The zone under osteoclasts (marked with dotted line) is the resorption pit generated by the osteoclast. Image adapted from (Stein 1999)

Many hormones including insulin, oestrogen, testosterone, parathyroid hormone (PTH), growth hormone (GH), calcitonin family of peptides, 1,25-dihydroxy vitamin D3, glucocorticoids and thyroid hormones are known to regulate bone remodelling (Canalis 1983, Mackie 2003). Bone remodelling is also regulated by the mechanical use of skeleton and growth factors such as

insulin like growth factor (IGF) I and II, platelet derived growth factor (PDGF), interleukins (IL1 and 6), transforming growth factor-b (TGF-b) and tumor necrosis factor (TNF) (Canalis 1983, Mackie 2003). An imbalance in the levels of any of these growth factors or hormones results in an imbalance in bone remodelling which in turn results in a compromised bone quality. Additionally, since many of these hormones also regulate differentiation of osteoblasts and osteoclasts, an altered hormone level can also result in alteration in cell population of either cell types eventually contributing to compromised bone quality.

Compromised skeletal quality increases bone fragility that leads to skeletal disorders characterised with frequent fractures, inflammation and pain. Skeletal disorders are amongst major health concerns worldwide. Apart from pathological disorders like osteoporosis, Paget's disease, osteonecrosis, osteogenesis imperfect, osteoarthritis and osteomyelitis, skeletal disorders can also result from metastatic cancer and prolonged cancer treatments like glucocorticoids, aromatase inhibitors and androgen deprivation (Confavreux et al 2007, Love et al 1992, Lukert 1992, Lukert et al 1992).

1.2 Osteoporosis

Amongst the various skeletal disorders, the most common disorder is Osteoporosis. Osteoporosis is defined as “*a skeletal disease characterized by compromised bone strength predisposing a person to an increased risk of fracture. Bone strength primarily reflects the integration of bone density and quality.*”(Klibanski 2001). Figure 1.9 below is a representative scanning electron micrograph image comparing healthy and osteoporotic bone.

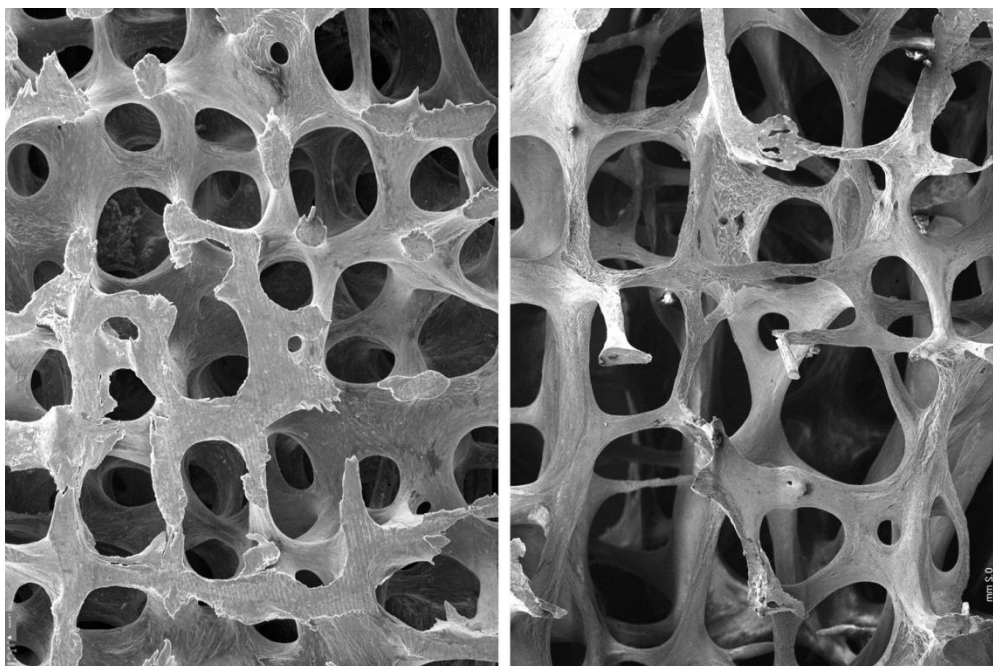


Fig 1.9: Scanning electron micrograph of normal (left) and osteoporotic bone (right). By kind permission of Prof. Tim Arnett (Bone Research Society). Osteoporotic bone shows compromised bone integrity.

According to National Health Service (NHS), about 3 million people are estimated to suffer from osteoporosis in the U.K that accounts for about 0.3 million fractures every year. The mortality rate of patients has been estimated to be as high as 10-20% due to frequent fractures (Lewiecki 2004). Death usually occurs due to hospital acquired infections due to frequent admissions to hospital. Patients who recover suffer loss of independence and shortened lifespan subsequently.

Although most commonly osteoporosis is associated with post-menopausal women, men and young adults can also be affected. Hormonal disorders such as reduction in oestrogen or testosterone, hyperthyroidism, pituitary gland disorders, hyperparathyroidism, Cushing's syndrome (adrenal gland) are commonly associated with osteoporosis. In men, osteoporosis can be caused by low testosterone levels, hypogonadism or use of glucocorticoids. In women the predominant reason for osteoporosis is menopause although, hysterectomy before the age of 45 or loss of

menstrual periods due to over dieting is also associated with osteoporosis. It is observed that women (80%) are more prone to develop osteoporosis than men (20%) (Lewiecki 2004).

1.2.1 Diagnosis and current therapies:

Osteoporosis is diagnosed by measuring bone mineral density (BMD) using dual energy X-ray absorptiometry scan (DEXA). The standard deviation of the difference in patient's BMD and that of a health young adult is calculated as the "T-score". A T-score above -1 is normal, between -1 and -2.5 is classified as osteopenia and below -2.5 is classified as osteoporosis.

According to the National Institute for health and Clinical Excellence (NICE) guidelines, treatment for osteoporotic patients depends on sex, whether patient is post-menopausal and if he/she has a previous history of fractures. All patients diagnosed of osteoporosis are prescribed calcium and vitamin D supplements. Exercise and change in lifestyle may be recommended to patients. Most common therapeutics used in the U.K, according to NICE guidelines, are summarised and detailed overleaf (Figure 1.10)

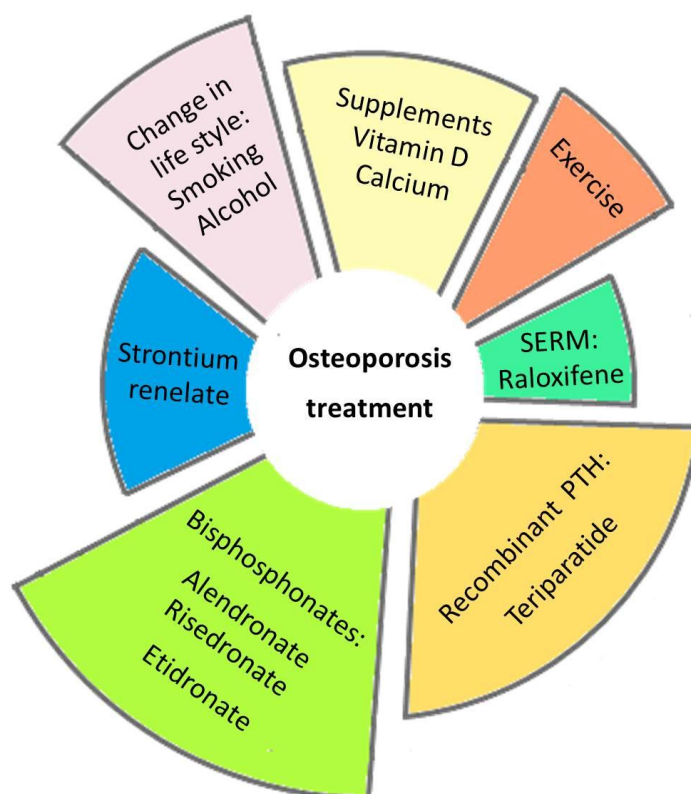


Fig 1.10: Schematic representation of major therapeutic approaches used to treat osteoporosis patients in the UK according to NICE guidelines.

A complete comprehension of the therapies for osteoporosis is beyond the scope of this project. However, the mode of action for a few main therapies is described below:

1.2.1.i Bisphosphonates: Bisphosphonates are a class of inorganic pyrophosphate analogues that have a high affinity to bone mineral during bone resorption (Rogers et al 1994). Nitrogen containing bisphosphonates such as Alendronate and Risedronate, act on the mevalonate pathway by hindering the prenylation of GTP-binding proteins, such as Rho, Ras and Rab by the enzyme farnesyl pyrophosphate synthetase (FPP) (Luckman et al 1998, Rogers et al 1999, van Beek et al 2003). This induces apoptosis in osteoclasts. Non-nitrogen containing bisphosphonate like Etidronate, Clodronate cripples osteoclast activity hence reducing bone resorption (Auriola et al 1997, Russell & Rogers 1999).

1.2.1.ii Strontium ranelate: Strontium ranelate, a strontium salt of ranelic acid, is a substitute for calcium. The nucleus size of Strontium is similar to Calcium and is hence absorbed by the body and incorporated in bone and teeth enamel. It increases bone formation by increasing osteoblast precursor proliferation and reduces bone resorption by hindering osteoclasts differentiation (Marie et al 1993, Meunier 2004, Meunier et al 2004).

1.2.1.iii Selective oestrogen receptor modulator (SERM): SERM - Raloxifene is a synthetic compound that selectively act as antagonist or agonist in different tissues (Jones et al 1984). Raloxifene is used to prevent fractures in post-menopausal breast cancer patients, as it acts as an antagonist in uterus and breasts. However, it acts as an agonist in bone hence protecting bone loss resulting from oestrogen deprivation (Jones et al 1984).

1.2.1.iv Recombinant PTH and anti-RANKL therapy - Teriparatide and Denosumab: Teriparatide is a recombinant human parathyroid hormone (1-34) of the whole 84 amino acid peptide which on regular administration of smaller doses results in anabolic skeletal effect (Deal & Gideon 2003, Dempster et al 1993, Hori et al 1988). Teriparatide can be prescribed in combination with Denosumab, a monoclonal antibody against RANKL to RANK which is important for osteoclast formation as a more efficient treatment than either agent alone (Lacey et al 1998, Tsai et al 2013).

In spite of their effectiveness to reduce fracture risk, these therapies have several side effects. Bisphosphonates are not prescribed to patients with stomach and kidney related pathological symptoms. There are reports of patients not taking bisphosphonates due to nausea, dyspepsia,

and diarrhoea (Ettinger et al 1998). There is compelling evidence to support that both bisphosphonates and Denosumab cause osteonecrosis of jaw resulting from reduced bone remodelling rate (Compston 2011, Odvina et al 2005). However this is only true when concentrations of drugs are administered as in oncology levels. Strontium ranelate is reported to increase risk of venous vein thromboembolism and is not suitable for patients suffering from phenylketonuria as it contains a phenyl group (NICE guidelines). In the NICE survey on 'The clinical effectiveness and cost effectiveness of prevention and treatment of osteoporosis' (2004), it was reported that despite reducing the risk of breast cancer related skeletal destruction SERMs result in deep vein thrombosis and is hence not prescribed to patients with thromboembolism. Another drug that is recently been discontinued by the European Medicines Agency 2012, is the nasal spray of synthetic salmon Calcitonin (sCT) due to increased risk of developing cancer. However the sCT injections are still administered but are restricted to Paget's disease patients and to vertebral fracture patients (European-Medicines-Agency 20 July 2012).

Since all the current major therapies except for Teriparatide, are anti-resorptive they lead to a low bone turnover state where bone formation also decreases with the decrease in bone-remodeling activity (Baron & Hesse 2012). The need for discovering bone anabolic therapies hence, demands itself. Ideally, the anabolic therapy should induce bone formation by the quiescent bone surface that is not simultaneously undergoing bone remodelling (Lane & Kelman 2003). Many promising anabolic therapies include parathyroid hormone related peptide analogues (PTHrP), Calcium sensing receptor and the members of the Calcitonin family of peptides.

Calcitonin family of peptides mainly comprise Calcitonin (CT), Calcitonin gene related peptide (CGRP), Amylin (AMY) and Adrenomedullin (AM). Each of these peptides influences skeletal regulation. However, with recent evidence of the accessory proteins that subtly modulate the receptor pharmacology of the CT family of peptides, new targets for skeletal therapies have been identified. In this study we focussed on the effects of accessory proteins called the Receptor Activity Modifying Proteins (RAMPs) on skeletal regulation through CT family peptide.

It is therefore important to understand the endocrinology of the CT family of peptides and to review the effects of these peptides and their receptors on the skeleton.

1.3 Calcitonin family of peptides

As mentioned earlier the calcitonin (CT) family of peptide comprise CT, CGRP, AMY and AM principally. Recently Intermedin is included in the group (Amara et al 1982, Cooper et al 1987, Copp & Cheney 1962, Kitamura et al 1993a). These peptides have a characteristic secondary structure. They all have a 6-7 amino acid (aa) ring formed by disulphide bonds between two Cys residues towards the N-terminus and amidation at the C-terminus of the peptide (Albrandt et al 1995). The structure, expression and function of each of these peptides are reviewed in the following sections.

1.3.1 Calcitonin (CT):

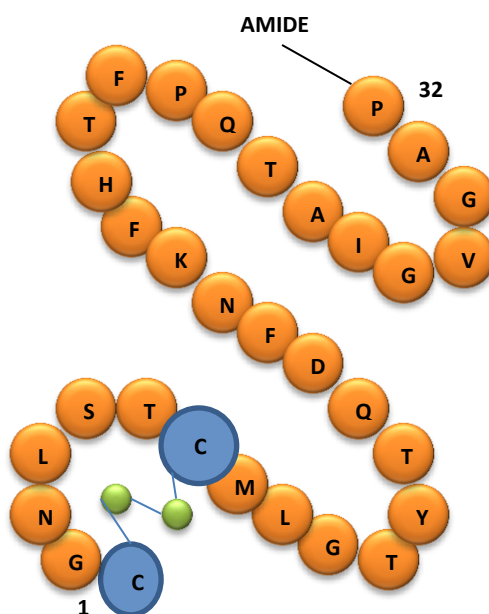


Fig 1.11: Calcitonin, 32 amino acid peptide with amidated C-terminus and a 6 ring structure at N-terminus formed due to disulphide bridge between C1 and C7. Adapted from MSc thesis: RAMPs potential role in regulation of bone mass and skeletal disorders, 2008, University of Sheffield.

Calcitonin (CT) the founder member of the CT family of peptide, is a 32 amino acid peptide with an amidated C-terminus and a disulphide bridge at the N-terminus forming a 7 amino acid ring (Fig 1.11). In humans mature CT results from a 141 amino acid precursor peptide known as the prepro-calcitonin (PreProCT) which originates from the calcitonin-1 gene (CALC-I) on chromosome 11 (Becker KL 1996, Becker L 1995, Copp & Cheney 1962). Alternate splicing of CT gene at exon 4 results in a 37 amino acid peptide, Calcitonin gene related peptide (CGRP)

(Amara et al 1982). CGRP is a neuropeptide and a potent vasodilator, which was first reported in rat and then in human (Evans et al 1983, Tippins et al 1984).

CT is primarily secreted by C cells in thyroid gland in response to increase in serum calcium levels (Copp & Cheney 1962, Neher et al 1968). CT is known to play an important role in calcium homeostasis as it regulates production of $1\alpha,25$ (OH) $_2$ D $_3$ and tubular reabsorption of calcium in the kidney (Sexton et al 1999, Shinki et al 1999). But most importantly CT inhibits extracellular Ca^{2+} sensing, thereby activating a potent anti-resorptive signal resulting in decrease in skeletal resorption (Zaidi et al 1996).

A single large dose of CT decreases serum levels of Luteinizing hormone (LH), testosterone and Follicle-stimulating hormone (FSH) in humans (Mulder 1993). On the other hand upon chronic administration of CT, increase in serum β -endorphin, cortisol and Adrenocorticotrophic hormone (ACTH) levels are reported in migraine patients (Becker L 1995).

CT interacts via a 7 transmembrane G – protein coupled receptor known as the Calcitonin receptor (CTR) which is highly expressed in renal cells, neural cells, breast cancer cell lines and most importantly in osteoclasts but not in osteoblasts (Findlay & Sexton 2004, Wang et al 2004). Activation of CTR results in intracellular adenylate cyclase and phospholipase C (PLC) enzyme activation mediated signalling (Findlay & Sexton 2004).

Osteoclasts are sensitized to parathyroid hormone induced (PTH-induced) stimulation, on CT withdrawal, resulting in increased serum Ca^{2+} levels and urinary deoxypyridinoline (DPD) cross links, which is a bone resorption marker (Zaidi et al 2002). CT also down regulates osteoclast mediated bone resorption (Wallach et al 1999). This phenomenon is supported by *in vitro* evidence of rapid cessation in mobility and size reduction of osteoclast upon CT administration (Chambers & Magnus 1982, Nicholson et al 1986). CT is also known to interfere with osteoclastogenesis, by hindering mononucleated cell fusion to form multinucleated osteoclasts (Takahashi et al 1988). It is one of the most potent antiresorptive hormones and is cleverly exploited during physiological calcium stress.

Despite convincing evidence, physiological importance of CT in skeletal maintenance is challenged by experiments in transgenic animals and unanswered phenomena like, why thyroidectomy or increased Ca^{2+} levels in case of medullary thyroid carcinoma fails to induce osteoporosis (Zaidi et al 2002) remain unknown. Global CT/CGRP knockout (KO) animals

interestingly exhibit osteosclerotic phenotype with increased trabecular bone volume due to elevated bone formation (Hoff et al 2002). Basal calcium metabolism parameters such as levels of serum Ca^{2+} , PTH, phosphorous and $1\alpha,25(\text{OH})_2\text{D}_3$ were the same in both KO and wild type (WT) animals (Hoff et al 2002). Interestingly there was an increase in serum Ca^{2+} and urinary DPD levels, 2 to 4 hr post exogenous human PTH (hPTH) treatment in KO but not WT. This suggested that hPTH induced bone resorption in KO animals. The resorptive effect of exogenous PTH was neutralised by the increased serum CT levels in WT animals suggesting that the bone resorption in KO animals was due to the lack of functional CT (Hoff et al 2002). Following this study Gagel et. al. in 2007 reported that osteosclerotic phenotype of the global CT/CGRP KO mice is lost after backcrossing to a C57BL/6 homogenous background; however there is instead an age related skeletal phenotype observed with increased cortical porosity (Davey et al 2008, Gagel RF et al 2007). Certainly, effect of CGRP on bone metabolism, confounds the phenotype resulting from CT/CGRP global KO (Davey et al 2008). It is not only important to carry out individual KO studies for each of these peptides, but also to understand the individual mechanisms through which they conserve skeletal tissues.

1.3.2 Calcitonin gene related peptide (CGRP):

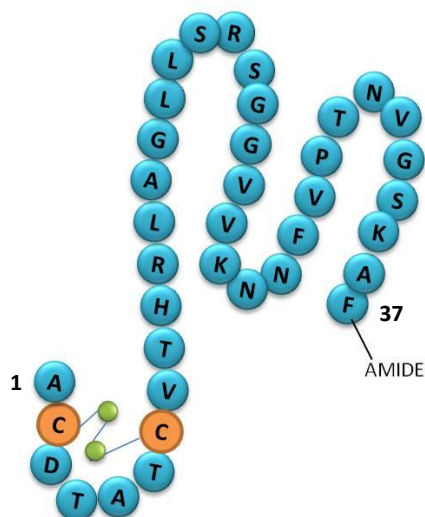


Fig 1.12: CGRP, 37 amino acid peptide with amidated C-terminus and a 6 ring structure at N-terminus formed due to disulphide bridge between C2 and C7. Adapted from MSc thesis: RAMPs potential role in regulation of bone mass and skeletal disorders, 2008, University of Sheffield.

As mentioned earlier the CALC 1 gene transcribes two distinct mRNAs that translate into a 32 amino acid CT and 37 amino acid long Calcitonin gene related peptide (CGRP) (Fig 1.12 and 1.13) (Amara et al 1982, Nagasaki et al 2004). It was reported that these two different mRNA

variants had a tissue specific expression (Amara et al 1984). CT is expressed primarily in C cells of thyroid, whereas CGRP is expressed mainly in brain, spinal cord and cranial nerve ganglia (Rosenfeld et al 1983). CGRP resulting from the CALC 1 gene is known as CGRP α . An isoform of CGRP α , CGRP β , is produced from a different gene which shares sequence homology with the CALC1 gene. In human, both these isoforms differ by a single amino acid (O'Connell et al 1993, Steenbergh et al 1985).

ALTERNATE SPLICING OF CALC1 GENE

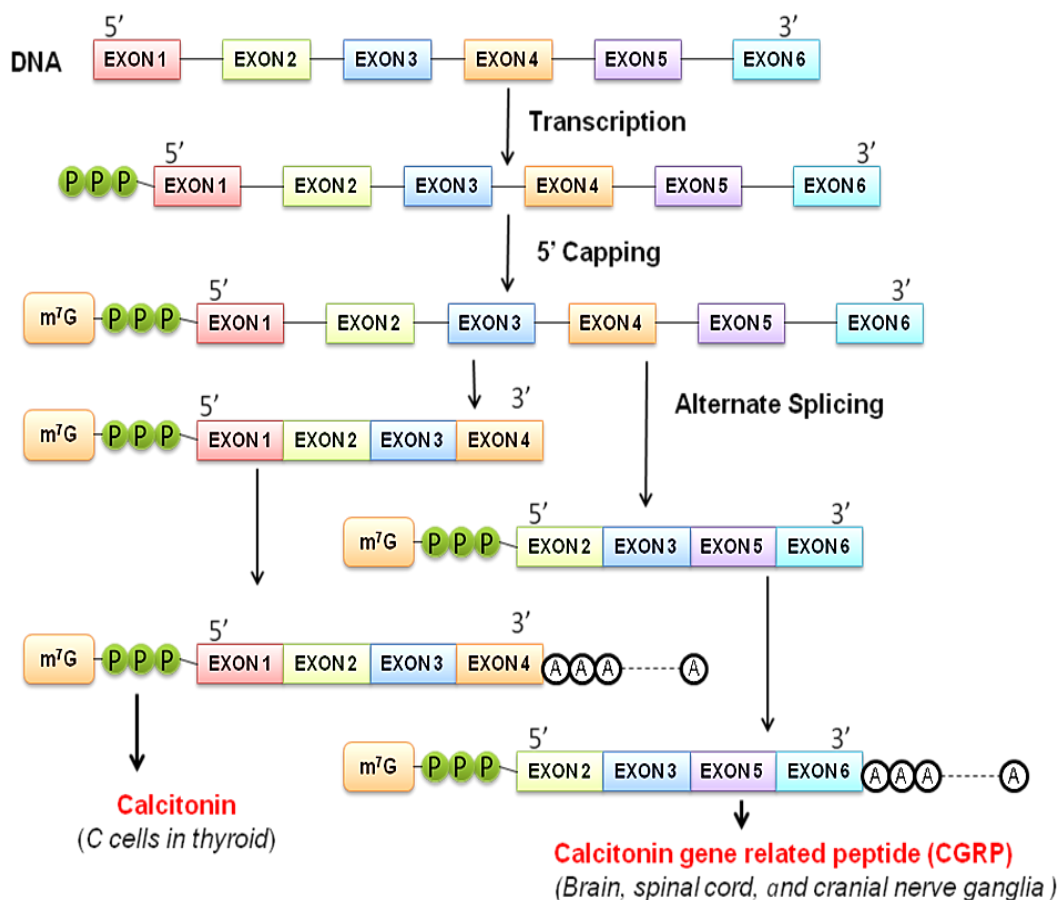


Fig 1.13: Schematic representation of alternate splicing of CALC 1 gene resulting in Calcitonin and Calcitonin gene related peptide (CGRP). Adapted from Nagasaki et. al. 2004. Image previously represented in MSc thesis: RAMPs potential role in regulation of bone mass and skeletal disorders, 2008, University of Sheffield.

Apart from the brain (Mulder et al 1985, Rodrigo et al 1985) and spinal cord, CGRP is also highly expressed in pituitary (Tschopp et al 1985), nerve fibres throughout cardiovascular system (Brain et al 1985), lungs, thyroid, pancreatic islets, gastrointestinal tract (Kraenzlin et al 1985),

urogenital tract (Ghatei et al 1985) and blood vessels. CGRP is a known neurotransmitter and a highly potent vasodilator. In skeletal muscles, CGRP increases cAMP accumulation and inhibits incorporation of glucose into glycogen thus reducing glucose uptake (Beaumont, Pittner et al. 1995).

Like CT, CGRP influences skeletal regulation. CGRP increases mineralisation in osteoblast cultures by inhibiting tumor necrosis factor α (TNF α) and activating interleukin 6 (IL6) and insulin like growth factor -1 (IGF-1) (Michelangeli et al 1989, Millet & Vignery 1997, Sakagami et al 1993, Shih & Bernard 1997). CGRP also induces subtle anti-resorptive effects by hindering osteoclast development (Shih & Bernard 1997). Systemic administration of CGRP induces increase in bone mineral density which is osteoblast mediated (Ballica et al 1999). Furthermore a similar effect on osteoblasts is observed *in vitro*.

1.3.3 Amylin (AMY):

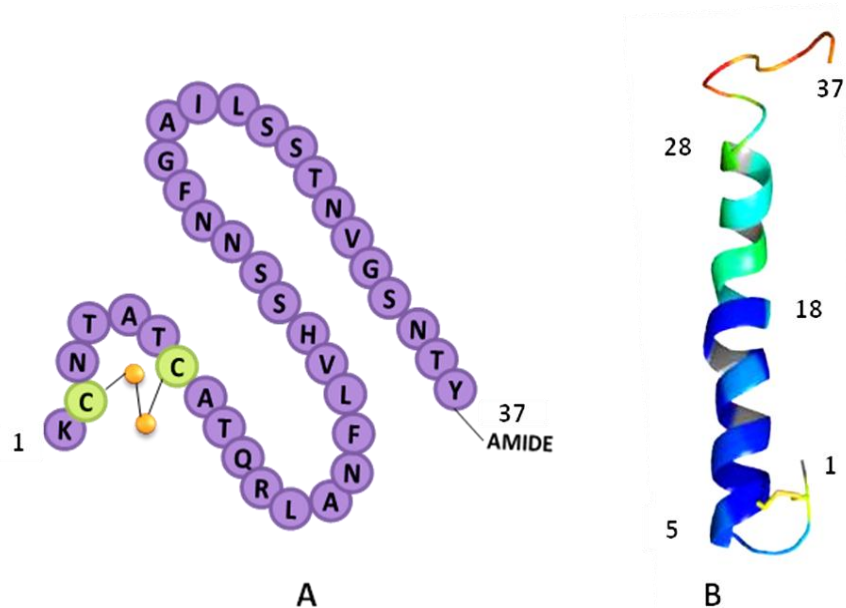


Fig 1.14: Amylin: a) 37 amino acid peptide with amidated C-terminus and a 6 ring structure at N-terminus formed due to disulphide bridge between C2 and C7. b) Micelle bound human AMY structure (Hauschka 1986, Patil et al 2009). Adapted from MSc thesis: RAMPs potential role in regulation of bone mass and skeletal disorders, 2008, University of Sheffield.

Amylin (AMY) or islet amyloid polypeptide (IAPP) was purified and sequenced from amyloid rich pancreas of type 2 diabetes patients, under the name diabetes-associated peptide (DAP). AMY gene, which is the gene for prepro-IAPP, is localized to the locus 12p12.3-p12.1 and shares

regulators with the insulin gene (Bronsky et al 2006, German et al 1992). It is a 37 amino acid peptide and has 46% and 43% sequence similarity with CGRP α and β respectively (Cooper et al 1987) (Fig 1.14).

AMY is principally stored in β cell secretory granules of pancreatic islets and co-secreted with insulin in response to glucose levels (Kanatsuka et al 1989, Lukinius et al 1989, Pieber et al 1993). Amylin, like CGRP, helps insulin in reducing glucose uptake by inhibiting the incorporation of glucose into glycogen in skeletal muscles (Beaumont et al 1995, Leighton & Foot 1990, Pittner et al 1994).

AMY is thought to increase glycogenolysis by cAMP mediated mechanism (Pittner, Beaumont et al. 1995). But a cAMP independent mechanism is also hypothesised, where there is an increase in intracellular glucose 6 - phosphate (G-6-P) which results in reduction of glucose phosphorylation by hexokinase, and retention of transported glucose (Castle et al 1998, Deems et al 1991, Pittner et al 1995). This function requires an intact disulphide bond between Cys2 and Cys7 and the amide at C-terminus (Pittner et al 1994). Both insulin and AMY expression and secretion rise with insulin resistant states, although in hyperglycaemic conditions, AMY secretion exceeds insulin levels (Pieber et al 1993). AMY also reduces food intake, gastric emptying and intestinal transit thereby regulating the rate of appearance of glucose in blood stream after meals (Clementi et al 1996, Lutz et al 1994). It is also expressed in intestine, stomach, lungs and brain (Asai et al 1990, Ferrier et al 1989).

Human AMY, forms stable aggregates called amyloid deposits, which underlines the disease pathogenesis of type 2 diabetes. The fibrillar structures in the deposits have a cytotoxic effect on the insulin producing β cells, causing cell death and eventually islet destruction (de Koning et al 1994). Interestingly rat AMY which differs from human AMY by 6 amino acids, in the 18–29 region; 3 of which are Proline substitutions at positions 25, 28 and 29, does not form fibrils (Green et al 2003, Leffert et al 1989). Owing to this pathogenic effect, human AMY is not used in research.

Another functional similarity between CGRP and AMY is that AMY increases intracellular cAMP levels and stimulates $\text{Na}^+\text{-K}^+$ pumps in skeletal muscle (Clausen 2000, Pittner et al 1994). This $\text{Na}^+\text{-K}^+$ pump stimulation results in Na^+ efflux and K^+ influx in skeletal muscles. Intravenous infusion of AMY in rats resulted in a 16% drop in plasma K^+ , which is inferred to be a result of K^+

uptake by skeletal muscle (Clausen 2000, Vine et al 1998). Results from this study implicate that AMY can be a potential therapeutic target to treat hyperkalemia (Clausen 2000).

The receptor for AMY is a heterodimer of CTR and RAMP1/2/3 (Christopoulos et al 1999, Muff et al 1999, Parameswaran & Spielman 2006). As mentioned earlier, in skeletal system, CTR is expressed in osteoclasts but not in osteoblasts (Findlay & Sexton 2004, Wang et al 2004). This indicates that osteoblasts lack the AMY receptor. AMY administration resulted in hypocalcaemia (Une et al 1993). AMY also reduces basal PTH mediated resorption in calvarial bone of neonatal mice, which is thought to be due to effect of AMY on osteoclasts (Pietschmann et al 1993). Interestingly Jill Cornish in 1995, reported, that along with increase in intracellular cAMP, AMY also stimulated osteoblast proliferation in both *in vivo* and *in vitro* models (Cornish et al 1995). This implicates the presence of a AMY receptor on osteoblasts (Cornish et al 1998b). Since AMY does both, decrease the rate of bone resorption and increase osteoblast proliferation, it becomes a potential candidate for treating local skeletal defects (Ellegaard et al 2010). Another interesting aspect of this combined function is that N-terminal fragment AMY(1-8), retains the osteoblast proliferative function but loses the antiresorptive regulation (Cornish et al 1998b). AMY administration partially reverses osteopenia in ovariectomized (OVX) rats (Horcajada-Molteni et al 2000). Systemic administration of both full length and AMY (1-8) in mice, for 4 weeks, resulted in increased bone volume at nanomolar concentrations (Cornish et al 2000, Cornish et al 1998a). Local administration of AMY (1-8) resulted in increase in bone volume, tibial length, and cortical and trabecular thickness in male mice (Cornish et al 2000). However this report is questioned by a recent research which demonstrated that AMY (1-8) lacks skeletal anabolic activity in bone *in vivo* and *in vitro* (Ellegaard et al 2010)

AMY or IAPP KO mice were generated by Gebre-Medhin's group in 1998 who studied insulin secretion and glucose tolerance in these models (Gebre-Medhin et al 1998). Their study suggested that AMY KO males but not females, had increased body mass, increased insulin response and reduced plasma glucose levels (Gebre-Medhin et al 1998). A similar sex dependent phenotype was observed by Rachel Davey's group in 2006. This group studied the same model for skeletal phenotype and it was observed that AMY KO males had increased femoral length and growth plate height (Davey et al 2006). The KO males also had increased trabecular thickness (TbTh) in the distal femora with no change in net trabecular bone volume (BV) (Davey et al 2006). Although in both the sexes, adult AMY KOs had a net decrease in trabecular BV and increased trabecular number (N) (Davey et al 2006).

1.3.4 Adrenomedullin (AM):

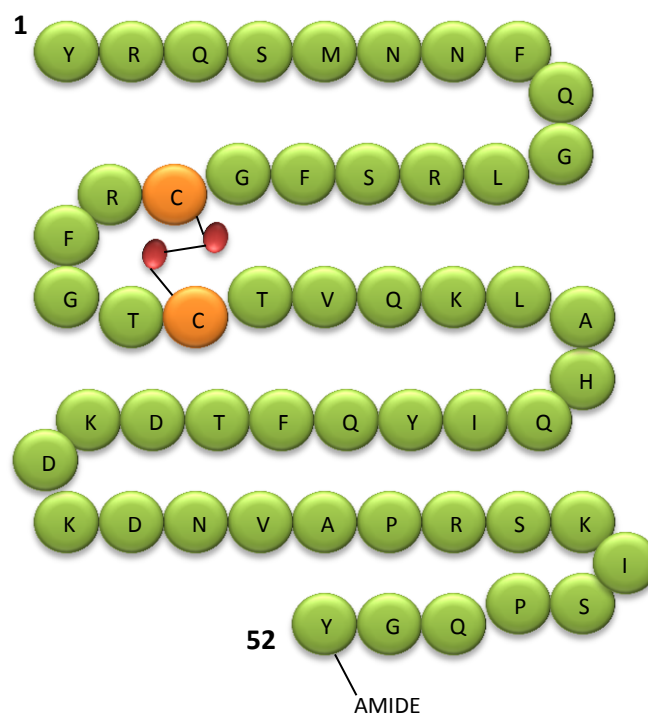


Fig 1.15: Adrenomedullin: a) 52 amino acid peptide with amidated C-terminus and a 6 ring structure due to disulphide bridge between C16 and C21 (Kitamura et al 2002, Mohan & Baylink 1991). Adapted from MSc thesis: RAMPs potential role in regulation of bone mass and skeletal disorders, 2008, University of Sheffield.

Adrenomedullin (AM) was discovered as a hypotensive peptide by monitoring elevated rat platelet cAMP activity and was found abundantly in normal adrenal medulla and in pheochromocytoma tissues arising from adrenal medulla (Kitamura et al 1993a). Two transcripts arise from the AM gene AM1 and AM2 (recently termed as Intermedin) (Bell & McDermott 2008). AM shares a slight sequence homology to both CGRP and AMY, although the 14 amino acid elongations at the amino terminal is not observed in any other member of CT family of peptides (Kitamura et al 2002, Kitamura et al 1993a). In humans, AM is a 52 amino acid peptide with an intramolecular disulphide bond between C16 and C21 and has an amidated Tyrosine at the carboxy terminus (Kitamura et al 1993a) (Fig 1.15).

Mature AM peptide arises from a precursor peptide called the preproadrenomedullin (preproAM) which contains 185 amino acid residues (Kitamura et al 1993b). This preproAM is thought to synthesise both proadrenomedullin (proAM) and a 20 amino acid hypotensive peptide called the "Proadrenomedullin N-terminal 20 peptide (PAMP)" (Kitamura et al 1994, Kitamura et al 1993b). AM gene consists of 4 exons, where the mature AM is encoded in exon 4 and PAMP is encoded

in exon 2 (Okazaki et al 1996). There are 2 activator protein 1 (AP1) binding sites and 8 activator protein 2 (AP2) binding sites upstream of 5' region of exon1. Additionally exon 1 also has consensus sequences for cAMP-regulated enhancer (CRE) (Fink et al 1988, Okazaki et al 1996). It is believed that AP2 mediates transcription activation on protein kinase C and cAMP induction and so AM expression is thought to be regulated by these two signal transduction pathways (Kitamura 2002, Imagawa 1987). Since AM is known to stimulate platelet cAMP, presence of AP2 binding site and presence of CRE sequence suggest a feedback mechanism (Kitamura 2002). Apart from this, AM gene promoter has a nuclear factor kB (Nf-kB) site and the 5' flanking region has TATA, CAAT and CC boxes which are important in the transcriptional regulation of AM gene (Kitamura et al 2002).

AM receptors are heterodimers of CLR and RAMP2/3 (Christopoulos et al 1999, Muff et al 1999, Parameswaran & Spielman 2006). At cellular level, AM induces various signal transduction pathways. Dose dependent increase in intracellular cAMP on AM administration is a well-established phenomenon (Kitamura et al 1993a). Increase in intracellular ionic calcium Ca^{2+} is reported in bovine aortic endothelial cells (Shimekake et al 1995). Apart from cAMP and protein kinase C, AM is also thought to induce nitric oxide (NO) pathway. It has been reported that most of the vasodilator activity of AM results from NO generation in the vasculature (Yang et al 1996). This was confirmed by the counter action of the nitric oxide synthase (NOS) inhibitor and de-endothelialisation (Yang et al 1996). Increase in intracellular Ca^{2+} on AM administration, is hypothesised to activate phospholipase C, which in turn produces NOS and NO (Kitamura et al 2002).

Normal human plasma AM concentration is 1- 10 pmol/l suggesting AM expression in peripheral tissues (Hinson et al 2000). AM is expressed in lung and kidney apart from the adrenal medulla (Kitamura et al 1993a). In the cardiovascular system, AM is synthesised by heart and blood vessels (Kitamura et al 1993b). AM is also expressed in the reproductive organs- uterus, ovary, oviduct, testis, prostate and the epididymis (Cameron & Fleming 1998, Chan et al 2008a, Chan et al 2008b, Li et al 2010, Li et al 2008, Upton et al 1997, Yang et al 1996). In the adrenal medulla, AM is stored in granules and is released by regulatory pathways, whereas in other tissues it is hypothesised to be rapidly synthesized and secreted in blood or act as an autocrine-paracrine regulator (Bean et al 1994, Kitamura et al 2002). In most of the tissues mentioned above, co-expression of AM and its receptors is reported, this emphasises the autocrine-paracrine regulation (Kitamura et al 2002).

AM is considered to be one of the most potent endogenous vasodilators (Cockcroft et al 1997). The importance of AM in normal development of vascular smooth muscles was recently elucidated by Kathleen Caron's group (Caron & Smithies 2001). Extreme hydrops fetalis was observed in E12.5 mice embryos of AM global KO (Fig 1.16). The yolk sac of KO animals was distended with fluids resulting from the massive oedema (Fig 1.16).

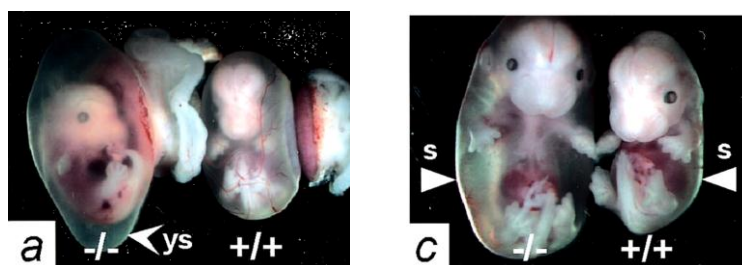


Fig 1.16: Fig 3 from Caron et. al. showing a) the distended yolk sack and c) extreme hydrops fetalis in AM KO(-/-) E12.5 mice embryos. With kind permission from Prof Caron (University of North Carolina) (Caron & Smithies 2001).

Abnormality in the lymphatic vessel development was suggested to be a plausible explanation in the observed phenotype, as lymphatic vessels sprout from veins at E12.5 in mice, which coincides with the onset of hydrops in these animals (Caron & Smithies 2001).

In rat models, intra-cerebroventricular administration of AM induces hypertension, tachycardia and consequent increase and decrease in renal synaptic nerve activity (Kitamura et al 2002, Saita et al 1998). In kidney, AM dilates both afferent and efferent arterioles, reflecting a renal vasodilator and diuretic activity of the peptide (Hirata et al 1995, Kitamura et al 2002).

Effect of AM peptide (full length or AM-(27–52) fragment) stimulation, varies in different tissue preparations. AM inhibits proliferation of vascular smooth muscle cells and induces significant proliferation in primary canine chondrocytes from articular cartilage, and in both primary osteoblasts and in osteoblastic cell lines (Cornish et al 1997, Cornish et al 2003, Kano et al 1996). This mitogenic effect of AM was similar to the effect resulting from insulin like growth factor – 1 (IGF-1) and transforming growth factor- β , which might be of significance (Cornish et al 1997). Two different secondary messengers involved with GPCR activation - cAMP and diacylglycerol. Both these secondary messengers are hypothesised to be responsible for the two contradictory proliferative effects in different tissues (Cornish et al 1997). The effect on osteoblasts, is hypothesised to involve mitogen-activated protein kinase (MAPK) signal transduction in contrast to cAMP activation (Cornish et al 2003). IGF -1, AMY and AM are

thought to share the same molecular mechanism to result the mitogenic effect on osteoblasts (Cornish et al 2004). Local administration of AM resulted in a 2-4 fold increase in bone formation indices and a dose dependent increase of bone area (Cornish et al 1997). Interestingly, unlike AMY, AM does not influence osteoclast mediated bone resorption drawing our attention to the difference in receptor expression in osteoclasts and osteoblasts (Cornish & Reid 2001).

1.4 Receptors of the CT family of peptides

Functional receptors for the CT family of peptide arise from heterodimers formed between family-B (Secretin-like) GPCRs - Calcitonin receptor (CTR) or Calcitonin like receptor (CLR) and accessory proteins called the Receptor activity modifying proteins – RAMPs. The structural and functional aspects of individual proteins are discussed briefly in the following sections.

1.4.1 Calcitonin receptor (CTR) and Calcitonin like receptor (CLR):

Calcitonin receptor was cloned in 1993 by Sexton *et. al.* and was identified to be a 474 aa peptide which acted as a receptor for CT (Sexton et al 1993). The gene for CTR – CALCR is localised to 7q21.3 on the chromosome (Sexton et al 1993). Soon another functional receptor - CLR (461 aa) was discovered which was identified to be a receptor for CGRP, and the gene - CALCRL was found to be localised to 2q32.1 (Fluhmann et al 1995, Gorn et al 1992). Both CTR and CLR have a typical GPCR structure of seven transmembrane domains (TM₁ – TM₇) which are connected by three intracellular loops (IC₁, IC₂ and IC₃) and three extracellular loops (EC₁, EC₂ and EC₃) and have a intracellular carboxy terminus and extracellular amino terminus (Fig 1.17 overleaf) (Harmar 2001). The intracellular C-terminus interacts with GTPase/G protein, a heterotrimer complex formed by α (associated with GTP), β and γ subunits (Harmar 2001). An in-depth GPCR activation discussion is beyond the scope of this review, but briefly - a typical GPCR activation results from a conformational change in GPCR following ligand interaction that dissociates the G $_{\alpha}$ subunit from the G $_{\beta}$ and G $_{\gamma}$ subunit, which further activates downstream intracellular signalling pathways like cAMP or phosphatidylinositol signalling (Harmar 2001). These downstream signal transductions depends on the type of α subunit G $_{\alpha_s}$, G $_{\alpha_i/o}$, G $_{\alpha_q/11}$ and G $_{\alpha_{12/13}}$ (Harmar 2001).

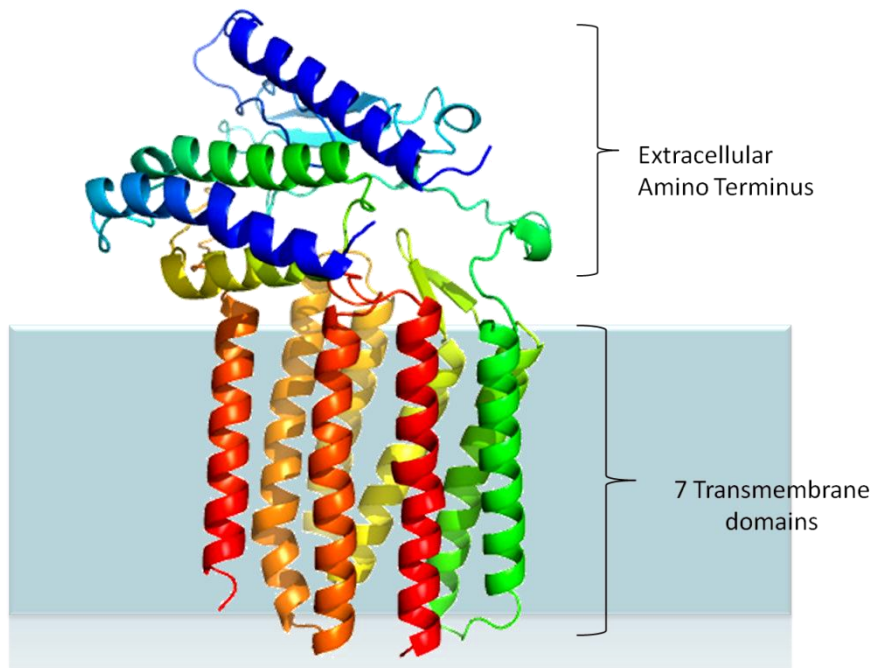


Fig 1.17: Predicted CLR structure showing 7 transmembrane domains and a large extracellular amino terminus that takes part in forming the receptor. Courtesy of Prof. Tim Skerry, Prof Artymiuk, and Dr Richards (University of Sheffield). Previously reported in MSc thesis: RAMPs potential role in regulation of bone mass and skeletal disorders, 2008, University of Sheffield.

Since CTR and CLR were identified to be receptors for CT, which was a known to be a hypocalcaemic peptide, there was an impetus in skeletal research with respect to CTR and CLR. CTR is expressed in osteoclasts but not in osteoblast, whereas CLR is expressed in both osteoclasts and osteoblasts (Findlay & Sexton 2004, Nicholson et al 1986, Wang et al 2004). Homozygous deletion of exon 6 and 7 of CTR results in embryonic lethality whereas haplo-insufficient CTR animals had increased bone formation with no influence on bone resorption (Dacquin et al 2004). To study the effects of CTR deficiency, Davey *et al* generated a viable global CTR KO mice line which had >94% but <100% deletion of CTR, using the Cre-lox system that excised exon 13, 14 and 3'UTR (Davey et al 2008). These KO animals showed protection against induced hypercalcaemia (Davey et al 2008). Global CLR deficiency resulted in embryonic lethality – midgestation death due to extreme hydrops fetalis (Dackor et al 2006).

1.4.2 Receptor Activity Modifying Proteins (RAMPs):

The known receptor pharmacology of CT family of peptides changed dramatically on the discovery of accessory proteins called the receptor-activity-modifying-proteins (RAMPs), by Linda McLatchie and her group in 1998 (McLatchie et al 1998). Until then, functional receptors for CGRP, AM and AMY remained unidentified. Rhodopsin-like receptors (RDC1), CLR and G10D (GPCR 182) were amongst the hypothesised receptors for CGRP and AM (Fluhmann et al 1995, Kapas et al 1995, McLatchie et al 1998). McLatchie cloned the first RAMP protein by expression-cloning strategy using SK-N-MC cell complementary DNA library. *Xenopus* oocytes were injected with pools of RNA, complementary to the cDNA libraries, and were then screened for cAMP response on CGRP stimulation. Following repeated screening and subdivision, a cDNA encoding 148 amino acids peptide was isolated, which was called RAMP1. Interestingly RAMP1 like CLR, on its own did not result in a cAMP response to CGRP. It was later determined that both RAMP1 and CLR form a heterodimer which forms a functional receptor for CGRP and that RAMP1 was also obligatory for CLR trafficking to the cell surface (McLatchie et al 1998). RAMP1 protein sequence has a single transmembrane domain towards the carboxy terminal and a long amino terminal signal sequence (Fig 1.18).

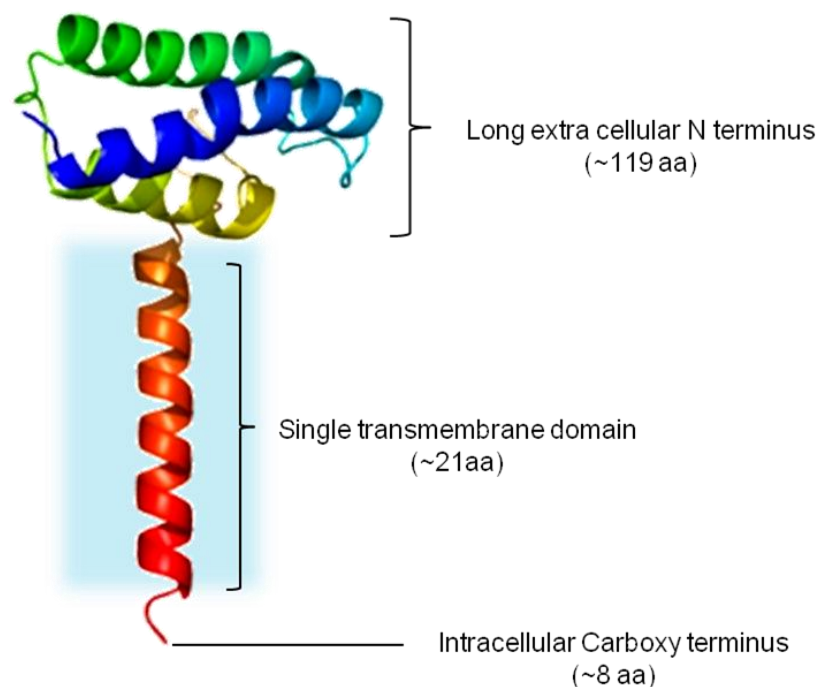


Fig 1.18: Proposed RAMP1 structure by Prof. Artymuk, Prof Skerry and Dr Richards (University of Sheffield). This proposed structure exhibits a large extracellular domain, followed by a single transmembrane domain and a short intracellular carboxy terminus. Previously published in MSc thesis: RAMPs potential role in regulation of bone mass and skeletal disorders, 2008, University of Sheffield.

The long N-terminal sequence determines the ligand specificity of CLR by actively forming a part of the receptor or by altering CLR structure in such a way that it forms a functional receptor (Fraser et al 1999). The transmembrane domain is thought to stabilize the heterodimer complex, and C-terminus interacts with intracellular proteins like G proteins (Fraser et al 1999). RAMP1 also altered terminal glycosylation of CLR and this mature form of CLR had a higher molecular weight, and was responsible for its CGRP receptor phenotype (McLatchie et al 1998).

Subsequently, two isoforms- RAMP2 (175 amino acid peptide) and RAMP3 (148 amino acid peptide) which were 31% identical to RAMP1 were cloned and isolated (McLatchie et al 1998). It was observed that all the RAMP isoforms have evolutionarily conserved 4 Cys residues (Cys40, Cys57, Cys72 and Cys104), but RAMP1 and RAMP3 have an extra pair of Cys residues which result in disulphide bonds at 1-5, 2-4 and 3-6 (McLatchie et al 1998, Steiner et al 2003). These disulphide bonds not only determine the protein structures, but are also indispensable in RAMP-GPCR heterodimer processing (Steiner et al 2003). There are N-glycosylation sites in RAMP2 and RAMP3 which are not present in RAMP1 (Flahaut et al 2003, McLatchie et al 1998). RAMP3 has a PDZ binding motif at its C terminus which is absent in RAMP1 and RAMP2 (Bomberger et al 2005, Pietschmann et al 1993). This PDZ motif plays an important role in receptor trafficking as it interacts with the Na⁺/H⁺ exchanger regulatory factor-1 (NHERF-1), which inhibits internalisation of receptor complex post ligand stimulation by tethering it to the actin cytoskeleton (Bomberger et al 2005). Both RAMP1 and RAMP3 form stable homodimers. Although not necessary for RAMP-GPCR interaction, these homodimers may dynamically regulate the availability of RAMP isoforms for receptor interaction (Sexton et al 2001).

RAMP2 and RAMP3 effectively transport CLR to the cell surface similar to RAMP1 (McLatchie et al 1998). Both RAMP2 and RAMP3 when co-transfected, one at a time with CLR, showed response to AM but not to CGRP, and again this response was not noticed when RAMP2, RAMP3 or CLR were expressed on their own (McLatchie et al 1998). RAMP2 and RAMP3 do not glycosylate their partner CLR when presented at cell surface which might be the reason why CLR loses its CGRP receptor phenotype (McLatchie et al 1998). Interestingly, it was observed that the CLR/RAMP complex are formed in the Golgi which are then processed, transported to cell membrane, recycled and degraded in their heterodimer form (McLatchie et al 1998). Internalisation of the CLR-RAMP complex is implicated to be β -arrestin and dymin dependent and degradation is thought to be due to arrestin interaction (Hilaret et al 2001a, Hilaret et al 2001b). Most certainly it was correctly hypothesised that CLR/RAMP3 complex escapes this degradation

and is recycled due to the PDZ domain present in RAMP3 mentioned earlier (Bomberger et al 2005).

It was discovered that RAMPs not only form heterodimer with CLR but also with CTR, although CTR does not require RAMPs for its cell surface transport. In 1999, Christopoulos *et. al.* reported 3 functional receptors for AMY arising from interaction between CTR and RAMPs (Christopoulos et al 1999, Muff et al 1999). Using radio-ligand binding and cAMP assays, it was discovered three functional receptors for AMY are formed due to dimerization of CTR with each of the RAMP isoforms. Hence it was discovered that RAMPs not only chaperone partner GPCRs to cell surface but also give ligand specificity to the receptors. Receptor interactions of RAMPs with CTR and CLR are summarised below in Fig 1.19.

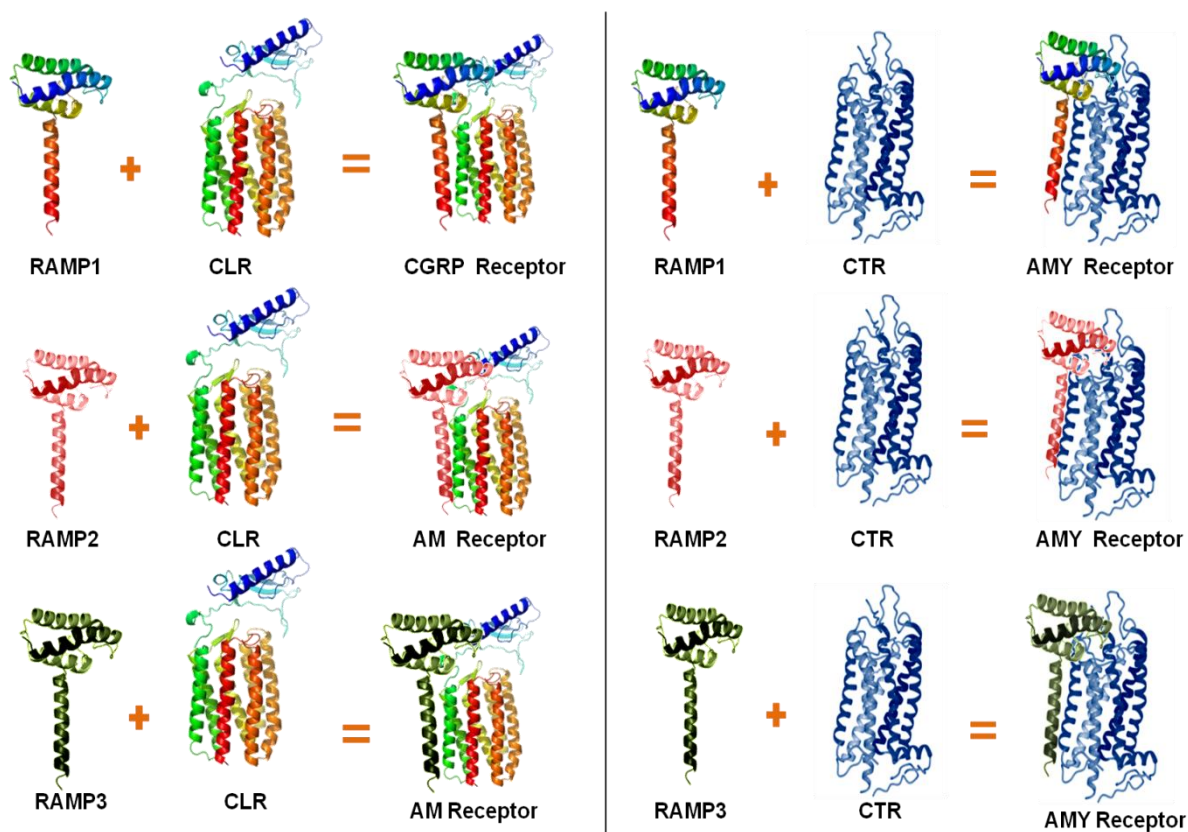


Fig 1.19: A schematic representation of RAMP interactions with CLR (left) and CTR (right) which result in different functional receptors for the CT family peptides. Adapted from Parameswaran *et. al.* 2006. Image created using proposed protein structures of RAMP1 and CLR by Prof Artymiuk, Prof Skerry and Dr Richards for University of Sheffield.

A number of RAMP-GPCR interactions have been identified to date. So far, it has been reported that RAMPs interact with GPCR class II receptors: PTH receptor 1 and 2 (RAMP2 and 3), glucagon receptor (RAMP3) and vasointestinal peptide/pituitary adenylate cyclase-activating peptide 1 (VIP/VPAC1) receptor (RAMP1 and 3) (Christopoulos et al 2003), and with a GPCR class III receptor - calcium sensing receptor (CaSR) (RAMP1 and 3) (Bouschet et al 2005, Christopoulos et al 2003, Foord et al 2005). This wide range of RAMP – GPCR interaction is no surprise considering the tissue expression profile of RAMPs. A schematic representation mRNA expression of RAMP isoforms in a few different tissues is shown below in Fig 1.20 (McLatchie et al 1998, Parameswaran & Spielman 2006).

Tissue	RAMP1	RAMP2	RAMP3
Brain	++	-	++
Heart	+++++	++++	++++
Kidney	-	+	+++
Liver	+	-	++
Lungs	-	++++	++++
Pancreas	+++++	+	++++
Skeletal muscle	+++++	+++	++++
Uterus	+	+++++	+++
Bladder	+	+	+
GTI	+	+	+

Fig 1.20: A schematic representation of mRNA expression in different tissues. (+) indicate the level of expression and (-) indicates very low or undetected expression. Fig adapted from Parameswaran et. al. 2006 and is based on the information published by McLatchie in 1998.

Transgenic mice models revealed the functional characteristics of RAMP isoforms. In an attempt to study vasodilatory regulation of CGRP through CLR/RAMP1 receptor, global RAMP1 KO mice were generated. These RAMP1 deficient mice exhibited hypertension without having an effect on heart rate (HR) and had increased serum pro-inflammatory cytokines (TNF- α , IFN- γ , IL-12, and IL-6) levels and increased serum CGRP levels post lipopolysaccharide (LPS) administration. This suggested a potential regulation of blood pressure and inflammatory response by CGRP through CLR/RAMP1 receptor (Tsujikawa et al 2007).

RAMP2 transgenic animals show an altogether different phenotype. Global RAMP2 KO animals are embryonically lethal and die mid-gestation due to Hydrops fetalis, a phenotype similar to one observed in AM and CLR deficient mice (Caron & Smithies 2001, Dackor et al 2006, Ichikawa-Shindo et al 2008) (Fig 1.21). This suggests that a severe phenotype results from the loss of AM signalling.

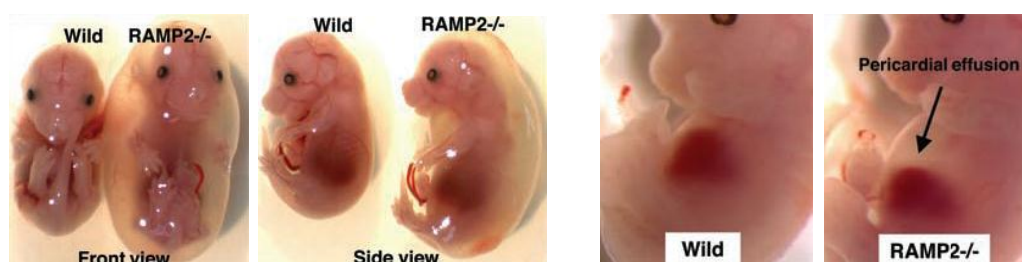


Fig 1.21: Images of RAMP2 KO neonatal mice displaying increased fluids in the body due to hydrops fetalis (first two panels) and pericardial effusion (last two panels) similar to AM KO mice. With kind permission from Prof Shindo Takayuki (Ichikawa-Shindo et al 2008).

RAMP2 heterozygous mice are viable but have reduced litter size and increased serum calcium and prolactin levels (Dackor et al 2007). On the other hand, overexpression of RAMP2 in smooth muscles of mice showed increase in AM sensitivity. These transgenic mice had enhanced reduction of blood pressure on AM administration (Tam et al 2006).

RAMP3 KO animals are born healthy with no known abnormalities up to 6 months. After 6 months, RAMP3 KO animals did not show normal physiological age related gain in weight when compared wild-type RAMP3 animals (Dackor et al 2007). Loss of RAMP3 neither affects blood pressure nor fertility of the animal (Dackor et al 2007).

Embryonic lethality exhibited by RAMP2 KOs, severely affected blood pressure in RAMP1 KO animals and unaffected physiology of RAMP3 KO animals demonstrates that RAMP isoforms have significantly different functions and that they play an important role in pathological and physiological regulation.

1.5 Importance of investigating receptors for CT family of peptides

To date, there is compelling evidence that all the members of the CT family of peptide either have an anti-resorptive or an anabolic effect on the skeleton. CT and AMY inhibit osteoclast mediated resorption by either affecting the cell adhesion to bone surface or by inhibiting maturation and AMY, AM and CGRP induce osteoblast proliferation (Fig 1.22).

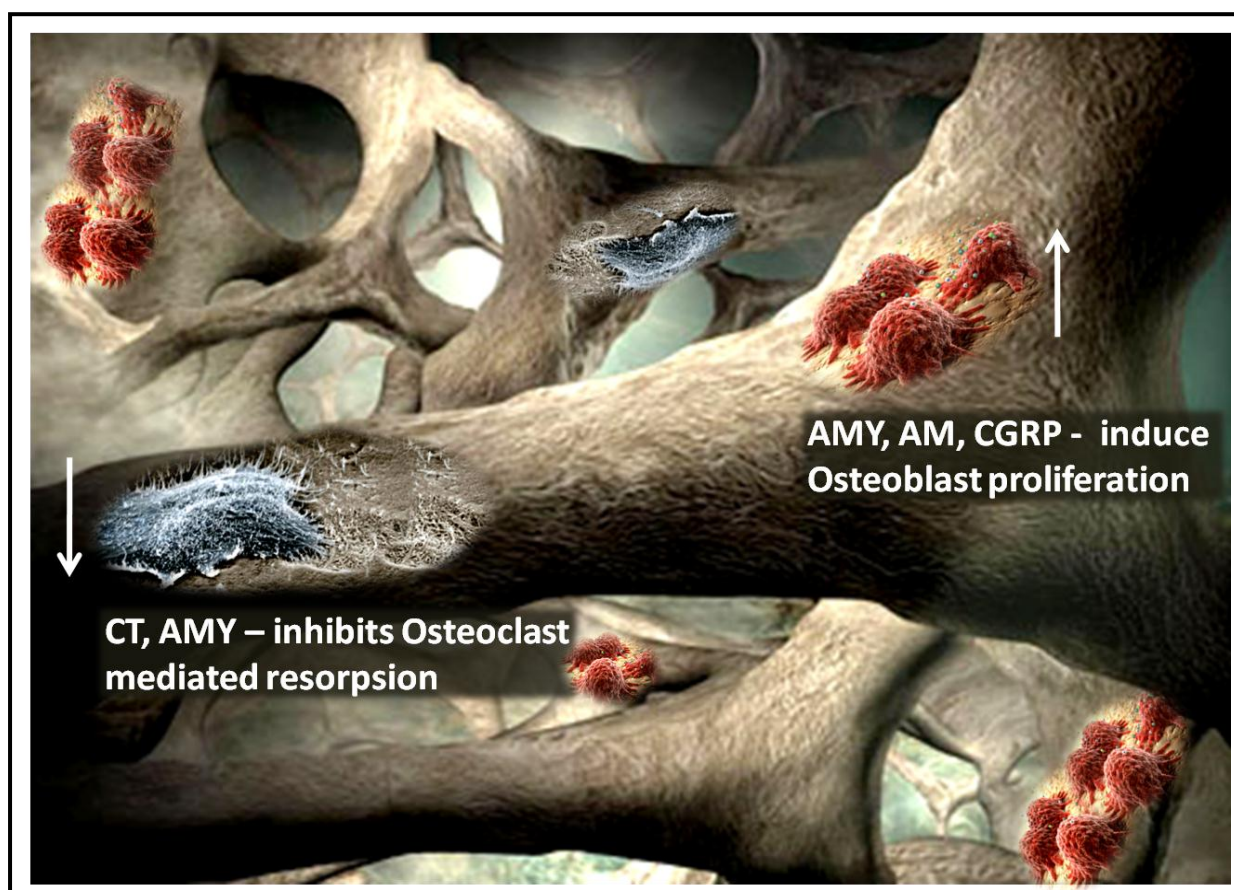


Fig 1.22: Overall anabolic effect of CT family of peptides on skeleton. CT and AMY inhibit the activity of the bone resorbing cells – osteoclasts (blue) and AM, AMY and CGRP induce proliferation of bone forming cells – osteoblasts (red). Diagram created using images kindly provided by Tim Arnett (Osteoclast) and Karin LaPudala (bone matrix created for Eveo).

Since all the CT family peptides have such profound effect on the skeleton by inducing bone formation, silencing these peptides or their receptors, was thought to result in reduction in bone density. However, knockout experiments show opposite phenotypes. CT/ CGRP deficient models have increased bone density (Hoff et al 2002) (Fig 1.23 overleaf).

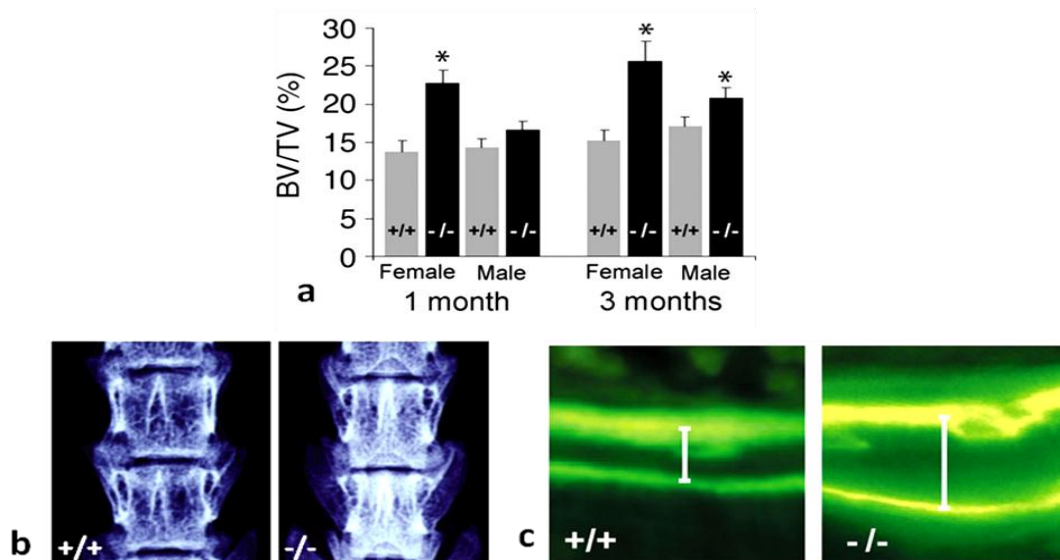


Fig 1.23: Results published by Hoff et al. showing **a)** Increase in bone volume to tissue volume ratio (BV/TV) in 1 and 3 month old male and female CT/CGRP KO mice, **b)** Increased bone density in vertebrae of CT/CGRP KO animals and **c)** Increased growth in CT/CGRP KO animals (Hoff et al 2002). Figures reproduced with permission.

This unexpected phenotype encouraged similar research in the receptors for these peptides. We studied the transgenic RAMP2 +/- and RAMP3 -/- animals created by Dr Caron for Adrenomedullin research. Our pilot research showed interesting data that suggested that both these isoforms had skeletal regulation (Fig 1.24). Further investigation confirmed the hypothesis that RAMPs 2 and 3 but not RAMP1 play an important role in regulating skeletal phenotype (Pacharne 2008).

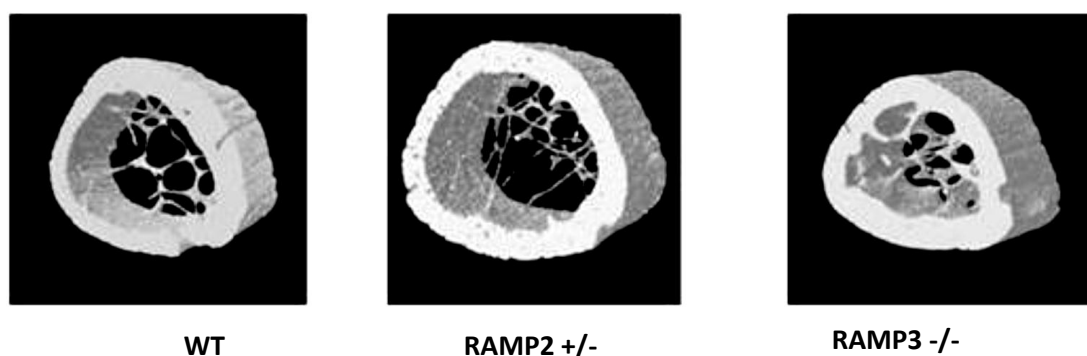


Fig 1.24: MicroCT analysis of femurs from WT, RAMP2 +/- and RAMP3 KO animals. RAMP2 animals had increase lumen & cortical. RAMP3 on the other hand and a two fold increase in bone density and increased trabecular and cortical thickness. Previously reported in MSc thesis: RAMPs potential role in regulation of bone mass and skeletal disorders, 2008, University of Sheffield.

Although it is certain that RAMP2 and RAMP3 influence skeletal regulation, the exact mechanism through which this occurs remains unknown. Furthermore, molecular mechanisms pertaining to RAMP and their ligands (CT family of peptides) are also not yet clearly understood. For, e.g., – the mechanisms by which AMY influences osteoblast proliferation, in spite of absence of AMY receptors on these cells, and whether is there a compensatory mechanism between RAMP isoforms, definitely require further investigation. Considering the complicated receptor pharmacology of RAMPs it is very important to clearly identify the specific receptor combination and the resulting downstream mechanisms that regulate the skeletal phenotype.

1.6 Hypothesis, aim and objectives

In light of evidence from our pilot study that RAMP2 and RAMP3 but not RAMP1 regulate skeletal development in mice, and that alteration in the RAMP2 gene result in a decrease in the bone volume, whereas silencing the RAMP3 gene completely, resulted in increase in the bone volume, **we hypothesized that *silencing the gene for receptor activity modifying protein 3 -RAMP3 in 129/SvEv mice, results in an advanced skeletal phenotype.***

With an aim to test whether RAMP3 is a potential therapeutic for treating skeletal disorders, we tested our hypothesis by determining:

- The skeletal phenotype of WT and RAMP3 KO 129/SvEv mice at different ages by microCT, dynamic histomorphometry and histology.
- The skeletal response to ovariectomy in both WT and RAMP3 KO 129/SvEv mice by microCT analysis.
- The primary calvarial osteoblast differentiation profile of WT and RAMP3 KO by mineralizing fibroblast-colony-forming assay.
- The expression of RAMPs 1/2 and 3 mRNA and protein expression during primary osteoblast differentiation in WT and RAMP3 KO osteoblasts.
- The effect of RAMP expression in primary WT and RAMP3 KO osteoblasts on Amylin, Adrenomedullin, PTH and Wnt and DKK stimulation.

Further, given the evidence that osteoblasts do not express the traditional calcitonin receptor (CTR) that forms a functional receptor for Amylin, but still respond to Amylin stimulation, **we hypothesized that osteoblasts either express a novel Amylin receptor, or have a transcription variant of the CTR.**

To test this hypothesis, we determined:

- The complete sequence of the CTR transcript variant expressed in WT 129/SvEv differentiated primary osteoblast by PCR technique using over lapping primers.
- The expression of CTR protein in both WT and RAMP3 KO differentiating primary osteoblast.

Chapter 2: Accelerated skeletal development in RAMP3 KO mice.

2.1 Introduction

Literature evidence to date supports the notion that RAMP1 plays an important role in the regulating blood pressure and inflammatory responses induced by Calcitonin gene related peptide (CGRP) through the CLR/RAMP1 receptor and that RAMP2 plays a key role in regulating vascularization induced by Adrenomedullin (AM) through the CLR/RAMP2 receptor (Caron & Smithies 2001, Tsujikawa et al 2007). The involvement of RAMPs in skeletal regulation was not elucidated until 2011 where our pilot study showed that RAMP2 heterozygous 129/SvEv mice had increased bone volume, reduced bone mineral density and under developed vertebra with increased inter-vertebral spaces (Kadmiel et al 2011). Furthermore, even with very few number of animals (n=3 each genotype), this pilot study also gave us encouraging evidence of RAMP3 KO mice having increased bone cortical thickness and bone mineral density.

As discussed earlier, RAMP3 forms one of the obligatory functional receptors for Amylin (AMY) and Adrenomedullin (AM) with GPCRs CTR and CLR respectively, and is associated with PTH receptor 2 and Calcium sensing receptor (CaSR) (Bouschet et al 2005, Christopoulos et al 2003, Christopoulos et al 1999, McLatchie et al 1998). RAMP3 chaperons the partner GPCRs to the cell membrane and most importantly, determines the ligand specificity of the partner GPCR (Bouschet et al 2005, McLatchie et al 1998). All the four ligands; AMY, AM, PTH and Calcium are potent skeletal regulators, and have both anabolic and anti-resorptive effect on the skeleton (discussed previously in Introduction, Section 1.3). With the need to develop anabolic therapeutic targets, it is important to determine whether RAMP3 regulates the anabolic effect of these ligands on the skeleton.

The skeletal phenotypes resulting from alteration of the ligands AMY and AM are discussed in detail earlier. Global deletions of GPCRs CTR, CLR, PTHR, CaSR are embryonically lethal. CTR KO-Cre skeletal model mentioned earlier show protection against induced hypercalcaemia (Davey et al 2008). Parathyroid cell specific CaSR KO mice show severe impediment of skeletal development, and heterozygous mice show reduced cortical and trabecular bone volume and thickness (Chang et al 2008). PTHR2 KO mice have not yet been studied with respect to skeletal phenotype.

The WT and RAMP3 KO 129/SvEv mice used in our work were generated from the animals obtained from Dr Kathleen Caron's research group in North Carolina USA, who have successfully established stable 129/SvEv transgenic embryonic stem (ES) cell models for CT peptides and

RAMPs (Dackor et al 2007). The 129/SvEv mouse strain is one of the most stable strains used for gene targeting and gene trap approaches to manipulate embryonic stem (ES) cells (Auerbach et al 2000). A study of establishment and chimera analysis of ES cells, suggests that C56BL/6-derived ES cell lines have a greater tendency to lose their ability to colonize the germ-line than 129-derived ES cell lines making 129/SvEv ES cells more suitable for generating transgenic models (Auerbach et al 2000).

The wild type skeletal phenotype of the 129/SvEv strain is not yet well characterised. However to date, this strain has been used to study various skeletal phenotype with respect to G protein α -subunit gene *Gnai3*, Wnt1-inducible signalling protein 3, undifferentiated mesenchymal stem cell (MSC) specific Sox 5/6/9 etc. (Akiyama et al 2002, Kutz et al 2005, Plummer et al 2012). A comparative study of homeobox genes *Hox a1/b1/b2* on pure 129SvEv background and 129SvEv-C57BL/6J hybrid background showed no difference in the skeletal phenotype on account of the difference in strains (Buckley 2002)

This chapter focuses on the characterisation of the skeletal phenotype of WT and RAMP3 KO 129/SvEv mice to test the hypothesis, **that silencing the gene for receptor activity modifying protein 3 -RAMP3 in 129/SvEv mice, results in an advanced skeletal phenotype.**

This was done by determining,

- Bone morphometric parameters of WT and RAMP3 KO 129/SvEv mice at post natal day 5, 4 weeks and 8 weeks of age by microCT analysis.
- The bone apposition rate of young adult mice at the age of 8 weeks, by dynamic histomorphometry.
- The differences in growth plate and number of osteoblasts and osteoclasts in the long bones of young adult mice at the age of 8 weeks, by histology.

2.2 Methods and materials

2.2.1 Animals:

RAMP2 heterozygous (Het) and RAMP3 knockout (KO) mouse on 129/SvEv strain were obtained from Dr Kathleen Caron (Department of Cell and Molecular Physiology, University of North Carolina).

RAMP3 KO mice were generated by Dr Caron's group on the 129/SvEv background mouse strain. Briefly, 129S6/SvEv-TC-1 embryonic stem cells were electroporated with linearized targeting vectors that excised exon 2 and 3 along with the stop codon and 3' untranslated region of RAMP3 gene, and inserted a Neomycin cassette by homologous recombination (Dackor et al 2007). Similarly, RAMP2 Het animals were also generated by Dr Caron's group on 129/SvEv mouse strain by targeting RAMP2 promoter, 5'-untranslated region translation start site, and exons 1 and 2 (Dackor et al 2007).

Wild-type (WT) 129/SVEV mice were generated and colonies were established in the University of Sheffield (Department of Animal and Plant science) from the founder RAMP2 heterozygous (Het) and RAMP3 knockout (KO) mice obtained from Dr Kathleen Caron. First generation (F1) of mice obtained from RAMP3 KO and RAMP2 Het crossing resulted in the progeny that comprised half R3 +/- R2 +/+ genotype progeny and half R3 +/- R2 +/- genotype progeny. The R3 +/- R2 +/+ male and females were then crossed to obtain the second generation (F2) that comprised half RAMP3 +/- RAMP2 +/+, one quarter RAMP3 -/-RAMP2+/+ and one quarter RAMP3 +/+ RAMP2 +/+ populations. The RAMP3 +/+ RAMP2 +/+ animals were the WT 129/SVEV animals that were used to generate the colony. Figure 2.1 illustrates this breeding plan.

Both the WT and RAMP3 KO breeding colonies in Sheffield were then backcrossed for nine generations to obtain congenic colonies (Simpson et al 1997). Animals from the 11th generation were used to breed animals for the experiments.



FIRST GENERATION

RAMP 2 \ RAMP 3	+/+	+/+	+/-	+/-
+/+	+/+ +/+	+/+ +/+	+/- +/-	+/- +/-
+/+	+/+ +/+	+/+ +/+	+/- +/-	+/- +/-
+/-	+/+ +/+	+/+ +/+	+/- +/-	+/- +/-
+/-	+/+ +/+	+/+ +/+	+/- +/-	+/- +/-



SECOND GENERATION

RAMP 3 \ RAMP 3	+	-
+	+/+	+/-
-	+/-	-/-

RAMP 2 \ RAMP 2	+	+
+	+/+	+/+
+	+/+	+/+



THIRD GENERATION – FOUNDER 129/SVEV WT PAIR

Fig 2.1: A schematic representation on WT 129/SvEv mice generation from RAMP3 KO and RAMP2 Het mice.

2.2.2 Genotyping:

2.2.2.i Genomic DNA extraction: Genomic DNA was extracted from the mouse ear-clips using the DNeasy Blood & Tissue Kit (Qiagen®). Bench protocol, provided by the manufacturer, for the kit was used for DNA extraction. Briefly, the tissues sample was lysed with Proteinase K at 56°C. The genomic DNA was then separated in the DNeasy™ Mini spin columns. It was then washed and eluted in elution buffer.

Buffer solutions used (in order) per ear-clip are as follows:

ATL buffer:	180µl
Proteinase K:	20µl
AL buffer + Absolute ethanol (1:1):	400µl each
AW1 and 2 (wash) buffer:	500µl each
AE (elution) buffer:	200µl each

2.2.2.ii PCR for genotyping: Identical PCR reaction mix and PCR conditions were used to genotype RAMP3 KO and RAMP2 Het mice. GoTaq® DNA Polymerase kit (Promega® Cooperation, Madison, USA) was used to determine WT/RAMP3 genotype. Each 25µl reaction mix contained 5µl of 5X Green GoTaq® reaction buffer (final conc. 1x), dNTP at a final concentration of 0.2mM (10mM each dNTP stock), MgCl₂ at a final concentration of 1.5mM (25mM each stock) and 2.5 units GoTaq® DNA Polymerase. Proportions for PCR mix are mentioned below along with the respective PCR conditions. PCR primer sequences are summarised in table 3.1 overleaf. PCR amplicons were visualized by electrophoresis in 1.5% Agarose gel (Sigma®) prepared in Tris-base-EDTA buffer containing 0.5ug/ml ethidium bromide.

PCR reaction mix:

5X Green GoTaq® reaction buffer:	5µl
MgCl ₂ :	0.75µl
dNTP mix :	0.5µl
Forward Primer:	1.25µl
Reverse primer:	1.25µl
GoTaq® DNA Polymerase:	0.5µl
Genomic DNA:	1-2µg
Nuclease free water:	upto 25µl

Thermocycler conditions:

- 1) Hold 95°C Enter
- 2) 95°C – 1.30min
- 3) 95°C – 30sec
- 4) 58°C - 30 sec (BOTH RAMP2/3)
- 5) 72°C – 1.30min
(Repeated 3-5, 30 cycles)
- 6) 72°C - 3min
- 7) Hold at 4°C

Table 2.1: RAMP3 and WT genotyping primer sequences

<i>Genotype</i>	<i>Primer ID</i>	<i>Primer Sequence</i>	<i>T_m</i>	<i>Amplicon</i>
<i>RAMP3 KO</i>	<i>Mr3.1</i>	5' GTGCTCAAGGGTTCTGTCTG 3'	59.4 ⁰ C	650bps (WT) 800bps(R3)
	<i>Mr3.10</i>	5' GACCTGGTTCATCTCTGGCTCC 3'	64.0 ⁰ C	
	<i>Neo60</i>	5' GCTTCCTCTTGCAAACCACA 3'	57.9 ⁰ C	
<i>RAMP2 Het</i>	<i>Mr2.45F</i>	5' TCTGTCTGGATGCTGCCTTGC 3'	61.8 ⁰ C	900bps (WT) 675bps (R2)
	<i>Mr2.46R</i>	5' GAAGTCAGGCAGTCAGGGTTG 3'	61.8 ⁰ C	
	<i>NeoOligo</i>	5' GACGAGTTCTTCTGAGGGGA 3'	59.4 ⁰ C	

2.2.3 Animal housing and humane culling:

Animals were culled humanely in accordance to home office regulations Schedule 1, Animals (Scientific Procedures) Act 1986 at required ages. Neonatal mice were culled by anaesthetic overdose of Pentobarbital (solution for euthanasia - JM Loveridge Ltd, UK) (dosage 0.1ml per 100grms). Adult mice were culled by cervical dislocation following anaesthesia.

2.2.4 Age groups:

Sex-matched WT and RAMP3 KO mice were used to study skeletal phenotype at three different ages: Post natal day 5 (PND5), 4 weeks and 8 weeks.

Intervention (Chapter3): Skeletal phenotype in response to ovariectomy (OVX) was studied in female WT and RAMP3 KO mice at the age of 12 weeks (baseline group/OVX conducted) and 16 weeks (sham and OVX group)

2.2.5 Treatments:

2.2.5.i Dual Calcein labelling treatment:

Eight week old WT and RAMP3 mice were injected with Calcein (100mg/kg) twice, one week apart before culling. The first label was administered in the 7th week and the second in the 8th week. Animals were culled the day after the second labelling while monitoring the animal's health during the course of the entire treatment.

2.2.6 Specimen preparation:

Culled animals were dissected immediately after death in clean conditions with sterile instruments following weight and tail length measurements. First the skin was removed, then viscera and soft tissues. Organs of interest (brain and uterus) were either snap-frozen in liquid nitrogen or fixed in 10% buffered formalin. Intact skeleton was stripped off soft tissue before separating long bones and vertebrae.

Skeletons of post natal day 5 animals were treated with Alcian blue and Alizarin red stains. (Procedure detailed below in Section 3.2.7).

Femora and tibiae of adult mice were dissected and fixed appropriately depending on whether they were being processed for histology, dynamic histomorphometry or microcomputer tomography. Third and fourth caudal vertebrae were then dissected, separated and fixed for microCT analysis.

2.2.7 Alcian Blue / Alzarin Red staining:

Skeletal staining was performed to study the extent of ossification in neonatal skeleton. Post natal day 5 skeletons were stained with Alcian Blue / Alzarin Red. The right hind limb was separated before staining and fixed in 70% ethanol for MicroCT analysis. The rest of the skeleton was used for staining. Briefly, the staining procedure consists of the following steps.

Dehydration: First the pups were fixed and dehydrated in 90% ethanol for 7 days, with changes of ethanol on the 3rd and the 5th day.

Alcian Blue staining: After dehydration, pups were immersed in freshly prepared Alcian blue solution (appendix) for 3 days at room temperature to stain the collagen present in the skeleton.

Rehydration: Following the Alcian staining, pups were rehydrated sequentially with:

- i) 70% ethanol for 4-6 hrs with ethanol change at 2-3 hours,
- ii) Followed by 40 % ethanol rehydration for 4-6 hrs with ethanol change at 2-3 hours.
- iii) Followed by 15 % ethanol rehydration for 4-6 hrs with ethanol change at 2-3 hours.
- iv) Finally - water for 3 days (or until the pups sank).

KOH treatment: After rehydration, pups were treated with freshly prepared 1% KOH for 1-2 days at room temperature until the soft tissue holding the skeleton together, became transparent. Samples were carefully monitored as there is a risk of skeleton falling apart if this treatment continues for a long period.

Alzarin Red staining: Skeletons were then immersed in freshly prepared Alzarin Red S solution (appendix), until the bone was stained purple (2-3 days). Care was taken to change the Alzarin Red S solution every day to enhance the staining.

KOH treatment: Skeletons were again treated with freshly prepared 1% KOH solution for 2-3 hours at room temperature. Subsequently the KOH solution was replaced and the 2-3 hour incubation was repeated. At least 3 repetitions of this step was carried out to obtain adequate transparency. Skeletons were photographed and stored in 100% glycerol.

2.2.8 Weights and Tail lengths:

Whole body weight: All animals were weighed, on portable digital weighing scales immediately post-culling.

Uterus weight: The uteri of female mice of each group (baseline, sham and ovariectomy) were weighed immediately post-culling on a digital weighing scale.

Tail lengths were measured from the base of the tail to the apex (Fig. 2.2) using GuoGen MC 01120028 digital callipers.

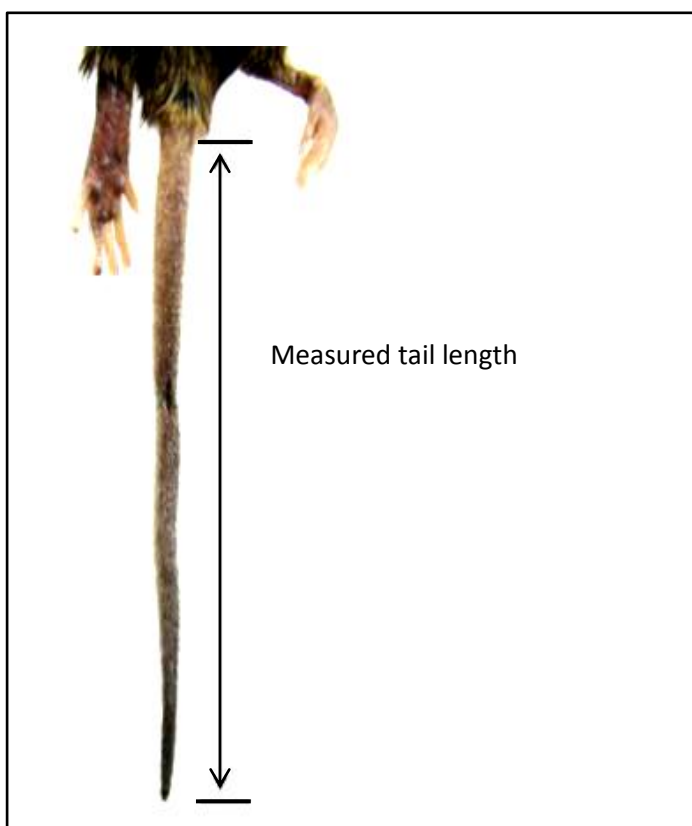


Fig 2.2i: A schematic representation of measured region of the mouse tail.

Femur and tibial lengths in post natal day 5 pups were measured from the photographs of Alizarin red and Alcian blue stained skeletons using the software ImageJ™. Briefly, every skeleton was photographed with a scale alongside it. Known distance on the photographed scale, was used to incorporate a digital scale in the software, which then gave measurement of each bone when a line was drawn over the bone in each image (Fig2.2ii)

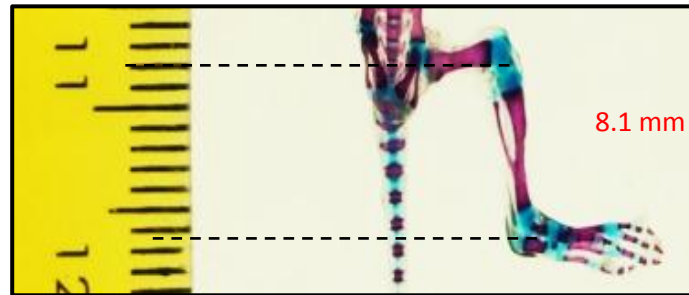


Fig 2.2ii: Representation of method used to measure tibia length in postnatal day 5 mice.

2.2.9 Micro Computed Tomography (MicroCT) Analysis:

Computed tomography is amongst the most useful techniques used to explore details of 3D structures in a non-destructive way. This cutting edge technology generates cross sections of 3D structures, using an X-ray source. These cross sections can then be interpolated in different planes to study different internal structures. Micro Computed Tomography (MicroCT) is the same system but has resolution in the order of few micrometres.

MicroCT analysis was carried out in the SkyScan 1172 Desktop X-ray microCT system (SkyScan N.V. Belgium) featuring a high performance resolution of 10 Megapixel (Mp). It has an X-ray source which is 20-100 kV for less than 5 μ m spot size and 20- 80 kV for less than 8 μ m spot size which is accompanied with a 12 bit cooled X-ray camera. Spatial resolutions of either 4.5 or 17 μ m were used depending on specimen and area to be scanned.

2.2.9.i Specimen processing:

For each animal, both left and right femur, tibiae and caudal were fixed in 70% ethanol immediately after dissection. Bone specimens of animals that were labelled with Calcein green were stored in dark at room temperature.

2.2.9.ii MicroCT scanning:

Each bone was wrapped in cellophane wrap and then mounted in plastic container which was placed in the microCT scanner. The position of the bone in the machine was adjusted and confirmed so that the required region of the bone is scanned appropriately. A 0.5mm aluminium filter and medium-pixel camera was specifically used for adult mouse bones. Care was taken to remove the Aluminium filter for neonatal bones.

Whole long bones were scanned at lower resolution: 17.5 μ m with an averaging 2 frame rotation to reduce the size of the scanned file without affecting the analysis, whereas trabecular and cortical regions were scanned at a higher resolution: 4.5 μ m with 360° rotation to ensure detailed imaging and analysis.

2.2.9.iii Reconstruction:

Scanned image datasets were then reconstructed in NRecon® (Version 1.4.1.0) in order to convert raw microCT images into greyscale cross-section images. The greyscale image datasets

generated for individual bone was then analysed by interpolating region of interests (ROIs) in CT Analyser Version 1.7.0.5 software. The threshold levels for reconstruction and for analysis for different bones are summarized in the following table (Table 2.2).

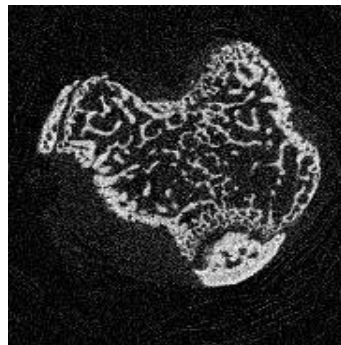
Table 2.2: Summary of the resolutions and threshold levels used for reconstruction and 3D analysis for different areas of different bones

Age and Bone	Resolution (μm)	Reconstruction threshold (Arbitrary value)	3D analysis threshold (Arbitrary value)
PND 5 whole Femur /Tibia	10 μm	0.16	100 - 255
Adult Whole Femur / Tibia / vertebra	17.5 μm	0.16	100 - 255
Adult Femur/ Tibia trabecular	4.5 μm	0.16	80 - 255
Adult Femur/Tibia cortical	4.5 μm	0.16	90 - 255

2.2.9.iv Regions of Interest (ROIs) for analysis:

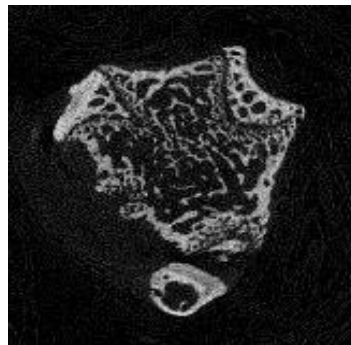
For whole bone analysis, ROIs were drawn around the whole bone in each cross section throughout the dataset, whereas for cortical and trabecular analysis, only a defined section of the whole bone was selected. This was done by setting an offset and height (1.0mm) for the region of the bone to be analysed. The offset was from a particular reference point, which is usually a physical marker of the bone. Reference point- physical markers used for tibia and femur trabecular and cortical analysis are represented overleaf in Fig 2.3 and Table 2.3 summarises the offset and height values used specific bone.

Proximal Tibia: trabecular &
cortical analysis



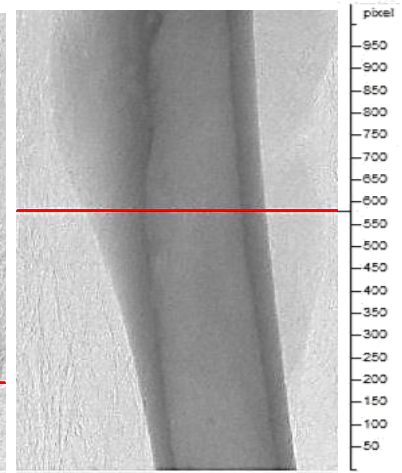
10 slices below growth plate

Distal femur:
Trabecular analysis



20 slices above growth plate

Femoral shaft:
cortical analysis



Slice from which third
trochanter reduces rapidly

Fig 2.3: Summary of the physical markers used to determine regions of interest for cortical and trabecular analysis. Each top panel (x-ray image generated by microCT) is the area of bone scanned at 4.5 μm resolution with a 0.5mm aluminium filter and medium camera. Bottom panels (black) represent the bone cross section generated on reconstruction of microCT scans, at the marked levels (red lines) in top panels.

Table 2.3: Summary of the physical markers and ROI settings used to measure high resolution bone area by MicroCT.

Bone Analysis	Reference point	Offset value	ROI height
Femur trabecular	20 slices above growth plate (distal end)	46 (0.2mm)	229 (1.00mm)
Tibia trabecular and cortical	10 slices below growth plate (proximal end)	-275	229 (1.00mm)
Femur cortical	Slice - third Trochanter reduces rapidly	-687 (3.0mm)	229 (1.00mm)

Once the specific area of the bone was defined using the reference point, trabecular and cortical area in the cross-sections was marked. Figures 2.4 (A) and (B) represent the ROIs drawn in the first and last slices of the dataset to analyse tibia trabecular and cortical ROI selection. Analysis was carried out by interpolating the ROIs of the entire dataset.

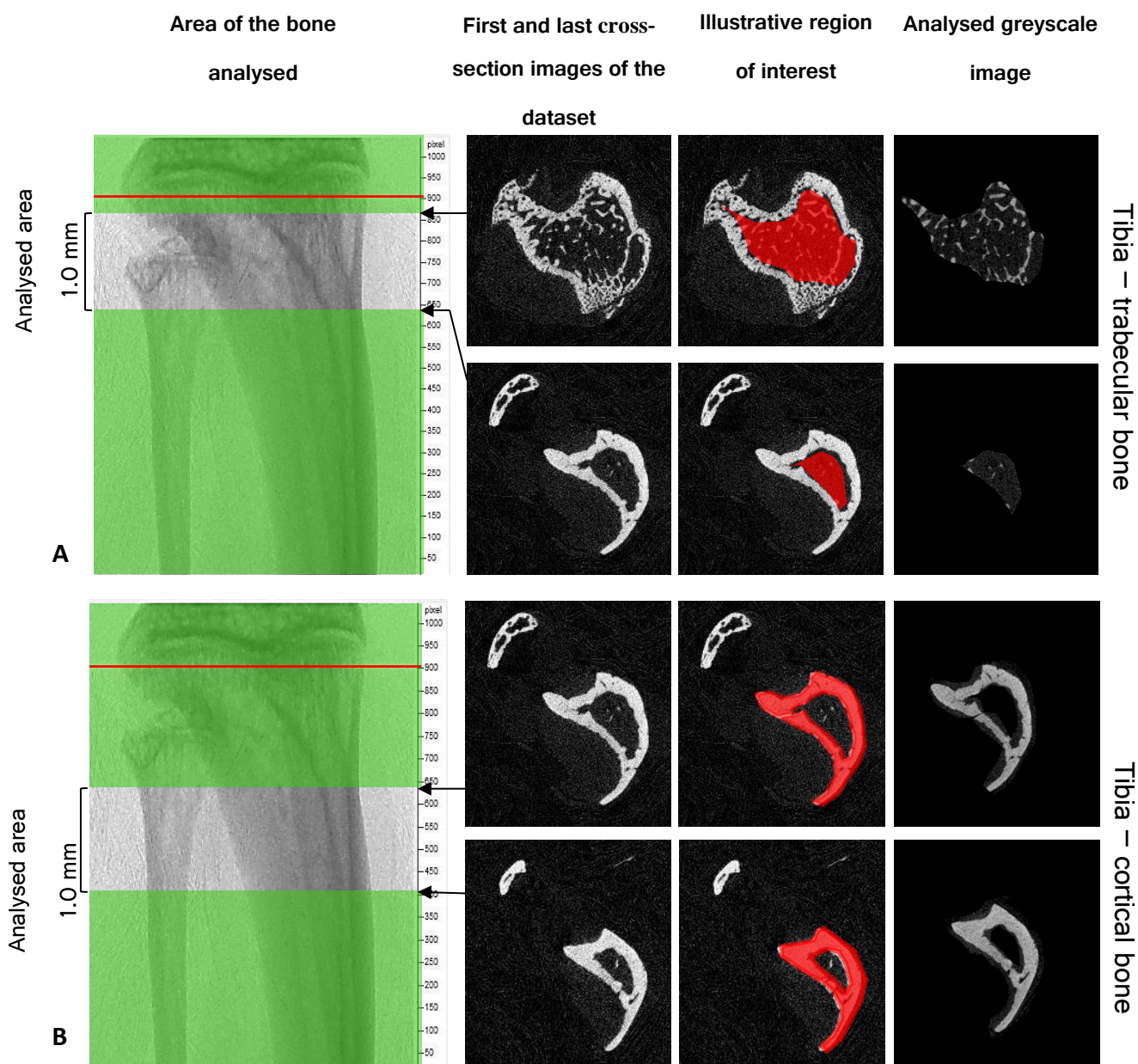


Fig. 2.4: Representative image depicting the microCT region of interests used to analyse tibia trabecular (A) and cortical (B) bone morphometric parameters. On the left, the green –grey panel show the part of bone scanned at 4.5µm resolution with a medium camera. The Red lines at the proximal end of the tibia show the physical marker used to decide the 1.0mm ROIs for analysis. Black and grey panels (both A and B): the first and the last cross section of each analysed area of the bone (left), the ROI marked in red for each section (middle) and the final analysis grey-scale image(right).

Similarly, Fig 2.5 (A) and (B) represent the ROIs drawn in the first and last slices of the dataset to analyse femur trabecular and cortical ROI selection. Analyses were then carried out by interpolating the ROIs of the entire dataset.

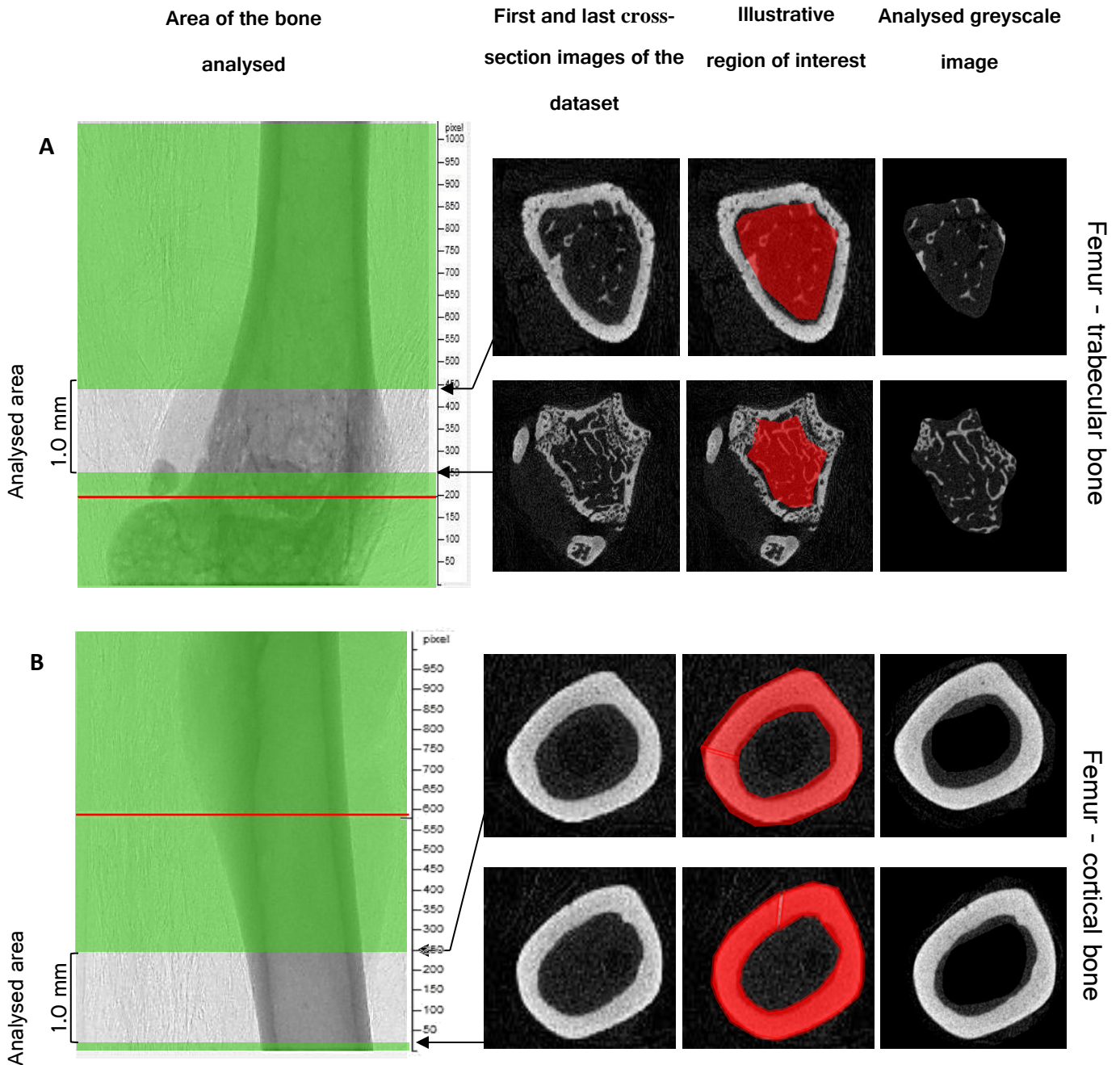


Fig 2.5: Representative image depicting the microCT region of interests used to analyse femur trabecular (A) and cortical (B) bone morphometric parameters. On the left, the green –grey panel show the part of bone scanned at $4.5\mu\text{m}$ resolution with a medium camera. The Red lines at the proximal end of the tibia show the physical marker used to decide the 1.0mm ROIs for analysis. Black and grey panels (both A and B): the first and the last cross section of each analysed area of the bone (left), the ROI marked in red for each section (middle) and the final analysis grey-scale image (right).

2.2.9.v Morphometric measures:

Quantification of bone morphometric parameters was automatically calculated for individual bone scan by the algorithms in the analysis software: CT Analyser (Version 1.7.0.5). The marked ROIs were uploaded in the batch analyser called the BATMAN, an allied tool of microCT Analyser. A predefined greyscale threshold was used for whole bone, trabecular and cortical bone. (summarised previously – Table 2.3). The BATMAN also corrects artificial speckles in the scans.

The typical order of tests run on every batch was as follows:

- i) Thresholding (defines grey scale of the scans),
- ii) Despeckle (set to remove white speckles/ artefacts within the 3D space with volume “less than” 10 voxels in the ROI) and,
- iii) 3D analysis (calculates the morphometric parameters)

2.2.10 Results:

2.2.10.i Quantitative results:

MicroCT analysis results were quantified to determine bone morphometric parameters such as whole, cortical and trabecular bone volume (BV), tissue volume (TV), bone volume to tissue volume ratio (BV/TV), cortical and trabecular thickness (Th), trabecular separation (Sp), trabecular number (N) and bone pattern factor (Pf). These parameters were generated through the BATMAN.

2.2.10.ii Qualitative results: 3D rendering:

Qualitative analysis of the bone structure was carried out by rendering realistic 3D models of the scanned bone datasets in Golden software's Voxler 1.1. Models were also generated on the CTVol the generic rendering software of the microCT machine Skyscan1172. Since the Volxer software had enhanced algorithms to create clip-planes and reduced opacity densitometric models, this software was preferred over the CTVol. Models were generated for whole bones, trabecular regions of femur and tibia and cortical regions of femur and tibia. Briefly, the ROI dataset was uploaded in the Voxler software. The 3D model was generated by using graphical output 'VolRender'. Models were represented in either grayscale or in rainbow colour gradient (densitometric model) with different opacities. For adult bones, densitometric models were generated at '0.1408450704' opacity. Transverse and longitudinal sections of a whole bone

model were obtained using an additional algorithm called 'ClipPlane'. Figure 2.6 is a screenshot of the software whilst rendering a femur model with the 'VolRender' and 'ClipPlane' tools.

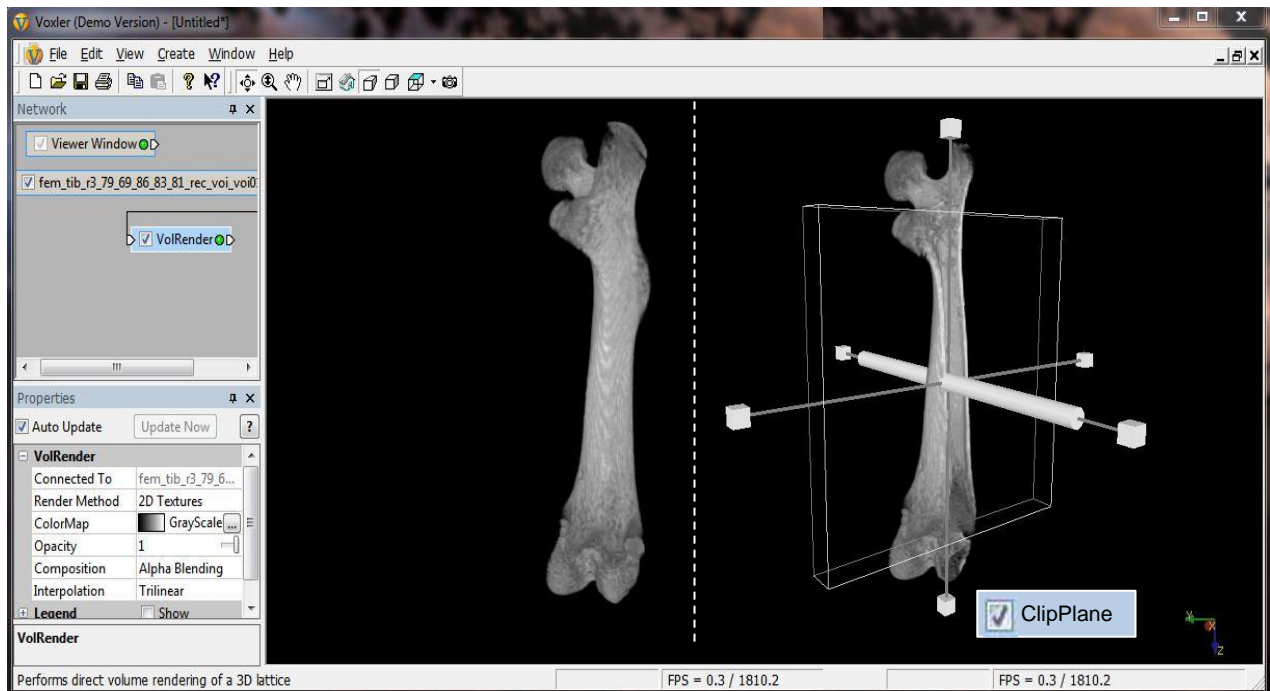


Fig 2.6: A screen shot of the software Voxler™ whilst rendering a femur model. The 'VolRender' generates the 3D model as seen on left. The additional graphical tool 'ClipPlane' allows the user to cut through the model and view the inner structure of the model as seen in on the right.

2.2.11 Dynamic histomorphometry: Dual Calcein labelling:

Eight week old WT (n=5) and RAMP3 KO (n=6) mice were studied to determine bone apposition rate by dynamic histomorphometry. Quantification of the bone apposition rate was done using the OsteoMeasure™ system (OsteoMetrics®) on a upright microscope with fluorescence (Leitz DMRB from Leica with Sony DCX-950P 3CCD digital camera).

Specimen processing: Post microCT, left tibiae (fixed in 70% ethanol), were embedded in resin. Resin embedding and sectioning of bone was carried out by the staff members of bone analysis laboratory, core facility (University of Sheffield). Six longitudinal mid sections, 3µm apart, were analysed per specimen for each experiment.

Endocortical dual calcein labels were measured on both lateral and medial sides of the tibia. An off-set of 250µm is left immediately after the growth plate on the lateral side. Six areas of interests 250µm x 250µm totalling 3mm, were then measured on each side of the bone. (Fig. 2.7).

Calculations: Bone apposition rate was calculated using the following formula:

$$\text{Bone apposition rate} = \text{Inter label thickness (In.L.Th)} / \text{time between labels (day)}.$$

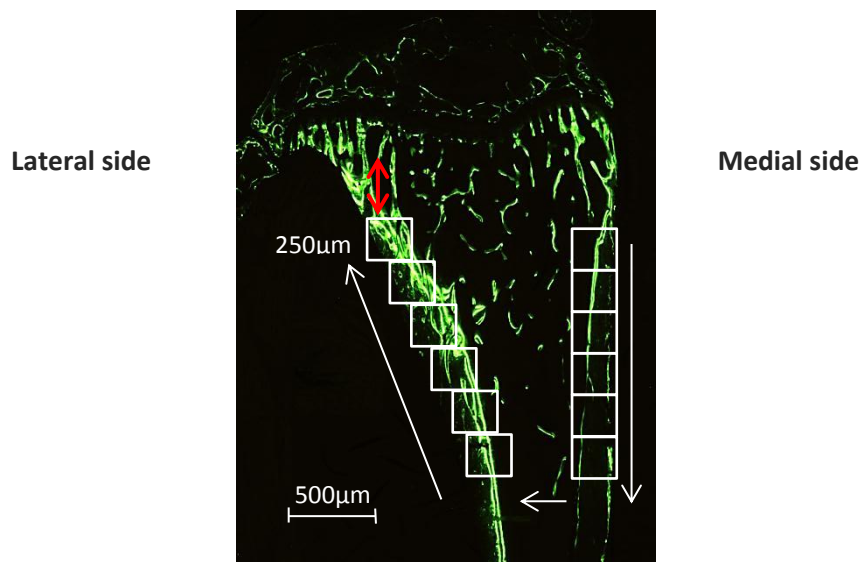


Fig 2.7: Representative image depicting the method used to measure the endocortical dual Calcein labels in Tibia. An offset of 250µm (red double headed arrow) is left after the growth plate. The first 500µm field of interest starts after the offset. In total, 6 x 500µm areas (3mm) were measured on each, lateral and medial side. Arrows mark the direct of measurement (successive field of interests). WT n=5 and RAMP3 KO n=6. Image generated from protocol provided by Darren Laith (Bone analysis laboratory, core facility, University of Sheffield, 2013).

2.2.12 Histology: Haematoxylin and Eosin (H&E) staining and Tartrate-resistant acid phosphatase (TRAP) stained sections:

Eight week old WT and RAMP3 KO (n=6 each genotype) mice were used to carry out histological analysis.

2.2.12.i Specimen processing: Right tibiae were fixed in ice cold 4%paraformaldehyde. Bones were then decalcified and embedded in paraffin wax blocks before sectioning and staining (bone analysis laboratory, core facility - University of Sheffield). Briefly bones were decalcified in EDTA at room temperature for 4 weeks using 10-20 times volume of EDTA to volume of bone. The EDTA solution was changed each week. On completion of decalcification process, bones were embedded in paraffin wax and sectioned. Out of the six longitudinal mid sections 3µm apart, three alternate sections were used for haematoxylin & eosin staining and the other three sections were used for TRAP staining (bone analysis laboratory, core facility - University of Sheffield).

2.2.12.ii Haematoxylin and Eosin (H&E) stained sections were used to study the bone versus cartilage differences. These sections were also used to determine the differences between the ratio of proliferative to hypertrophic zones in WT and RAMP3 KO samples. **Tartrate-resistant acid phosphatase (TRAP)** stained sections were used to determine the number of osteoblast and osteoclasts and the osteoblast-osteoclast coverage. These measurements were performed on both the endocortical and the trabecular surface of tibia. **Virtual sections:** H&E and TRAP sections were scanned in the ScanScope® (Aperio®) scanner. All histological analyses were then carried out manually on virtual sections in ImageScope™ (Aperio®), the e-slide viewing software.

2.2.12.iii Virtual analysis:

Trabecular area: Scanned images of the H&E and TRAP sections were uploaded in the ImageScope™ software. Trabecular area in the section was measured by marking a ~2.0mm distance in the marrow cavity from the midpoint of the growth-plate. The trabecular region in the section of the bone was manually marked in an overlapping virtual layer. The software then simultaneously calculates the number of trabecular area manually drawn and the area of each trabecular unit (see Fig. 2.8). The average thickness of the trabecular units was calculated by the formula:

Trabecular thickness: Total area of all the trabecular units / Number of trabecular units.

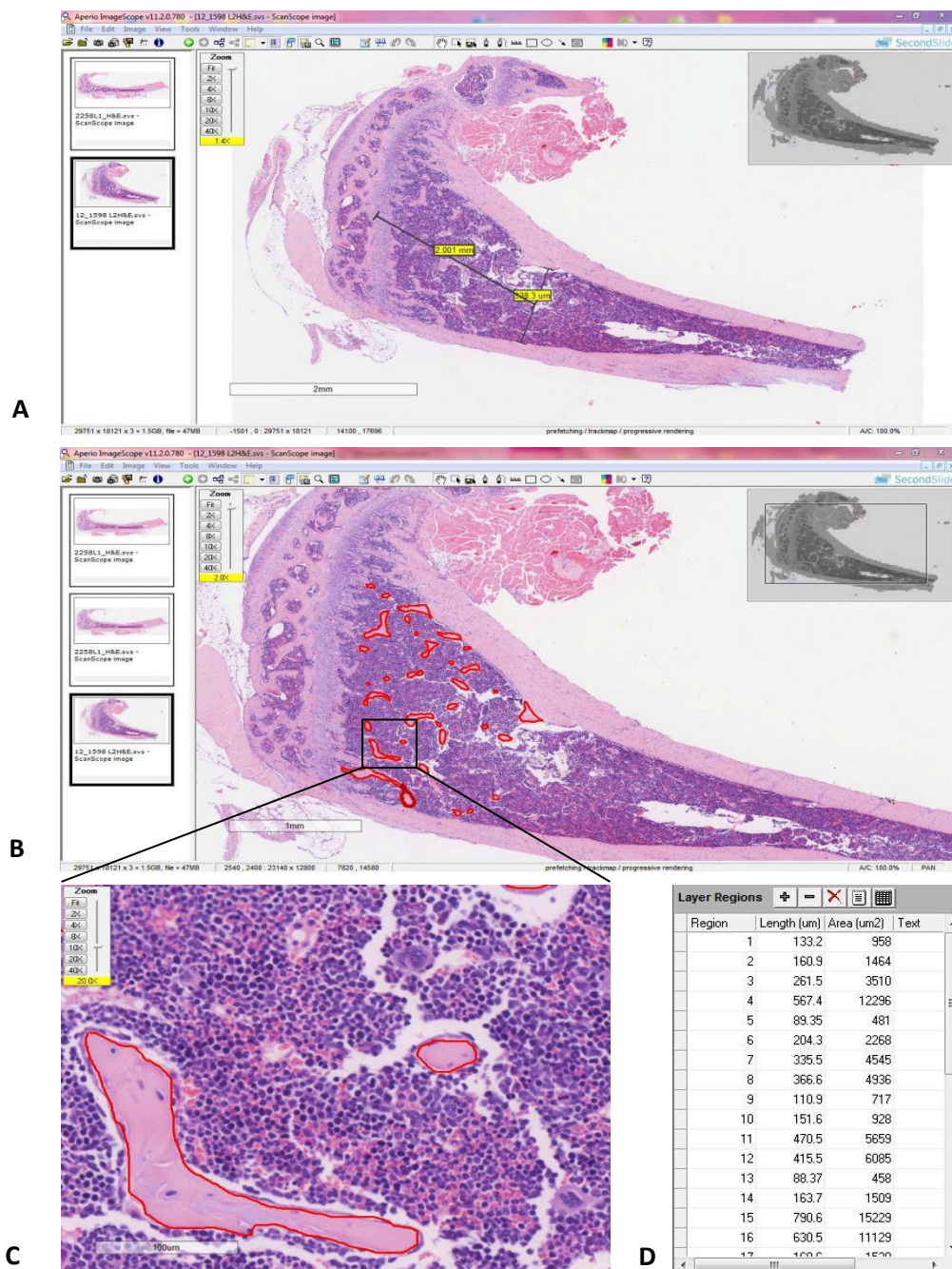


Fig 2.8: Representative image depicting the method used to quantify the trabecular area in e-slide using ImageScope®. The top panel is a screen-capture showing the marking of 2.0mm distance from the growth (A). Middle panel (B) shows the region of interests drawn around the trabecular units. Panel C, is a zoomed image showing the accuracy of trabecular marking. The measurements of manually marked regions generated by the software is shown in panel D. n=6 each group.

2.2.12.iv Osteoblast and osteoclast numbers: Number of Osteoclasts (N.Ob.), osteoblast covered bone surface (Ob.S.), number of osteoclasts (N.Oc.) and osteoclast covered bone surface (Oc.S.) were determined on both the endocortical surface of the bone and the trabecular bone. Cells were manually marked on the viewing software. Active osteoblasts were quantified. They were differentiated from the bone lining cells by their cuboidal shape. Osteoclasts with 3 or more nuclei were quantified. Similar to the dual calcein labels, the endocortical measurements were done in 12, 300 μ m x 300 μ m regions: 6 on the medial and 6 on the lateral side. Trabecular measurements were done in a 750 μ m x 750 μ m area. An offset of 300 μ m from the growth-plate was maintained in both endocortical and trabecular measurement (Fig. 2.9).

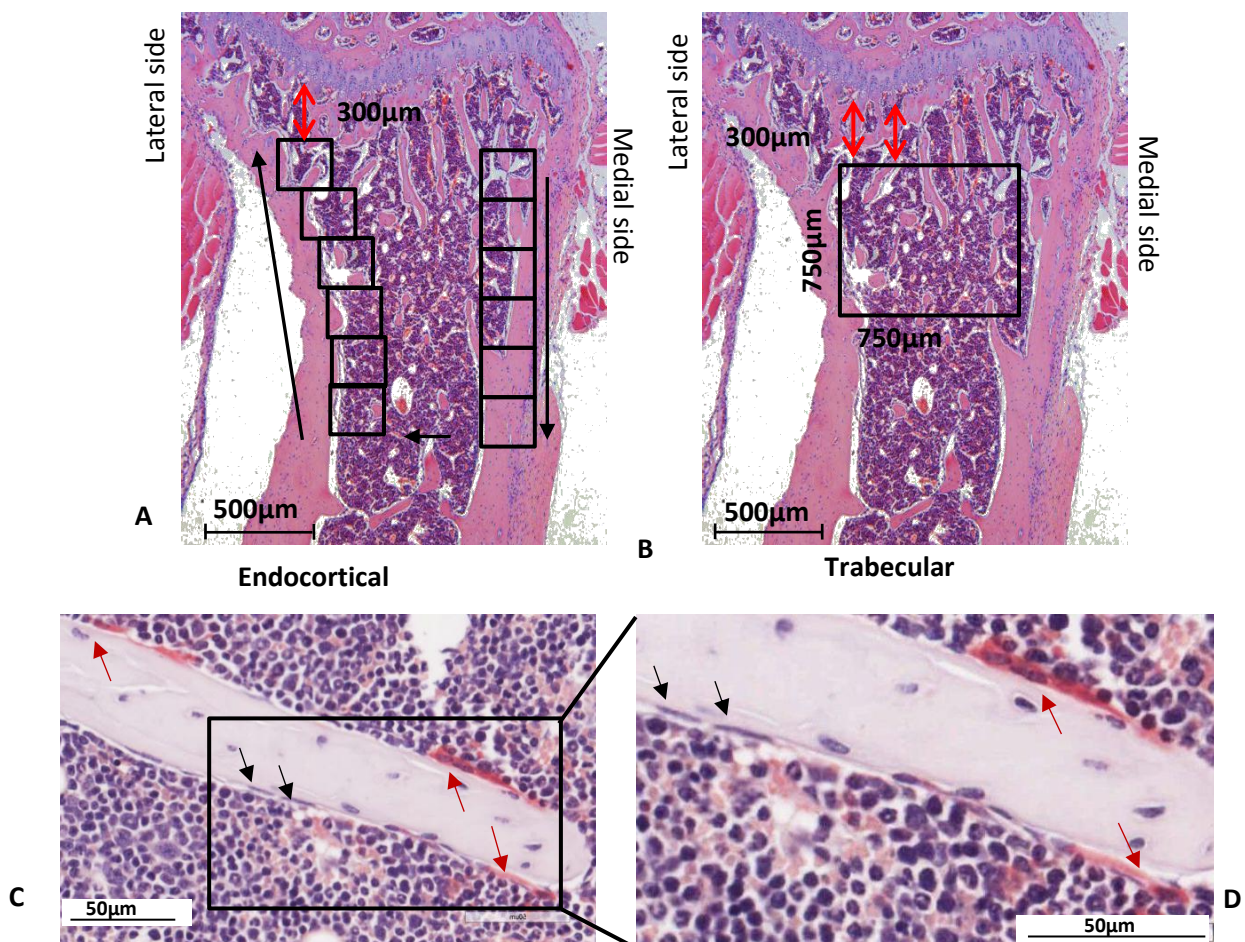


Fig 2.9: Panels A and B representative images depicting the method used to measure the endocortical (A) and trabecular (B) bone cell measurements in tibia. An offset of 300 μ m (red double headed arrow) is left after the growth plate. Panels C and D (zoomed ROI of C) show TRAP positive osteoclast in red (Red arrows) and osteoblasts lined on the bone surface (black arrows). n=6 each group. Image A, generated from protocol provided by Darren Laith (Bone analysis laboratory, core facility, University of Sheffield, 2013).

2.2.12.v Growth plate analysis: The proliferative and hypertrophic zones of the growth plate were studied in order to characterise the growth plate of WT and RAMP3 KO mice. Using virtual slides, number of proliferative cells (N.PC), number of hypertrophic cells (N. HC) and the ratio of proliferative zone to hypertrophic zone (PC:HC) were determined by manually marking the cells. Three H&E stained tibial longitudinal mid sections (6 μ m apart) were analysed per sample. An area of 1mm x 0.6mm mid growth plate region was analysed in each section. First, individual chondrocyte columns were manually marked as each column represents a clonal expansion of stem cells (Farnum & Wilsman 1993). Then proliferative and hypertrophic chondrocytes were marked manually with different colours in overlapping layers. Finally the extent of proliferative zone and hypertrophic zone within each column was marked. The software then simultaneously calculated the number of cells and PC/HC zone. Figure 2.10 below, details this process.

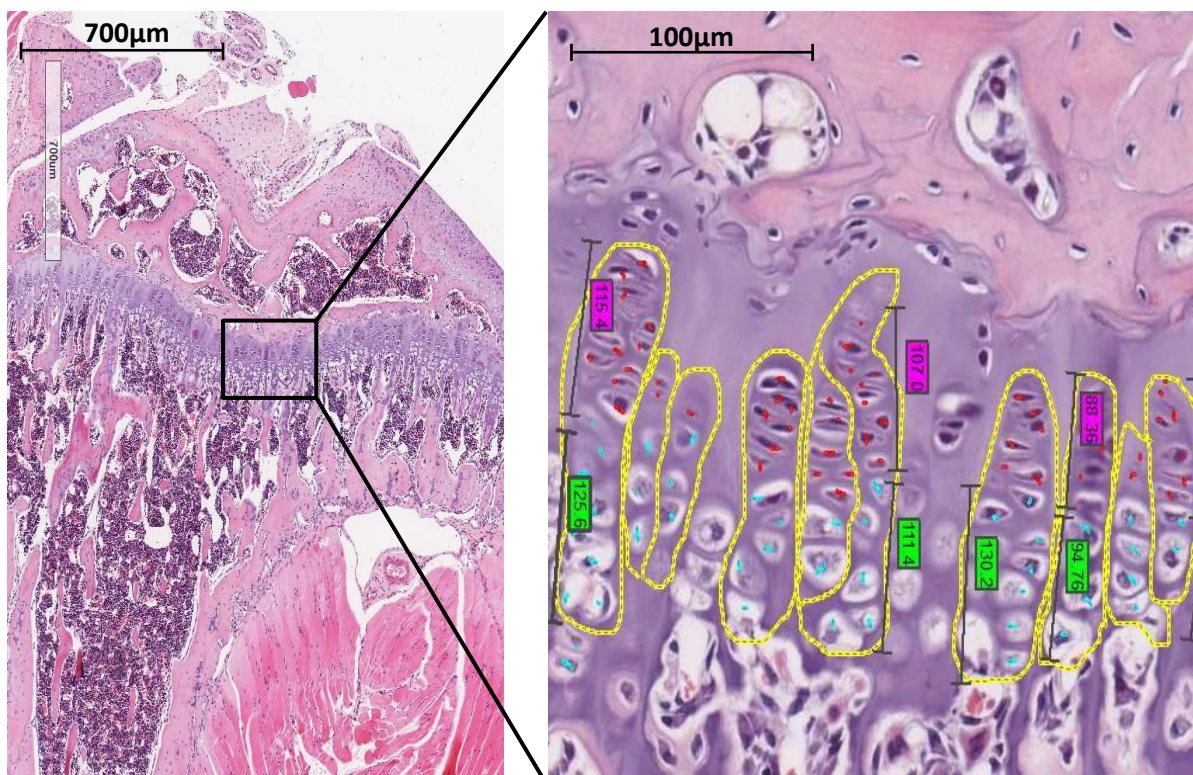


Fig 2.10: Representative image depicting the method used to analyse growth plate. The left panel is a tibial section with the manually marked analysis region (black box). The right panel is the zoomed region of analysis with the different markings. The yellow manual drawing marks individual chondrocyte column, pink dots mark proliferative cells, light blue dots mark the hypertrophic cells. Proliferative zone length is marked by black line with pink label, whereas the hypertrophic zone length is marked with black line with green label.

Using the GraphPad Prism Version 5.01, data was statistically analysed using either unpaired two tailed Student's T- test with 95% confidence interval or paired two-way ANOVA test followed by Bonferroni's post multiple comparison correction test depending on the experimental dataset. P value < 0.05 was considered significant. The level of significance was indicated by number of '*' signs presented on the plots.

Unpaired data sets were represented as box and whisker plots with upper and lower quartiles of the dataset. Paired datasets were represented as bar graphs. Specific statistical test and its representation are detailed in respective results section.

2.3 Results

2.3.1 Five day old pups:

Skeletal phenotype of postnatal day 5 WT and RAMP3 KO males and females were determined using Alcian Blue / Alizarin Red skeletal staining and microCT. Since skeletal staining interfered with the microCT analysis, right femur and tibia of the pups were dissected for microCT prior to staining the rest of the intact skeleton. The phenotype of WT and RAMP3 KO mice at post natal day 5 is detailed below. Unpaired two tailed Student's T- test with 95% confidence interval and P value < 0.05 considered significant was used to analyse the data statistically.

2.3.1.i Whole body weights, tail lengths and whole bone lengths

RAMP3 KO male and female mice had significantly (*) higher whole body weight compared to WT mice. Figure 2.11 below represents the differences in whole body weights in both male and female WT and RAMP3 KO mice.

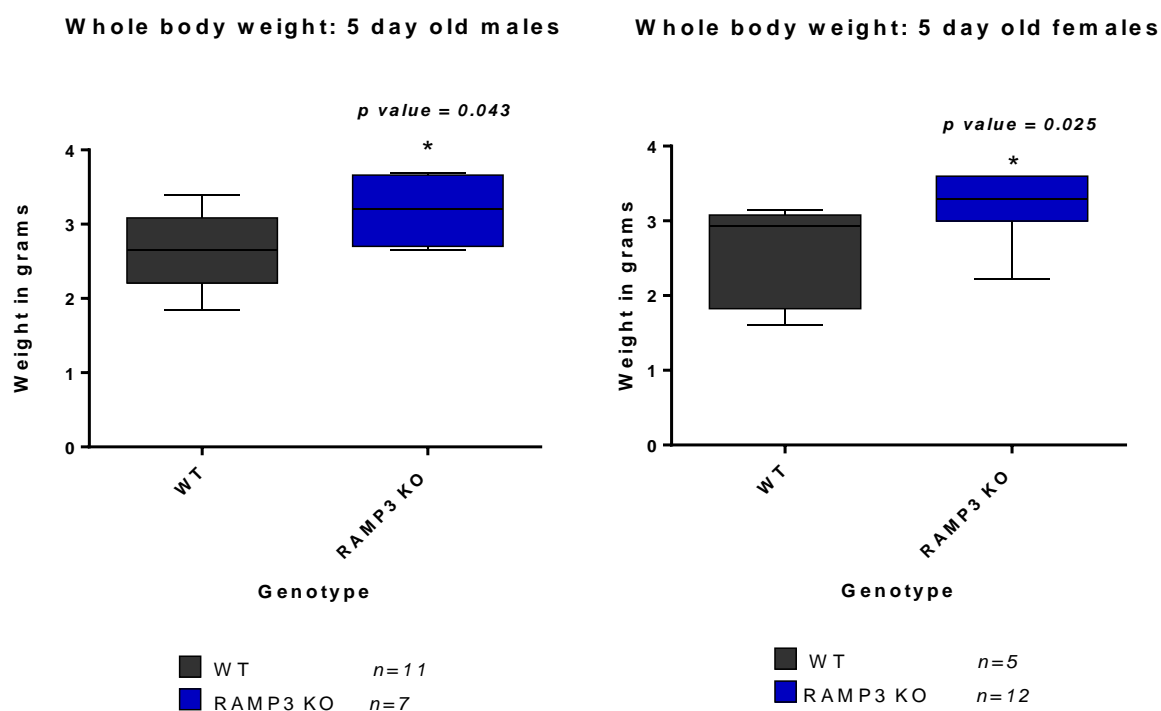


Fig 2.11: Box and whisker plot showing whole body weights in post natal day 5 old WT and RAMP3 KO male (left) and female (right) mice. Unpaired Student's T- test showed a significant increase in both RAMP3 KO male (p value=0.043) and female (p value=0.025) body weights compared to WT male and females. In males WT $n=11$ and RAMP3 KO $n=7$. In females, WT $n=5$ and RAMP3 KO $n=12$.

Although there was no significant difference in female tail lengths, it was observed that RAMP3 KO male mice had significantly (*) longer tails compared to WT male mice (Fig. 2.12i).

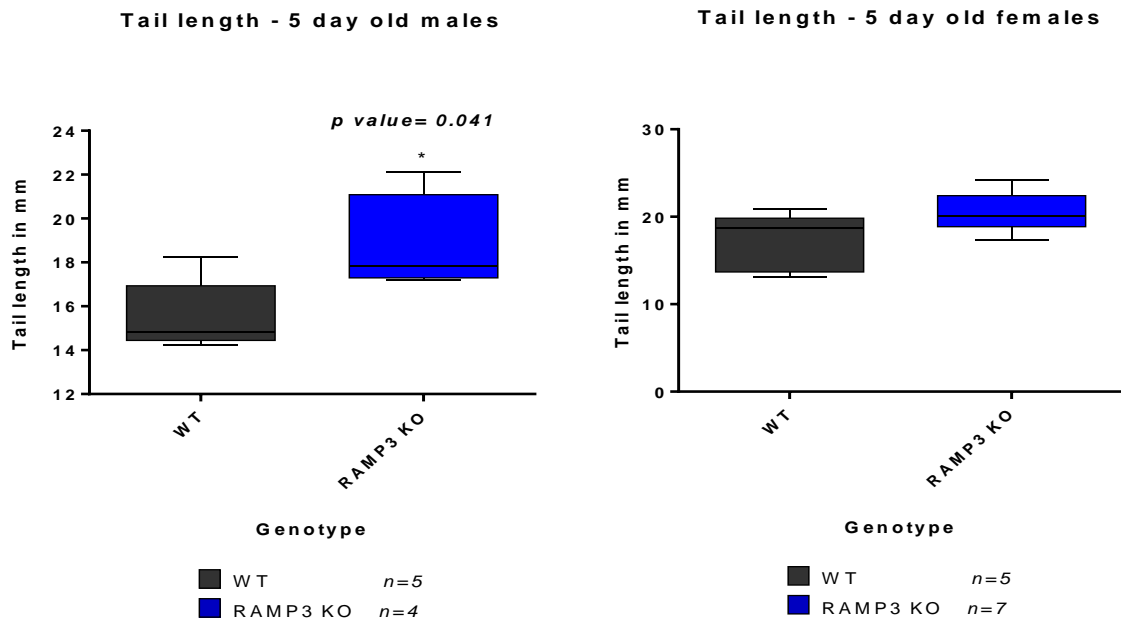


Fig 2.12i: Box and whisker plot showing differences in tail lengths in post natal day 5 old WT and RAMP3 KO male (left) and female (right) mice. Unpaired Student's T- test demonstrated a significant increase in RAMP3 KO male (p value=0.041) tail length. There was no significant difference in female tail lengths. In males, WT $n=5$ and RAMP3 KO $n=4$. In females, WT $n=5$ and RAMP3 KO $n=7$.

The femoral and tibial lengths of RAMP3 KO male and female mice were compared to that of WT mice. There were no significant differences in the whole bone lengths in either male or females (Figure 2.12ii).

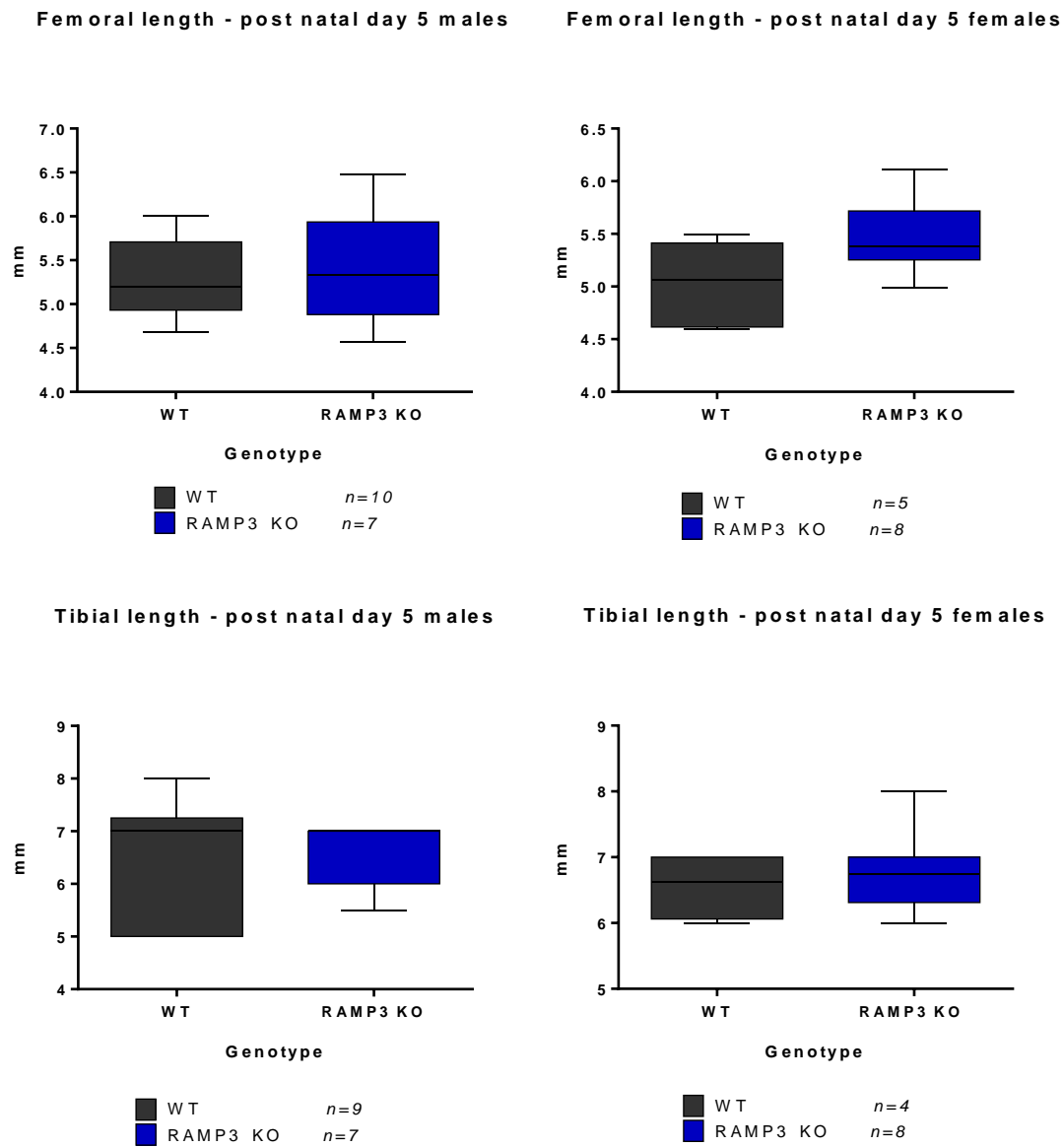


Fig 2.12ii: Box and whisker plot showing femoral and tibial lengths of male (A,C) and female (B,D) RAMP3 KO and WT mice. Unpaired Student's T- test demonstrated no significant differences between RAMP3 KOs and WTs.

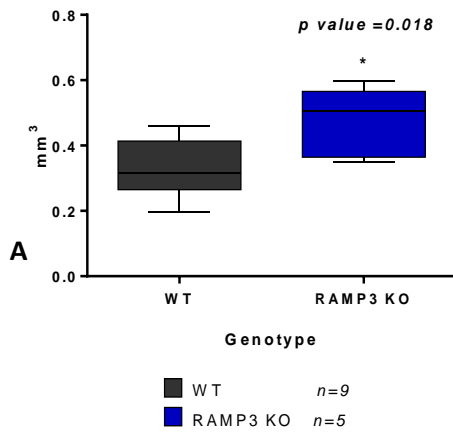
2.3.1.ii MicroCT analysis whole femur and tibia:

Whole femur and tibia of post natal day 5 mice were scanned at a 10.00 μm resolution. Since the samples were stained with Alcian blue and Alzarin red prior to the microCT analysis, bone mineral density was not analysed. Also since the femurs and tibia-fibula complexes in the females were broken, they were excluded from the comparisons and this resulted in reduced numbers (WT n=4). RAMP3 KO male and female mice had significantly increased femoral bone volume (BV) compared to male and female WT mice (Fig. 2.13 (A) and (B) overleaf). However, neither male nor females had significant differences in tibial BV (Fig 2.13 (C) and (D) overleaf). Mean \pm SEM (standard error of mean) values for each group and the statistical significance is tabulated below (Table 2.4).

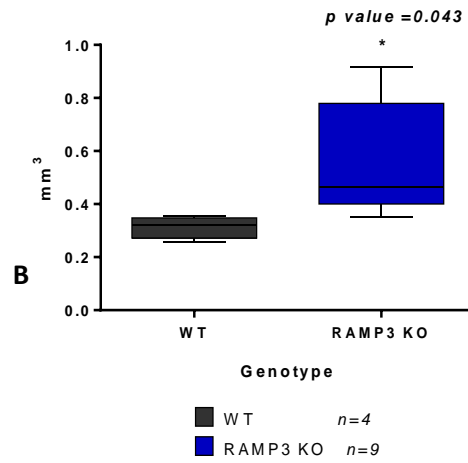
Table 2.4: Statistical analysis of 5 day old whole femur and tibia bone volume

Bone morphometric parameter	Units	WT Mean \pm SEM.	RAMP3 KO Mean \pm SEM.	P Value	Significance
PND5 male femur BV	mm^3	0.33 \pm 0.029 n=9	0.47 \pm 0.047 n=5	0.0189	*
PND5 female femur BV	mm^3	0.31 \pm 0.02 n=4	0.56 \pm 0.70 n=9	0.0435	*
PND5 male tibia-fibula BV	mm^3	0.38 \pm 0.031 n=10	0.39 \pm 0.047 n=6	0.7843	NS
PND5 female tibia-fibula BV	mm^3	0.42 \pm 0.054 n=4	0.57 \pm 0.071 n=7	0.1909	NS

Whole femur bone volume - 5 day old male



Whole femur bone volume - 5 day old female



Whole tibia-fibula bone volume - 5 day old males Whole tibia-fibula bone volume - 5 day old females

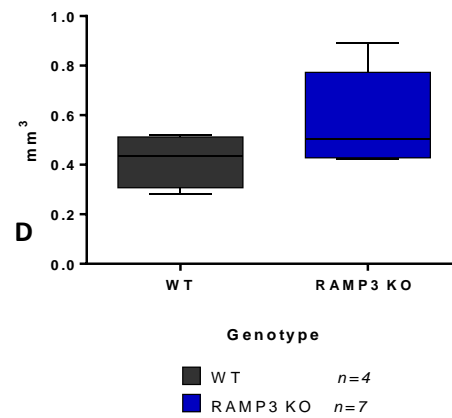
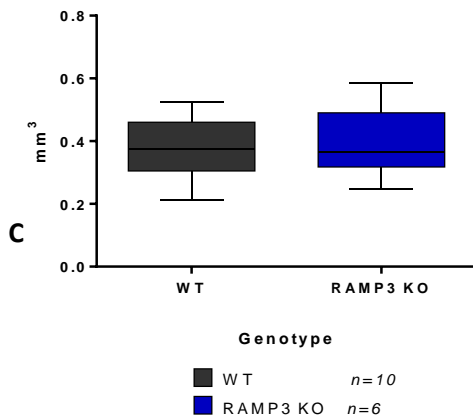


Fig 2.13: Box and whisker plots showing the differences in whole femur (A,B) and tibia(C,D) bone volume (BV) in males (A,C) and females (B,D). Both male and female RAMP3 KO whole femur BV is significantly more than WT whole femur BV. In males, WT n=9 (femur) and n=10 (tibia-fibula), RAMP 3 KO n=5 (femur) and n=6 (tibia-fibula). In females, WT n=4 (femur and tibia-fibula) and RAMP 3 KO n=9 (femur) and n=7 (tibia- fibula).

2.3.1.iii Three dimension model rendering:

Femoral microCT scans were used to render 3D bone models to study the structural differences between WT and RAMP3 KO bones. Densitometric femur models translate microCT analysis into visual differences. As seen in Fig. 2.14, RAMP3 KO representative model has increased opacity when compared to WT femur.

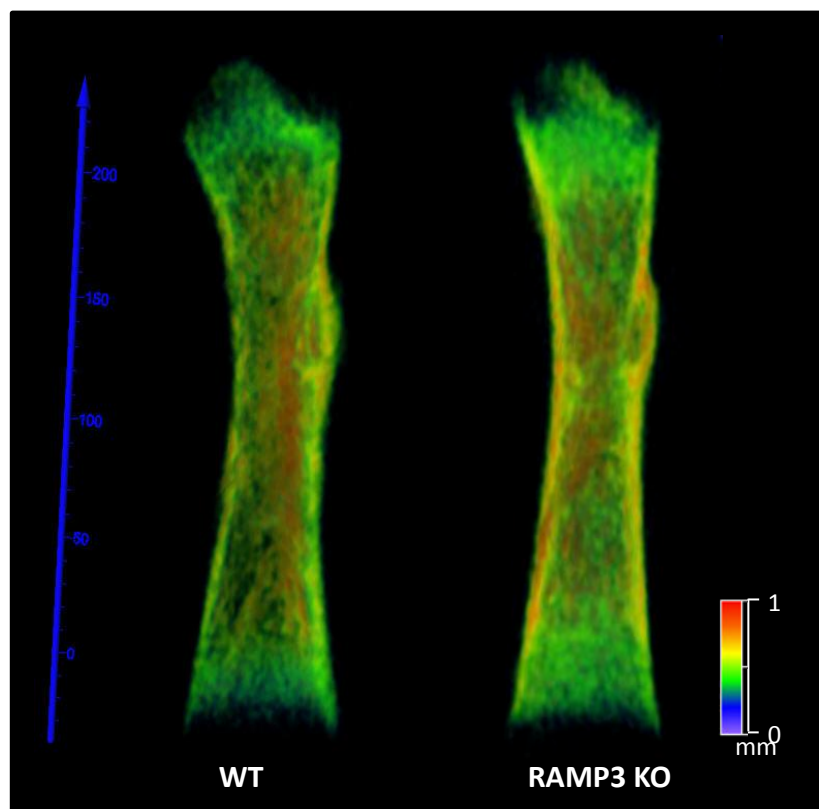


Fig 2.14: Representative 3D femur models of post natal day 5 mice. Densitometric model represents the density of the structure by gradient colours: purple being least dense and red being most dense (legend: right bottom). Blue scale (left) represents voxels and the scale to the right represents the millimetres and the densitometric gradient. WT femur (left) models appears more transparent compared to RAMP3 KO femur (right) suggesting increased density in the RAMP3 KO femur.

2.3.1.iv Skeletal staining:

Fourteen WT and fifteen RAMP3 KO sex-matched 5 day old mice were stained with Alcian Blue / Alizarin Red to reveal gross skeletal differences. The RAMP3 KO mice had bigger, more mineralised and more developed skeleton compared to WT of the same age. Advanced development of the skeleton was most evident in the RAMP3 KO vertebrae which had larger vertebral body and more developed and more mineralised spinous and transverse processes than the WT vertebrae (Fig. 2.15). The advanced development in RAMP3 KO skeleton was seen irrespective of the gender of the mice and was robust to differences in inter-litter pup sizes.

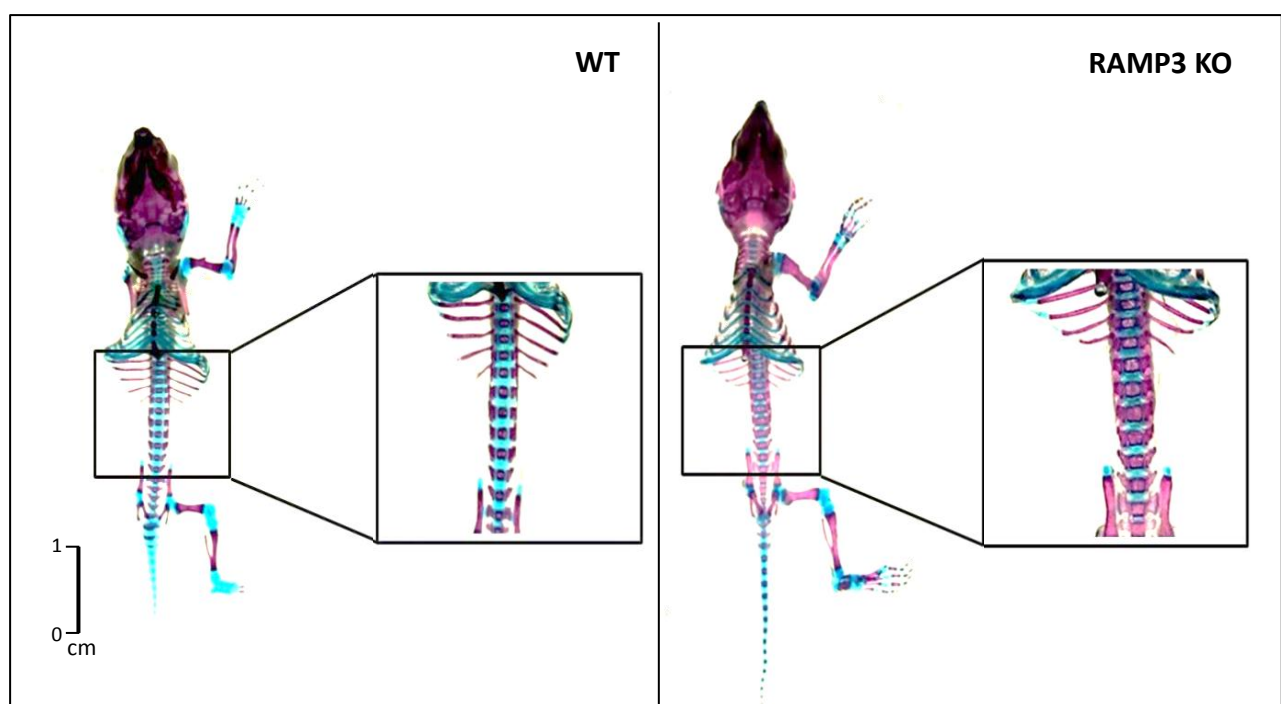


Fig 2.15: Representative Alcian blue / Alizarin red stained skeletons of WT (left) and RAMP3 KO (right) post natal day 5 mice. Alcian blue stains the cartilage blue and Alizarin red stains the mineralised tissue purple. RAMP3 KO skeleton is larger and shows advanced development evidently seen in the zoomed spine panel. RAMP3 KO vertebral body is larger; more mineralised and has more developed transverse process compared to WT vertebrae. WT $n = 14$ (10 males, 4 females) and RAMP3 KO $n = 15$ (6 males, 9 females).

2.3.2 Four week old mice:

The skeletal phenotype of 4 week old WT and RAMP3 KO male and female mice was determined using microCT. The phenotype of WT and RAMP3 KO mice at this age is detailed below. Unpaired two tailed Student's T- test with 95% confidence interval and P value < 0.05 considered significant was used to analyse the data statistically.

2.3.2.i Whole body weight

Unlike post natal day 5, 4 week old RAMP3 KO male and female mice had significantly (*) lower whole body weight compared to WT mice. Figure 2.16 below represents the differences in whole body weights in both male and female WT and RAMP3 KO mice.

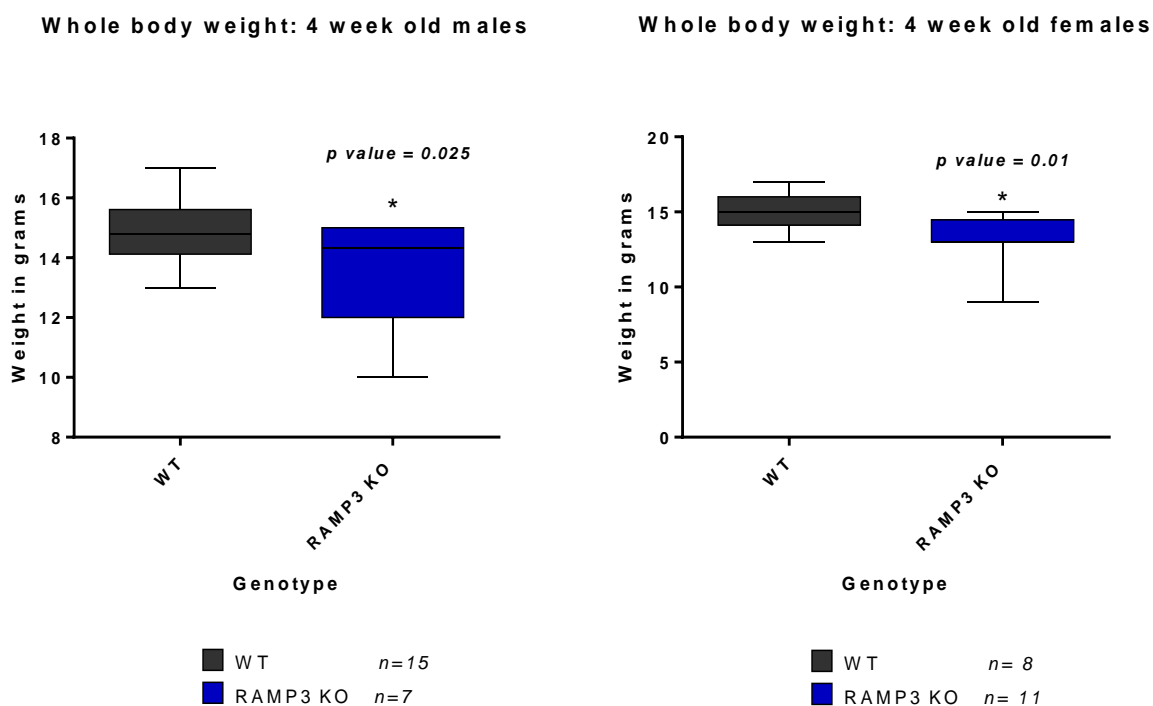


Fig 2.16: Box and whisker plot showing whole body weights in 4 week old WT and RAMP3 KO male (left) and female (right) mice. Unpaired Student's T- test showed a significant increase in both RAMP3 KO male (p value=0.025) and female (p value=0.01) body weights compared to WT male and females. In males WT $n=15$ and RAMP3 KO $n=7$. In females, WT $n=8$ and RAMP3 KO $n=11$.

2.3.2.ii MicroCT analysis and three dimensional skeletal models:

As mentioned before, whole bones were scanned at 17.5 μ m and cortical and trabecular sections were scanned at 4.5 μ m. The analysed dataset was checked for outliers using GraphPad prism. Following this, the cleaned up data was subjected to unpaired two tailed Student's T- test with 95% confidence interval and P value < 0.05 was considered significant.

Data obtained from microCT analysis was used to aid visual understanding of the skeletal phenotype. These 3D models where rendered in Voxler® as solid models and gradient models (densitometric models).

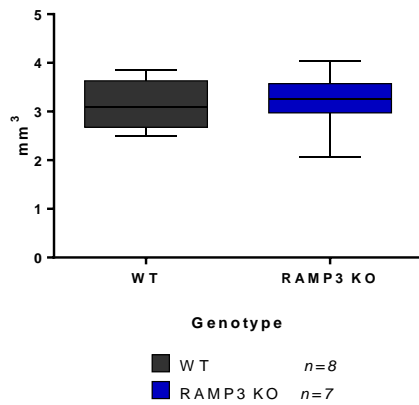
2.3.2.ii.a Whole femur:

Four-week old WT and RAMP3 KO mice displayed a gender dependent difference in whole femur bone volume. No significant difference was observed between male WT and RAMP3 KO femur bone volume (BV). Although, in females, RAMP3 KO femur BV was significantly higher than WT femur BV. Table 2.5 details mean \pm standard error of mean (SEM) for WT and RAMP3 KO samples along with the statistical significance (red). Figure 2.17 (overleaf) are box and whisker plots representing the femur bone volume in males (A) and females (B).

Table 2.5: Statistical analysis: 4 week old male whole femur bone volume

Bone morphometric parameter	Units	WT Mean \pm SEM.	RAMP3 KO Mean \pm SEM.	P Value	Significance
4 week male whole femur BV	mm ³	3.14 \pm 0.18 n=8	3.20 \pm 0.23 n=7	0.8387	NS
4 week female whole femur BV	mm ³	2.90 \pm 0.11 n=8	3.33 \pm 0.12 n=9	0.0201	*

Whole femur bone volume - 4 week old males



Whole femur bone volume - 4 week old females

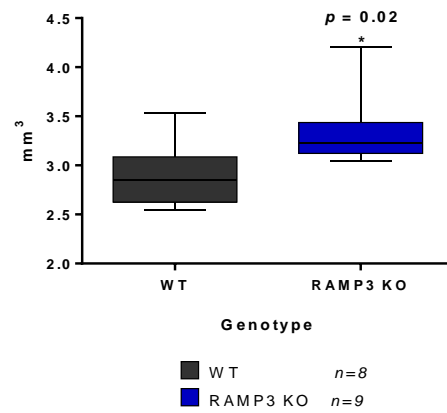


Fig 2.17: Box and whisker plot showing whole femur bone volume in 4 week old WT and RAMP3 KO male (left) and female (right) mice. Unpaired Student's T- test suggests a significant increase in female RAMP3 KO whole femur bone volume (p value=0.020) when compared to WT (right). No significant differences observed in male femur comparisons (left). In males, WT $n=8$ and RAMP3 KO $n=7$ and in females, WT $n=8$ and RAMP3 KO $n=9$.

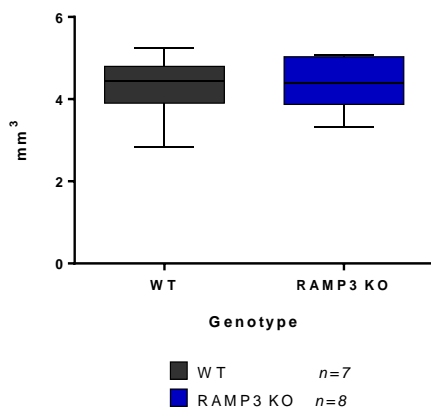
2.3.2.ii.b Whole tibia-fibula:

Similar to whole femur BV, whole tibia-fibula BV showed sex dependent skeletal phenotype. No significant difference was observed between male WT and RAMP3 KO tibia-fibula BV (Fig. 2.18 left). However, RAMP3 KO females had significantly higher tibia-fibula whole BV than WTs (Fig. 2.18 right). Table 2.6 details mean \pm standard error of mean (SEM) for WT and RAMP3 KO samples along with the statistical significance (red).

Table 2.6: Statistical analysis: 4 week old male whole tibia-fibula bone volume

Bone morphometric parameter	Units	WT Mean \pm SEM.	RAMP3 KO Mean \pm SEM.	P Value	Significance
4 week male whole tibia-fibula BV	mm ³	4.27 \pm 0.29 n=7	4.39 \pm 0.22 n=8	0.7411	NS
4 week female whole tibia-fibula BV	mm ³	3.95 \pm 0.16 n=8	4.64 \pm 0.11 n=9	0.0022	**

Whole tibia-fibula bone volume - 4 week old male



Whole tibia-fibula bone volume - 4 week old females

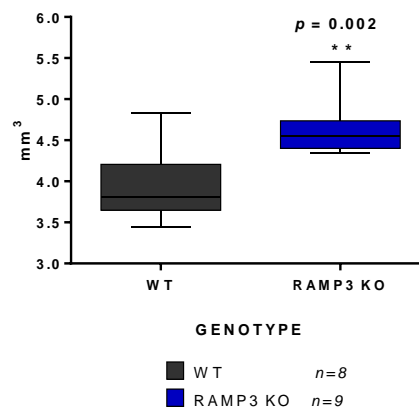


Fig 2.18: Box and whisker plot showing tibia-fibula whole bone volume in 4 week old WT and RAMP3 KO male (left) and female (right) mice. Unpaired Student's T- test demonstrated a significant increase in female RAMP3 KO whole femur bone volume (p value=0.002) when compared to WT (right). No significant differences observed in male femur comparisons (left). In males, WT $n=7$ and RAMP3 KO $n=8$ and females, WT $n=8$ and RAMP3 KO $n=9$.

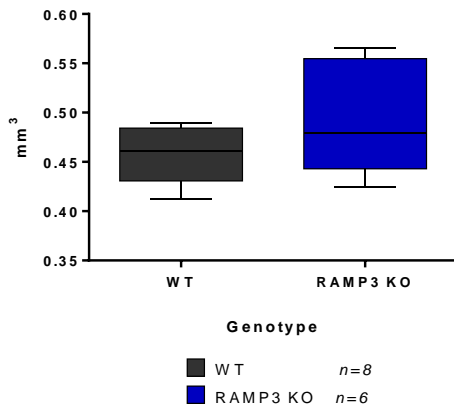
2.3.2.ii.c Femur cortical bone:

Cortical microCT analysis was performed at a higher resolution to enable detailed micro-architectural analysis. Neither male nor female RAMP3 KO mice had statistically significant differences from WT in their femoral cortices (Fig. 2.19 overleaf). Table 2.7 below, details mean \pm standard error of mean (SEM) for WT and RAMP3 KO samples along with the statistical significance.

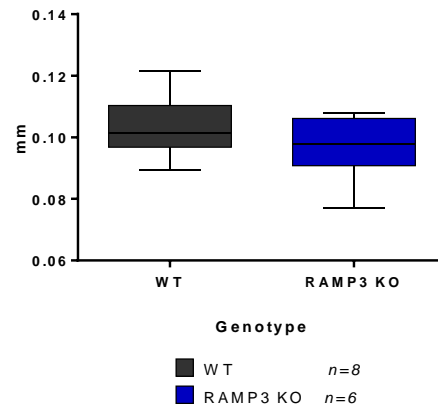
Table 2.7: Statistical analysis of 4 week old male femur cortical bone.

Bone morphometric parameter	Units	WT Mean \pm SEM.	RAMP3 KO Mean \pm SEM.	P Value	Significance
4 week male femur cortical BV	mm ³	0.46 \pm 0.00 n=8	0.49 \pm 0.02 n=6	0.1702	NS
4 week male femur cortical Th	mm	0.10 \pm 0.00 n=8	0.08 \pm 0.00 n=6	0.2668	NS
4 week female femur cortical BV	mm ³	0.45 \pm 0.00 n=10	0.45 \pm 0.00 n=9	0.7526	NS
4 week female femur cortical Th	mm	0.10 \pm 0.00 n=10	0.10 \pm 0.00 n=11	0.9901	NS

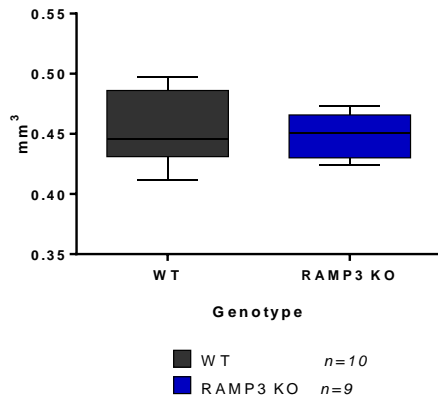
Femur Cortical bone volume - 4 week old males



Femur Cortical thickness - 4 week old males



Femur Cortical bone volume - 4 week old females



Femur Cortical thickness - 4 week old females

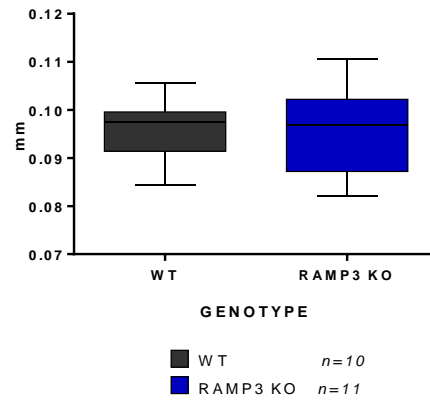


Fig 2.19: Box and whisker plot showing femur cortical bone volume (left) and thickness (right) in 4 week old WT and RAMP3 KO male (top) and female (bottom) mice. Unpaired Student's T- test showed neither male nor female WT and RAMP3 KO have significant differences in cortical bone volume and thickness. In males WT n=8 and RAMP3 KO n=6 (BV and Th) and in females, WT n=10 (BV and Th) and RAMP3 KO n=9 (BV) and n=11 (Th)

2.3.2.ii.d Tibia cortical bone:

Similar to femur cortical analysis, neither male nor female WT and RAMP3 KO mice had any statistically significant differences observed in their tibial cortices (Fig. 2.20 overleaf). Table 2.8 below, details mean \pm standard error of mean (SEM) for WT and RAMP3 KO samples along with the statistical significance.

Table 2.8: Statistical analysis of 4 week old male tibia cortical bone.

Bone morphometric parameter	Units	WT Mean \pm SEM.	RAMP3 KO Mean \pm SEM.	P Value	Significance
4 week male tibia cortical BV	mm ³	0.53 \pm 0.01 n=7	0.54 \pm 0.37 n=5	0.4569	NS
4 week male tibia cortical Th	mm	0.09 \pm 0.00 n=6	0.09 \pm 0.01 n=7	0.9794	NS
4 week female tibia cortical BV	mm	0.51 \pm 0.00 n=9	0.51 \pm 0.01 n=10	0.7961	NS
4 week female tibia cortical Th	mm	0.08 \pm 0.00 n=9	0.09 \pm 0.00 n=11	0.8290	NS

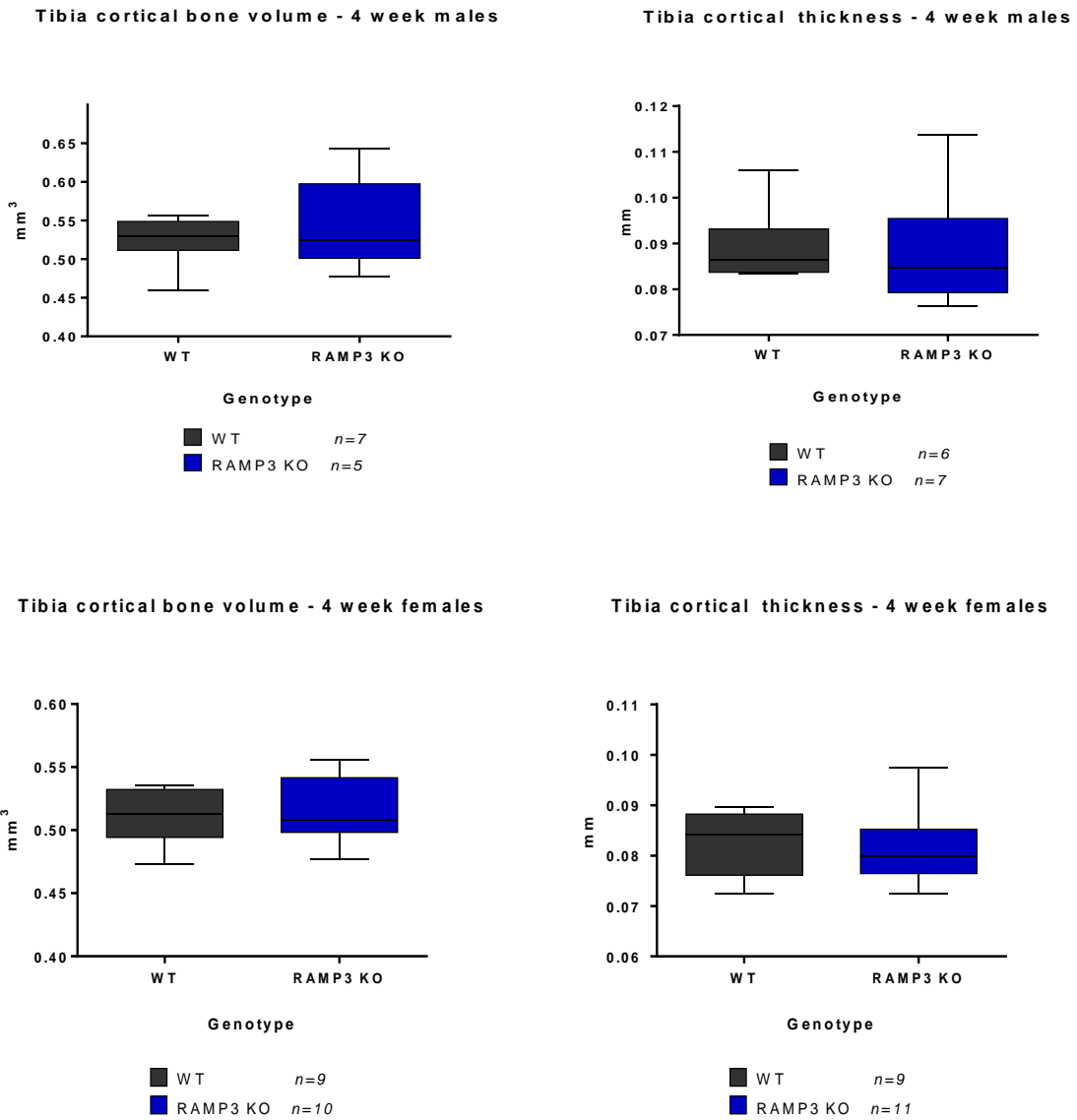


Fig 2.20: Box and whisker plot showing tibia cortical bone volume (BV) –left, and thickness (Th) –right, in 4 week old WT and RAMP3 KO male (top) and female (bottom) mice. Unpaired Student’s T- test showed neither male nor female WT and RAMP3 KO have significant differences in cortical bone volume and thickness. In males WT n=7 (BV) and 6 (Th) and RAMP3 KO n=5 (BV) and 7 (Th). In females, WT n=9 (BV and Th) and RAMP3 KO n=10 (BV) and n=11 (Th)

2.3.2.ii.e Femur trabecular bone:

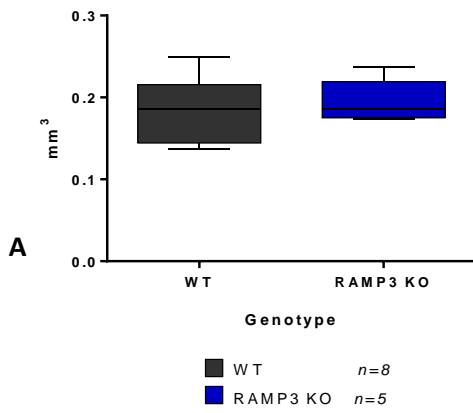
Trabecular microCT analysis measured bone morphometric parameters that included total bone volume (BV), bone volume to tissue volume ratio (BV/TV), Thickness (Th), separation between individual trabecular units (Sp), number of trabecular units (N) and pattern factor that quantitatively describes the ratio of inter-trabecular connectivity (Pf).

In WT and RAMP3 KO male 4 week old mice, there was no significant difference between femur trabecular bone morphometric parameters. However, in females, RAMP3 KO mice had highly significant increase in trabecular thickness, increase in pattern factor and reduction in trabecular number compared to WT female mice. This suggested that RAMP3 KO female mice have an overall thicker and well-connected trabecular meshwork at this age. Table 2.9 below, details mean \pm standard error of mean (SEM) for WT and RAMP3 KO samples along with the statistical significance (red). Figures 2.21 and 2.22 represent the trabecular differences.

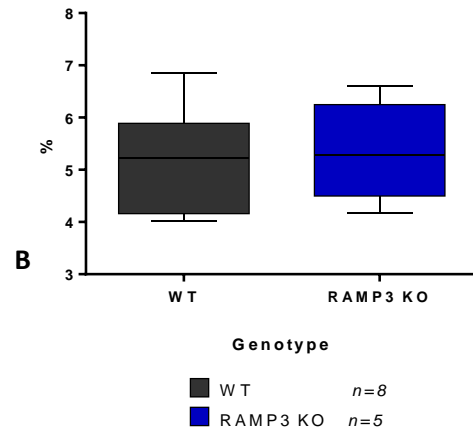
Table 2.9: Statistical analysis of 4 week old male and female femur trabecular bone.

Bone morphometric parameter	Units	WT Mean \pm SEM.	RAMP3 KO Mean \pm SEM.	P Value	Significance
4 week male femur trabecular BV	mm ³	0.18 \pm 0.01 n=8	0.20 \pm 0.01 n=5	0.5697	NS
4 week male femur trabecular BV/TV	%	5.18 \pm 0.37 n=8	5.36 \pm 0.42 n=5	0.7667	NS
4 week male femur trabecular Th	mm	0.03 \pm 0.00 n=8	0.04 \pm 0.00 n=6	0.2320	NS
4 week male femur trabecular Sp	mm	0.30 \pm 0.01 n=8	0.30 \pm 0.01 n=6	0.8160	NS
4 week male femur trabecular N	1/mm	1.57 \pm 0.11 n=8	1.54 \pm 0.10 n=6	0.8773	NS
4 week male femur trabecular Pf	1/mm	31.63 \pm 2.87 n=8	30.77 \pm 1.83 n=6	0.8200	NS
4 week female femur trabecular BV	mm ³	0.18 \pm 0.01 n=9	0.17 \pm 0.011 n=9	0.7137	NS
4 week female femur trabecular BV/TV	%	5.22 \pm 0.17 n=9	5.00 \pm 0.20 n=11	0.4169	NS
4 week female femur trabecular Th	mm	0.03 \pm 0.00 n=9	0.035 \pm 0.00 n=9	0.002	***
4 week female femur trabecular Sp	mm	0.29 \pm 0.01 n=9	0.32 \pm 0.01 n=11	0.1298	NS
4 week female femur trabecular N	1/mm	1.65 \pm 0.06 n=9	1.47 \pm 0.06 n=11	0.0477	*
4 week female femur trabecular Pf	1/mm	27.87 \pm 1.77 n=9	32.22 \pm 0.97 n=9	0.0471	*

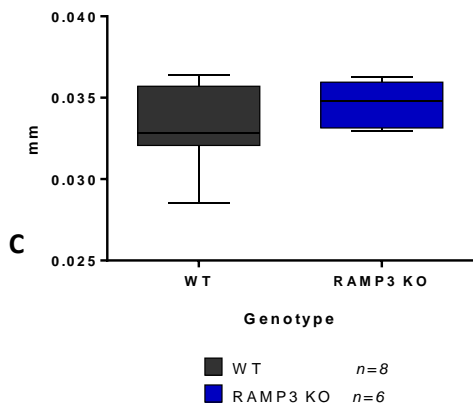
Femur trabecular bone volume- 4 week old males



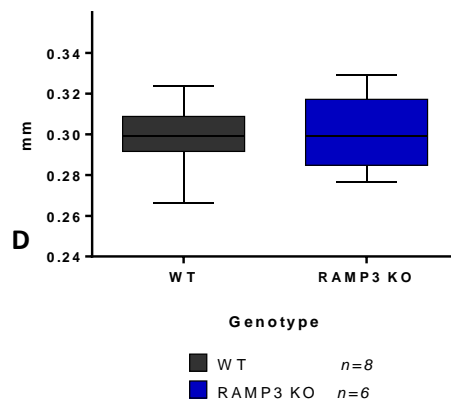
Femur trabecular BV/TV - 4 week males



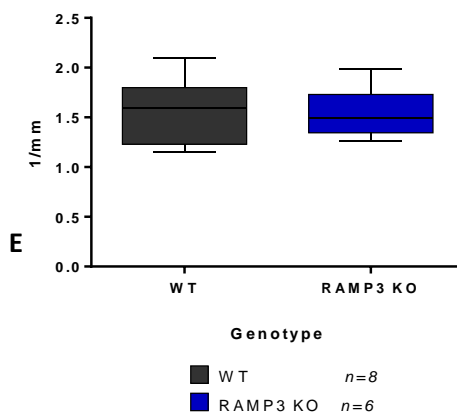
Femur trabecular thickness - 4 week males



Femur trabecular separation - 4 week males



Femur trabecular number - 4 week males



Femur trabecular pattern factor - 4 week males

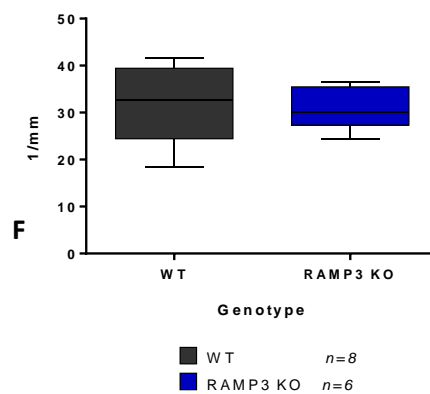
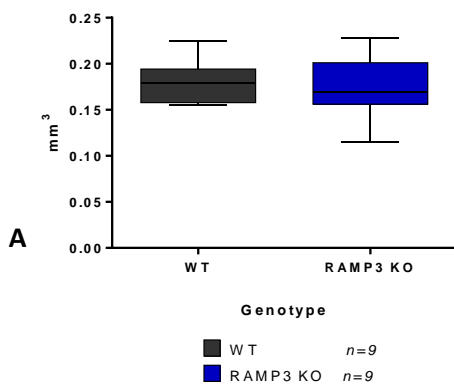
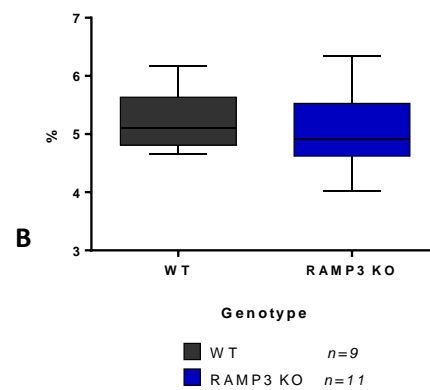


Fig 2.21: Box and whisker plot showing femur trabecular analysis in 4 week old WT and RAMP3 KO males. Unpaired Student's T- test showed that male WT and RAMP3 KO do not have any significant differences in trabecular BV (A), BV/TV (B), Th(C), Sp (D), N (E) and Pf(F). In males WT n=8 and RAMP3 KO n=5 (BV and BV/TV) and 6 (Th,Sp,N and Pf).

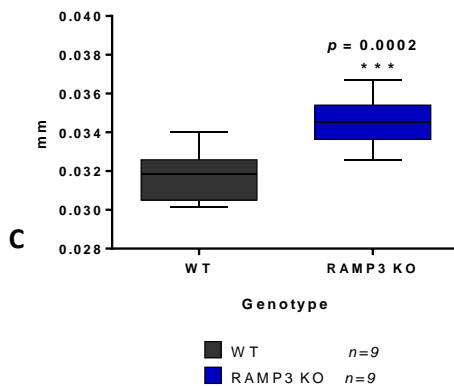
Femur trabecular bone volume- 4 week old females



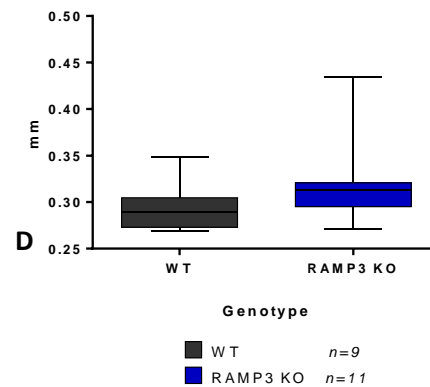
Femur trabecular BV/TV - 4 week females



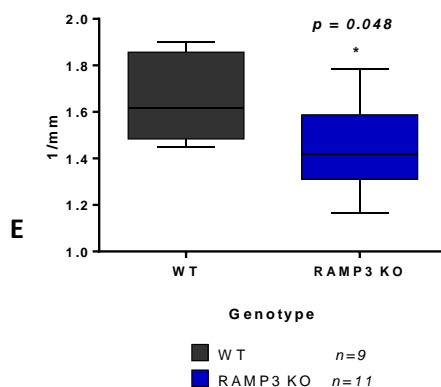
Femur trabecular thickness - 4 week females



Femur trabecular separation - 4 week females



Femur trabecular number - 4 week females



Femur trabecular pattern factor - 4 week females

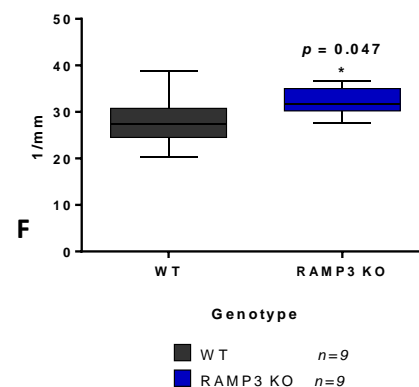


Fig 2.22: Box and whisker plot showing femur trabecular analysis in 4 week old WT and RAMP3 KO females. Unpaired Student's T- test showed that female RAMP3 KO trabecular bone has significant increase in trabecular Th, $p=0.0002$ (C) and Pf, $p=0.047$ (F). Trabecular N on the other hand is significantly lower ($p=0.048$) in RAMP3 KO when compared to WT (E). No significant differences were observed in trabecular BV (A), BV/TV (B) and Sp (D). In females WT $n=9$ and RAMP3 KO $n=9$ (BV,Th,Pf) and 11 (BV/TV,Sp and N).

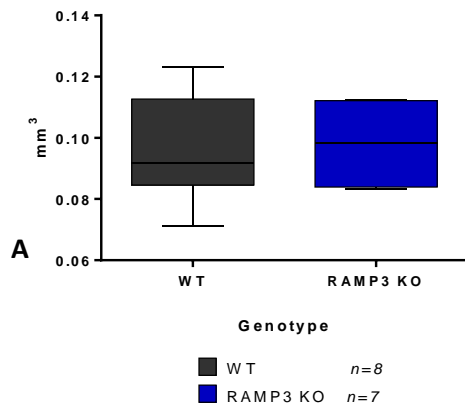
2.3.2.ii.f Tibia trabecular bone:

Like the femur trabecular analysis, tibia trabecular bone showed a sex dependent skeletal phenotype. Male WT and RAMP3 KO mice did not have differences in trabecular bone. However, in females, RAMP3 KO mice had significant increase in trabecular thickness compared to WT female mice. Table 2.10 below, details mean \pm standard error of mean (SEM) for WT and RAMP3 KO samples along with the statistical significance (red). Figures 2.23 and 2.24 represent the trabecular differences observed.

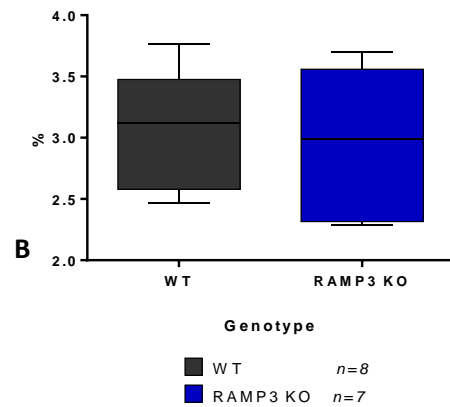
Table 2.10: Statistical analysis of 4 week old male and female tibia trabecular bone.

Bone morphometric parameter	Units	WT Mean \pm SEM.	RAMP3 KO Mean \pm SEM.	P Value	Significance
4 week male tibia trabecular BV	mm ³	0.03 \pm 0.00 n=8	0.04 \pm 0.00 n=7	0.8417	NS
4 week male tibia trabecular BV/TV	%	3.08 \pm 0.17 n=8	3.00 \pm 0.21 n=7	0.7853	NS
4 week male tibia trabecular Th	mm	0.03 \pm 0.00 n=8	0.04 \pm 0.00 n=7	0.2488	NS
4 week male tibia trabecular Sp	mm	0.42 \pm 0.01 n=8	0.41 \pm 0.02 n=7	0.7138	NS
4 week male tibia trabecular N	1/mm	0.91 \pm 0.05 n=8	0.87 \pm 0.06 n=7	0.5954	NS
4 week male tibia trabecular Pf	1/mm	39.36 \pm 1.67 n=8	41.42 \pm 1.92 N=7	0.4313	NS
4 week female tibia trabecular BV	mm ³	0.10 \pm 0.01 n=8	0.10 \pm 0.01 n=10	0.7631	NS
4 week female tibia trabecular BV/TV	%	3.19 \pm 0.14 n=8	3.19 \pm 0.19 n=10	0.9916	NS
4 week female tibia trabecular Th	mm	0.03 \pm 0.00 n=7	0.04 \pm 0.00 n=10	0.0024	**
4 week female tibia trabecular Sp	mm	0.43 \pm 0.02 n=8	0.44 \pm 0.03 n=10	0.6506	NS
4 week female tibia trabecular N	1/mm	0.94 \pm 0.05 n=8	0.92 \pm 0.05 n=10	0.7370	NS
4 week female tibia trabecular Pf	1/mm	36.80 \pm 0.76 n=7	38.15 \pm 0.89 n=10	0.2970	NS

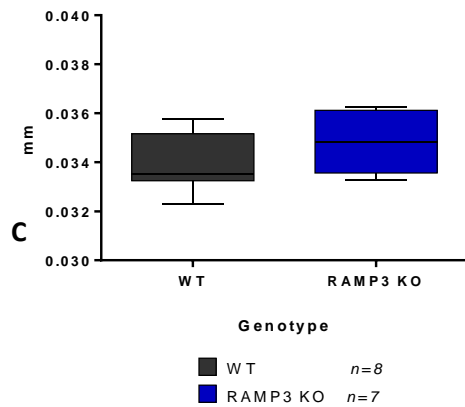
Tibia trabecular bone volume- 4 week old males



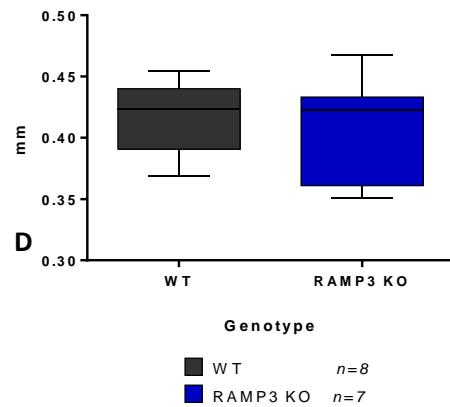
Tibia trabecular BV/TV - 4 week males



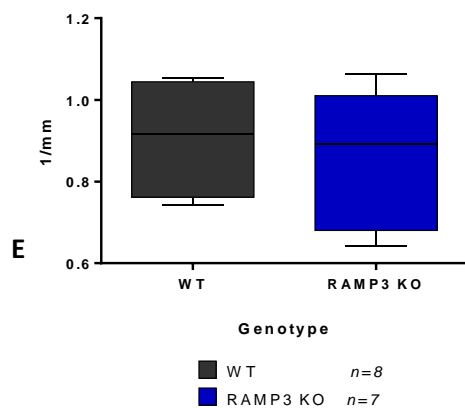
Tibia trabecular thickness - 4 week males



Tibia trabecular separation - 4 week males



Tibia trabecular number - 4 week males



Tibia trabecular pattern factor - 4 week males

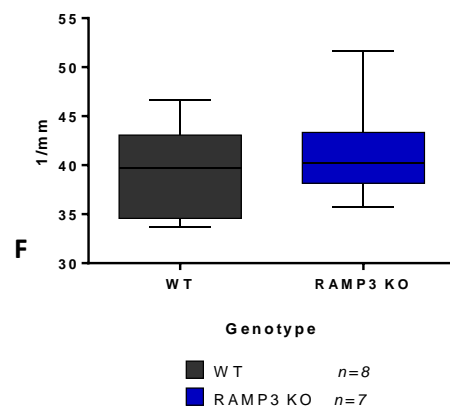
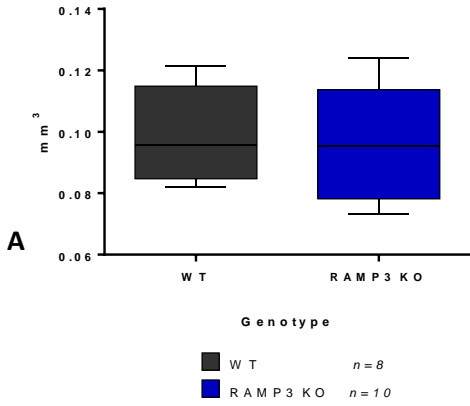
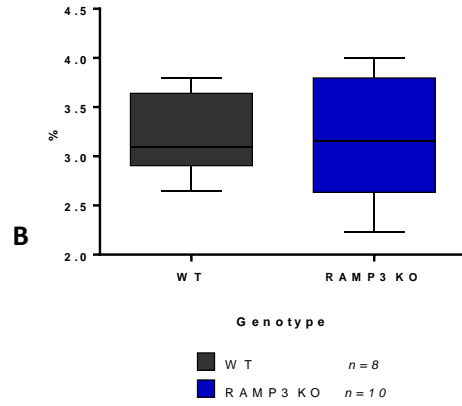


Fig 2.23: Box and whisker plot showing tibia trabecular analysis in 4 week old WT and RAMP3 KO males. Unpaired Student's T- test demonstrated that male WT and RAMP3 KO do not have any significant differences in trabecular BV (A), BV/TV (B), Th(C), Sp (D), N (E) and Pf(F). In males WT n=8 and RAMP3 KO n=7.

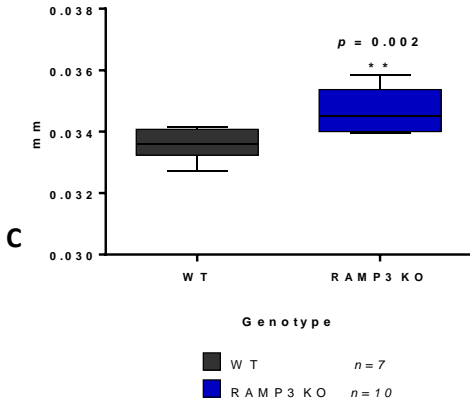
Tibia trabecular bone volume - 4 week old females



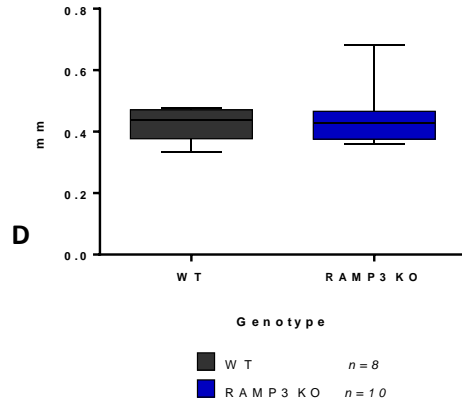
Tibia trabecular BV/TV - 4 week females



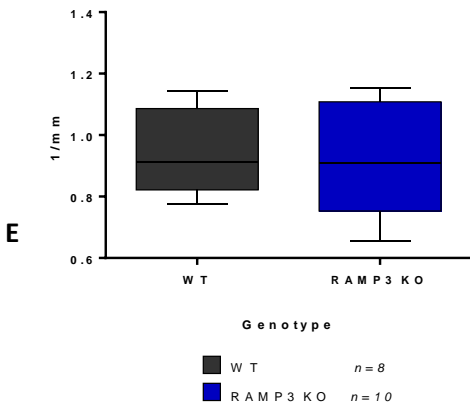
Tibia trabecular thickness - 4 week females



Tibia trabecular separation - 4 week females



Tibia trabecular number - 4 week females



Tibia trabecular pattern factor - 4 week females

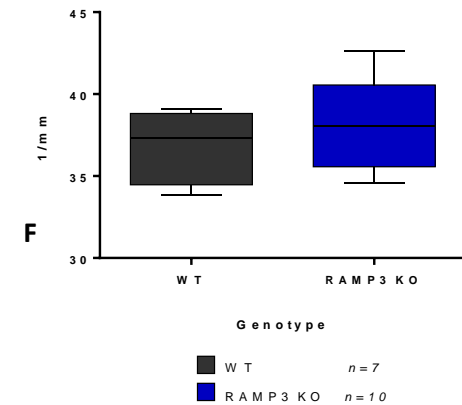


Fig 2.24: Box and whisker plot showing tibia trabecular analysis in 4 week old WT and RAMP3 KO females. Unpaired Student's T- test showed that female RAMP3 KO trabecular bone has significant increase in trabecular Th, $p=0.002$ (C) compared to WT. No significant differences observed in trabecular BV (A), BV/TV (B), Sp (D), N (E) and Pf(F). WT $n=8$ (BV, BV/TV, Sp, N) and $n=7$ (Th, Pf). RAMP3 KO $n=10$.

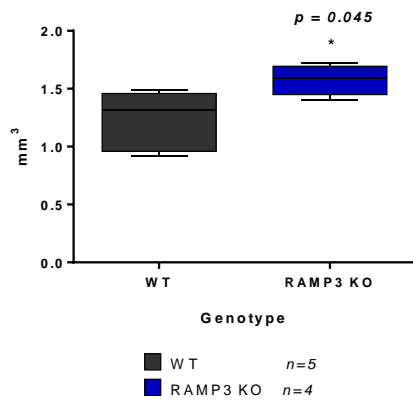
2.3.2.ii.g Caudal vertebra:

Whole 4th caudal vertebrae of WT and RAMP3 KO 4 week old male and females were scanned for microCT analysis at 17.5 μ m resolution and the whole vertebral bone volume (BV) and thickness (Th) were determined. Cortical and trabecular analysis was not performed separately and the physical marker references could not be identified. Hence consistent scanning areas could not be determined. Protocol is yet to be optimised. Both male and female caudal vertebrae had significantly increased vertebral BV in RAMP3 KO mice compared to WTs (Fig. 2.25 (left column)). In males RAMP3 KO vertebrae also had a significant increase in bone thickness (Fig 2.25 (top right)). Table 2.11 below details the mean \pm standard error of mean (SEM) for WT and RAMP3 KO samples along with the statistical significance (red).

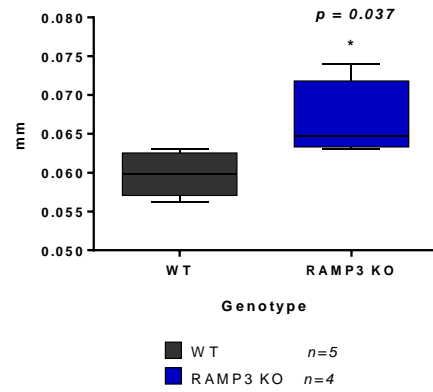
Table 2.11: Statistical analysis of 4 week old male and female caudal vertebra.

Bone morphometric parameter	Units	WT Mean \pm SEM.	RAMP3 KO Mean \pm SEM.	P Value	Significance
4 week male caudal vertebra BV	mm ³	1.23 \pm 0.12 n=5	1.58 \pm 0.07 n=4	0.0445	*
4 week male caudal vertebra Th	mm	0.06 \pm 0.00 n=5	0.07 \pm 0.00 n=4	0.0367	*
4 week female caudal vertebra BV	mm ³	1.24 \pm 0.08 n=8	1.48 \pm 0.07 n=8	0.0324	*
4 week female caudal vertebra Th	mm	0.06 \pm 0.00 n=8	0.07 \pm 0.00 n=8	0.0806	NS

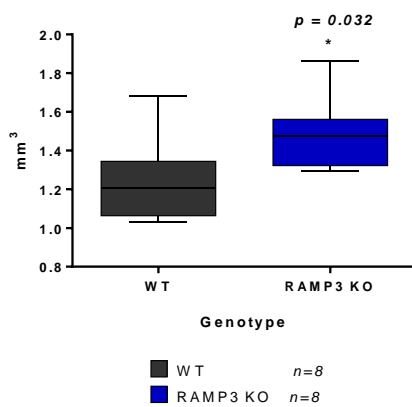
Caudal vertebra bone volume - 4 week old males



Caudal vertebra thickness - 4 week old males



Caudal vertebra bone volume - 4 week old females



Caudal vertebra thickness - 4 week old males

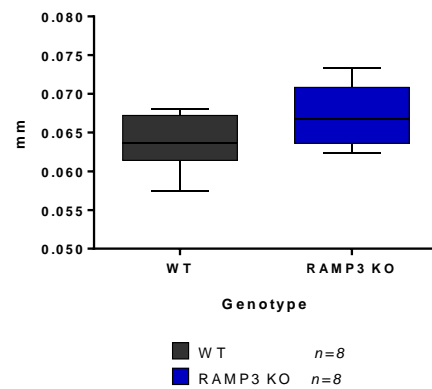


Fig 2.25: Box and whisker plot showing caudal vertebral bone analysis in 4 week old WT and RAMP3 KO females. Unpaired Student's T- test demonstrated that both male and female RAMP3 KO caudal vertebrae had significantly increased vertebral BV when compared to WT: male $p=0.045$ and female $p=0.032$ (A,B). Vertebral thickness was significantly higher in RAMP3 KO male vertebra, $p=0.037$ (C). In males WT $n=5$ and RAMP3 KO $n=4$ and in females, WT and RAMP3 KO $n=8$.

2.3.2.ii.h Three dimension skeletal models of 4 week old mice:

Both solid and gradient 3D models were generated to study the structural differences between RAMP3 KO and WTs. Gradient densitometric whole femur models revealed that RAMP3 KO have denser femurs, although, statistical significance was only achieved in female femurs. Figure 2.26 below, is a representative image of whole femur gradient models where purple is least density of the structure and red is highest density of the structure.

The Figure 2.27 overleaf summarises representative images of femur cortical, tibia trabecular and whole vertebral models. Solid grey-scale models of femur cortical, tibia trabecular and whole vertebrae overleaf, reflect the microCT analysis. No obvious structural differences were observed in femur cortical models. Tibia trabecular models showed thicker trabecular units in RAMP3 KO models compared to WTs. Female RAMP3 KO tibia trabecular model depicts the significant increase in trabecular thickness determined in microCT analysis. Lastly, whole vertebra solid models suggest genotype-dependent structural differences in vertebrae. RAMP3 KO vertebral models appear to have slender but well defined vertebral body with denser transverse process compared to WTs.

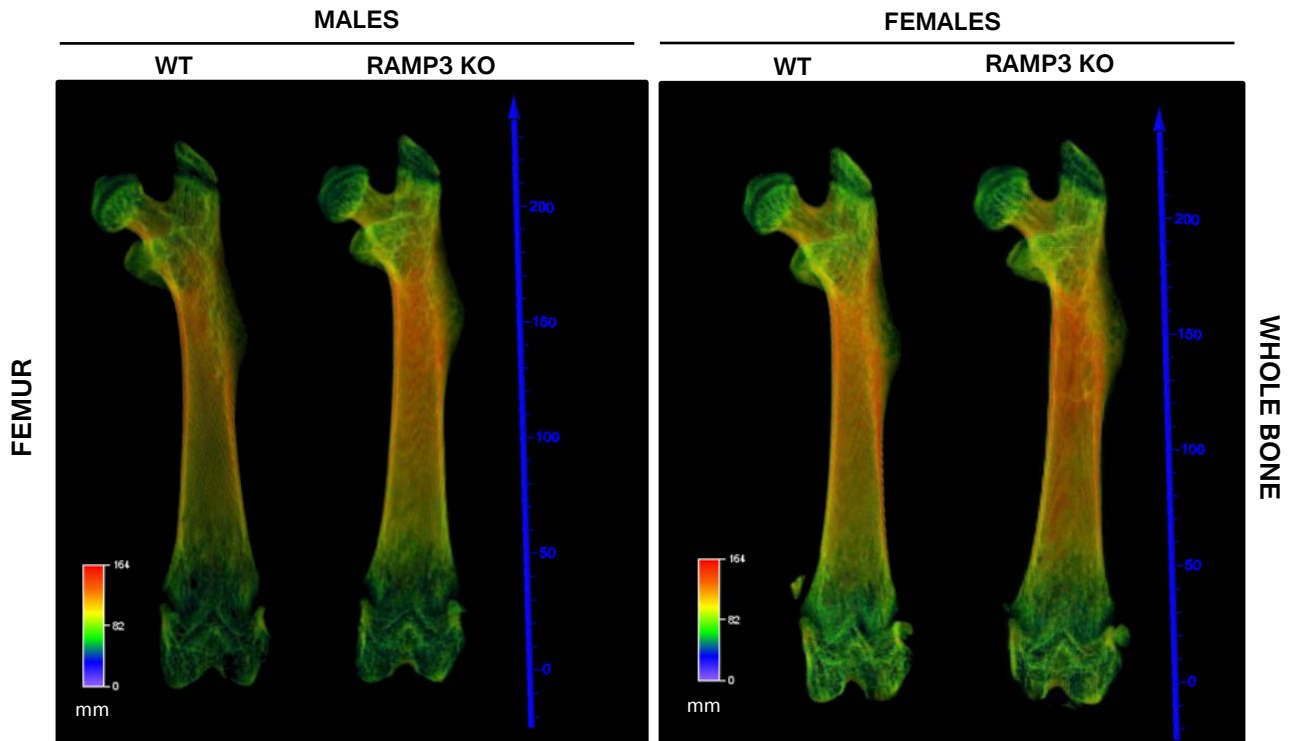


Fig 2.26: Representative 3D skeletal gradient models of 4 week old, WT and RAMP3 KO male (left panels) and female (right panels) mice. Gradient models of whole femur suggest that RAMP3 KO femurs in general are denser to WT femur however microCT data suggests statistical significance in difference of BV in female RAMP3 KO whole femur and WTs only.

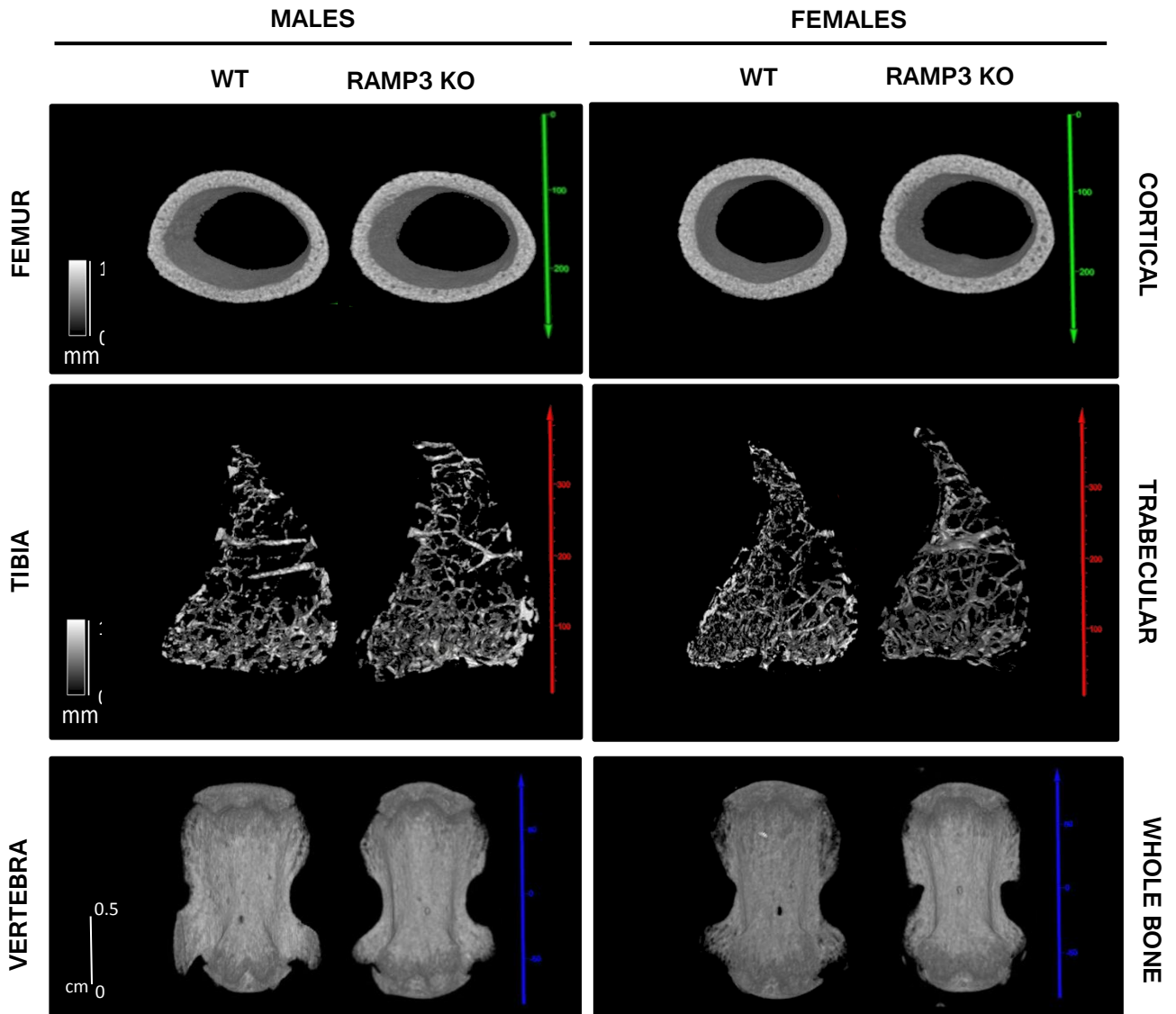


Fig 2.27: Representative 3D skeletal models of 4 week old, WT and RAMP3 KO male (left panels) and female (right panels) mice. Within each image, left model is of WT and right of RAMP3 KO. Top-most panel is of femur cortical solid grey-scale models that do not show any structural differences in RAMP3 KOs and WTs. Middle panel of tibia trabecular solid model show thicker trabecular units in RAMP3 KO females (right most). The last panel of caudal vertebra show structural differences between WT and in the RAMP3 KO. It is evident that RAMP3 KO vertebrae are slender with denser vertebral bodies and transverse process.

2.3.3 Eight week old mice:

Skeletal phenotypes of 8 week old WT and RAMP3 KO male and female mice were determined by microCT. Histology and dynamic histomorphometry was performed on male tibiae. The phenotype of WT and RAMP3 KO mice at this age is detailed below. Unpaired two tailed Student's T- test with 95% confidence interval and P value < 0.05 considered significant was used to analyse the data statistically.

2.3.3.i Whole body weight

Eight week-old RAMP3 KO male had significantly (***) higher whole body weight compared to WT mice. There was no significant difference in the body weights of female mice. Figure 2.28 below represents the differences in whole body weights in both male and female WT and RAMP3 KO mice.

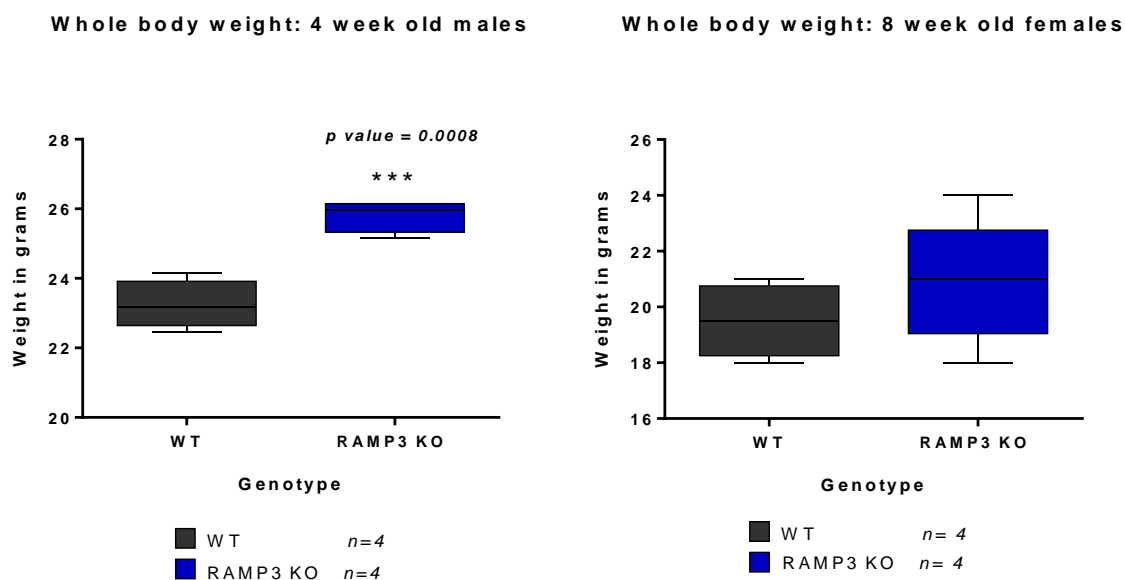


Fig 2.28: Box and whisker plot showing whole body weights in 8 week old WT and RAMP3 KO male (left) and female (right) mice. Unpaired Student's T- test showed a significant increase in RAMP3 KO male (p value=0.0008) compared to WT males. $n=4$ each genotype.

2.3.3.ii MicroCT analysis:

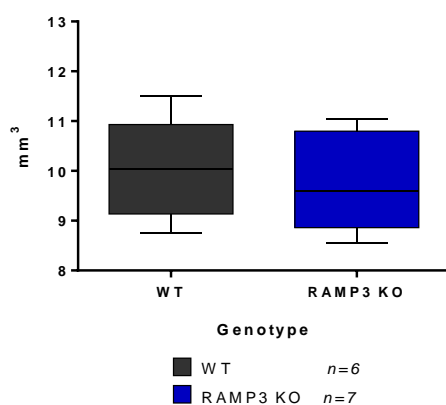
2.3.3.ii.a Whole femur and tibia:

MicroCT analysis suggested that at 8 weeks of age, RAMP3 KO male mice had significantly lower tibia-fibula bone volume compared to WT. There was no statistically significant difference between femurs of WT and RAMP3 KO male mice. Table 2.12 below details the arithmetic means \pm standard error of means (SEM) along with statistical significance (red). Figure 2.29 is a graphical representation of the same.

Table 2.12: Statistical analysis of 8 week old male whole femur and tibia.

Bone morphometric parameter	Units	WT Mean \pm SEM.	RAMP3 KO Mean \pm SEM.	P Value	Significance
8 week male whole femur BV	mm ³	10.06 \pm 0.412 n=6	9.64 \pm 0.37 n=7	0.4630	NS
8 week male whole tibia-fibula BV	mm ³	11.18 \pm 0.19 n=5	10.31 \pm 0.21 n=6	0.0136	*

Whole femur bone volume - 8 week males



Whole tibia-fibula bone volume - 8 week males

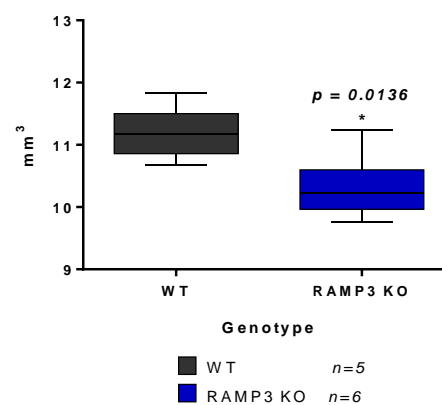


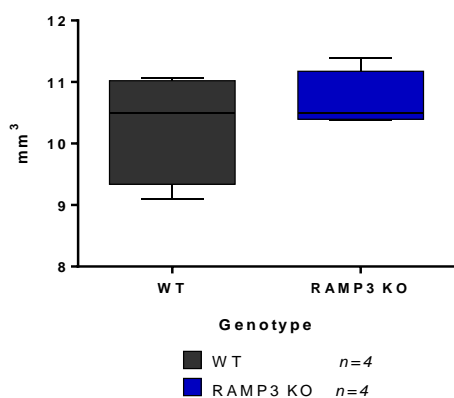
Fig 2.29: Box and whisker plot showing whole femur (left) and tibia (right) bone volume of 8 week old WT and RAMP3 KO male mice. Unpaired Student's T- test showed a significant decrease in RAMP3 KO tibia-fibula bone volume (p value=0.0136) compared to WT males but not in the femur bone volume. For femur analysis $n=6$ (WT) and 7(RAMP3KO) and for tibia-fibula analysis $n= 5$ (WT) and 6 (RAMP3 KO).

MicroCT analysis suggested that at 8 weeks of age, there are no statistically significant difference between femora and tibia-fibula complexes of WT and RAMP3 KO female mice. Table 2.13 below details the arithmetic means \pm standard error of means (SEM) along with statistical significance (red). Figure 2.30 is a graphical representation of the same.

Table 2.13: Statistical analysis of 8 week old male whole femur and tibia.

Bone morphometric parameter	Units	WT Mean \pm SEM.	RAMP3 KO Mean \pm SEM.	P Value	Significance
8 week female whole femur BV	mm ³	10.28 \pm 0.45 n=4	10.69 \pm 0.24 n=4	0.4594	NS
8 week female whole tibia-fibula BV	mm ³	11.03 \pm 0.28 n=4	11.17 \pm 0.18 n=4	0.6704	NS

Whole femur bone volume - 8 week females



Whole tibia-fibula bone volume - 8 week females

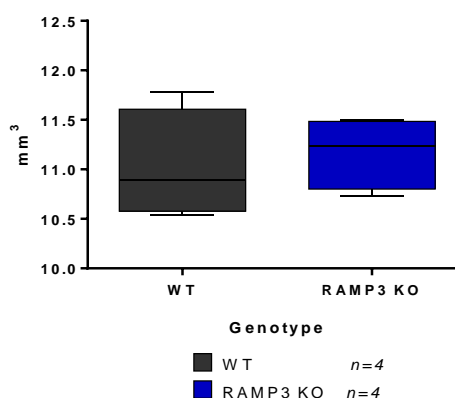


Fig 2.30: Box and whisker plot showing whole femur (left) and tibia (right) bone volume of 8 week old WT and RAMP3 KO female mice. Unpaired Student's T- test showed no significant differences in whole bone volume of WT and RAMP3 KO femora and tibia-fibula complexes.

2.3.3ii.b Femur cortical bone:

No significant differences were observed in 8 week old WT and RAMP3 KO male and female femur cortices. Table 2.14 below details the means \pm standard error of means (SEM) along with statistical significance. Figure 2.31 overleaf is a graphical representation of the same.

Table 2.14: Statistical analysis of 8 week old male whole femur cortical bone.

Bone morphometric parameter	Units	WT Mean \pm SEM.	RAMP3 KO Mean \pm SEM.	P Value	Significance
8 week male femur cortical BV	mm ³	0.83 \pm 0.02 n=7	0.77 \pm 0.04 n=6	0.4630	NS
8 week male femur cortical Th	mm	0.23 \pm 0.01 n=7	0.23 \pm 0.01 n=6	0.5480	NS
8 week female femur cortical BV	mm ³	0.71 \pm 0.02 n=4	0.70 \pm 0.02 n=4	0.8408	NS
8 week female femur cortical Th	mm	0.21 \pm 0 n=4	0.2 \pm 0.01 n=4	0.4263	NS

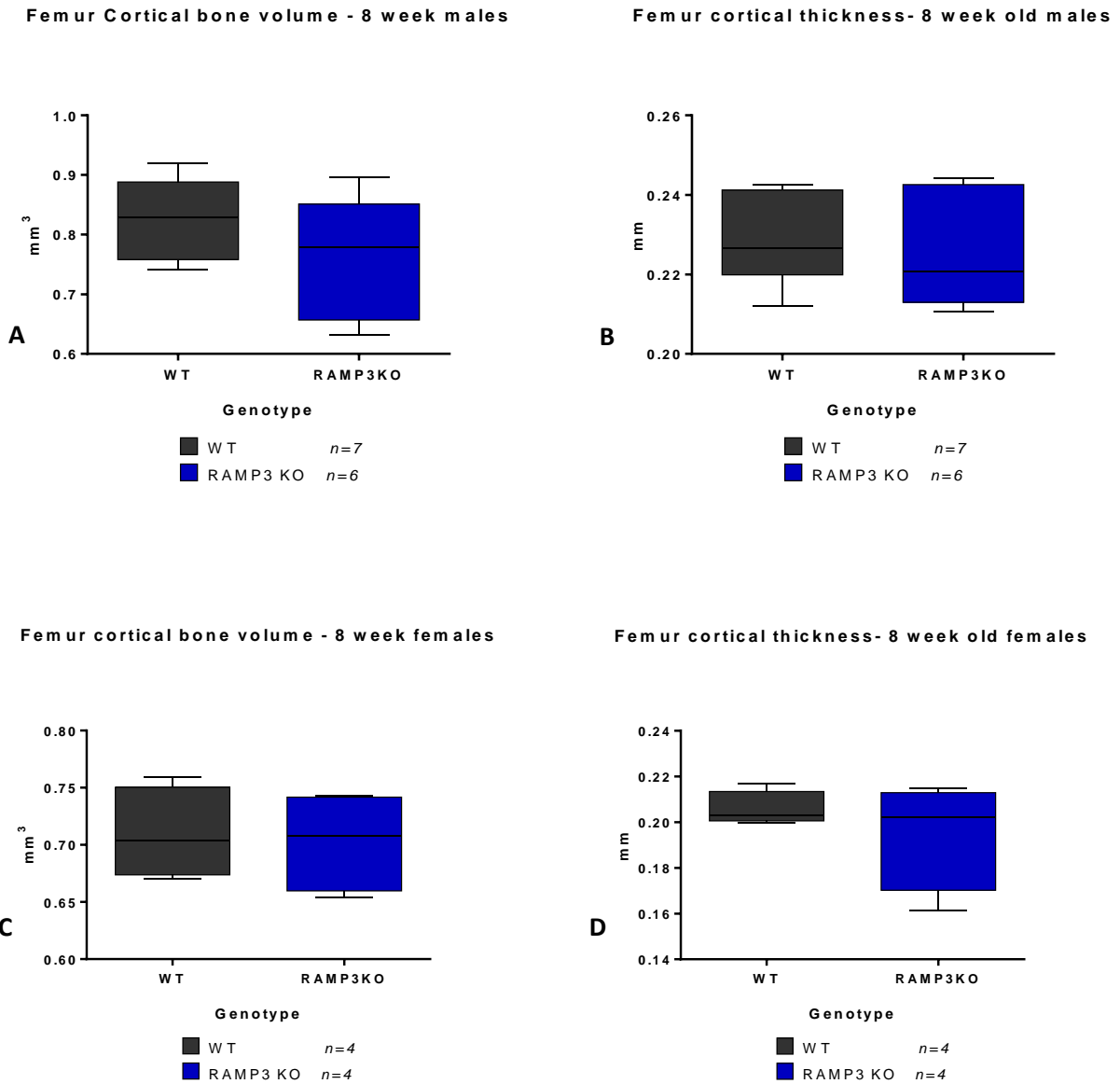


Fig 2.31: Box and whisker plot showing femur cortical bone volume (left) and thickness (right) of 8 week old WT and RAMP3 KO male (A,B) and female (C,D) mice. Unpaired Student's T- test demonstrated no significant differences in the bone volume and thickness between WT and RAMP3 KO male and female, femur cortices. Males: n=7 (WT) and 6 (RAMP3 KO). Females: n=4 each genotype.

2.3.3.ii.c Tibia cortical bone:

No significant differences were observed in 8 week old WT and RAMP3 KO male and female tibia cortical bone volume and female tibia cortical thickness. However, in RAMP3 KO male mice, tibia cortical thickness was significantly reduced. Table 2.15 below details the means \pm standard error of means (SEM) along with statistical significance (red). Figure 2.32 is a graphical representation of the same.

Table 2.15: Statistical analysis of 8 week old male whole tibia cortical bone.

Bone morphometric parameter	Units	WT Mean \pm SEM.	RAMP3 KO Mean \pm SEM.	P Value	Significance
8 week male tibia cortical BV	mm ³	0.87 \pm 0.03 n=7	0.82 \pm 0.02 n=7	0.2139	NS
8 week male tibia cortical Th	mm	0.18 \pm 0.00 n=7	0.16 \pm 0.00 n=7	0.0203	*
8 week female tibia cortical BV	mm ³	0.74 \pm 0.02 n=4	0.84 \pm 0.07 n=4	0.2588	NS
8 week female tibia cortical Th	mm	0.18 \pm 0.06 n=4	0.18 \pm 0 n=4	0.6396	NS

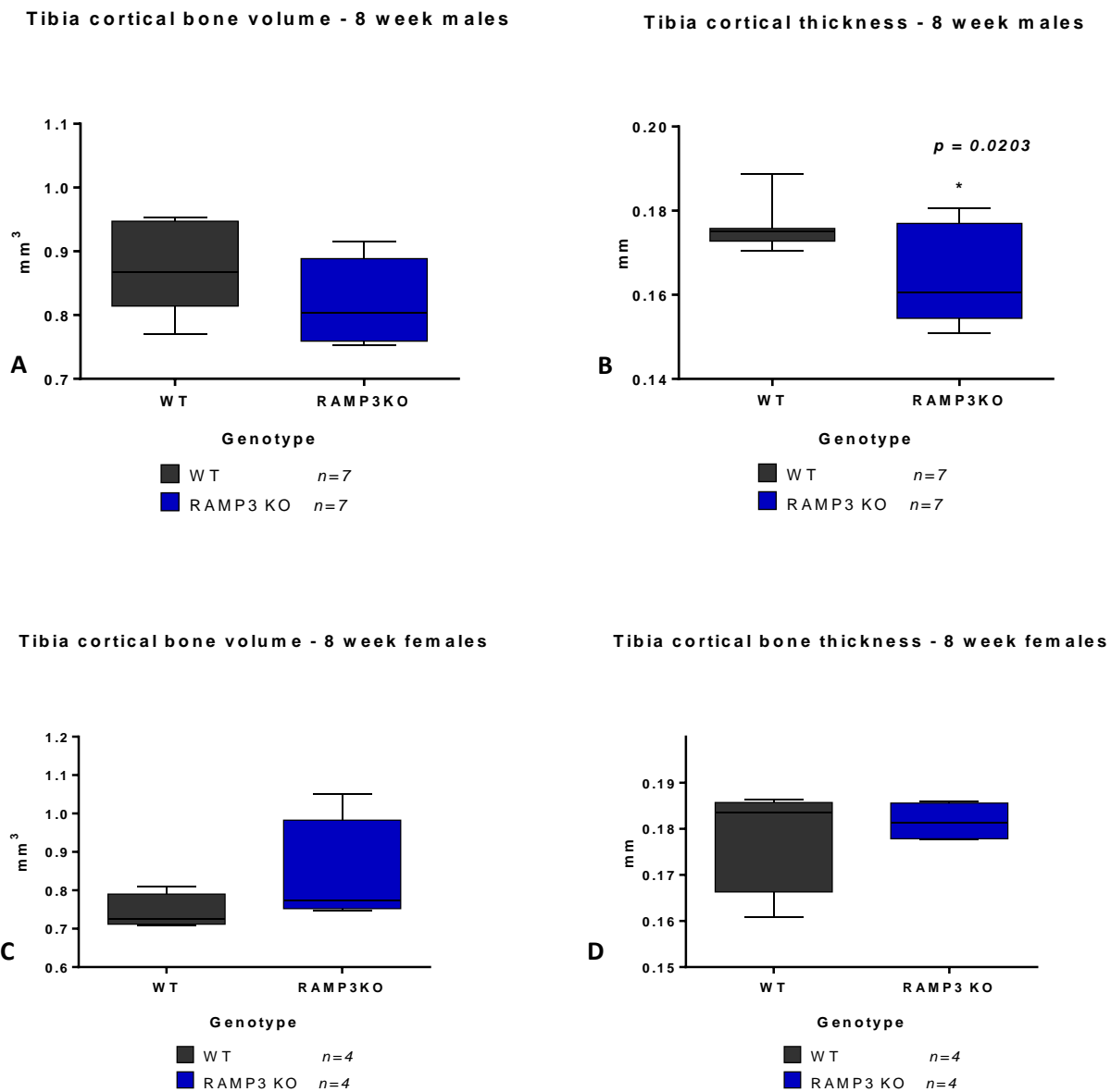


Fig 2.32: Box and whisker plot showing whole tibia cortical bone volume (left) and thickness (right) of 8 week old WT and RAMP3 KO male (A,B) and female (C,D) mice. Unpaired Student's T- test demonstrated a significant decrease in RAMP3 KO tibia thickness (p value=0.0203) compared to WT male mice (B). No significant difference was detected in the tibial bone volume in both males and females and cortical thickness in females. Males: $n=7$ each group, females: $n=4$ each group.

2.3.3.ii.d Femur trabecular bone:

Eight week old male WT and RAMP KO mice did not show any significant difference in femur trabecular architecture, except for pattern factor. RAMP3 KO mice had significantly higher femur trabecular pattern factor (Pf) compared to WT. In females, RAMP3 KO mice had a significant increase in femur trabecular thickness compared to WTs. Table 2.16 below, details the mean \pm standard error of mean (SEM) for WT and RAMP3 KO samples along with the statistical significance (red). Figures 2.33 and 2.34 are graphical representation of the statistical analysis in males and females.

Table 2.16: Statistical analysis of 8 week old male whole tibia cortical bone.

Bone morphometric parameter	Units	WT Mean \pm SEM.	RAMP3 KO Mean \pm SEM.	P Value	Significance
8 week male femur trabecular BV	mm ³	0.27 \pm 0.01 n=6	0.27 \pm 0.01 n=6	0.8491	NS
8 week male femur trabecular BV/TV	%	6.99 \pm 0.49 n=4	6.24 \pm 0.44 n=4	0.2960	NS
8 week male femur trabecular Th	mm	0.04 \pm 0.00 n=6	0.04 \pm 0.00 n=6	0.9635	NS
8 week male femur trabecular Sp	mm	0.34 \pm 0.01 n=6	0.36 \pm 0.01 n=6	0.2121	NS
8 week male femur trabecular N	1/mm	0.83 \pm 0.05 n=5	0.94 \pm 0.11 n=6	0.4182	NS
8 week male femur trabecular Pf	1/mm	22.84 \pm 1.00 n=7	25.80 \pm 0.76 n=7	0.0368	*
8 week female femur trabecular BV	mm ³	0.3 \pm 0.01 n=4	0.31 \pm 0.01 n=4	0.6110	NS
8 week female femur trabecular BV/TV	%	8.0 \pm 0.3 n=4	8.6 \pm 0.3 n=4	0.1899	NS
8 week female femur trabecular Th	mm	0.04 \pm 0.001 n=4	0.05 \pm 0.0012 n=4	0.0299	*
8 week female femur trabecular Sp	mm	0.32 \pm 0.011 n=4	0.32 \pm 0.003 n=4	0.9321	NS
8 week female femur trabecular N	1/mm	1.89 \pm 0.05 n=4	1.91 \pm 0.08 n=4	0.8665	NS
8 week female femur trabecular Pf	1/mm	20.6 \pm 1.0 n=4	19.3 \pm 0.5 n=4	0.2913	NS

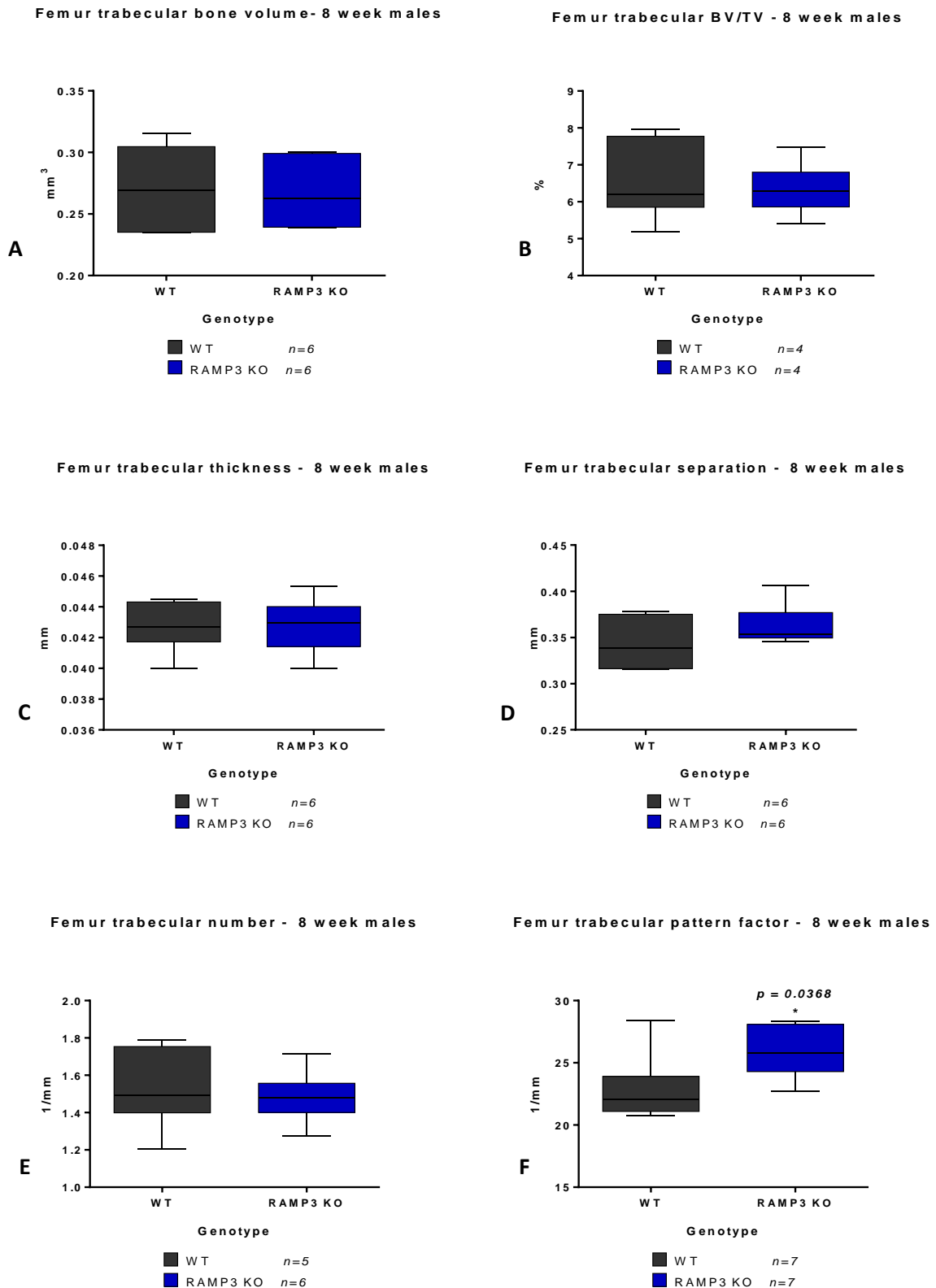
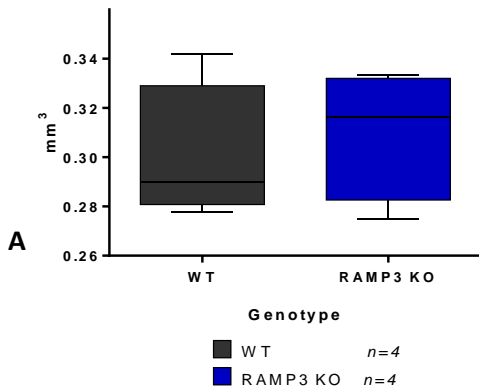
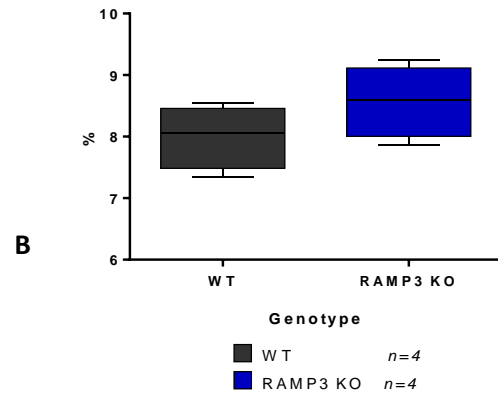


Fig 2.33: Box and whisker plot showing femur trabecular analysis in 8 week old WT and RAMP3 KO males. Unpaired Student's T- test showed that male WT and RAMP3 KO do not have any significant differences in trabecular BV (A), BV/TV (B), Th(C), Sp (D), N (E). However femur trabecular Pf (F) in RAMP3 KO mice is higher than WT mice. WT n=6 (BV, Th and Sp), n=4 (BV/TV), n=5 (N) and n=7 (Pf). RAMP3 KO n=6 (BV, Th, Sp and N), n=4 (BV/TV) and n=7 (Pf).

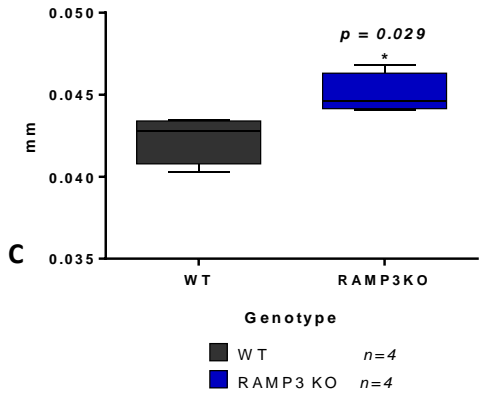
Femur trabecular bone volume- 8 week females



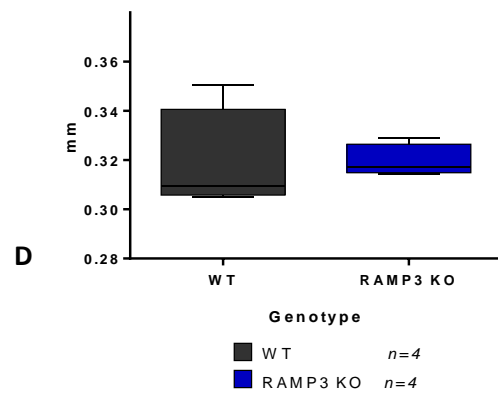
Femur trabecular BV/TV - 8 week old females



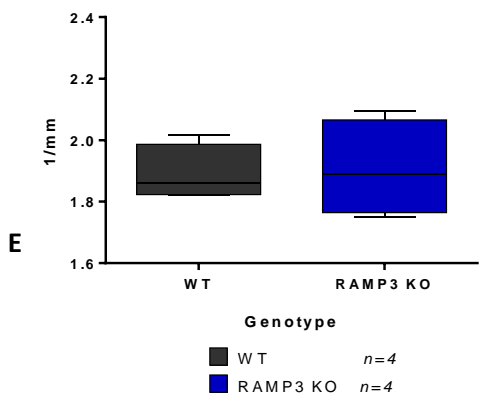
Femur trabecular thickness - 8 week females



Femur trabecular separation - 8 week females



Femur trabecular number - 8 week females



Femur trabecular pattern factor - 8 week females

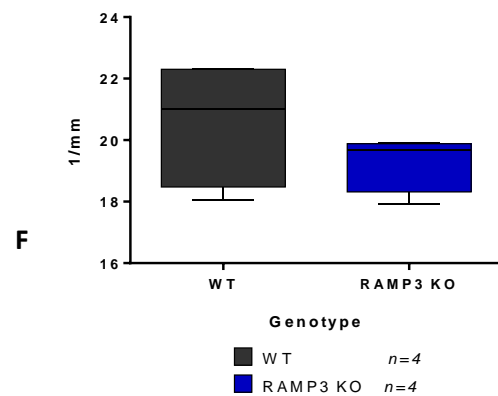


Fig 2.34: Box and whisker plot showing femur trabecular analysis in 8 week old WT and RAMP3 KO females. Unpaired Student's T- test showed that female WT and RAMP3 KO do not have any significant differences in trabecular BV (A), BV/TV (B), Sp (D), N (E) and Pf (F). However femur trabecular Th(C) in RAMP3 KO mice is significantly higher than WT mice ($p=0.029$). $n=4$ each group.

2.3.3.ii.e Tibia trabecular bone:

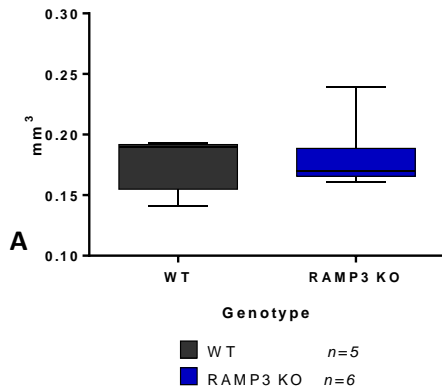
MicroCT analysis of tibia trabecular bone of 8 week old WT and RAMP3 KO males suggested a significant increase in trabecular thickness of RAMP3 KO mice compared to WT. There were no other trabecular differences determined. In females, the RAMP3 KO mice had a significant increase in tibia trabecular bone volume/tissue volume ratio (BV/TV), trabecular thickness (Th), and trabecular number (N). There was a significant reduction in trabecular separation (Sp).

Table 2.17 below, details mean \pm standard error of mean (SEM) for WT and RAMP3 KO samples along with the statistical significance (red). Figures 2.35 and 2.36 are graphical representation of the statistical analysis of male and female tibia trabecular bone.

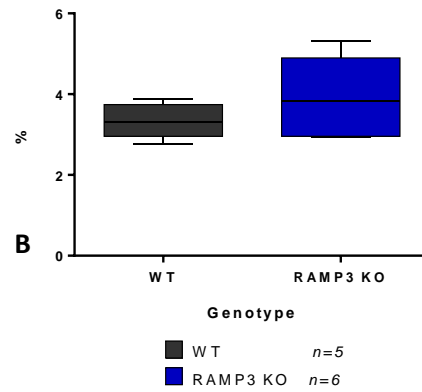
Table 2.17: Statistical analysis of 8 week old male whole tibia trabecular bone.

Bone morphometric parameter	Units	WT Mean \pm SEM.	RAMP3 KO Mean \pm SEM.	P Value	Significance
8 week male tibia trabecular BV	mm ³	0.18 \pm 0.019 n=5	0.18 \pm 0.01 n=6	0.8465	NS
8 week male tibia trabecular BV/TV	%	3.34 \pm 0.19 n=5	3.94 \pm 0.40 n=6	0.2437	NS
8 week male tibia trabecular Th	mm	0.04 \pm 0.00 n=5	0.04 \pm 0.00 n=6	0.0155	*
8 week male tibia trabecular Sp	mm	0.61 \pm 0.02 n=5	0.55 \pm 0.05 n=6	0.2741	NS
8 week male tibia trabecular N	1/mm	0.83 \pm 0.05 n=5	0.94 \pm 0.11 n=6	0.4182	NS
8 week male tibia trabecular Pf	1/mm	52.10 \pm 10.29 n=5	50.02 \pm 8.36 n=6	0.8769	NS
8 week female tibia trabecular BV	mm ³	0.13 \pm 0.01 n=4	0.13 \pm 0.01 n=4	0.7735	NS
8 week female tibia trabecular BV/TV	%	4. \pm 0.2 n=4	5.25 \pm 0.22 n=4	0.0058	**
8 week female tibia trabecular Th	mm	0.04 \pm 0.001 n=4	0.05 \pm 0.001 n=4	0.0436	*
8 week female tibia trabecular Sp	mm	0.53 \pm 0.01 n=4	0.42 \pm 0.03 n=4	0.0150	*
8 week female tibia trabecular N	1/mm	0.93 \pm 0.04 n=4	1.17 \pm 0.04 n=4	0.0047	**
8 week female tibia trabecular Pf	1/mm	29.23 \pm 2.5 n=4	28.43 \pm 0.74 n=4	0.7696	NS

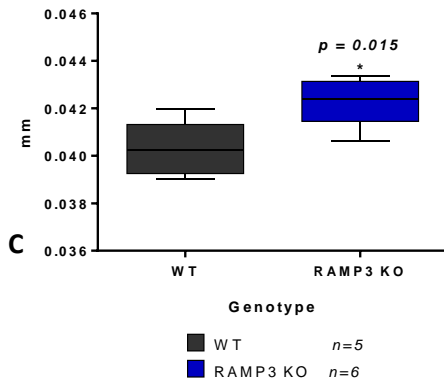
Tibia trabecular bone volume- 8 week males



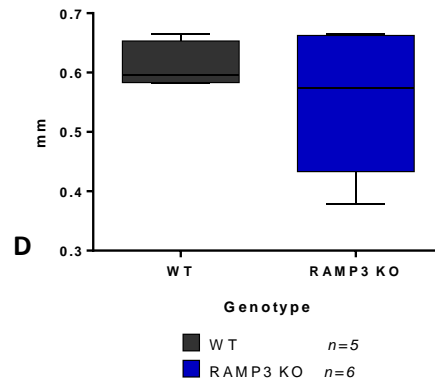
Tibia trabecular BV/TV - 8 week males



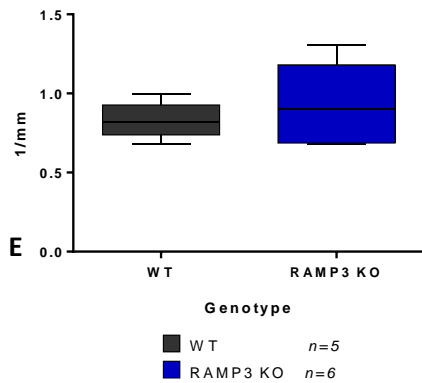
Tibia trabecular thickness - 8 week males



Tibia trabecular separation - 8 week males



Tibia trabecular number - 8 week females



Tibia Trabecular Pattern factor- 8 week males

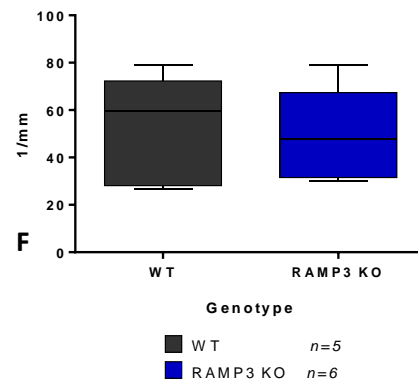
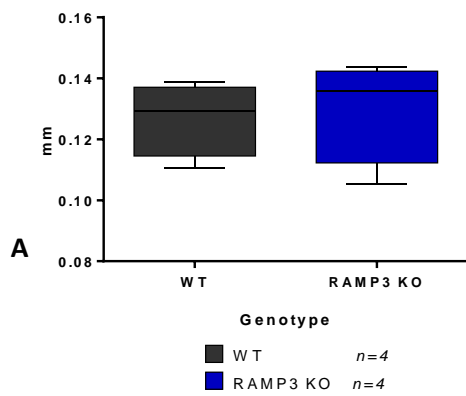
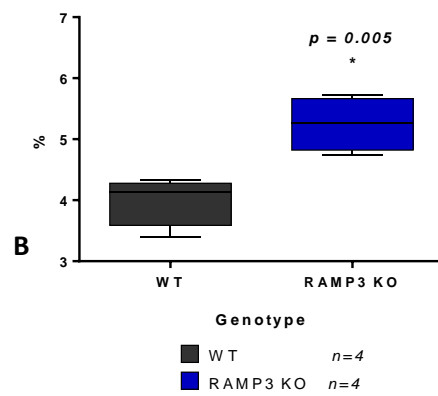


Fig 2.35: Box and whisker plot showing tibia trabecular analysis in 8 week old WT and RAMP3 KO males. Unpaired Student's T- test showed that male RAMP3 KO trabecular bone has significant increase in trabecular Th, $p=0.035$ (C) compared to WT. No significant differences observed in trabecular BV (A), BV/TV (B), Sp (D), N (E) and Pf(F). WT $n=5$ and RAMP3 KO $n=6$.

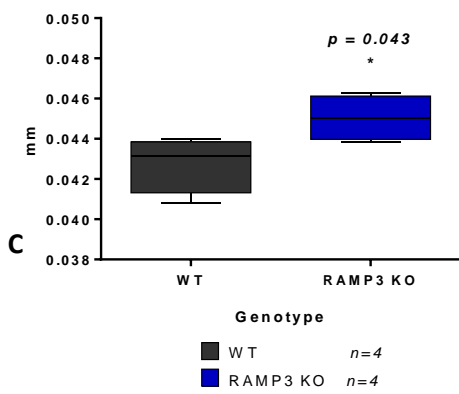
Tibia trabecular bone volume- 8 week old females



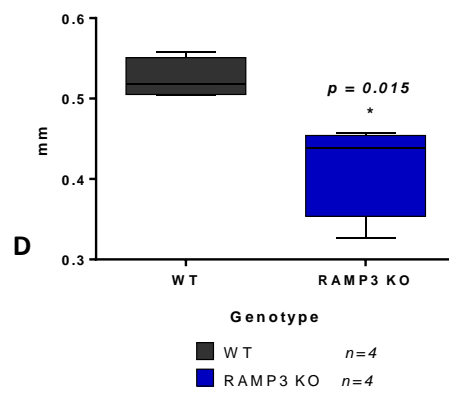
Tibia trabecular BV/TV - 8 week females



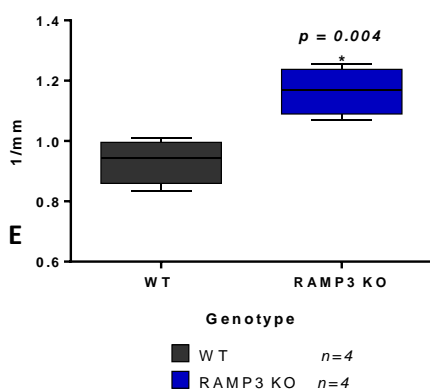
Tibia trabecular thickness - 8 week females



Tibia trabecular separation - 8 week females



Tibia trabecular number - 8 week females



Tibia Trabecular Pattern factor- 8 week females

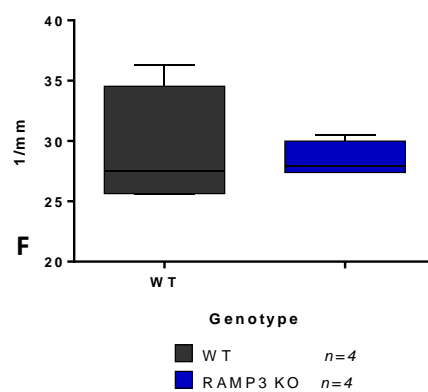


Fig 2.36: Box and whisker plot showing tibia trabecular analysis in 8 week old WT and RAMP3 KO females. Unpaired Student's T- test showed that male RAMP3 KO trabecular bone has significant increase in trabecular BV/TV ($p=0.015$), Th ($p=0.043$), N ($p=0.004$) and a significant decrease in trabecular separation (Sp) ($p=0.015$) compared to WT. $n=4$ each group.

2.3.3.ii.f Three dimension skeletal models: Three-dimensional models were generated from microCT scans of bones using Voxler rendering software (Fig. 2.37 below). Individual models reflected the data observed in microCT analyses.

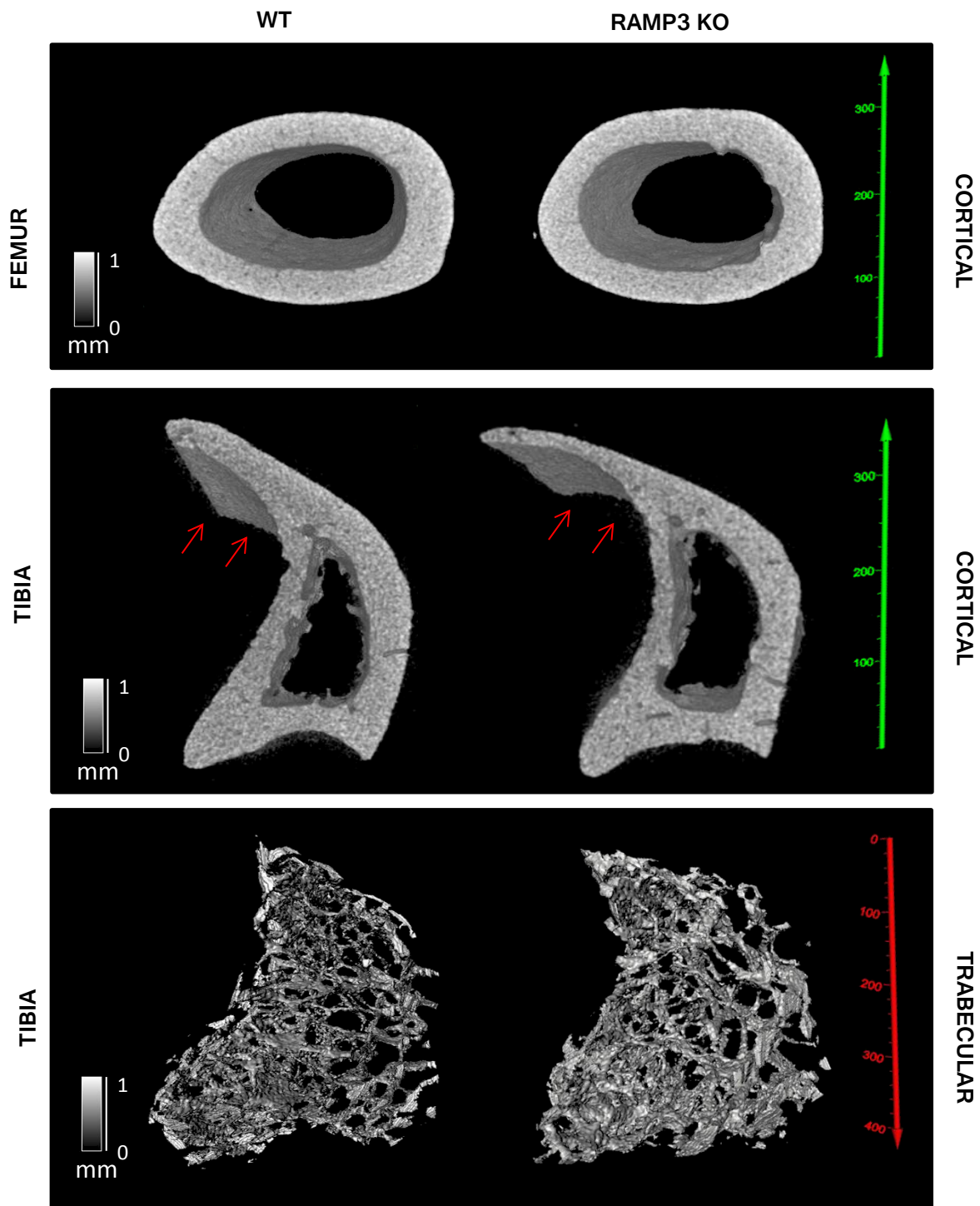


Fig 2.37: Representative 3D skeletal models of femur cortical, tibia cortical and tibia trabecular bone (from top to bottom). WTs are to the left and RAMP3 KO are to the right. RAMP3 KO tibia show longer and thinner tibial crest (red arrows) responsible for reduction in total tibia cortical thickness of RAMP3 KOs in microCT. The last bottom panel shows thicker trabecular structure in RAMP3 KO models compared to WT, again reflecting the increase in trabecular thickness in RAMP3 KOs seen in the microCT analysis earlier.

2.3.3.iii Dynamic histomorphometry:

The distance between double calcein labels was determined on lateral and medial endocortical surface by fluorescent microscopy. The inter-label width determined was then used to calculate the bone apposition rate on the endocortical surface. Figure 2.38 shows representative images of whole tibia longitudinal section and an enlarged view of an analysed region on the lateral endocortical surface. The following Fig. 2.39 overleaf shows representative fields of view of lateral and medial endocortical surface of WT (n=4) and RAMP3 KO (n=4). Table 2.18 (overleaf) summaries the mean \pm SEM values of inter-label width and bone apposition rate and respective statistical significance (red). Lastly, Fig. 2.40 is a graphical representation of the inter-label width and bone apposition rate analysis.

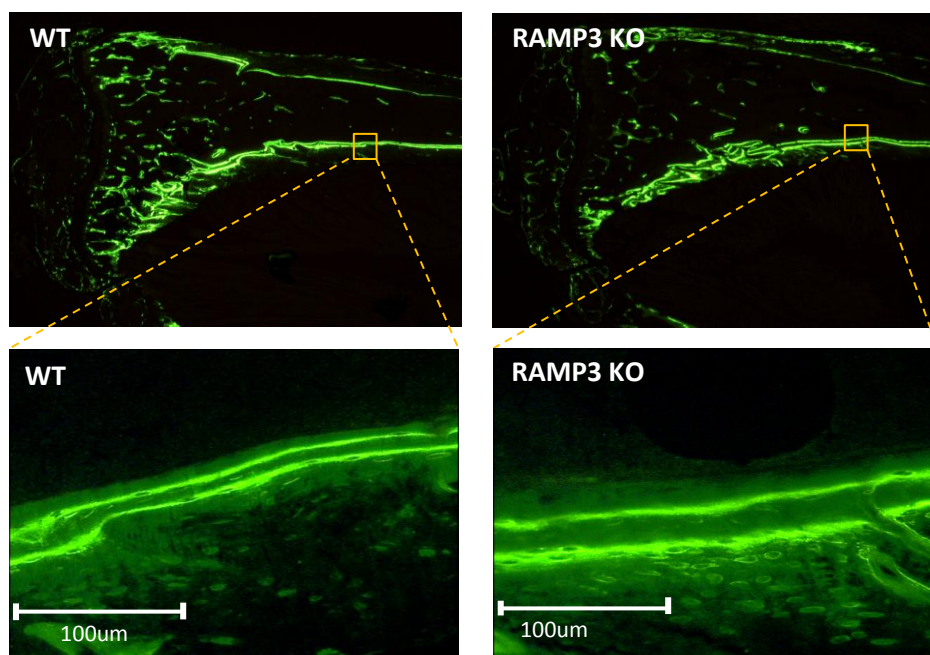


Fig 2.38: Representative images of plastic embedded whole tibia longitudinal section of WT (left, top) and RAMP3 KO (right, top) 8 week old male mice. Bottom panels are zoomed images of an analysed region of the lateral endocortical surface showing increased inter-label width in the RAMP3 KO (right, bottom) compared to WT (left, bottom). WT n=5 and RAMP3 KO n=6.

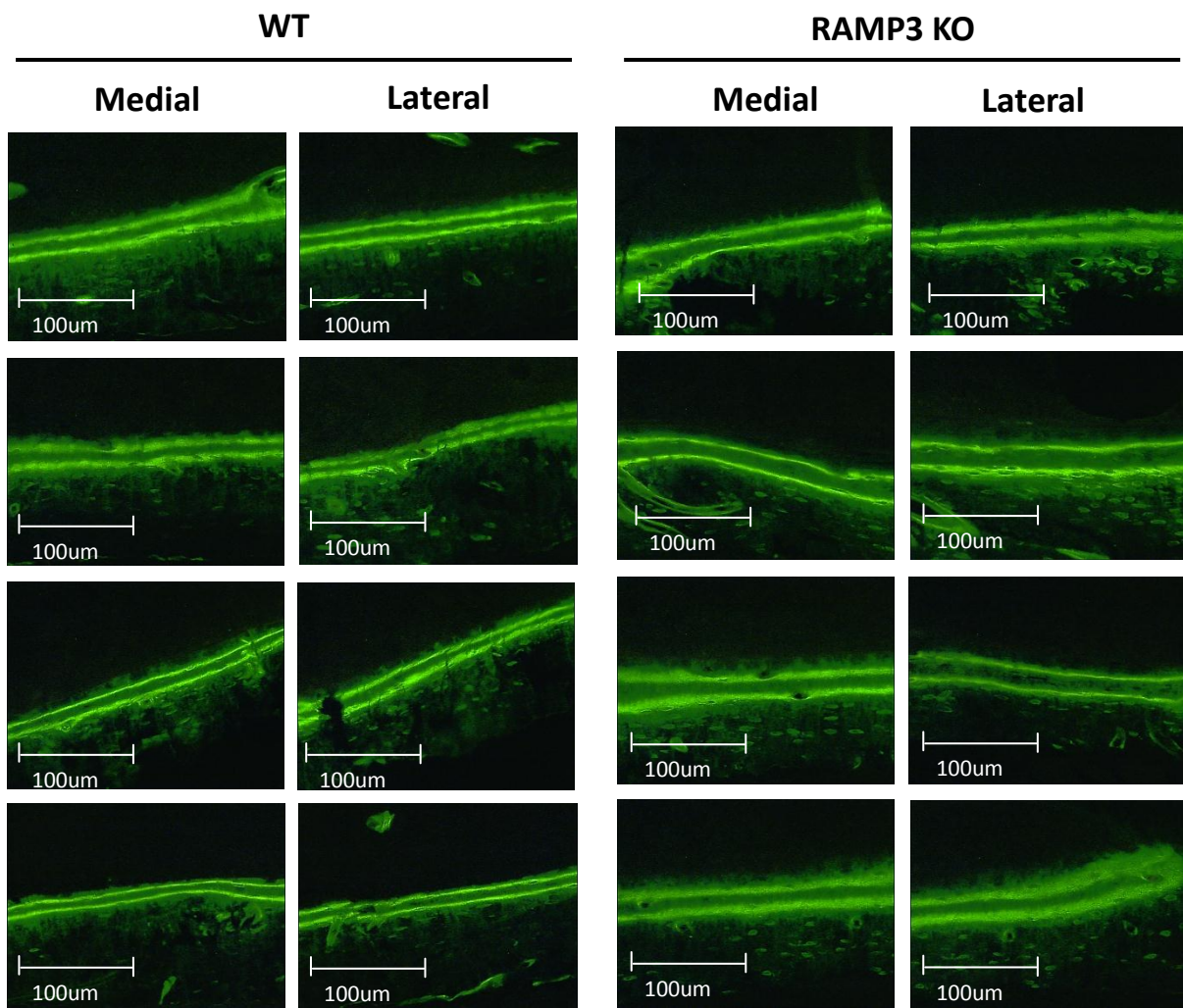


Fig 2.39: Representative 'fields of view' of medial and lateral endocortical surface of four WT (left) and four RAMP3 KO (right) plastic embedded tibia longitudinal sections. Increased inter-label width is evident in all eight RAMP3 KO panels compared to the WTs. n = 4.

Table 2.18: Statistical analysis – dynamic histomorphometry of 8 week old males

Bone morphometric parameter	Units	WT Mean \pm SEM.	RAMP3 KO Mean \pm SEM.	P Value	Significance
8 week male inter Calcein label width	μm	10.66 \pm 0.85 n=5	14.88 \pm 1.19 n=6	0.0218	*
8 week male bone apposition rate	$\mu\text{m/day}$	1.52 \pm 0.12 n=5	2.12 \pm 0.17 n=6	0.0223	*

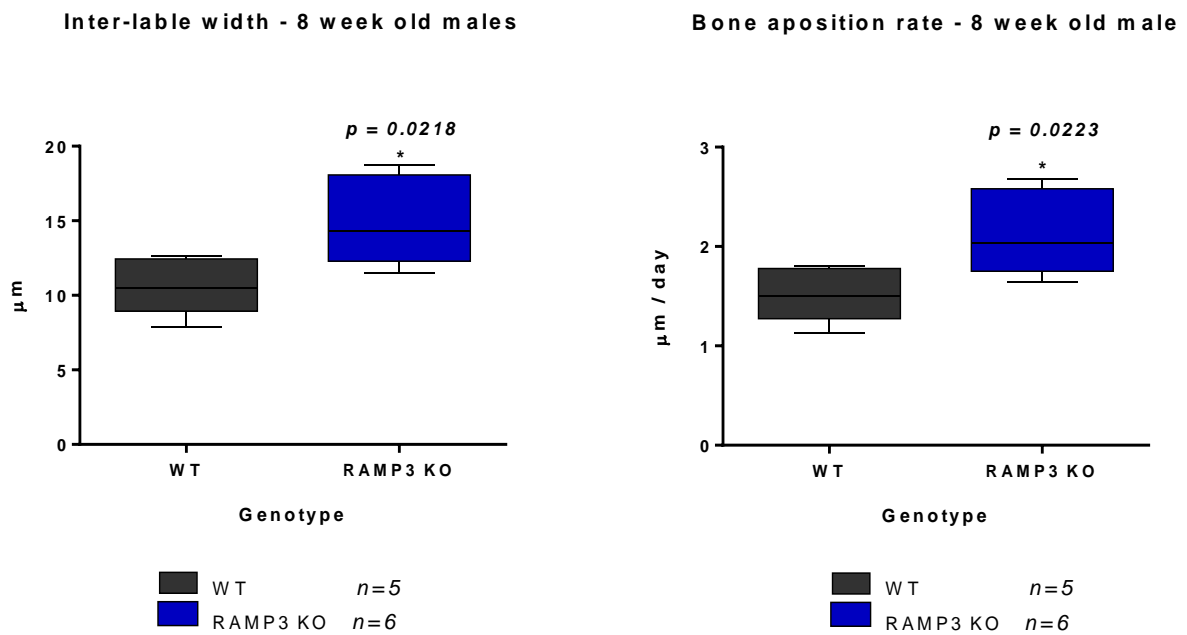


Fig 2.40: Box and whisker plots for inter label width (left) and bone apposition rate (right) of 8 week old male tibia-endocortical surfaces. RAMP3 KO mice have significant increase in both, the inter-label width ($p=0.0218$) and the bone apposition rate ($p=0.0223$). WT n=5 and RAMP3 KO n=6.

2.3.3.iv Histology:

Both Haematoxylin and Eosin (H&E) stained and Tartrate-resistant acid phosphatase (TRAP) stained tibia sections revealed differences in trabecular area, number of osteoblasts and osteoclasts and growth plate of WT and RAMP3 KO mice in histological analyses.

Noticeable structural differences observed in tibia sections: RAMP3 KO tibia were narrower, had differences in the arrangement of chondrocytes in the growth plate and increase in the area and surface of trabecular unit compared to WT (Fig. 2.41).

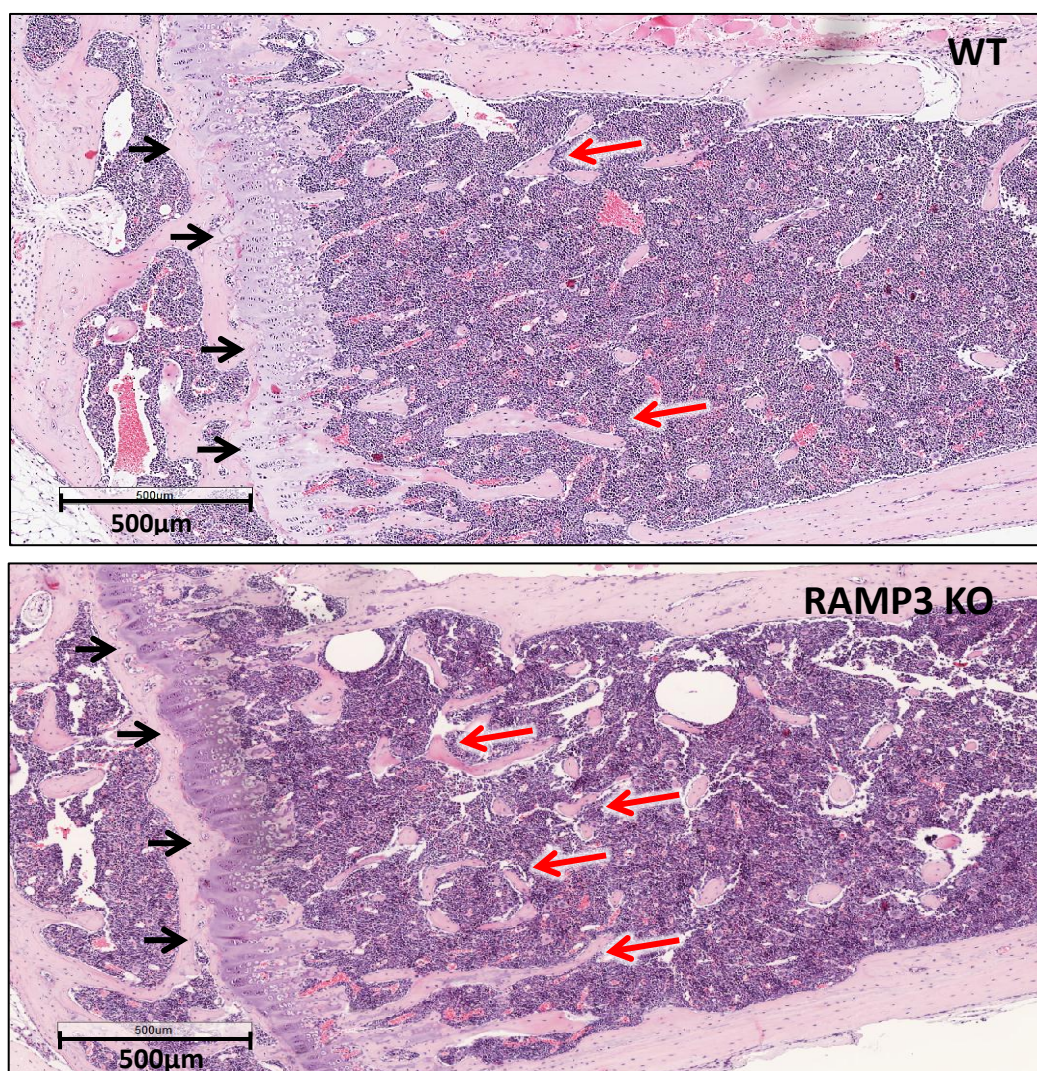


Fig 2.41: Representative H&E stained longitudinal tibia section of WT (top) and RAMP3 KO (bottom) 8 week old males. The tibiae in RAMP3 KO mice were observed to be narrower than WT. RAMP3 KO and WT mice had differences in the arrangement of chondrocyte in the growth plate (black arrows). Trabecular area and surface was higher in RAMP3 KO mice (red arrows).

2.3.3.iv.a Trabecular analysis

H&E stained sections showed significant increase in total trabecular area and trabecular thickness (average trabecular area per trabecular unit) in RAMP3 KO males compared to WT males. Unpaired Student's t-test was used to determine the statistical significance. Table 2.19 summarises mean \pm SEM values and respective statistical significance. Figure 2.42 is a graphical representation of the same.

Table 2.19: Statistical analysis – Histology: trabecular analysis 8 week old males.

Bone morphometric parameter	Units	WT Mean \pm SEM.	RAMP3 KO Mean \pm SEM.	P Value	Significance
8 week male tibia total trabecular area	μm^2	187746 \pm 14532 n=5	265877 \pm 20627 n=5	0.0147	*
8 week male tibia total trabecular surface	μm	13422 \pm 959.4 n=5	16074 \pm 1327 n=5	0.1440	NS
8 week male tibia average trabecular area per trabecular unit (trabecular thickness)	μm^2	5566 \pm 525.5 n=5	8365 \pm 1077 n=5	0.0477	*
8 week male tibia total number of trabecular units	Arbitrary number	34.00 \pm 1.30 n=5	33.20 \pm 3.43 n=5	0.8327	NS

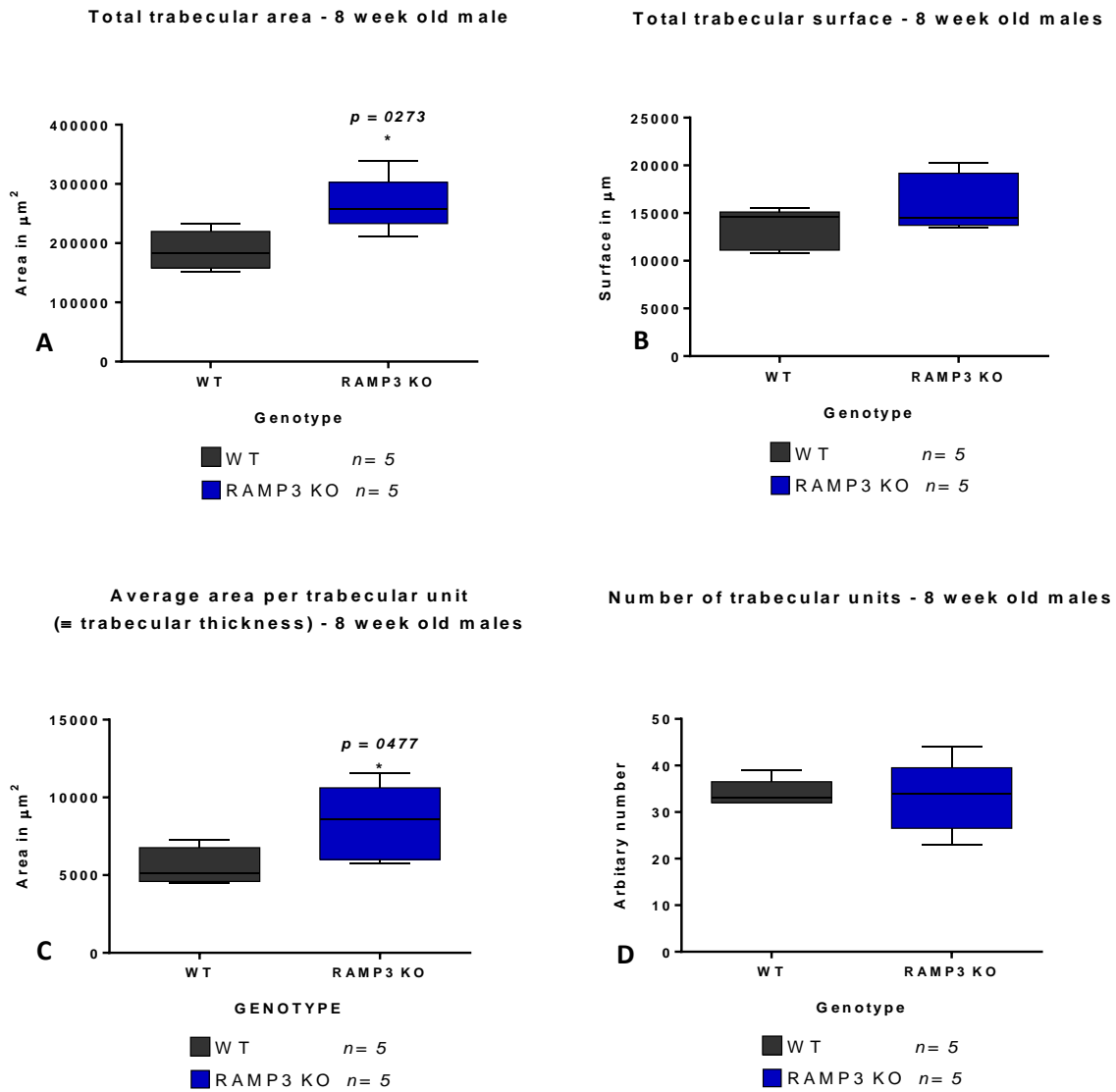


Fig 2.42: Box and whisker plots representing statistical analysis of trabecular measurements in tibia sections of 8 week old RAMP3 KO and WT male mice. Unpaired t-test suggests, RAMP3 KO mice have significantly increased total trabecular area (A) and average trabecular area per unit (trabecular thickness) (C). No significant difference was determined in trabecular surface (B) and number of trabecular unites (D) between RAMP3 KO and WT mice. Three sections were measured per sample. $n=5$ each group.

2.3.3.v Osteoblasts and osteoclasts quantification:

Number of osteoblasts and osteoclasts were determined on the endocortical and trabecular surfaces of tibia in RAMP3 KO and WT males. Considering difference in cell population on the medial and lateral endocortical surface, the number of osteoblasts and osteoclasts were counted and analysed separately for each side. Unpaired Student's t-test was used to determine the statistical significance of the differences between WT and RAMP3 KO mice.

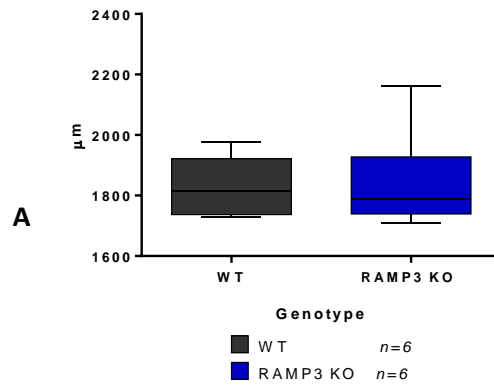
2.3.3.v.a Medial endocortical osteoblast and osteoclast quantification:

No significant differences were observed in medial endocortical bone surface (En.S), number of osteoblast (Ob.N), number of osteoclast (Oc.N), osteoblast covered bone surface (Ob.S) or osteoclast covered bone surface (Oc.S) between WT and RAMP3 KO 8 week male mice. Table 2.20 below summarises the mean \pm SEM values and statistical significance if any (red). Figure 2.43 overleaf is a graphical representation of the same.

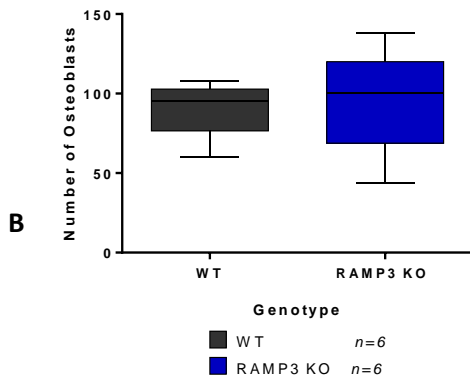
Table 2.20: Statistical analysis –medial endocortical osteoblast and osteoclast quantification.

Bone morphometric parameter	Units	WT Mean \pm SEM.	RAMP3 KO Mean \pm SEM.	P Value	Significance
Tibia, medial endocortical bone surface	μm	1830 \pm 42.87 n=6	1841 \pm 67.22 n=6	0.8916	NS
Tibia, medial endocortical osteoblast number	Arbitrary number	90 \pm 7 n=6	96 \pm 13 n=6	0.7300	NS
Tibia, medial endocortical osteoclast number	Arbitrary number	1 \pm 0 n=6	3 \pm 2 n=6	0.2518	NS
Tibia, medial endocortical osteoblast covered bone surface	μm	1282 \pm 85.15 n=6	1290 \pm 157.1 n=6	0.9663	NS
Tibia, medial endocortical osteoclast covered bone surface	μm	102.3 \pm 64.96 n=6	96.16 \pm 53.85 n=6	0.9437	NS

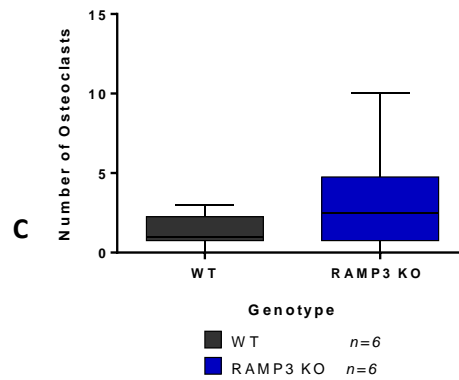
Tibia medial endocortical bone surface -
8 week old males



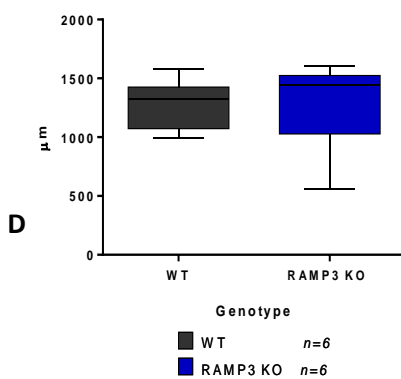
Tibia medial endocortical osteoblast number -
8 week old males



Tibia medial endocortical osteoclast number -
8 week old males



Tibia medial endocortical osteoblast covered bone surface -
8 week old males



Tibia medial endocortical osteoclast covered surface -
8 week old males

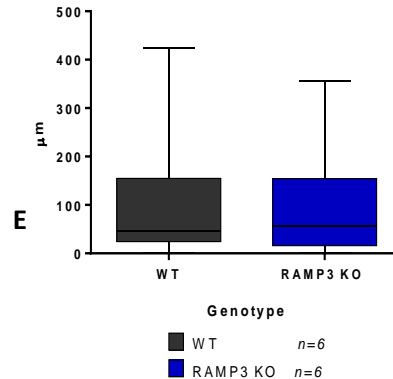


Fig 2.43: Box and whisker plots showing statistical analysis of medial endocortical osteoblast & osteoclast quantification in 8 week old male WT and RAMP3 KO mice. There was no significant difference in endocortical bone surface (En.S) (A), osteoblast number (Ob. N) (B), osteoclast number (Oc. N.) (C), osteoblast covered bone surface (Ob.S) and osteoclast covered bone surface (Oc.S) between the groups. n=6 each group.

2.3.3.v.b Lateral endocortical osteoblast and osteoclast quantification:

No significant differences were observed in lateral endocortical bone surface (En.S), number of osteoblast (Ob.N), number of osteoclast (Oc.N), osteoclast covered bone surface (Oc.S) between WT and RAMP3 KO 8 week male mice. However, RAMP3 KO mice had a significant reduction in osteoblast covered bone surface (Ob.S) indicating smaller osteoblasts in RAMP3 KO mice. Unpaired Student's t-test was used to determine the statistical significance between the WT and RAMP3 KO mice. Table 2.21 below summarises the mean \pm SEM values and statistical significance (red). Figure 2.44 overleaf is a graphical representation of the same.

Table 2.21: Statistical analysis - lateral endocortical osteoblast and osteoclast quantification.

Bone morphometric parameter	Units	WT Mean \pm SEM.	RAMP3 KO Mean \pm SEM.	P Value	Significance
Tibia, lateral endocortical bone surface	μm	2110 \pm 150.2 n=6	1864 \pm 72.76 n=6	0.1718	NS
Tibia, lateral endocortical osteoblast number	Arbitrary number	141 \pm 9 n=6	140 \pm 10 n=5	0.9282	NS
Tibia, lateral endocortical osteoclast number	Arbitrary number	1 \pm 1 n=6	1 \pm 1 n=6	0.8892	NS
Tibia, lateral endocortical osteoblast covered bone surface	μm	1990 \pm 84.28 n=6	1679 \pm 56.40 n=6	0.0118	*
Tibia, lateral endocortical osteoclast covered bone surface	μm	46.17 \pm 43.72 n=6	22.56 \pm 15.11 n=6	0.6208	NS

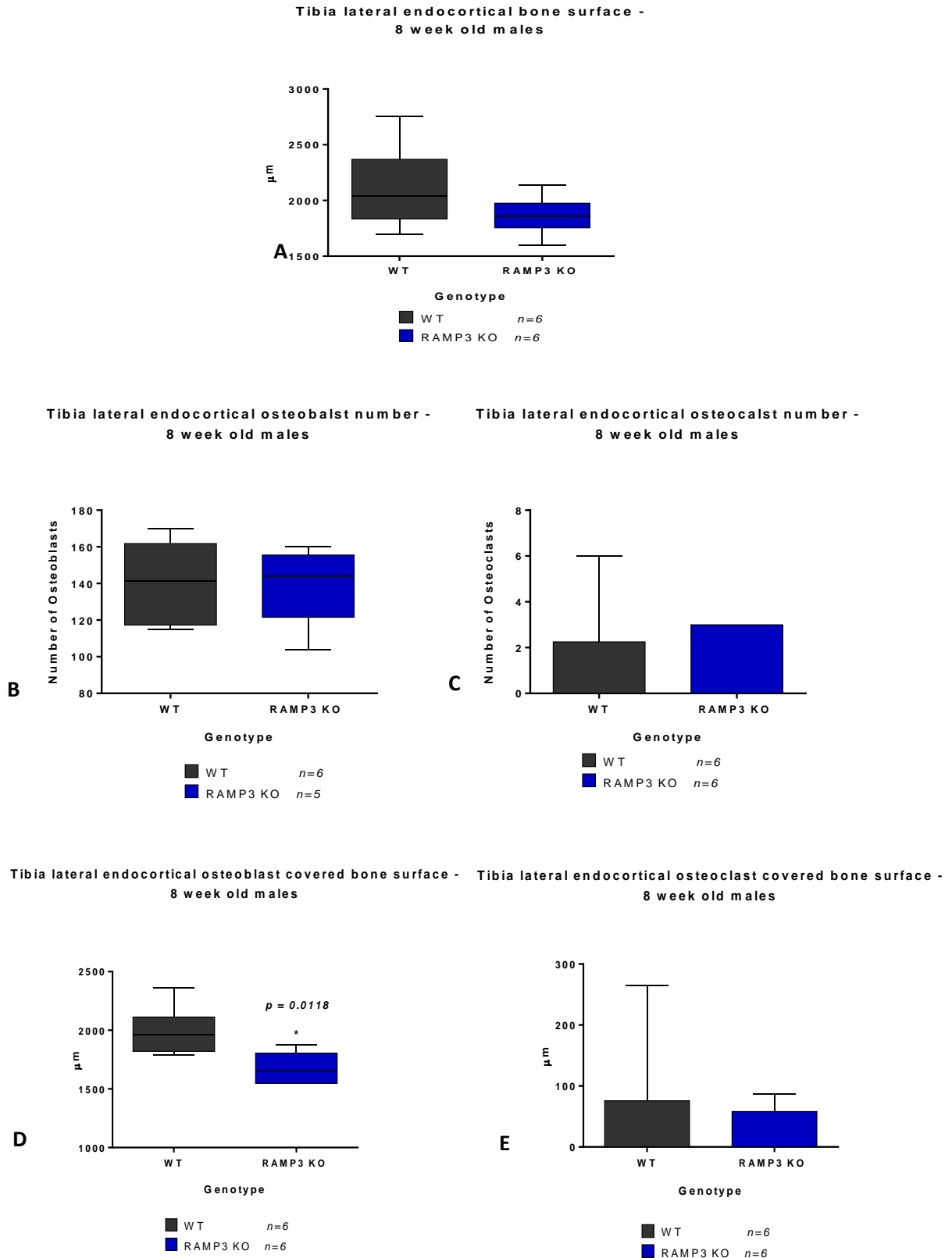


Fig 2.44: Box and whisker plots representing statistical analysis of lateral endocortical osteoblast and osteoclast quantification in 8 week old male WT and RAMP3 KO mice. There was no significant difference in endocortical bone surface (En.S) (A), osteoblast number (Ob. N) (B), osteoclast number (Oc. N.) (C) and osteoclast covered bone surface (Oc.S). There was a significant reduction in osteoblast covered bone surface (Ob.S) ($p = 0.0118$). WT $n = 5$ (Ob. N) and $n = 6$ (En.S, Oc. N, Ob.S, Oc.S).

2.3.3.v.c Trabecular osteoblast and osteoclast quantification:

In trabecular osteoblast and osteoclast quantification, RAMP3 KO mice had significantly higher trabecular bone surface, higher osteoblast number and a higher osteoblast covered bone surface compared to WT mice. There was no significant difference in osteoclast number and osteoclast covered bone surface. Table 2.22 below summarises the mean \pm SEM values and statistical significance (red). Figure 2.45 overleaf is a graphical representation of the same.

Table 2.22: Statistical analysis - lateral endocortical osteoblast and osteoclast quantification.

Bone morphometric parameter	Units	WT Mean \pm SEM.	RAMP3 KO Mean \pm SEM.	P Value	Significance
Tibia, trabecular bone surface	μm	2925 \pm 257.0 n=5	4189 \pm 339.3 n=5	0.0178	*
Tibia, trabecular osteoblast number	Arbitrary number	94 \pm 11 n=5	137 \pm 12 n=5	0.0336	*
Tibia, trabecular osteoclast number	Arbitrary number	18 \pm 2 n=5	27 \pm 5 n=5	0.1414	NS
Tibia, trabecular osteoblast covered bone surface	μm	1433 \pm 155.6 n=5	1992 \pm 174.3 n=5	0.0437	*
Tibia, trabecular osteoclast covered bone surface	μm	530.0 \pm 111.6 n=5	721.6 \pm 84.06 n=5	0.2075	NS

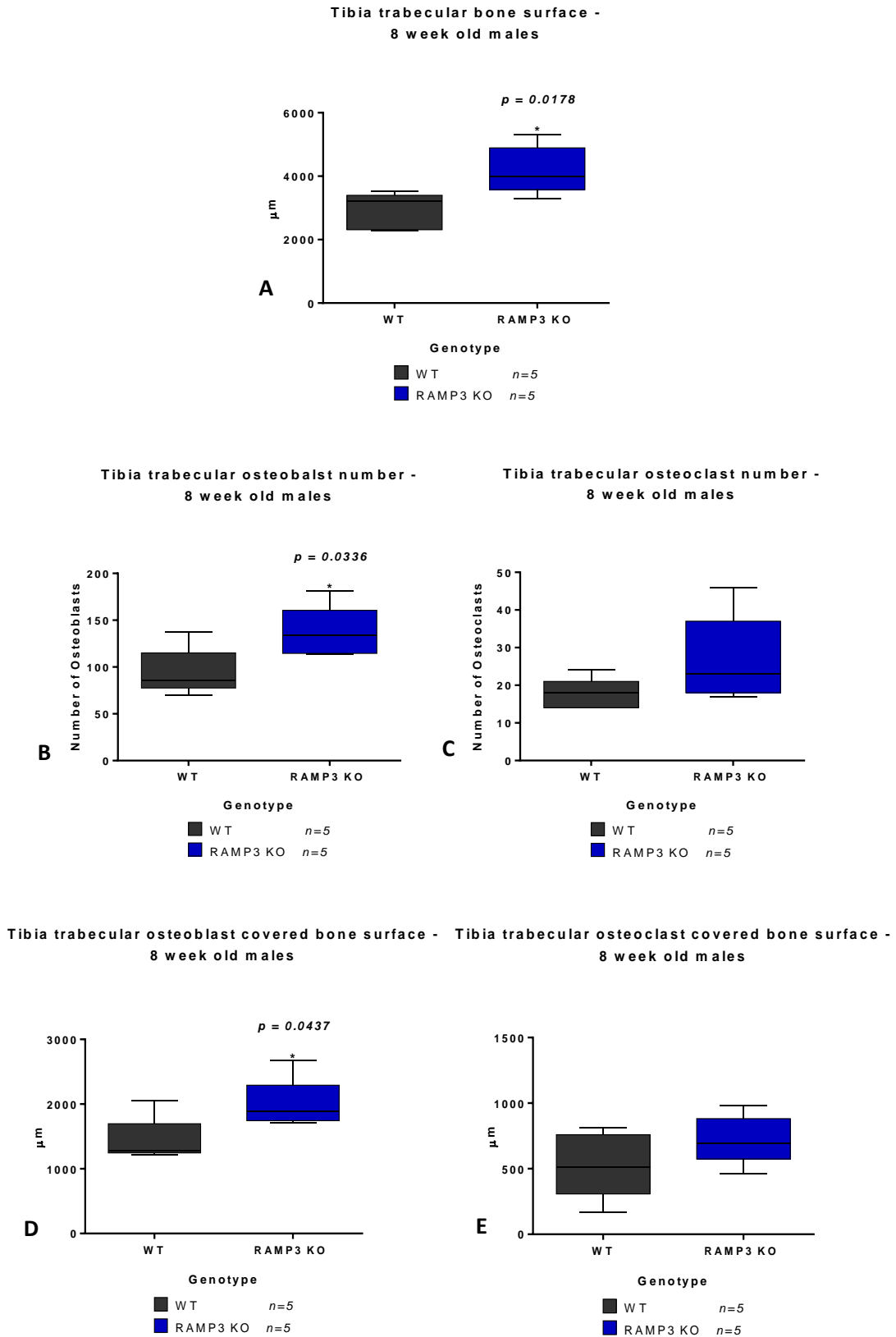


Fig 2.45: Box and whisker plots demonstrating statistical analysis of trabecular osteoblast and osteoclast quantification in 8 week old male WT and RAMP3 KO mice. There was a significant increase in trabecular bone surface ($p=0.0178$) (T.S) (A), osteoblast number ($p=0.0338$) (Ob. N) (B) and osteoblast covered bone surface ($p=0.0437$) (Ob.S). There was no significant difference in osteoclast number (Oc. N.) (C) and osteoclast covered bone surface (Oc.S). $n=5$ in both groups.

2.3.3.vi Growth plate analysis

H&E tibial sections were analysed to determine differences in growth plates of WT and RAMP3 KO mice. It was observed that RAMP3 KO mice had larger chondrocyte columns in the growth plate with larger proliferative chondrocyte zone. On the other hand, the hypertrophic zone was variable in both WT and RAMP3 KO mice. Figure 2.46 below shows three representative growth plates each genotype.

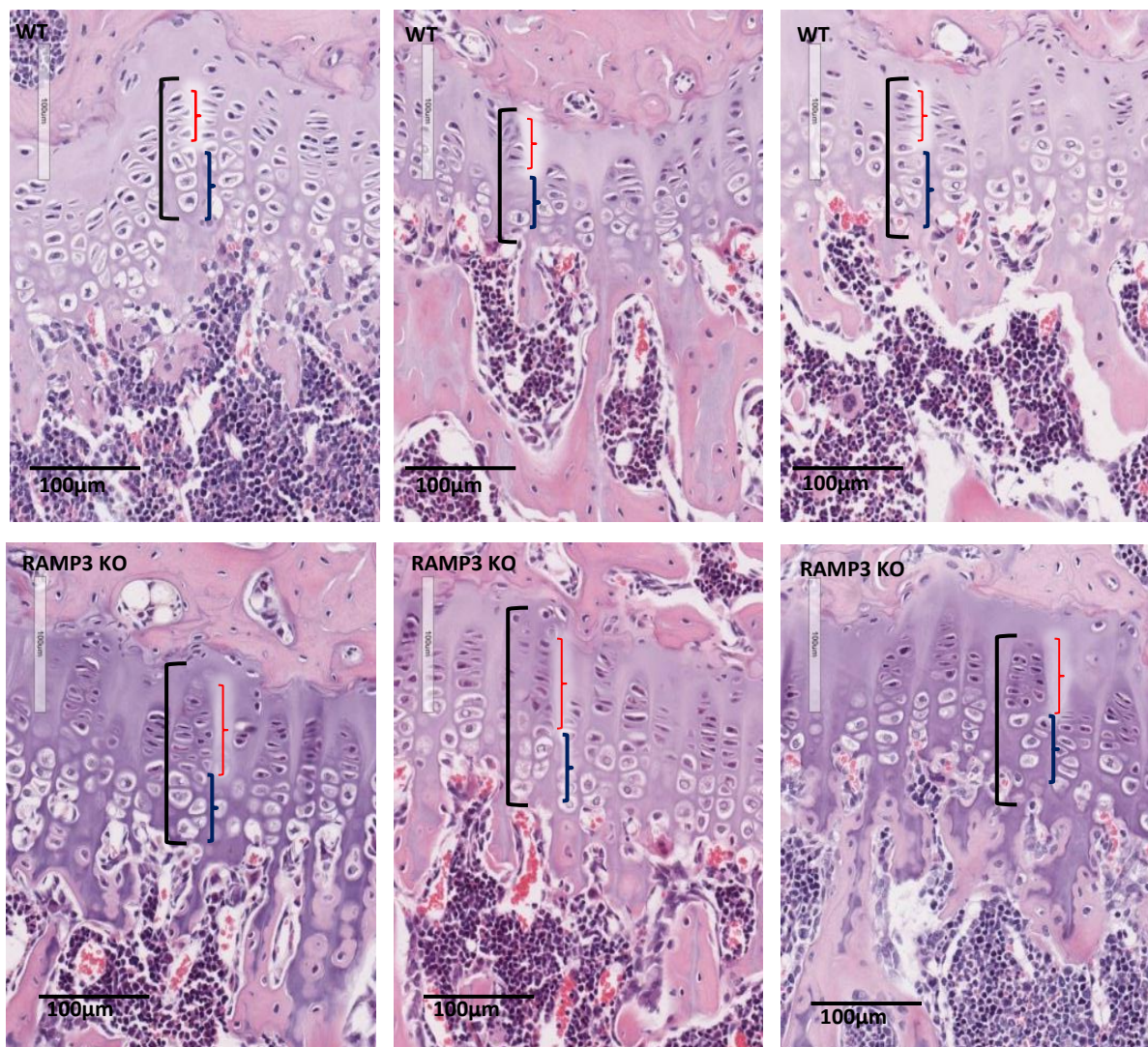


Fig 2.46: Representative images of tibial growth plates. Top three panels are WT and bottom three panels are of RAMP3 KO mice. RAMP3 KO growth plates appear to have larger chondrocyte columns (black box bracket) compared to WTs. Additionally, RAMP3 KOs had larger proliferative zone indicated by red brace bracket. Hypertrophic chondrocyte number appears to be variable in both the RAMP3 KO and WTs (blue brace bracket). Three H&E sections per bone were studied for growth plate analysis (n=6 each group).

2.3.3.vi.a Growth plate measurements: Total chondrocyte column length of 15 columns (per section of bone) was measured along with individual measurements of the proliferative and hypertrophic zones. Additionally, the average numbers of proliferative and hypertrophic cells per chondrocyte column were determined. In total 3 sections were analysed per sample where, n=6 WT and RAMP3 KO. Unpaired Student's t-test was used to determine the statistical significance in the differences between WT and RAMP3 KO mice. Table 2.23 summarizes mean \pm SEM values of these quantifications with significant differences (red). Figure 2.47 overleaf is a graphical representation of the same.

Table 2.23: Statistical analysis tibial growth plate of 8 week old male mice

Bone morphometric parameter	Units	WT Mean \pm SEM.	RAMP3 KO Mean \pm SEM.	P Value	Significance
Total chondrocyte column length	μm	162.0 \pm 6.51 n=6	189.7 \pm 7.47 n=6	0.0188	*
Proliferative zone length	μm	60.00 \pm 3.22 n=6	88.89 \pm 7.83 n=6	0.0066	*
Hypertrophic zone length	μm	102.0 \pm 4.84 n=6	100.8 \pm 4.07 n=6	0.8604	NS
Number of proliferative chondrocytes	Arbitrary number	6 \pm 1 n=6	7 \pm 1 n=6	0.3077	NS
Number of hypertrophic chondrocytes	Arbitrary number	6 \pm 0 n=6	5 \pm 1 n=6	0.7060	NS

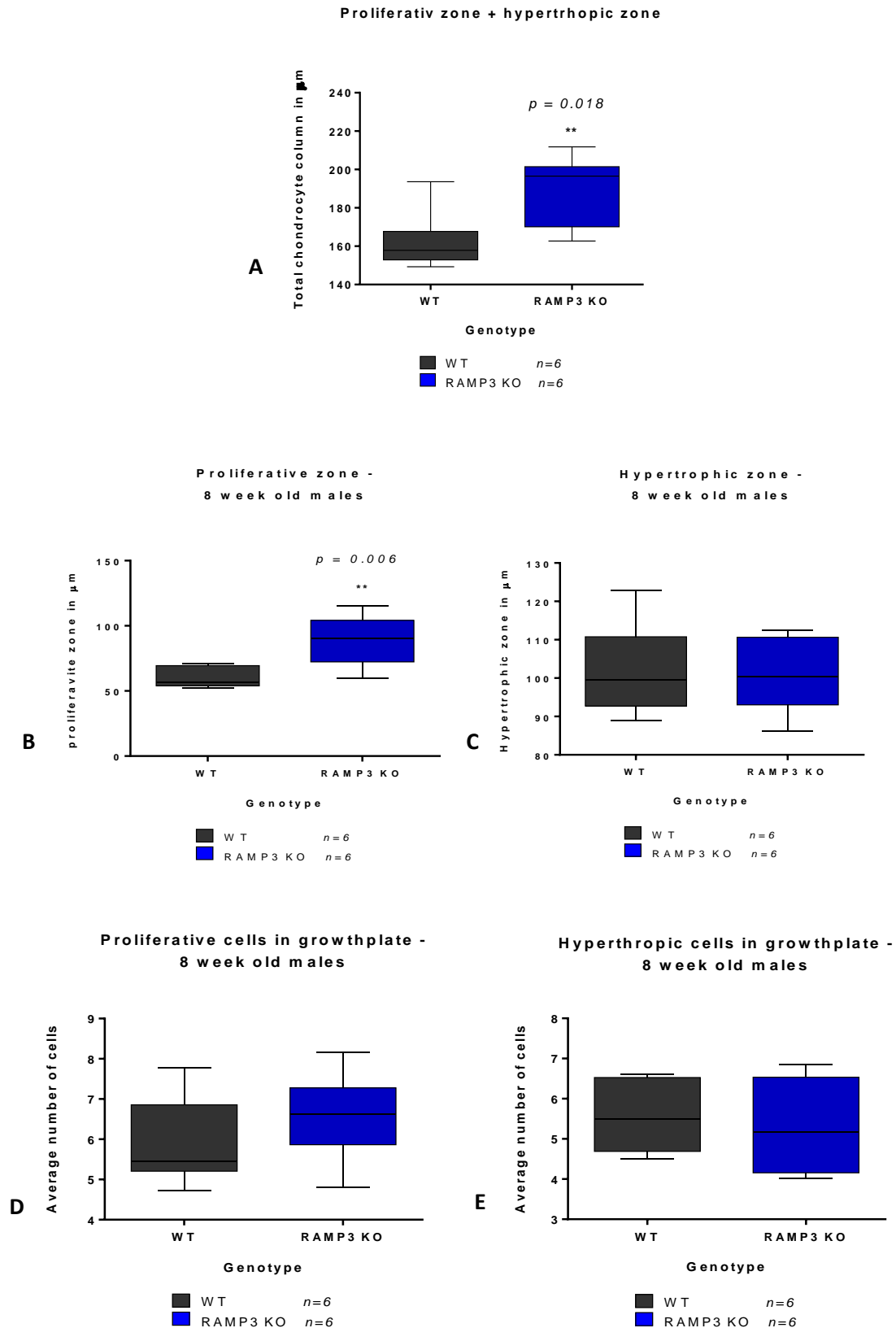


Fig 2.47: Box and whisker plots representing statistical analysis of growth plates of 8 week old male WT and RAMP3 KO mice. RAMP3 KO had significantly larger chondrocyte columns (A). RAMP3 KOs had significantly larger proliferative zones ($p = 0.006$) (B) but there was no difference in hypertrophic zones (C) There was no significant difference in the number of proliferative and hypertrophic cells (D and E). $n=6$ in both groups.

2.4 Discussion

2.4.1 Technical limitations:

2.4.1.i Animals: The WT 129/SvEv mice used in this study were generated from RAMP2 +/- cross RAMP3 -/- mice that were back crossed for 9 generations to obtain a founder breeding pairs on a congenic background. However, these animals were not monitored for behavioural changes. There were no physiological abnormalities reported in the breeding animals for up to 2 years of age in both WT and RAMP3 KO breeding lines. Since it has been reported that the RAMP3 KO adult mice had reduced body weights compared to WTs, we monitored the body weights of WT and RAMP3 KO mice up to 16 weeks of age (Dackor et. al. 2007). In contrast to Dackor et al, we observed that RAMP3 KO mice had reduced body weight at 4 weeks of age, although at time point other than 4 weeks (Fig. 2.16): post natal day 5 (PND5), 8 weeks, 12 weeks and 16 weeks, RAMP3 KO mice either had increased body weights or that there was no difference (Figs. 2.11, 2.28, 3.2). We also observed that the differences in body weights were not sex-dependent. It can be suggested that our observations, with respect to body weights, are different from what has been reported because of the difference in generating and breeding WT 129/SvEv mice. Since our WT 129/SvEv mice were generated from RAMP2 +/- and RAMP3 -/-, there could be a phenotypic trait passed on to the future generation by the RAMP3 KO parent.

2.4.1.ii MicroCT analysis: Major skeletal analyses in our study is carried out using microCT. The maximum resolution that can be achieved by the microCT scanner Skyscan 1172 in University of Sheffield is of 4.5µm and at this resolution the camera is limited to a region of the long bone and does not scan the whole bone. For whole bone, the maximum resolution that can be used at a medium camera is 17.5 µm. A larger camera or an oversize scan can be used to scan the whole long bone at 4.5µm, but the raw dataset generated goes beyond 4GB in size. The reconstruction and analysis of the huge datasets need computer equipped with extra hard drives to cope with the huge data processing for each sample. The use of medium camera and above mentioned resolutions, were the most efficient and economical settings that have been standardised for Skyscan 1172 microCT scanner. Another technical limitation of microCT analysis is that, the measurements of bone morphometric parameters are done as the quantifications of the greyscale pixels in the cross section data set of the reconstructed scan. Site specific differences, for example: lateral v/s medial cortical thickness, cannot be measured as the measurements made are average quantifications. This abolishes the significance of the site specific differences in the

skeleton. The structural differences can only be addressed through the 3D models generated from the scans; however the details of the rendering are limited by the resolution of the scan.

2.4.1.iii Histology. Eight week old male tibiae were used to conduct histological analysis. The most challenging technical limitation confronted during histological measurements was inconsistent bone sections. This limited the histological measurements to smaller areas to avoid inconsistency and contributed to larger error bars that affected the statistical analysis. Another difficulty faced with initial histology samples was improper sample fixing and delay in initiation of decalcification process as samples were first scanned for microCT prior to histology. These problems were later rectified by promptly decalcifying right side bones and scanning the left side bones which were later processed for dynamic histomorphometry which did not need decalcification.

2.4.2 Silencing RAMP3 gene results in an accelerated skeletal development.

It was observed that RAMP3 KO mice had an accelerated skeletal development at birth. As observed in figures 2.13 and 2.15 at PND5 of age, RAMP3 KO mice have more developed vertebral bodies which are larger and have developed transverse process compared to WTs. The microCT analysis suggests that, compared to WTs, RAMP3 KOs also have increased femoral bone volume and increased bone density which is evident from the increased opacity in RAMP3 KO 3D femur model (Fig 2.14) These differences were independent of the sex of the animals.

At 4 weeks of age, RAMP3 KO males and females still maintain the sex independent accelerated development in the caudal vertebra which have slender and denser bone structure (Fig. 2.27). This increase in bone volume is supported by the microCT analysis data (Fig 2.25). There is an increase in femur and tibia-fibula bone volume of RAMP3 KO mice (Figs. 2.17 and 2.18); however, this difference is only in female which is accounted by an increase in tibia trabecular thickness and trabecular pattern factor which is evident from the 3D trabecular models (Figs. 2.26 and 2.27). The increase in the bone morphometric parameters is observed in 4 week old RAMP3 KO animals despite the reduced body weights in RAMP3 KOs at this age.

At 8 weeks of age, the RAMP3 KO males have increased whole tibia BV and females have increased whole femur BV (Fig. 2.29). Both male and female RAMP3 KOs have increased tibia trabecular thickness (microCT) and trabecular area (histology) (Figs. 2.35 and 2.41 respectively). The enhanced trabecular structure of RAMP3 KOs is obvious in the 3D models and H&E stained tibia sections (Figs. 2.36 and Fig. 2.41). The increase in trabecular area was

resulted from a significant increase in the number of osteoblasts and osteoblast covered trabecular bone surface (Fig. 2.45). Hence there was a significant increase in osteoblast activity on the trabecular surface of the RAMP3 KO tibiae. There was no significant increase in the number of osteoclasts and osteoclast covered region (Fig.2.45). It was also observed that the 8 week old male tibiae had a decrease in tibia cortical bone thickness. Interestingly this reduction in the tibia cortical bone thickness in RAMP3 KOs was due to the thinner, longer and enhanced curvature of the tibial crest seen in 3D cortical model (Fig. 2.36). There is evidence that RAMP3 KO male tibiae have decreased response to bone loading (Livesey et al 2013, University of Sheffield, yet to be published data). The change in the structure of the tibia cortical bone that is observed in this study could be due to one of the reasons why RAMP3 KO male tibiae have resistance to bone loading as observed by Livesey et al. Despite the reduction in tibia cortical thickness in RAMP3 KO mice determined by the microCT techniques, dynamic histomorphometry suggested an increase in bone apposition rate in both medial and lateral periosteal regions of the RAMP3 KO tibiae (Figs. 2.38 and 2.39). This suggested that the differences in the cortical bone were not identified by the microCT analysis even at 4.5 μ m resolution. There could be other differences in the bone morphometric parameters at other time points that were not identified by microCT. Interestingly the number of osteoblasts and osteoclasts on the lateral endocortical surface of RAMP3 KO mice were not significantly different from that of WT mice (Fig. 2.43). However, the lateral endocortical bone surface covered with osteoblasts in RAMP3 KOs was significantly less compared to the WTs (Fig. 2.44). This suggested that the osteoblasts on the lateral endocortical surface of RAMP3 KO mice were smaller in size compared to the osteoblasts in WTs (Fig. 2.48 below). One of the reasons for smaller osteoblasts in RAMP3 KOs could be that they were proliferating, which could imply that the RAMP3 KO osteoblasts had increased proliferation compared to WT on the lateral endocortical surface. Moreover, active osteoblasts are smaller but more cuboidal in shape compared the flattened bone lining cells. It can hence be postulated that the RAMP3 KOs have more active osteoblasts compared to the WTs.

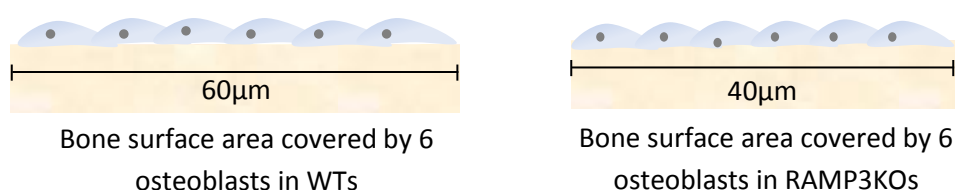


Fig 2.48: Schematic representation of lateral endocortical bone surface in WT and RAMP3 KO mice hypothesising that the reduction in the osteoblasts covered surface in RAMP3 KOs could result from smaller osteoblasts and there were no differences in the number of osteoblasts in WTs and RAMP3 KOs.

The advanced skeletal phenotype observed in postnatal day 5 animals followed by a suggestively anabolic skeletal phenotype, encouraged us to study the growth plate of RAMP3KO animals. Growth plate analysis of 8 week old males revealed a significant increase in the length of the chondrocyte columns in RAMP3 KO mice compared to WT (Fig. 2.47). Interestingly the increase in the length was due to the expanded proliferative zone, although the number of proliferative cells in the columns of RAMP3 KO was not significantly different from that of the WT (Fig. 2.47). The increase in the proliferative zone could be because of the increase in size of the proliferative cells which is when the proliferative cells become pre-hypertrophic. So the differentiation of proliferative cells to pre-hypertrophic could be enhanced in the RAMP3 KO mice. By having more pre-hypertrophic cells in the proliferative zone, it can be suggested that in RAMP3 KO the differentiation of proliferative chondrocyte to hypertrophic chondrocytes is accelerated which is followed by acceleration in the mineralization of the growth plate. This could in turn explain the acceleration in endochondral ossification *in utero* that results in the advanced development of the skeleton seen in the postnatal day 5 old RAMP3 KO mice. These findings give novel evidence to involvement of RAMP3 in chondrocyte differentiation and endochondral ossification. To date there is evidence of Indian hedgehog (Ihh) regulated differentiation of pre-hypertrophic chondrocytes into hypertrophic chondrocytes with a negative feedback loop on PTHrP expression, although these are no studies on RAMP3 involved Ihh-PTHrP chondrocyte differentiation (Kornenberg 2005, Scheijen et al 2003, St-Jacques et al 1999). There is also evidence that RAMP3 expression profoundly increase in the uterus in an oestrogen dependent manner (Hewitt et al 2005, Watanabe et al 2006). Therefore, RAMP3 can play a regulatory, although not obligatory role like RAMP2, in embryogenesis, implying that RAMP3 and RAMP2 play distinct and non-redundant roles in animal development (Dackor et al 2007). In future, it will be helpful to study the chondrocyte differentiation in neonatal RAMP3 KO mice, and to determine RAMP1/2/3 expression in the growth plates of WT and RAMP3 KO mice.

The significant differences observed in histological analysis are diminished in the microCT analysis. The technical limitations discussed earlier could account for the reduction of the significance of the differences observed by microCT analysis. Judging from the histological differences observed at 8 weeks of age, there would certainly be interesting differences supporting enhanced skeletal development in RAMP3 KO at PND5 and 4 weeks of age at cellular level. Regardless of the technical limitations, it can be stated that RAMP3 KO mice have advanced skeletal development at early age, which could provide protection to age related bone

loss phenomena like osteoporosis. Increased number of osteoblasts in the RAMP3 KO trabecular bone is suggestive of an anabolic skeletal phenotype in the RAMP3 KOs. It is also evident from 4 and 8 week old animals (see Figs. 2.17, 2.23, 2.24, 2.35 and 2.36) that the suggestively anabolic skeletal phenotype is statistically significant in female RAMP3 KOs compared to male RAMP3 KOs, hence it can be implied that oestrogen enhances the RAMP3 KO skeletal phenotype. In the next chapter we investigate the skeletal response to ovariectomy in an attempt to understand the role of RAMP3 in skeletal regulation in postmenopausal conditions. The molecular mechanisms responsible for the skeletal phenotype of RAMP3 KO mice are discussed in chapter 8.

In conclusion, RAMP3 KO mice have, accelerated skeletal development at birth and in adult tibiae there is:

- Significant increase in trabecular thickness without increase in total bone volume.
- Difference in the shape of the tibial crest,
- Significant increase in the bone apposition rate,
- Significant increase in the number of osteoblasts in the trabecular bone,
- Significant increase in the osteoblast covered trabecular surface and
- Significant increase in the thickness of the growth plate.

Chapter 3: Skeletal response of RAMP3 KO mice to ovariectomy.

3.1 Introduction

It has been suggested that a women can expect to lose about 35% of her cortical bone and 50% of her trabecular bone as she ages, whereas a man can expect to lose only about two-thirds of these amounts (Riggs et al 1982). About half of this bone loss in women is in the first decade after menopause (Riggs & Melton 1992). Postmenopausal osteoporosis is characterised by loss of bone that results in frequent fractures, mostly of vertebrae, hip, distil forearm and proximal femur following minimal trauma. This progression in bone loss is due to an increase in bone resorption and decrease in bone formation which occurs from increase in the rate of activation of the Bone Mineralizing Units (BMU) (Storm et al 1990). The onset of trabecular bone loss precedes the loss of cortical bone with aging. In postmenopausal women this loss of trabecular bone is aggravated. There is strong evidence to propose, that the bone loss in postmenopausal women mainly affects the trabecular bone in the vertebra, hip and the proximal ends of femur (Melton et al 1986, Riggs & Melton 1986). This loss of trabecular bone, is not due to generalised thinning of the trabeculae but instead it is due to complete perforation and fragmentation of trabecular bone (Kleerekoper et al 1985, Parfitt et al 1983).

The details of current therapeutic approaches for treating osteoporosis are discussed in the main dissertation introduction (Section 1.2). In this section we shall focus on the role of oestrogen and oestrogen dependent CT family of peptides' role in skeletal regulation. In older women with established osteoporosis, there is evidence that hormone replacement therapy arrests the drastic loss of bone mineral density and reduces fracture rates (Christiansen 1990, Dequeker & Geusens 1989, Lufkin 1992, Lufkin et al 1992). Postmenopausal women treated with oestrogen for 5 years showed prevention of the bone loss that was observed within the placebo group. It was also observed that if the onset of the therapy is delayed by 5 years, bone formation increases in the first 3 years. In the later 2 years there was no increase in bone formation however the 1% bone loss seen in placebo group was not seen in the treatment group (Lindsay et al 1976).

The influence of oestrogen on differentiation and activity of osteoblasts is discussed earlier in section 1.1.3.i. Briefly, oestrogen regulates osteoblast differentiation and osteoblast induced osteoclast differentiation and activation. Oestrogen down regulates osteoclasts by inducing apoptosis through TFG- β (Khosla et al 1999). Oestrogen also inhibits the PTH induced osteoclast resorption by blocking the cAMP pathway in osteoblasts and also by decreasing interleukin-6 (IL-6), release from osteoblasts as IL-6 is a potent osteoclasts activator. Furthermore oestrogen also

induces OPG production that hinders RANKL–RANK association (Kaji et al 1996). The loss of oestrogen in postmenopausal women results in the loss these key regulatory pathways. Therefore hormone replacement therapy aims to restore this balance to protect the loss of bone mineral density.

Ovariectomy is the surgical procedure used to generate an experimental murine model for studying postmenopausal osteoporosis. Bone loss is induced by surgically removing the ovaries. Ovariectomy is performed when the animals attains sexual maturity as the bone loss can be studied after the animals attains the peak bone formation (8 weeks to 16 weeks). Amongst the Calcitonin (CT) family of peptides, Adrenomedullin (AM) is associated with vasodilation in OVX models (Ross et al 2006). Calcitonin (CT), Calcitonin gene related peptide (CGRP) and Amylin (AMY) have been shown to regulate the bone morphology and induce skeletal protection to bone loss following ovariectomy (OVX).

The role of Calcitonin in bone loss protection is very well understood. There is also evidence that prophylactic administration of CT results in protection against oestrogen induced –bone loss (Mazzuoli et al 1990a, Mazzuoli et al 1990b). As mentioned earlier in section 1.2, intranasal calcitonin spray is used as an osteoporosis treatment. However recent reports suggest that Novartis has withdrawn CT intranasal spray as a treatment for osteoporosis. CGPR inhibits bone resorption but not bone formation, however it is not as efficient as CT in preventing bone loss It was observed that CGRP-treated rats had a loss of 46% trabecular bone, whereas CT-treated rats had a loss of 21% (Valentijn et al 1997). In comparison to just OVX rats, OVX rat subjected to 3 µg/100 g BW/day injection of AMY, showed increase in both distal metaphyseal (representative of trabecular bone) and total femoral bone densities. However, this skeletal response was not seen in the diaphyseal femoral density (representative of cortical bone). Hence AMY induced a specific bone formation response in the trabecular bone and not in the cortical bone (Horcajada-Molteni et al 2000).

We now have robust evidence that the RAMP3 KO mice have an advanced skeletal phenotype with higher significance in female RAMP3 KO mice (Chapter 2). In a study to determine AM induced uterine relaxation, it was observed that both pregnancy and estradiol treatment to OVX rats amplified RAMP3 expression in uterine arteries while progesterone had no effect (Ross et al 2010). There is also evidence that RAMP3 expression profoundly increase in the uterus in an oestrogen dependent manner (Hewitt et al 2005, Watanabe et al 2006). Therefore we can

propose that, the absence of RAMP3 expression in RAMP3 KO female mice will influence the skeletal bone phenotype following ovariectomy.

As discussed earlier, the RAMP3 KO mice and WT mice used in our study are generated on 129/SvEv background. The skeletal response to ovariectomy (OVX) in 129/SvEv mice is not completely known. Hybrid 129/SvEv cross C57BL/6 mice have been used to study the response to OVX in AMP-activated protein kinase gene *Ampk α 1* KO mice, where WT hybrid 129/SvEv cross C57BL/6 mice show reduction in trabecular and cortical bone volume (Jeyabalan et al 2012). The WT and RAMP3 KO models used in our study shall provide novel data on the skeletal response to OVX on a pure 129/SvEv background

In this chapter we focus on determining whether the accelerated skeletal development in RAMP3 KO mice at early ages, provided protection to oestrogen dependent bone loss and if the oestrogen dependent skeletal regulation is influenced by the alteration in RAMP3 expression in the RAMP3 KO female mice. We hypothesized, *the skeletal response to ovariectomy, would be different in RAMP3 KO 129/SvEv female mice, in comparison to the WT 129/SvEv female mice.*

To test our hypothesis, we perform microCT skeletal analysis of:

- 10 baseline 12 week old female mice (5 WT and 5 RAMP3 KO),
- 10 sham operated 16 week old female mice (5 WT and 5 RAMP3 KO) and
- 10 OVX, 16 week old female mice (5 WT and 5 RAMP3 KO).

3.2 Methods and materials

The skeletal phenotype in response to ovariectomy (OVX) was studied in female WT and RAMP3 KO mice at the age of 12 weeks (baseline group/OVX conducted) and 16 weeks (sham and OVX group) by microCT. Protocols used for sample processing and microCT analysis are previous discussed in chapter 2, section 2.2.9. This section details the surgical intervention-ovariectomy used to mimic postmenopausal physiology in WT and RAMP3 KO mice.

3.2.1 Ovariectomy:

Skeletal response to ovariectomy (OVX) was studied in 12 week old WT and RAMP3 KO female mice. OVX (n=5/genotype) and sham operations (n=5/genotype) were conducted at 12 weeks of age and the animals were culled at 16 weeks of age. Baseline animals were culled at 12 weeks. (Bagi et al 1993, Bouxsein et al 2005).

Anaesthesia: Animals were anaesthetised using Isoflurane (IsoFlo™, Abbot®) at 2.5 – 3% in 100% oxygen. The anaesthesia was induced (4.5l/min during the first three minutes) and maintained (~2.5 l/min) through a face mask linked to an active-scavenge system to reduce environmental contamination. Loss of righting reflex was used to determine the state of consciousness.

Surgery: Ensuring the spine was straight; the animal was placed in ventral recumbency position, with the tail towards the surgeon. Limbs were taped to the surgery mat to maintain the animal in position. The dorsal mid-lumbar region was shaved and scrubbed with alcohol. A dorsal midline skin incision approximately 1.5 cm was over the lumbar spine. Fascia was separated by blunt dissection. On either sides lateral to the skin incision (3-5 mm away), a 0.5-1 cm incision was made in the muscle wall. Ovaries and oviducts were located and exteriorised through the muscle wall incisions on either sides (one at a time). To remove the ovary, the uterine horn was first clamped with a haemostat and ovary was cut above the clamp. The clamp was then removed and the tissue was replaced back into the abdomen. Similarly the other ovary was excised. The muscle wall was not sutured. The skin incision was sutured with Polyglactin 910 synthetic absorbable suture (Johnson and Johnson® W9443). Sham animals were operated with the same procedure except that their ovaries were exteriorised and replaced but not excised. The surgeries were performed by Dr Ning Wang (University of Sheffield).

Post operation recovery: Animals recovered from anaesthesia in recovery chambers that were temperature regulated at 22°C. Animals were then housed in their cages and monitored for the next 72 hours for suture breakage and general recovery. Sham and OVX groups were housed for 4 weeks post operation and were culled at 16 weeks of age.

3.3 Results

The response of the skeleton to ovariectomy was determined through microCT analysis. There were 10 baseline mice (5 WT and 5 RAMP3 KO) which were 12 weeks of age (age at which ovariectomy conducted), 10 sham mice of 16 weeks old (5 WT and 5 RAMP3 KO) and 10 ovariectomized mice of 16 week old (OVX) (5 WT and 5 RAMP3 KO).

3.3.1 Weight of Uterus

Whole uteri were weighed in sham and ovariectomized (OVX) mice immediately post sacrifice. Both WT and RAMP3 KO females showed a significant reduction in whole uterus weight, due to excision of ovaries, in OVX group compared to their respective sham group confirming that the surgical intervention was executed effectively (Fig 3.1).

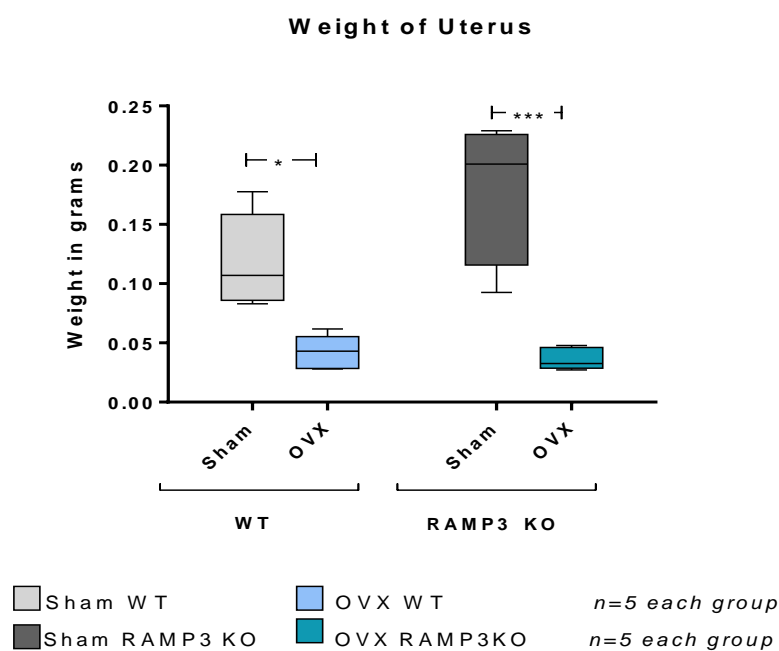


Fig 3.1: Box and whisker plot showing significant reduction of whole uterus weight in WT ($p=0.0215$) and RAMP3 KO ($p = 0.0001$) OVX mice compared to their respective sham group.

3.3.2 Whole body weights:

There was a pattern of increase in whole body weight post OVX in both WT and RAMP3 KO mice. However according to 2-way ANOVA and post multiple comparison Bonferroni's test, differences in the weights were not statistically significant (Fig. 3.2).

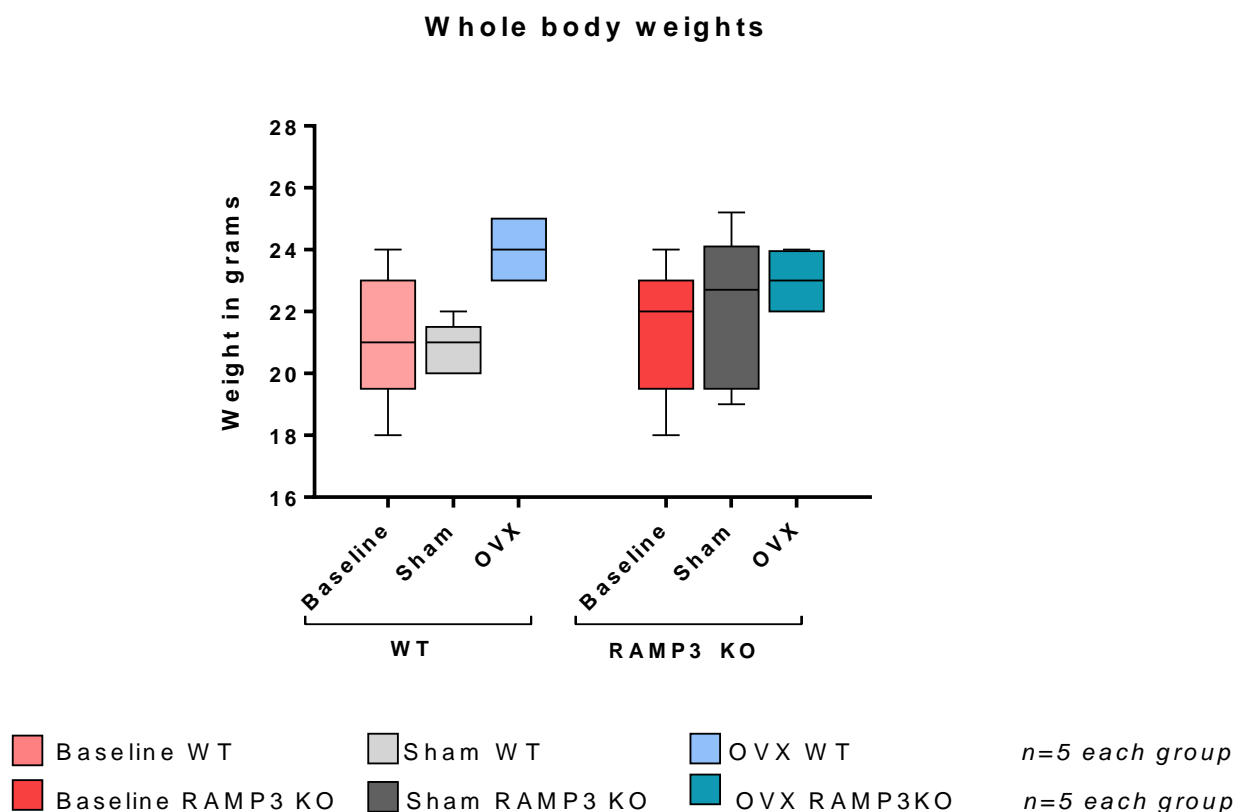


Fig 3.2: Box and whisker plot showing whole body weights of baseline, sham and OVX WT and RAMP3 KO mice. Two-way ANOVA test followed by Bonferroni's post multiple comparisons test was used to determine statistical significance of differences between the treatment and genotype. Neither the genotype nor the treatment resulted in significant difference in body weights. n = 5 in each group.

3.3.3 MicroCT analysis:

MicroCT analysis was used to determine the bone morphometric parameters for whole, cortical and trabecular, femur and tibia bone. Dataset was analysed using 2-way ANOVA statistical test. Additionally, Bonferroni's post-multiple analysis was used to determine whether the difference observed was between genotypes or between treatments.

3.3.3.i Whole femur and tibia bone volume:

There was no significant difference resulting from intervention in the total femur and tibia bone volume in either WT or RAMP3 KO mice. Figure 3.3 below is a graphical representation of the statistical analysis. Bone morphometric values and statistical significance is summarised in table 9.1 in the appendix.

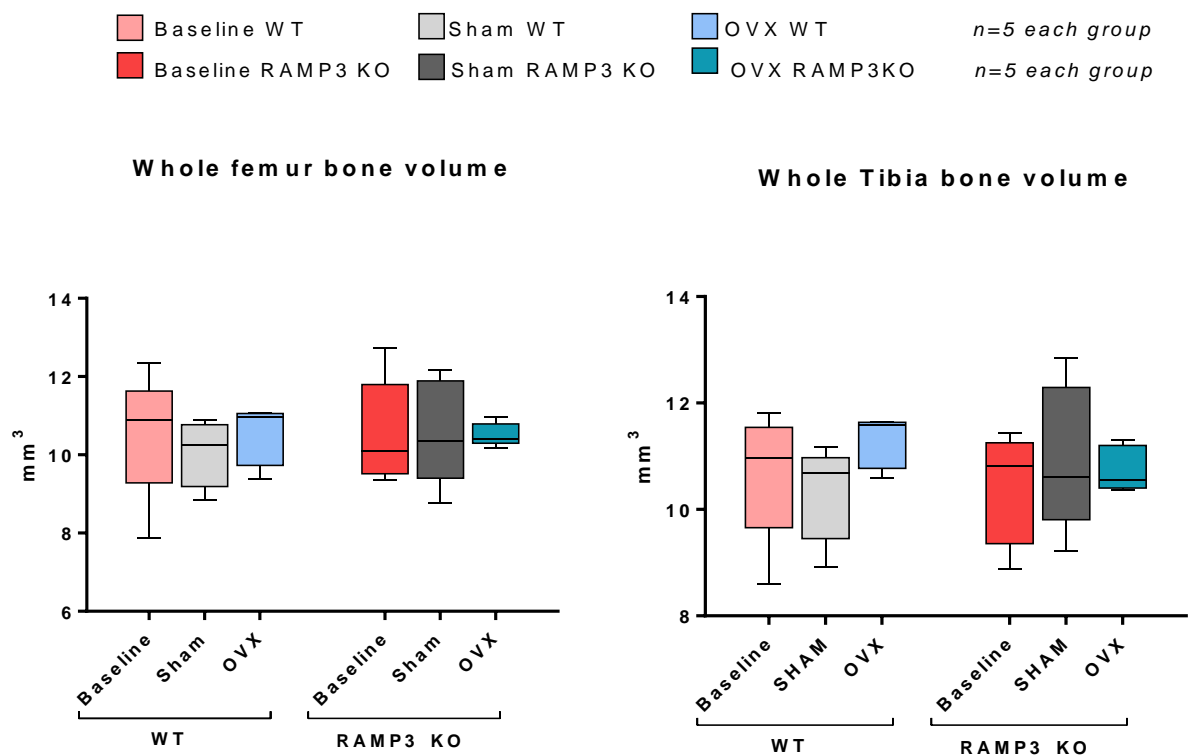


Fig 3.3: Box and whisker plot showing whole femur (left) and tibia (right) bone volume of baseline, sham and OVX in WT and RAMP3 KO mice. Two-way ANOVA test followed by Bonferroni's post multiple comparisons test was used to determine statistical significance of differences between the treatment and genotype. Neither the genotype nor the treatment resulted in significant difference in whole bone volumes of femurs and tibiae.

3.3.3.ii Femur cortical bone:

There was no significant difference resulting from intervention in the femur cortical bone volume and thickness in either WT or RAMP3 KO mice. Figure 3.4 below is the graphical representation of the statistical analysis. Bone morphometric values and statistical significance is summarised in table 9.1 in the appendix

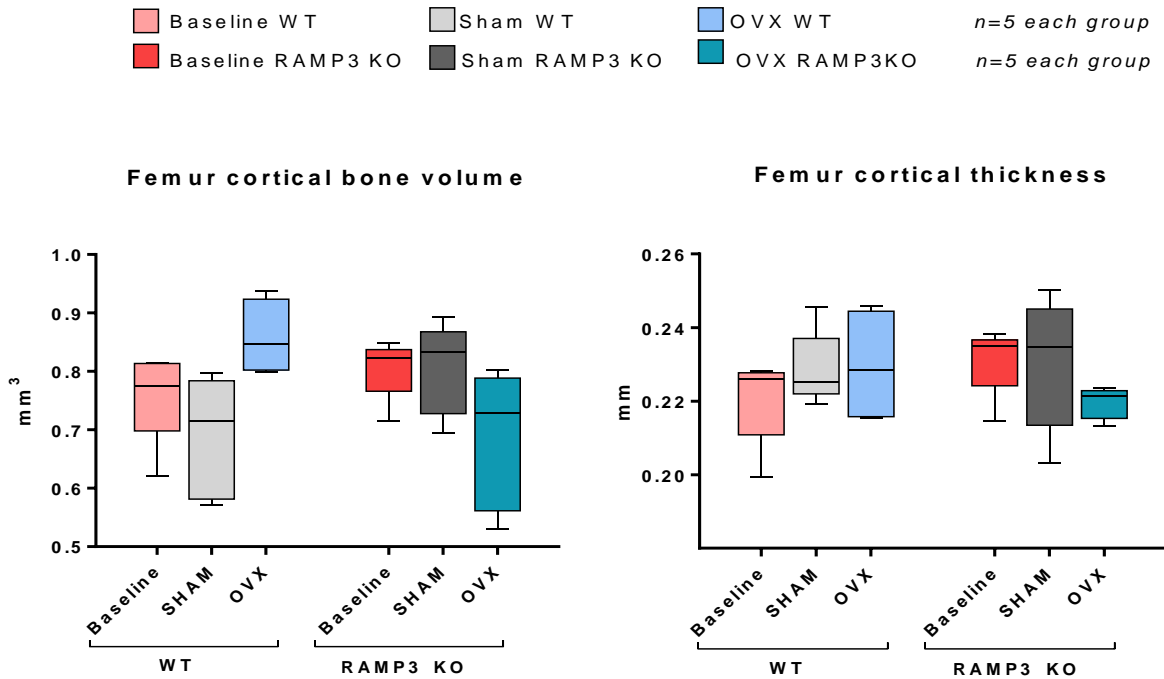


Fig 3.4: Box and whisker plot demonstrating femur cortical bone volume (left) and thickness (right) of baseline, sham and OVX groups within WT and RAMP3 KO mice. Two-way ANOVA test followed by Bonferroni's post-multiple comparisons test was used to determine statistical significance of differences between the treatment and genotype. Neither the genotype nor the treatment resulted in significant difference in femur cortical parameters.

3.3.3.iii Tibia cortical bone:

The tibia cortical bone volume was observed to be significantly higher in WT OVX treated mice compared to WT sham treated mice ($p = 0.0227$) while there was no significant difference in cortical bone volume within RAMP3 KO mice groups.

On the other hand, the tibia cortical thickness was significantly different in all RAMP3 KO treatment groups. Compared to the baseline mice, cortical thickness was significantly reduced in the sham treated mice ($p = 0.0001$) while the cortical thickness was significantly increased in OVX treated group compared to sham treated ($p = 0.0011$). Figure 3.5 below is a graphical representation of the statistical analysis. Bone morphometric values and statistical significance is summarised in table 9.1 in the appendix

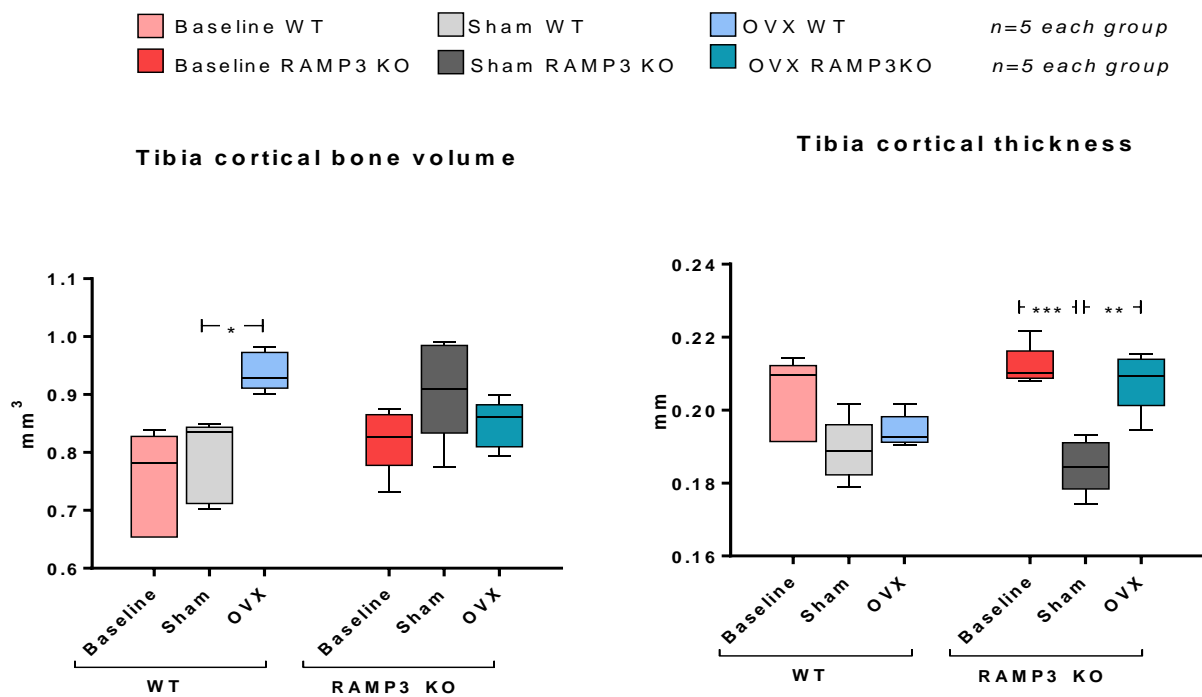


Fig 3.5: Box and whisker plot showing tibia cortical bone volume (left) and thickness (right) of baseline, sham and OVX WT and RAMP3 KO mice. Two-way ANOVA test followed by Bonferroni's post-multiple comparisons test was used to determine statistical significance of differences between the treatment and genotype. There was a significant increase in tibia cortical bone volume of WT OVX treated mice compared to WT sham treated mice ($p=0.0227$). Cortical thickness of RAMP3 KO sham treated mice was very significantly reduced than RAMP3 KO baseline mice ($p=0.0001$). However, cortical thickness of RAMP3 KO OVX treated mice was significantly increased than RAMP3 KO sham treated mice ($p=0.0011$).

3.3.3.iv Femur trabecular bone:

Unlike the femur cortical bone, femur trabecular bone showed difference in the bone parameters in response to the intervention. A pattern of reduction in trabecular BV, BV/TV, Th and N and increase in Sp in both WT and RAMP3 KO OVX treated mice when compared to respective baseline and sham treated groups was observed. However, according to the two-way ANOVA test followed by Bonferroni's post multiple comparisons test, these differences were not significant. Figure 3.6 overleaf is a graphical represents of the statistical analysis. Bone morphometric values and statistical significance is summarised in table 9.1 in the appendix

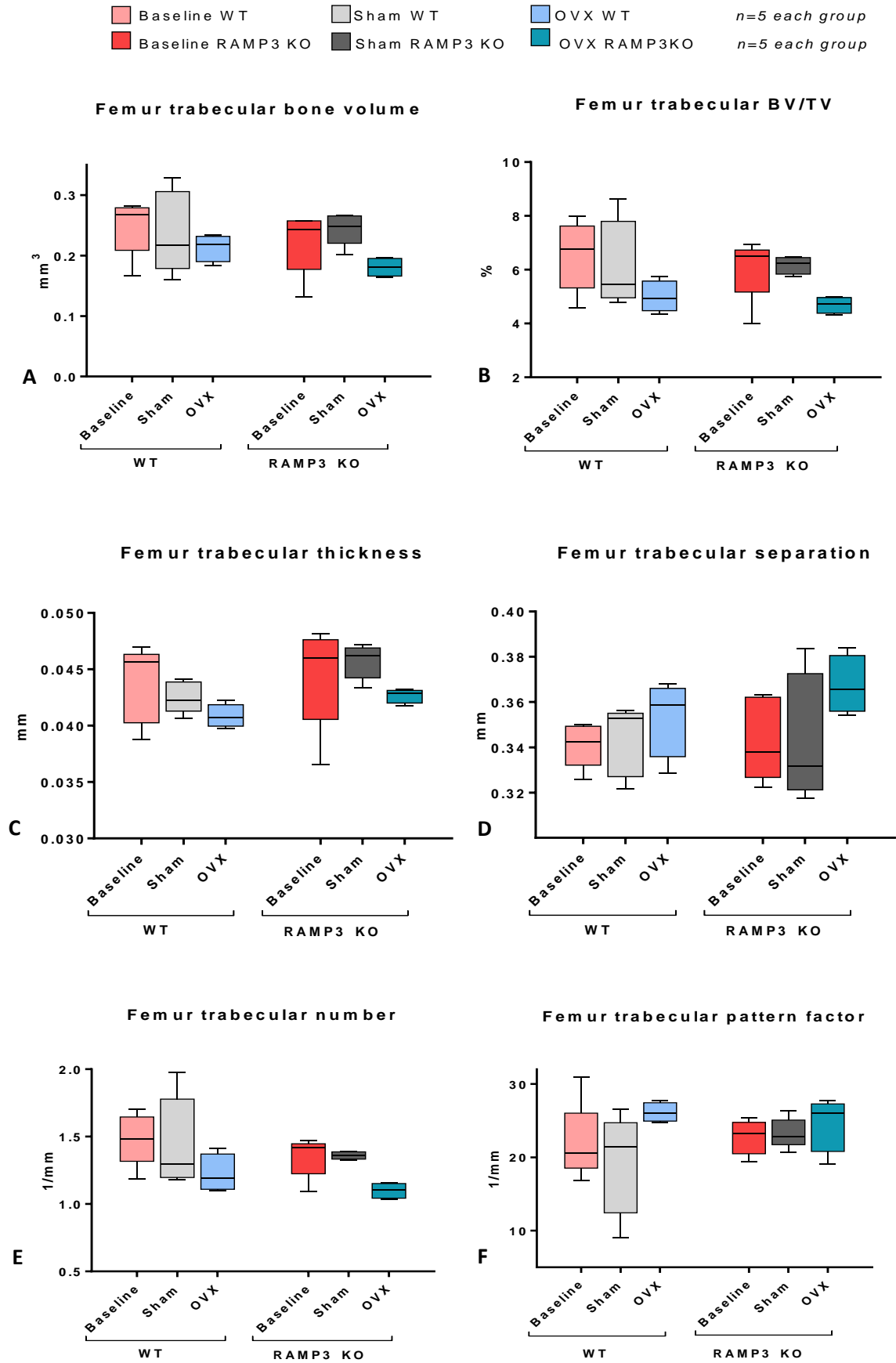


Fig 3.6: Box and whisker plot showing femur trabecular bone volume (A), BV/TV (B), thickness (Th) (C), separation (Sp) (D), Number (N) (E) and pattern factor (Pf) (F). No significant differences were observed in any of the trabecular parameters in any treatment groups of either genotype.

3.3.3.v Tibia trabecular bone:

Tibia trabecular bone showed the maximum response to intervention in both WT and RAMP3 KOs. Similar to femur trabecular bone, a pattern of reduction in trabecular BV, BV/TV, Th and N in both WT and RAMP3 KO OVX treated mice when compared to respective baseline and sham treated groups was observed. Two-way ANOVA test followed by Bonferroni's post multiple comparisons test was used to determine statistical significance of differences between the treatment and genotype. Bone morphometric values and statistical significance is summarised in table 9.1 in the appendix. Individual statistical differences in tibia trabecular bone parameters in graphically represented and in Figures 3.7, 3.8 and 3.9.

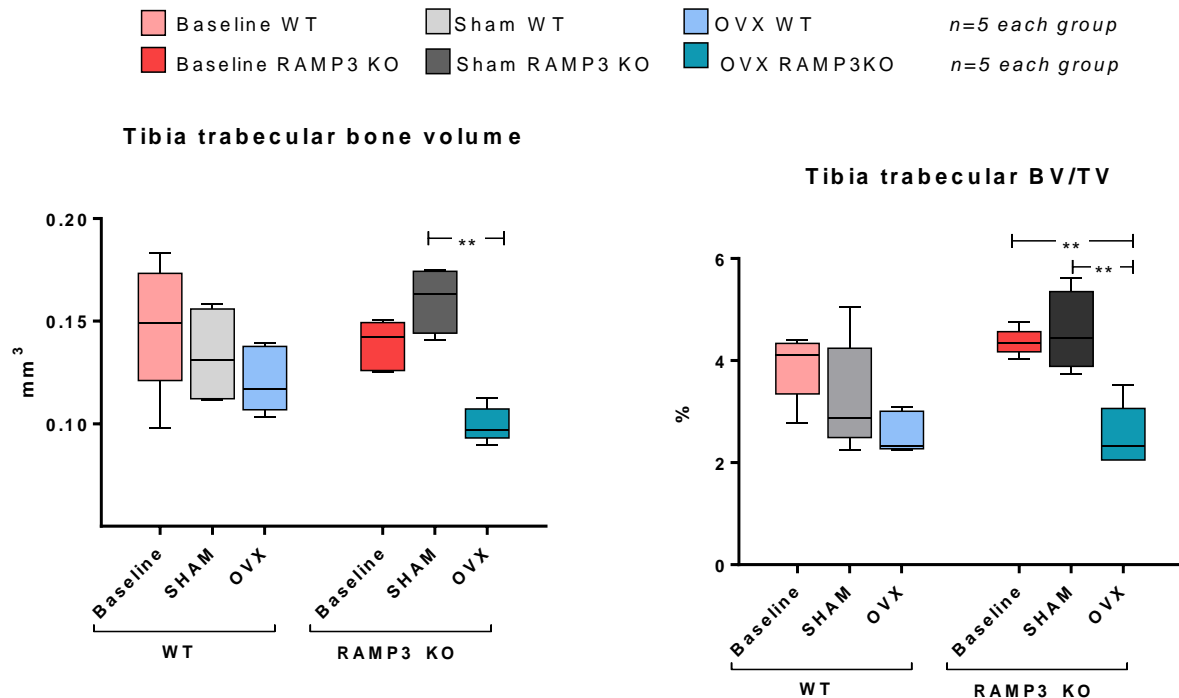


Fig 3.7: Box and whisker plot showing tibia trabecular bone volume (left) and bone volume to tissue volume ratio BV/TV (right) in WT and RAMP3 KO baseline, sham and OVX treated mice.. RAMP3 KO OVX treated mice had significant reduction in trabecular bone volume compared to sham treated mice ($p=0.0018$). There was significant reduction in RAMP3 KO OVX treated tibia trabecular BV/TV compared to both, sham treated ($p = 0.0024$) and baseline ($p = 0.0038$) mice. Although there was reduction in both BV and BV/TV in WT treatment groups, these differences were not significant.

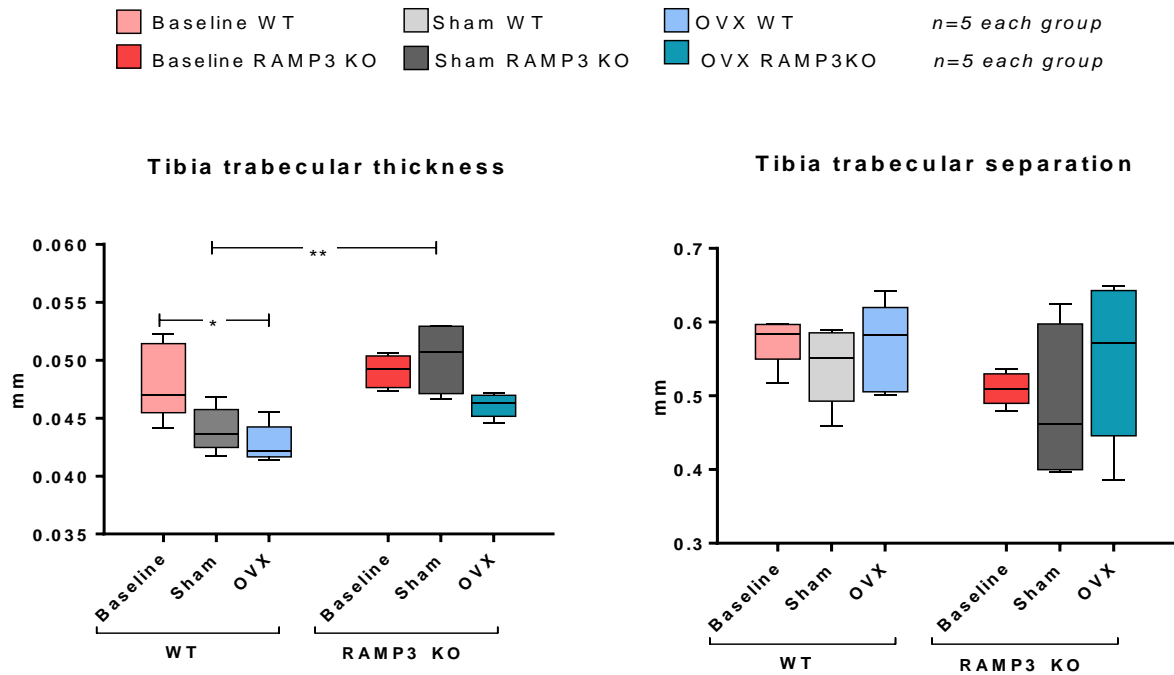


Fig 3.8: Box and whisker plot showing tibia trabecular thickness (left) and separation (right) in WT and RAMP3 KO baseline, sham and OVX treated mice. There is a significant decrease in WT OVX treated trabecular thickness compared to baseline mice ($p = 0.0108$). On the other hand, RAMP3 KO sham treated mice showed a significantly higher trabecular thickness compared to WT sham treated animals ($p=0.0041$). However, there were no statistically significant differences in trabecular separation.

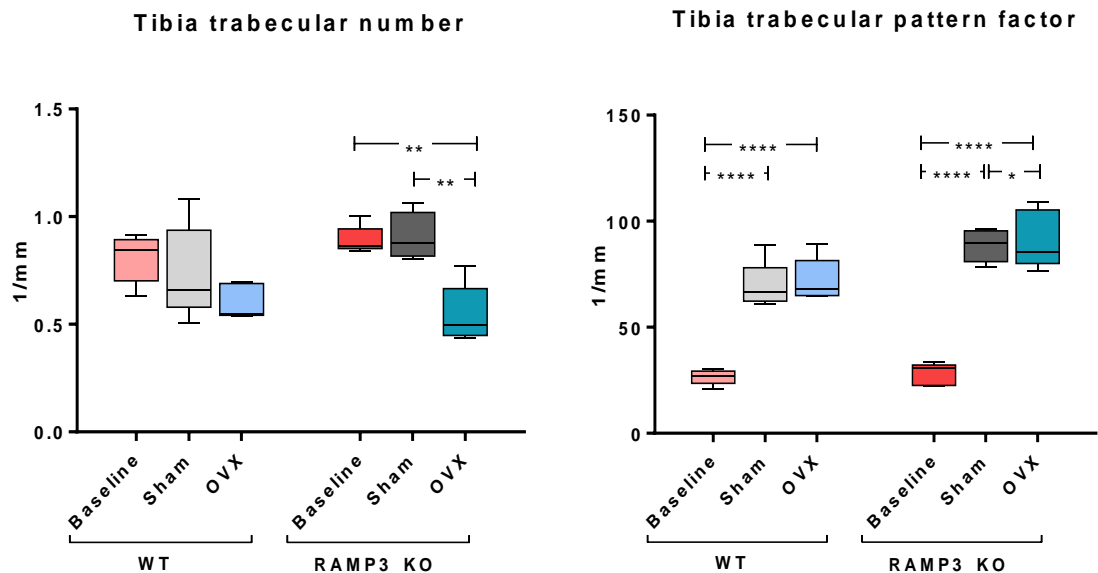


Fig 3.9: Box and whisker plot showing tibia trabecular number (left) and pattern factor (right) in WT and RAMP3 KO baseline, sham and OVX treated mice. A significant decrease was observed in RAMP3 KO OVX treated trabecular number compared to both baseline ($p = 0.0051$) and sham ($p = 0.0064$) treated mice. Both WT and RAMP KO baseline mice had significantly reduced trabecular pattern factor compared to sham ($p < 0.0001$) and OVX treated ($p < 0.0001$) mice. RAMP3KO OVX treated mice had higher trabecular pattern factor compared to sham treated mice ($p = 0.0170$).

3.3.4 Three dimension skeletal models:

Sham and OVX treated 3D trabecular models were generated and compared as these groups were both age and sex matched. There was a noticeable reduction in the trabecular bone volume in both WT and RAMP3 KO in response to OVX treatment. It was observed that, WTs had reduction in trabecular thickness whereas RAMP3 KOs had a reduction in trabecular number when compared to sham treated animals. This data was observed to be consistent with the previous microCT analysis (Fig.3.10).

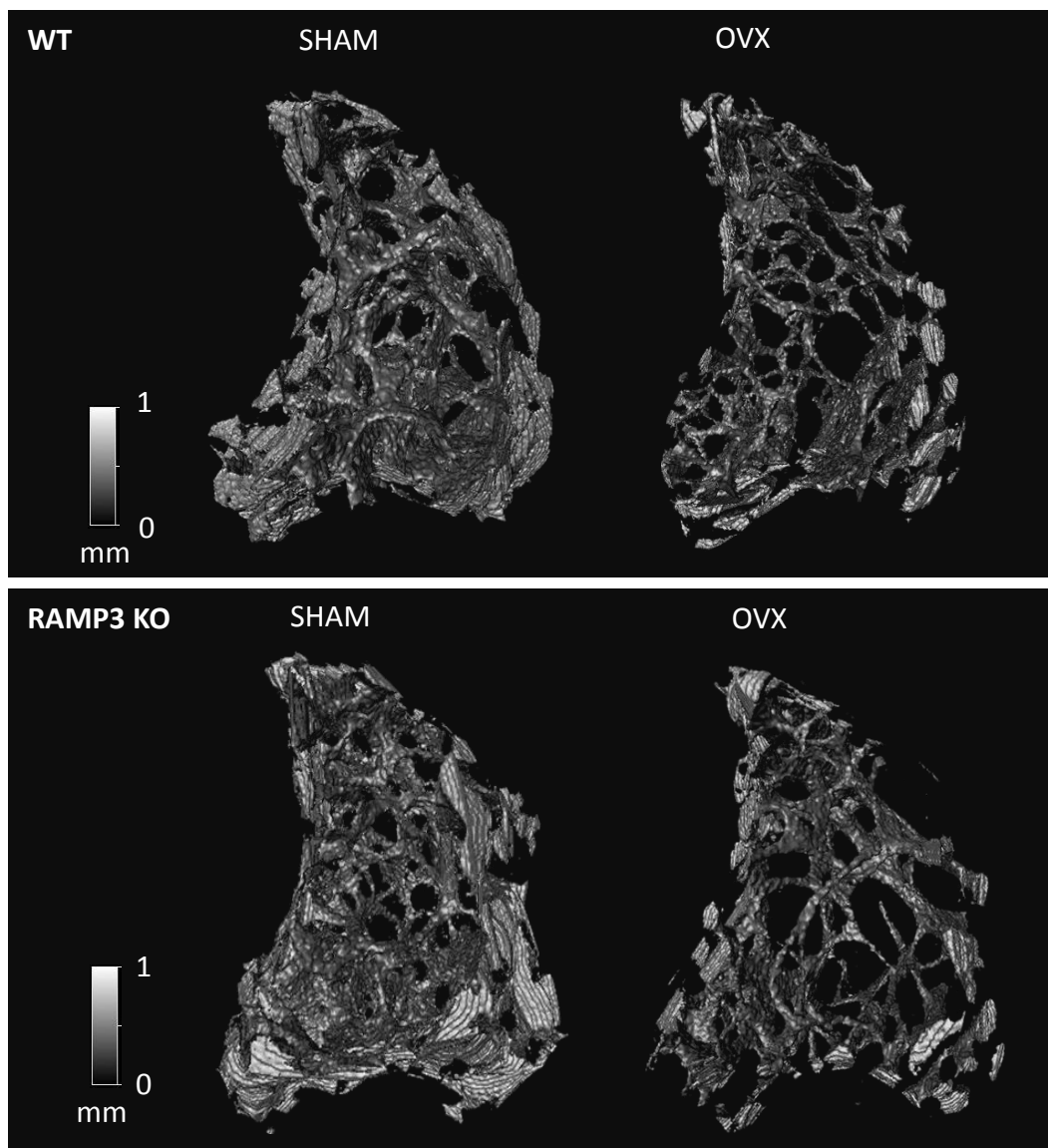


Fig 3.10: Representative solid grey-scale 3D tibia trabecular models reflecting the microCT analysis. Top panel shows WT models and bottom panels show RAMP3 KO models. Both WT and RAMP3 KO OVX treated trabecular models show reduction in bone volume compared to sham treated mice (left). WT OVX trabecular bone shows reduction in the thickness on individual trabecular unit. However, RAMP3 KOs demonstrated a reduction in the number of trabecular units and not the thickness of the trabecular bone.

3.4 Discussion

The 129/SvEv female mice did not show a classical ovariectomy associated bone loss response. Although there was a non-significant decrease femur cortical bone volume of OVX RAMP3 KO compared to sham RAMP3 KOs, it was puzzling to see an increase in the femur cortical bone volume in OVX WT compared to sham WT (see Figure 3.4). Furthermore, there was a significant increase in the tibia cortical BV of OVX WT mice compared to sham and baseline WT mice and a highly significant increase in the OVX RAMP3 KO tibia cortical thickness compared to the sham RAMP3 KO mice (see Figure 3.5).

An ovariectomy associated bone loss was observed in the femur trabecular bone of the OVX 129/SvEv mice compared to sham and baseline 129/SvEv mice in both the genotypes, although these differences were not significantly different (see Figure 3.6). Interestingly, the tibia trabecular thickness was significantly reduced in OVX WT compared to the baseline WTs, but it was not significantly different to the sham WT mice (see Figure 3.8). The OVX RAMP3 KO mice showed reduction in tibia trabecular thickness compared to the sham RAMP3 KO mice, but this difference was not significant. The reduction in the trabecular thickness in both the OVX WT and OVX RAMP3 KO in comparison to the respective sham groups is more evident in the 3D models (see Figure 3.10). As discussed earlier in Section 2.4, microCT analysis is limited to the resolution of 4.5µm. This resolution is evidently insufficient in detecting the site specific differences and is responsible for the reduced significance of the differences seen in this experiment. Given the evidence that regardless of the treatment, the differences in RAMP3 KO and WT mice skeleton have only been detected at 4.5µm and not at 17.5µm, we can conclude that quantification of the skeletal difference should not be limited to microCT technique.

The RAMP3 KO mice maintained a higher trabecular thickness in the tibia in both sham and OVX groups compared to the sham and OVX WT mice (see Figure 3.8 and 3.10). This could suggest that the RAMP3 KO mice retained more trabecular bone after the oestrogen induced bone loss due to the accelerated skeletal development at an early age (see Figure 3.8). However, since the WT 129/SvEv 129 mice do not exhibit a classical oestrogen response to the ovariectomy, it is not possible to compare the skeletal response of the RAMP3 KOs to the WTs. One of the possible explanations for the WT skeletal phenotype could be that the WT 129/SvEv mice generated for this project are decedents of RAMP2 +/- cross RAMP3-/- pair. Despite the nine generation back crossing to achieve congenicity, there could to be a skeletal trait that has been passed on to

the WT 129/SvEv used in this project by the RAMP3 KO founder parent. The RAMP3 KOs are bred from RAMP3KO male and female transgenic mice generated by Dr Caron, USA, hence the RAMP3 KOs do not have any other phenotypic influence. Since there is no literature evidence on the skeletal response of pure 129/SvEv WT mice, we cannot conclude that the skeletal response observed in the OVX WT 129/SvEvs is due to the background strain. It is first important to establish a protocol to depict postmenopausal physiology in the 129/SvEv mice. Ovariectomy can be performed at different ages and different post-ovariectomy period can be tried to determine the optimum conditions.

MicroCT analyses and 3D models (see Figure 3.9 and 3.10), of the trabecular bone give the impression that RAMP3 KO female mice to respond to ovariectomy, however they retain thicker trabecular units despite the bone loss, which could be due to the accelerated development of the skeleton in these animals at earlier an age (Chapter 2). Since the microCT analyses have their limitations, the skeletal analysis should not be limited to this technique. Histology and dynamic histomorphometry shall further help in understanding the skeletal response of the 129/SvEvs to ovariectomy.

In conclusion, the 129/SvEv mice respond to ovariectomy differently than other strains with:

- Increase in cortical bone volume and thickness,
- Insignificant decrease in trabecular thickness and
- No change in the total bone volume.

Chapter 4: Characteristics of primary osteoblasts from RAMP3 KO mice.

4.1 Introduction

Calcitonin (CT) family of peptides, have both anabolic and anti-resorptive effects on the bone. There are several studies that suggest the increase of bone formation markers on CT administration (Wallach et al 1999). CT also has an osteoblastic effect, as it has been shown previously that 100nm CT induces alkaline phosphatase activity in UMR- 106-06 rat osteoblastic cells (Iida-Klein et al 1992, Naot & Cornish 2008). Although it is suggested that AMY essentially has an anabolic effect on the skeleton compared to the activity of Calcitonin, there is evidence that AMY regulates bone resorption and not bone formation (Dacquin et al 2004, Naot & Cornish 2008). AMY deficient mice have an osteoporotic skeletal phenotype without having an effect in the rate of bone formation or the number of osteoblasts. Increased osteoclast number and activity is responsible for the skeletal phenotype of these animals. There were no differences in the alkaline phosphatase activity, type I collagen and mineralisation nodules of osteoblasts of the AMY deficient mice compared to WT mice (Figure S2 (Dacquin et al 2004)). Nevertheless, there is strong evidence that Calcitonin gene related peptide (CGRP), Adrenomedullin and Amylin all *in vitro*, induce osteoblast proliferation, suggesting an anabolic skeletal regulation by each of these peptides ((Cornish et al 1997, Cornish et al 1999, Naot & Cornish 2008, Villa et al 1997).

Differentiation of osteoblasts from mesenchymal stem cells (MSCs) is discussed in the main dissertation introduction section 1.1.3.i. This section focuses on characterising the primary calvarial osteoblasts of RAMP3 KO 129/SvEv mice with respect to the expression of phenotypic markers of osteoblast differentiation. Primary calvarial osteoblast cultures are advantageous in studying osteoblasts and their progenitors at various stages of differentiation with reduced complexity compared with organ cultures. However, these primary osteoblast cultures are not 100% pure as there are sub populations of non-osteoblastic cells (Klein-Nulens 2003). Osteoblast progenitor cells in the culture are pushed toward osteoblast differentiation with osteogenic medium that favours the proliferation and differentiation of osteoblastic cells populations.

Osteoblast growth and differentiation can be briefly divided into four stages: proliferation, extracellular matrix maturation, extracellular matrix mineralisation and apoptosis (Stein et al 2004, van Wijnen et al 2004). Figure 4.1 overleaf, is a schematic representation of the osteoblast differentiation stages and the expression pattern of a few principal differentiation markers.

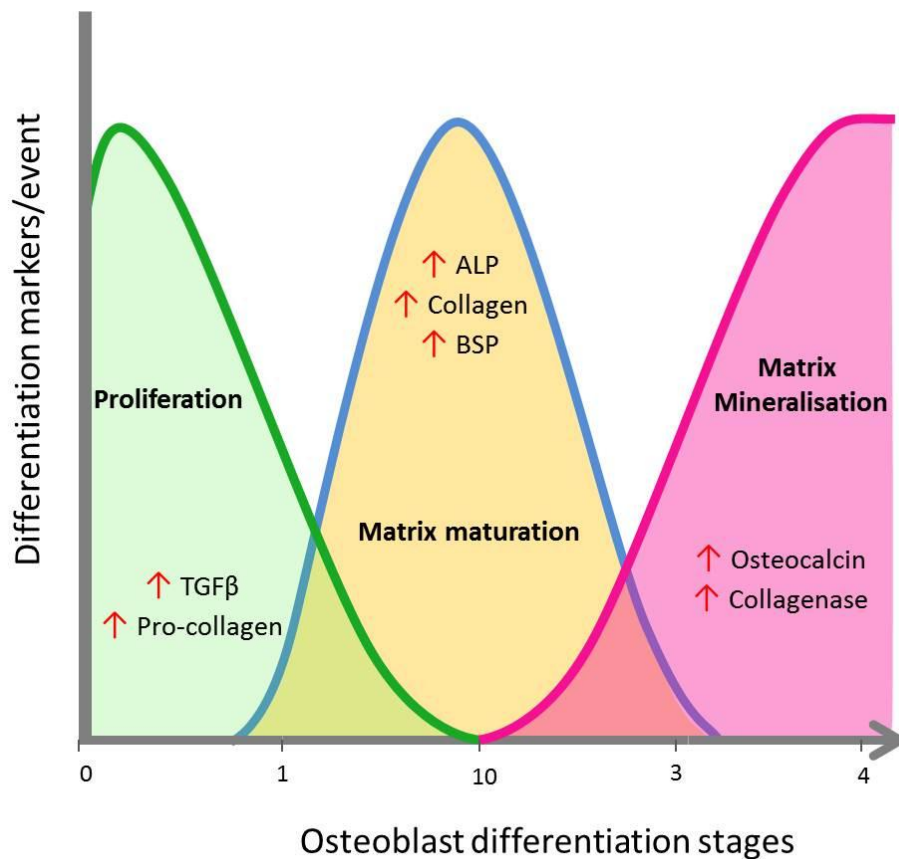


Fig 4.1, Schematic representation of various differentiation markers and events expressed during osteoblast differentiation. Image adapted from (Stein et al 2004)

First, the progenitor osteoblasts proliferate and differentiate into pre-osteoblasts. This is followed by differentiation of the pre-osteoblasts into mature osteoblasts. Some of the early differentiation markers of osteoblasts include alkaline phosphatase (ALP) and collagen (Fletcher et al 1997, Stein et al 2004). ALP is a member of tissue non-specific alkaline phosphatases (TNAP), a hydrolase enzyme that removes phosphate group from many molecules. In bone, ALP converts inorganic pyrophosphate (PPi) to inorganic phosphate (Pi) which combines with calcium to forms hydroxylapatite which is incorporated into the bone matrix (Balcerzak et al 2003). Hence by regulating the amount of PPi in the extracellular matrix, ALP enhances and regulates bone mineralisation. The extracellular matrix maturation stage is followed by its mineralisation. The mineralisation of the matrix requires up-regulation of a late osteoblast differentiation marker Osteocalcin (Oc) (Delmas et al 1986, Stein et al 2004). Some osteoblasts get embedded in the mineralised matrix and eventually the cells undergo apoptosis (Stein et al 2004).

In the previous chapters, we have assessed the skeletal phenotype of the RAMP3 KO mice by measuring the bone morphometric parameters. We have established that RAMP3 KO mice have enhanced skeletal development at young age that results in an adult skeleton with increased trabecular bone thickness, which is beneficial against bone loss induced due to aging. Furthermore, at 8 weeks of age, the RAMP3 KO 129/SvEv male mice had increased trabecular thickness with increase in the osteoblast number and osteoblast covered bone surface compared to the WT mice. On the lateral endochondral surface, the osteoblasts were smaller in the RAMP3 KO mice compared to the WTs which could be due to more dividing osteoblasts in RAMP3 KOs. These finding suggest that the skeletal phenotype observed in the RAMP3 KO 129/SvEv mice is an anabolic effect. To investigate whether this advanced skeletal phenotype is an anabolic phenomenon, we aimed to determine the osteoblast differentiation pattern of RAMP3 KO 129/SvEv mice.

ALP activity, mineralisation, collagen formation and number of colony forming units were determined for both WT and RAMP3 KO differentiating primary calvarial cultures which were differentiated in osteogenic media supplemented with ascorbic acid, dexamethasone and β -glycerophosphate (Jonsson et al 1999).

4.2 Methods and materials

4.2.1 Primary osteoblast cultures:

Each of the primary osteoblast cultures were established from three neonatal (male, post natal day 3) mouse calvariae by sequential enzymatic digestion of the bone matrix. Pups were culled with anaesthetic over-dose following which the calvariae were excised immediately using aseptic techniques

Following this cells were harvested from calvariae of WT/RAMP3 KO mice through a series of sequential digestions as described below:

First digestion: Excised calvariae were washed in Hank's balanced salt solution containing calcium and magnesium without phenol red (Lonza ®) followed by a 15 min digestion in 5ml Collagenase 1A (Sigma®) (1mg/ml prepared in Hank's balanced salt solution). The supernatant was discarded from this first digestion.

Second digestion: The calvariae were again digested at 37°C on a shaker at 200rpm in Collagenase 1A for 30 min and the supernatant was centrifuged at 200 x g for 5 minutes. Pelleted cells formed the first fraction of cells which were re-suspended in non-differentiation media: alpha Minimum Essential Media (MEM) (Sigma®) with 10% heat inactivated fetal calf serum (FCS) (Sigma®) and 0.5% penicillin-streptomycin solution and stored in ice.

Third digestion: The calvariae were washed twice with phosphate buffered saline (PBS) (Sigma®) and incubated at for 15 min at 37°C on a shaker at 200rpm in 5ml of 4mM tetrasodium EDTA pH7.0 (prepared in PBS). Supernatant was centrifuged at 200 x g for 5 minutes. Pelleted cells formed the second fraction of cells which were re-suspended in non-differentiation media and stored in ice.

Fourth digestion: The calvariae were washed twice with Hank's balanced salt solution and again digested in Collagenase 1A for 30 min at 37°C on a shaker at 200rpm. Supernatant was centrifuged at 200 x g for 5 minutes. Pelleted cells formed the third fraction of cells which were re-suspended in non-differentiation media and stored in ice.

All the three fractions of cells were then pooled together and plated in two sterile T75 culture flasks (Nunc™) in non-differentiation media and at 37°C with 5% CO₂. Once the flasks reached 80% confluency, cells were trypsinized (Trypsin-EDTA solution Gibco®) and re-seeded in either

in 6 well culture plates (Nunc™) or T25 culture flasks (Nunc™) alpha MEM according to the experimental setup. On the third day the culture medium was switched on to the differentiation medium containing 5mM/l β -Glycerophosphate, 10nM dexamethasone and 100 μ g/ml Ascorbic acid (day 0) and cells were differentiated up to 20 days. Protein and RNA extractions and fixation of cells for staining was done at day 0, 5, 10, 15 and 20. All buffers and solutions used for primary culture are detailed in the appendix 9.1.3.i.

4.2.2 Mineralizing fibroblast-colony-forming assays:

Mineralizing fibroblast colony forming assays are sequential staining protocols that allows the assessment of alkaline phosphatase (ALP), mineralization, collagen and colony forming units (CFU) (in the same order) all from one fixed set of cell (Scutt A. 2003). Differentiating primary calvarial osteoblasts were fixed with cold 100% ethanol after decanting the media and a PBS wash was given at day 0, 5 10, 15 and 20 of differentiation with/without stimulation. After each assay the stained cell cultures were photographed for analysis using ImageJ™ image editing software. Cells were first stained for ALP and then de-stained for mineralization assay. Following this the cells were de-stained and stained for Collagen staining. Lastly the cells were de-stained and stained for CFU. Brief staining and de-staining protocol used are as follows:

4.2.2.i Alkaline phosphatase staining:

Staining solution (prepared fresh before use): 20mM Tris pH7.5 with 0.5mg/ml of naphthol phosphate AS-BI and 1mg/ml fast red B.

Staining protocol: Fixed cells were allowed to dry and stained with ALP staining solution: 2ml per well of a 6 well plate, for 30 min at room temperature. Staining solution was then decanted. Plates were washed and dried for photographs.

De-staining protocol: Plates were de-stained with 100% ethanol overnight on shaker at 30 rpm. Plates were dried and before staining for mineralization assay.

4.2.2.ii Mineralisation assay:

Staining solution (prepared fresh): Alizarin red solution prepared by adding 1mg/ml alizarin red in distilled water and pH adjusted to 5.5 with ammonium hydroxide.

Staining protocol: Plates were stained with Alizarin red solution: 2ml per well of a 6 well plate, for 30 min at room temperature. Staining solution was then decanted. Plates were washed and dried for photographs.

De-staining protocol: Plates were de-stained with 5% perchloric acid prepared in distilled water for 5 min. Plates were then washed and dried before Collagen staining.

4.2.2.iii Collagen staining:

Staining solution (prepared fresh): 1mg/ml of sirius red in saturated picric acid.

Staining protocol: Plates were stained with Alizarin red solution: 2ml per well of a 6 well plate, for 18hrs at room temperature. Staining solution was then decanted. Plates were washed and dried for photographs.

De-staining protocol: Plates were de-stained with 0.1N NaOH mixed with methanol (50:50) until the collagen stain was completely removed. Plates were washed and dried before methylene blue staining.

4.2.2.iv CFU staining:

Staining solution (prepared fresh): 1mg/ml methylene blue in 10mM borate pH 8.8 adjusted with NaOH.

Staining protocol: Plates were first washed with borate buffer and then stained with 1% methylene blue solution for 30min staining solution was then decanted. Plates were then washed and dried for photographs. Number of colonies each well was quantified manually in ImageJ™ software.

4.2.2.v Image analysis:

Each stained plate was photographed and the image was opened in the Image J software. The circular region of each well was marked and saved as an 8-bit (grey scale image) image. Threshold was set for each stain and the 8-bit image was analysed for area and intensity of the stain. Figure 4.2 below summarizes the image analysis steps with collagen staining image as an example.

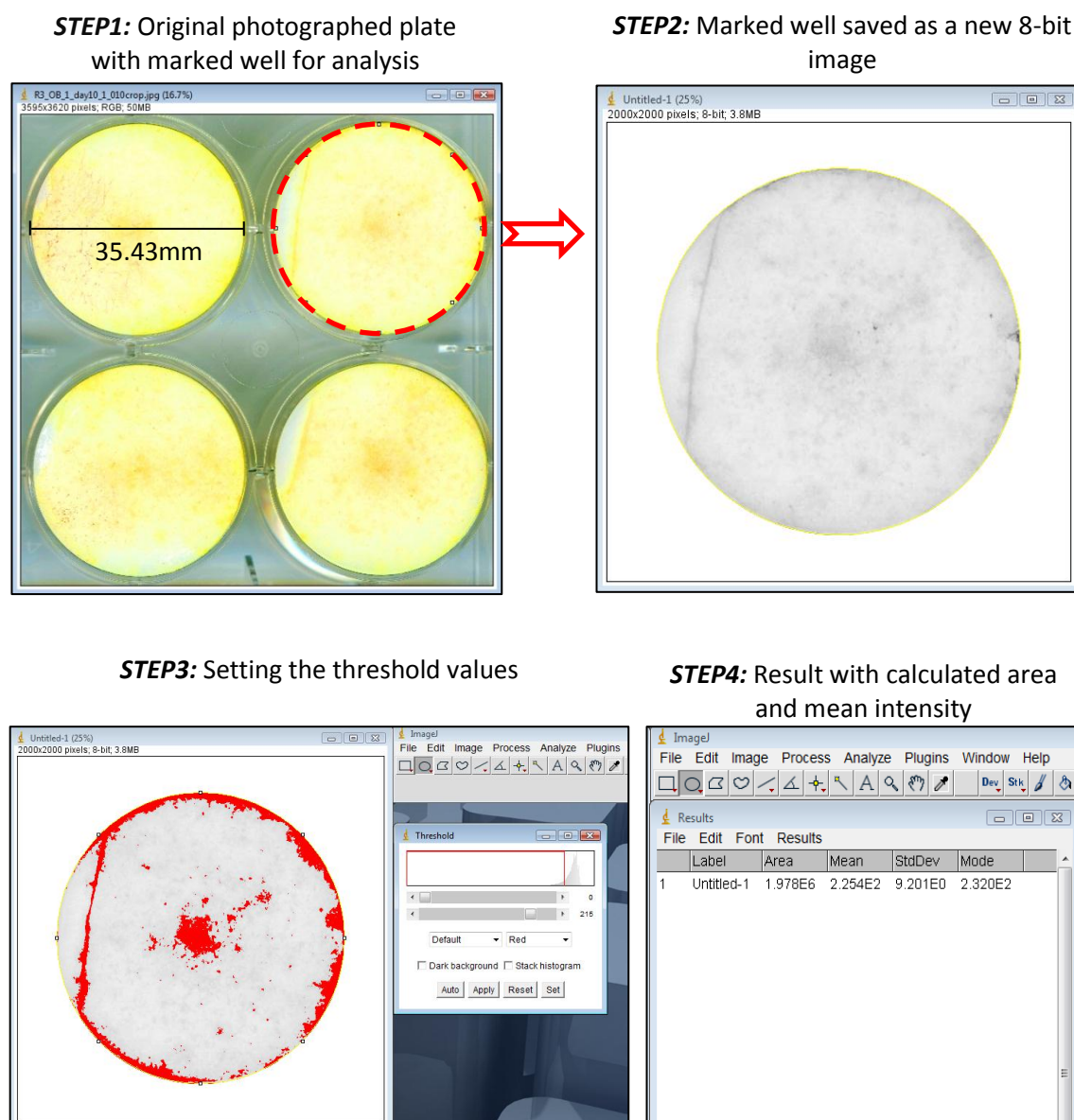


Fig 4.2: Summary of image analysis protocol used to quantify differentiating primary osteoblast culture staining. Top panels show the marking (left) and conversion of each stained well as an 8-bit image (right). Bottom panels show the adjustment of the threshold for collagen stain (in this example) (left) and the result output as the area and mean intensity of the stain (right).

4.3 Results

Differentiating primary osteoblasts were fixed at day 0, 5, 10, 15 and 20 from 4 WT and 4 RAMP3 KO primary osteoblast cultures. At each time point, each culture had 6 repeats for each assay. Mean intensity of each stain at each time point was statistically analysed using Two-way ANOVA test followed by Bonferroni's post multiple analysis test.

4.3.1 Alkaline phosphatase (ALP) activity:

ALP activity in WT osteoblast cultures dropped at day 10 and peaked to maximum at day 15 of differentiation. This peak in ALP at day 15 was not seen in RAMP3 KO cultures. Instead the maximum ALP activity was at day 5 in the RAMP3 KO cultures, after which the ALP activity reduced gradually until day 20 of differentiation. At day 10, the RAMP3 KO cultures had significantly higher ALP compared to WTs, whereas at day 15 the WT cultures had significantly higher ALP compared to RAMP3 KOs. Table 4.1 below summarises the statistical analysis dataset and Figure 4.3 overleaf shows representative ALP staining images of WT and RAMP3 KO cultures at each differentiation time point along with a graphical representation of the statistical analysis.

Table 4.1: Statistical analysis: Primary differentiating osteoblast – ALP assay

Bonferroni's Multiple Comparisons Test	Mean Diff.	95% CI Of Diff.	Significant?	Summary	P Value
WT Vs RAMP3 KO					
Day 0	0.70	-0.61 to 2.01	No	NS	0.8349
Day 5	0.57	-0.79 to 1.92	No	NS	> 0.9999
Day 10	2.41	1.07 to 3.75	Yes	****	< 0.0001
Day 15	-3.27	-4.58 to -1.96	Yes	****	< 0.0001
Day 20	-0.91	-2.32 to 0.51	No	NS	0.4911

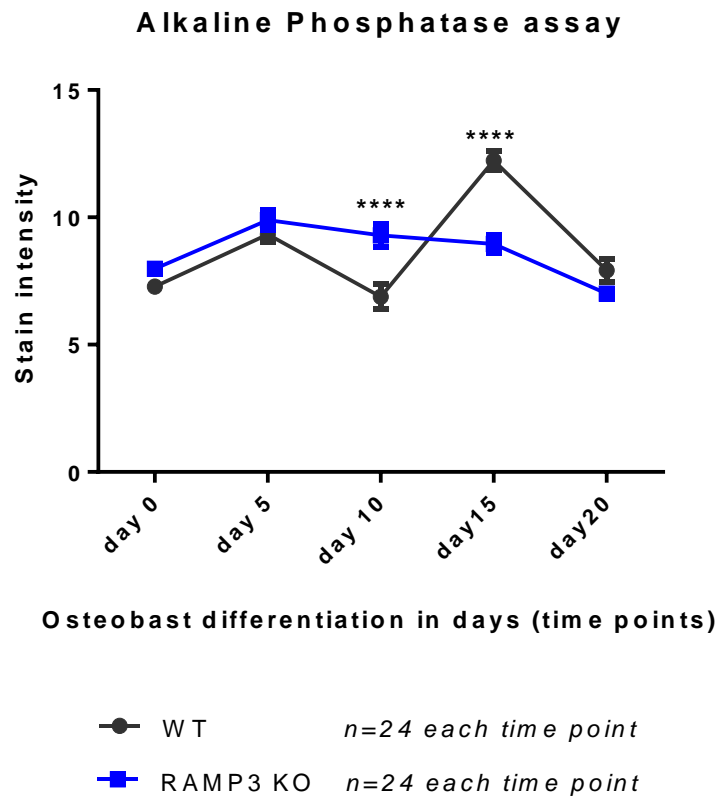
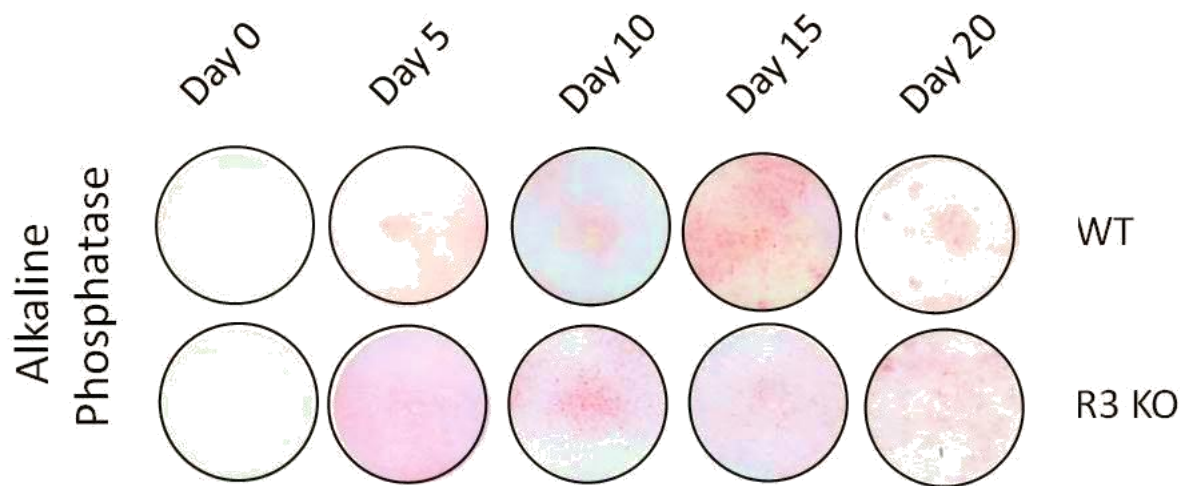


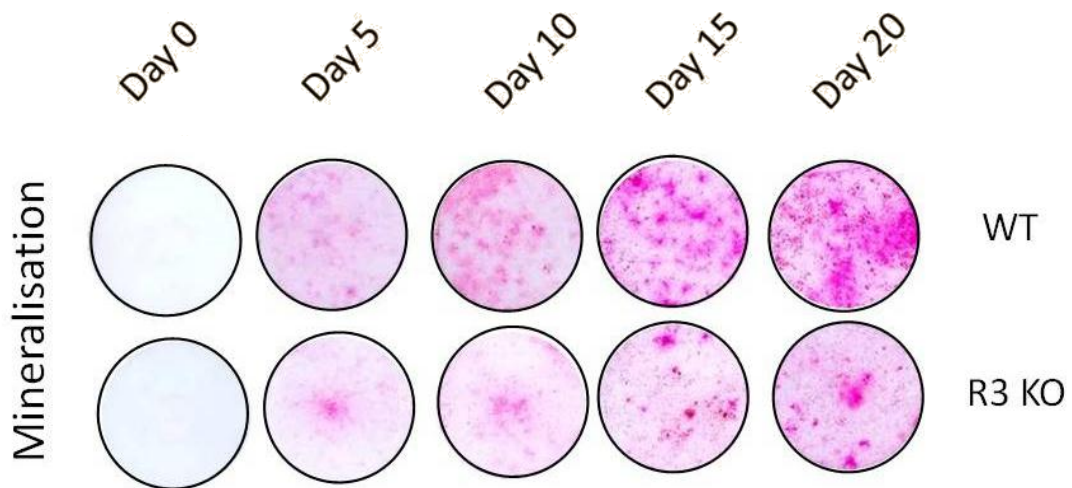
Fig 4.3: Representative ALP staining images of WT and RAMP3 KO primary osteoblast cultures at day 0, 5, 10, 15 and 20 of differentiation (top) along with statistical analysis to determine significant differences (bottom). RAMP3 KO cultures show maximum ALP activity at day 5 whereas WT have maximum ALP activity at day 15. ALP activity is significantly different between WT and RAMP3 KOs at day 10 and day 15 of differentiation ($p = < 0.0001$).

4.3.2 Mineralisation assay:

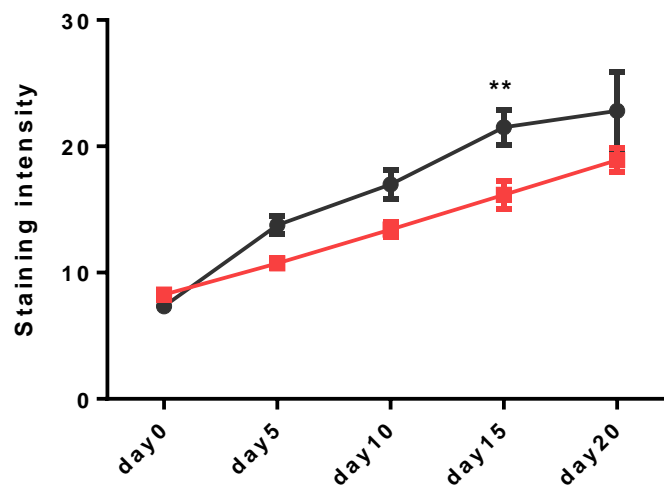
It was observed that the number of mineralising colonies was fewer in the RAMP3 KO cultures at each differentiation time point, compared to WT cultures. The total alizarin stain intensity was significantly higher in WT cultures at day 15, although, by day 20 the difference between WT and RAMP3 KO staining was not significant. Table 4.2 below summarises the statistical analysis dataset and Figure 4.4 overleaf shows representative mineralisation staining images of WT and RAMP3 KO cultures at each differentiation time point along with a graphical representation of the statistical analysis.

Table 4.2: Statistical analysis: Primary differentiating osteoblast – mineralisation assay

Bonferroni's Multiple Comparisons Test	Mean Diff.	95% CI Of Diff.	Significant?	Summary	P Value
WT Vs RAMP3 KO					
Day 0	0.92	-2.94 to 4.78	No	NS	> 0.9999
Day 5	-3.04	-6.86 to 0.78	No	NS	0.2003
Day 10	-3.59	-7.54 to 0.37	No	NS	0.0975
Day 15	-5.34	-9.20 to -1.47	Yes	**	0.0020
Day 20	-3.90	-8.52 to 0.73	No	NS	0.1489



Mineralisation assay



Osteoblast differentiation in days (time points)

● WT $n=24$ each time point
 ■ RAMP3 KO $n=24$ each time point

Fig 4.4: Representative mineralisation assay staining images of WT and RAMP3 KO primary osteoblast cultures at day 0, 5, 10, 15 and 20 of differentiation (top) along with statistical analysis to determine significant differences (bottom). RAMP3 KO cultures have less mineralising colonies compared to WT cultures at each time point. The intensity of alizarin staining in WT at day 15 is significantly higher than RAMP3 KO ($p=0.002$). At day 20 there is no significant difference between WT and RAMP3 KO mineralisation.

4.3.3 Collagen assay:

WT and RAMP3 KO primary osteoblast culture have similar collagen activity until day 10 of differentiation. After day 10 there is a significant drop in the collagen activity in RAMP3 KO osteoblast cultures compared to WT. Table 4.3 below summarises the statistical analysis dataset and Figure 4.5 overleaf shows representative collagen staining images of WT and RAMP3 KO cultures at each differentiation time point along with a graphical representation of the statistical analysis.

Table 4.3: Statistical analysis: Primary differentiating osteoblast - collagen assay

Bonferroni's Multiple Comparisons Test	Mean Diff.	95% CI Of Diff.	Significant?	Summary	P Value
WT Vs RAMP3 KO					
Day 0	-0.53	-3.94 to 2.89	No	NS	> 0.9999
Day 5	-0.21	-3.63 to 3.20	No	NS	> 0.9999
Day 10	0.74	-2.68 to 4.15	No	NS	> 0.9999
Day 15	-5.08	-8.80 to -1.36	Yes	**	0.0024
Day 20	-7.60	-11.70 to -3.49	Yes	****	< 0.0001

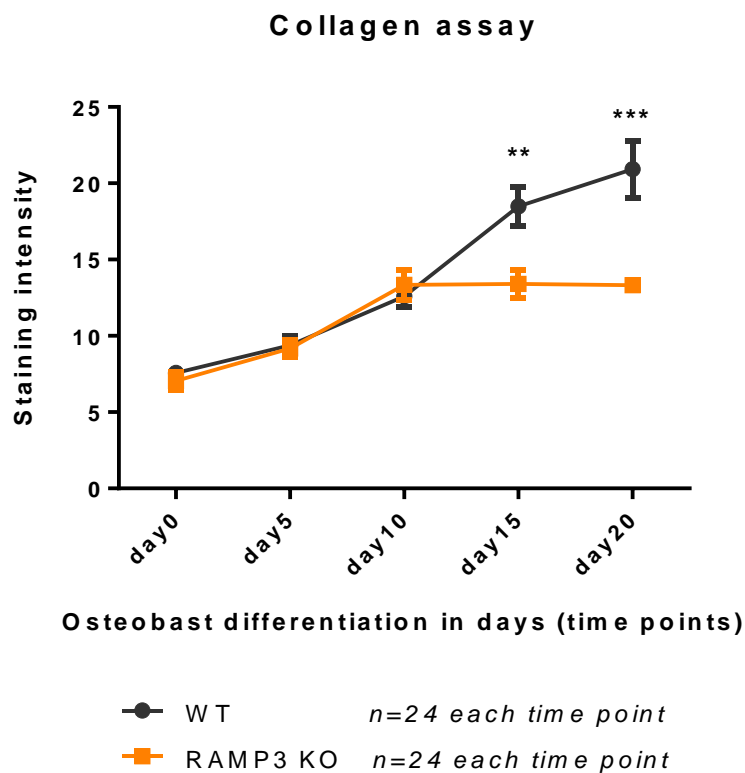
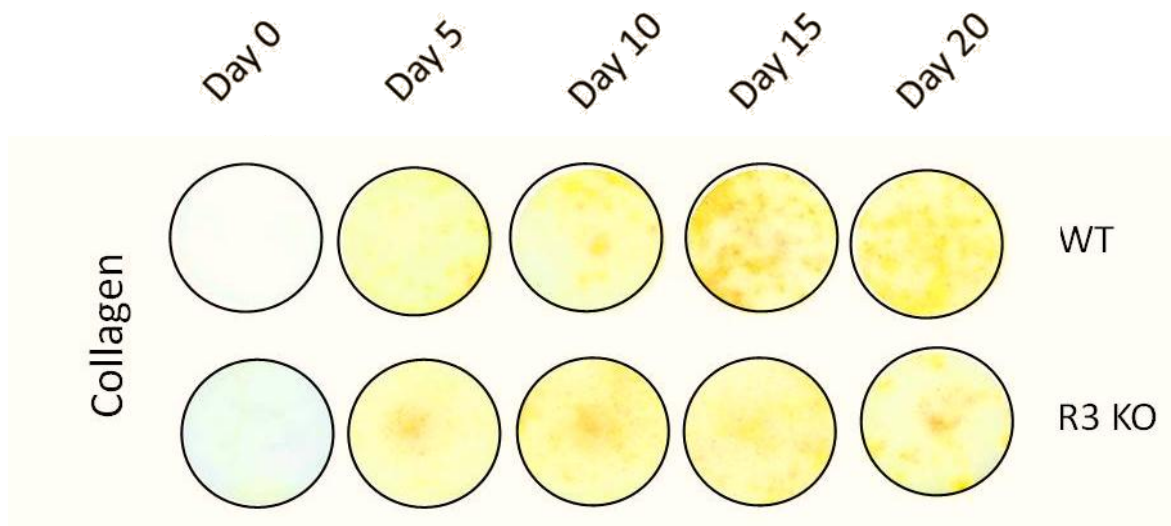


Fig 4.5: Representative collagen staining images of WT and RAMP3 KO primary osteoblast cultures at day 0, 5, 10, 15 and 20 of differentiation (top) along with statistical analysis to determine significant differences (bottom). There is no difference in WT and RAMP3 KO collagen activity at day 0, 5 and 10 of differentiation. After day 10, RAMP 3 KOs have a significant descent in collagen activity, $p=0.0024$ at day 15 and < 0.0001 at day 20.

4.3.4 Colony forming units assay:

Methylene blue staining of colony forming units suggested no statistically significant difference in the number of colony forming units in RAMP3 KO and WT osteoblast cultures, although RAMP3 KO osteoblasts appeared to have bigger individual colonies compared to WTs. Table 4.4 below summarises the statistical analysis dataset and figure 4.6 overleaf shows representative collagen staining images of WT and RAMP3 KO cultures at each differentiation time point along with a graphical representation of the statistical analysis.

Table 4.4: Statistical analysis: Primary differentiating osteoblast - collagen assay

Bonferroni's Multiple Comparisons Test	Mean Diff.	95% CI Of Diff.	Significant?	Summary	P Value
WT Vs RAMP3 KO					
Day 5	4.0	-25.53 to 33.53	No	NS	> 0.9999
Day 10	2.0	-27.53 to 31.53	No	NS	> 0.9999
Day 15	13.0	-16.53 to 42.53	No	NS	0.3928
Day 20	1.0	-28.53 to 30.53	No	NS	> 0.9999

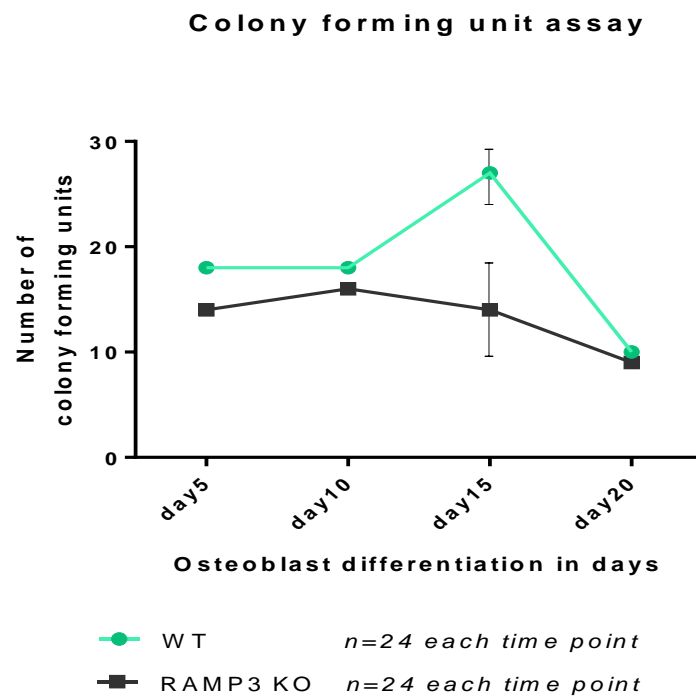
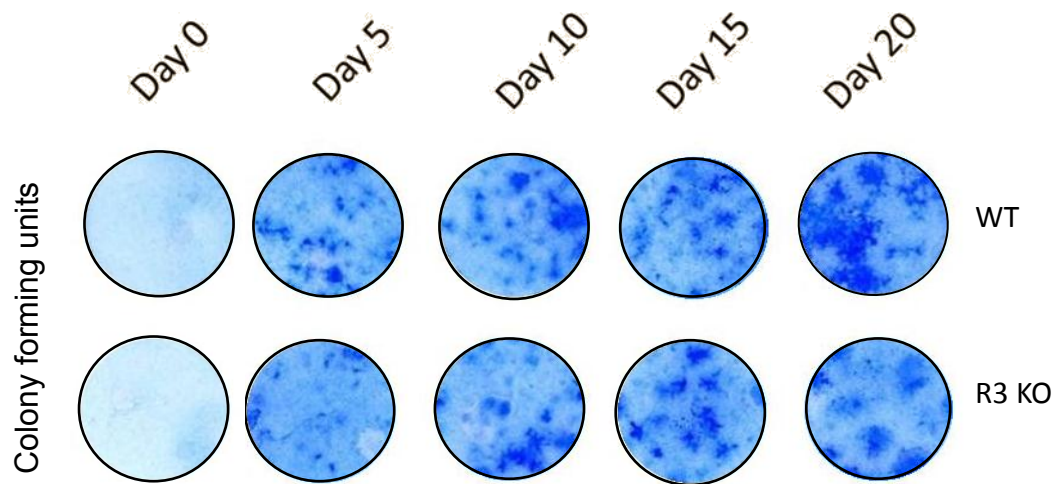


Fig 4.6: Representative methylene blue staining image of WT and RAMP3 KO primary osteoblast cultures at day 0, 5, 10, 15 and 20 of differentiation (top) along with statistical analysis to determine significant differences (bottom). There is no difference in the number of WT and RAMP3 KO colony forming units at any time point, however, RAMP3 KO cultures appear to have larger individual colonies compared to WTs.

4.4 Discussion

With an aim to characterise primary osteoblasts of RAMP3 KO mice, we differentiated four independent primary calvarial cultures of each WT and RAMP3 KO genotype and differentiated the cultures for 20 days. There are a few limitations of this study. Firstly, the cultures were not measured for proliferation at every time-point; hence cultures are not efficiently validated. Also since the study lacks a positive control of osteoblasts differentiation (Eg: Leptin stimulated cultures), the interpretation of the differentiation assays of these primary 129/SvEv cultures is hindered. Moreover, since the suture regions of the calvaria were included in the culture protocol there is a higher population of mixed fibroblasts population that do not represent the true osteoblast cultures.

The osteoblast phenotypic markers were assessed at day 0, 5, 10, 15, 20 of differentiation by 'mineralizing fibroblast-colony-forming assays' as described by (Scutt A. 2003). This technique is advantageous as all the markers: ALP, collagen, mineralisation and CFUs can be quantified from the same fixed cultures sequentially. Hence each assay can be correlated to the other assay for a set of cells. Moreover, since the quantifications were made from four independent cultures (each genotype) with 6 repeats each culture, each differentiation time point, these results can be considered robust.

RAMP3 KO primary calvarial osteoblast cultures showed significant difference in the expression of ALP activity. In WT 129/SvEv mice, the ALP activity showed an initial increase in ALP activity at day 5 followed by a drop in the ALP activity (day 10) which was in-turn followed by maximum ALP activity at day 15 (Fig.4.3). In RAMP3 KOs the ALP activity was similar to WT cultures until day 5 of differentiation, although, unlike the WT cultures, the ALP activity did not drop drastically at day 10 of differentiation in the RAMP3 KOs (Fig.4.3). The ALP activity in RAMP3 KOs steadily increased until day 5 and then gradually declined until day 20 of differentiation. The peak in ALP activity, as observed in the WT cultures at day 10, was absent in the RAMP3 KOs (Fig.4.3). This suggests that the differentiation of the osteoblast precursor into mature osteoblasts, is different in the RAMP3 KO mice. As discussed earlier in Section 1.1.3.i, Runx2, β -catenin, and osterix direct the differentiation of the pre-osteoblasts to form mature osteoblasts, we can imply that expression/regulation of these transcription factors is different in the RAMP3 KO mice compared to the WT 129/SvEv mice (Day et al 2005, Ducy et al 1997, Komori 2006). There is evidence that RAMP3 is one of the early genes response genes regulated by Wnt (Rohrs et al 2009).

Increase in phosphorylated β -catenin levels up-on Wnt3A stimulation, down regulate RAMP3. We can therefore hypothesize that there could be an up-regulation of Wnt/ β -catenin pathway in the RAMP3 KO primary osteoblast cultures (Kenny et al 2005, Ziegler et al 2005). This could result in an alteration in the ALP activity. From our results, it can be suggested that RAMP3 KO mice have a prolonged ALP activation phase which later on gradually declines. This would eventually result in a prolonged extracellular matrix maturation phase which can alter the skeletal phenotype. Fig 4.7 is a schematic representation of the difference of ALP activity in WT and RAMP3 KO osteoblasts, which would have alterations in the matrix maturation phase.

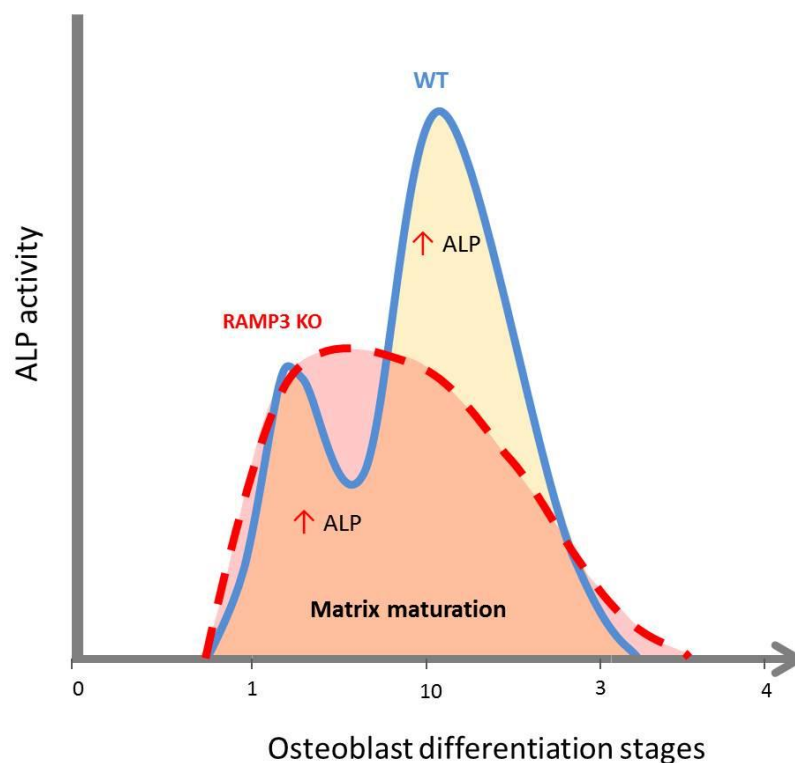


Fig 4.7: Schematic representation of the difference in the ALP activity in WT and RAMP3 KO osteoblasts, which will alter the matrix maturation phase of osteoblasts differentiation.

The number of CFUs in RAMP3 KO osteoblasts is fewer than the number of CFUs in WT osteoblasts, although the colonies in RAMP3 KOs are larger than the WT CFUs (Fig 4.6). In both the WT and RAMP3 KO, the number of CFUs reduced by day 20 of differentiation. This could however be a result of a technical error. Since the colonies grow bigger they overlap and merge into larger colonies, the software used to measure the colonies would just count the merged colonies as one an individual colony. Since there was heterogeneity between colonies irrespective of the genotype, it was not possible to calibrate / standardize the software.

The fewer, but bigger colonies of RAMP3 KO had reduced mineralisation compared to WT osteoblasts, throughout differentiation (Fig. 4.4). However, the difference in mineralisation is only significant at day 15 of differentiation and most interestingly, the RAMP3 KO osteoblasts are able to catch up with the WTs with respect to mineralisation by day 20 of differentiation (Fig. 4.4). This is not observed in collagen formation. RAMP3 KO osteoblasts have similar amounts of collagen compared to WTs until day 10 of differentiation, although, there is a significant reduction in collagen formation at day 15 and day 20 of differentiation (Fig. 4.5).

From these *in vitro* primary osteoblast experiments we can conclude that RAMP3 KO mice have fewer osteoblasts that have reduced collagen formation ability, but form larger mineralisation nodules and are capable to mineralising the same amount of bone as the WTs. Our *in vitro* findings do not correspond to the *ex vivo* osteoblast analysis of histological section. This can be due to two reasons. Firstly, despite the use of osteogenic stimulators to differentiate the osteoblasts *in vitro*, it is not possible to mimic the *in vivo* microenvironment which dictates the osteoblast differentiation in bone. Secondly, the primary osteoblast cultures used for the *in vitro* experiments were established from neonatal mice. Hence they do not reflect the differentiation of osteoblasts in adult mice. Furthermore, since RAMP3 KO mice have an age dependent skeletal phenotype, it would be helpful to study the same differentiation patterns in primary osteoblast cultures derived from adult marrow cultures of RAMP3 KO and WT 129/SvEv mice in the future.

In conclusion, RAMP3 KO primary osteoblasts have:

- Decreased but prolonged ALP activity.
- Decreased collagen formation and,
- Fewer but larger colony forming units.

Chapter 5: Expression of RAMP1,2 and 3 mRNA in differentiating primary osteoblasts.

5.1 Introduction

Receptor activity modifying proteins (RAMPs) are expressed in many tissues including the skeleton (Parameswaran & Spielman 2006). In humans, all the RAMP isoforms are highly expressed in the skeletal muscle, whereas in mouse RAMP1 and RAMP2 are highly expressed and expression of RAMP3 is yet to be fully determined (Parameswaran & Spielman 2006). RAMPs 1-3 are all ubiquitously expressed in rat and mouse primary osteoblasts and in cell lines including MC3T3-E1 and UMR106-006 osteoblast-like cell lines (Naot & Cornish 2008, Uzan et al 2004). RAMPs are also expressed in osteoclast cultures and the expression of individual RAMP isoform varies during the osteoclast differentiation (Granholm et al 2008). Nakamura et. al. in 2003 reported the presence of RAMP2 but not RAMP1 or 3 in mature osteoclast cultures and Granholm et. al. reported presence of RAMP1, 2 and 3 in osteoclast cultures (Granholm et al 2008, Nakamura et al 2005). Additionally, it was also observed that expression of RAMP1 and RAMP3 decreases when the cells become multinucleated (Granholm et al 2008). It can therefore be suggested that, RAMPs play an important role in regulating osteoclastogenesis.

The skeletal phenotype observed in the RAMP3 KO mice appears to be an anabolic skeletal effect rather than an anti-resorptive regulation. Given the evidence that the number of osteoclasts is neither different in the cortical bone nor in the trabecular bone and conversely with evidence that the number of osteoblasts is more in the trabecular bone of RAMP3 KOs we have demonstrated that the osteoblasts but not osteoclasts are affected in RAMP3 KO mice (Chapter 3). Furthermore we have also demonstrated that the primary osteoblast have a different osteoblast differentiation pattern compared to WTs (Chapter 4). This chapter focuses on determining whether the expression of RAMPs plays an important role in osteoblast differentiation and whether the RAMP3 KO mice have an altered RAMP expression profile in comparison to the WTs that could potentially result in an altered signal transduction in these KO animals.

Kadmiel et al have reported that RAMP 1 and 3 do not compensate for the absence of RAMP2 in RAMP2 KO mice which are embryonically lethal. However, RAMP1 and RAMP3 KO mice are viable which could perhaps be because other RAMPs compensates for these RAMP isoforms (Kadmiel et al 2012). Given that there is evidence that RAMP 1 and 3 forms intracellular homodimers and, although this is not yet proved experimentally, RAMP2 is also expected to form homodimers (Sexton et al 2001). We can therefore hypothesize that these reserves of RAMPs in

the cytoplasm can compensate for the loss of other RAMPs and form functional receptors that are presented on the cell surface.

To test our *investigate whether there is a differences in RAMP 1,2 and 3 mRNA expression between RAMP3 KO and WT primary osteoblasts*, we performed quantitative PCR (qPCR) in differentiating primary osteoblasts of RAMP3 KO and WT 129/SvEv mice.

Three independent primary osteoblasts cultures were established from WT and RAMP3 KO each. Total RNA was collected at day0, 5, 10, 15, and 20 of differentiation.

5.2 Methods and materials

5.2.1 Sample preparation:

5.2.1.i Total RNA from differentiating primary osteoblasts:

Detailed calvarial primary culture protocol is described in Section 5.2.1. Total RNA was collected from differentiating calvarial primary osteoblasts of WT (SVEV/129) and RAMP3 KO genotype on day 0, 5, 10, 15 and 20 of differentiation. One T25 flask-worth of each culture was harvested at each time point. The medium was removed and 500µl of TRIZOL® reagent was added to the cells. The cells were collected in 1.5 ml tubes by scraping. Total RNA was then extracted using the protocol provided by the manufacturer (Invitrogen™). RNA in each sample was quantified in NanoDrop® (Thermo Scientific, Wilmington, USA), a micro-volume UV-vis spectrophotometer, at A260 and the purity of preparation checked by determining the 260/280 ratio. Samples were then stored at -20°C.

5.2.1.ii Controls:

Mouse brain cDNA was used as a positive control in end point PCR. Total RNA was extracted from previously snap frozen WT (SVEV/129) mouse. The mouse brain (snap frozen tissue stored at -80°C) was weighed and allowed to thaw at -20°C for an hour prior being chopped into small pieces. The 100mg chopped tissue was placed in a 7 ml tissue grinder tube and 1ml of ice-cold TRIZOL® reagent was added. The tissue was first homogenized by 15 passes of the loose pestle and then by 15 passes of the tight pestle. This homogenate was used to extract total RNA according to manufacturer's guidelines (Invitrogen™). RNA was quantified and stored similar to total RNA from cell cultures.

5.2.1.iii DNase treatment:

Total RNA generated was subjected to DNase treatment to prevent genomic DNA contamination. Precision™ DNase kit (Primerdesign®) was used to treat the RNA samples. Briefly, the following reaction mix was incubated at 30°C for 10 min to degrade the DNA from the RNA sample:

RNA sample:	50.0µl
10X Precision™ DNase reaction buffer:	5.0µl
Precision™ DNase:	1.0µl (for upto 100µl of RNA sample)

DNase was inactivated by incubating the mixture at 55°C for 5 min. Samples were stored at -20°C.

5.2.1.iv Reverse transcription to generate cDNA

cDNA was generated from total RNA samples using Precision nanoScript™ Reverse transcription kit (Primerdesign®). Briefly, the cDNA was generated in two steps:

Step 1: Annealing

For every 1µg of RNA, a 10µl annealing reaction mix was prepared as below. The mix was then heated to 65°C for 5 min and the samples were then directly transferred from 65 °C to ice.

Annealing reaction mix:

RNA template:	1µg
RT oligoDT:	1µl
RNAse/DNAse free water: upto	10 µl
Final volume:	10.0µl

Step 2: Extension

To each of the 10µl annealing reaction mix (step 1) the following 10µl RT mix was added.

RT mix:

nanoScript 10X Buffer:	2.0µl
dNTP mix 10mM of each:	1.0µl
DTT 100mM:	2.0µl
RNAse/DNAse free water:	4.0µl (5.0µl for RT- samples)
nanoScript enzyme:	1.0µl (not added for RT- samples)

Annealing reaction mix:	10.0µl
Final volume:	20.0µl

This reaction mix was then placed in a PCR machine with the following conditions:

- 1) 55°C - 20 min
- 2) 75 °C - 15min
- 3) Hold at 4 °C

Samples were then stored at -20 °C.

5.2.2 End point PCR:

GoTaq® DNA Polymerase kit (Promega® Cooperation, Madison, USA) was used to detect RAMP1/2/3 expression in cDNA of WT and RAMP3 KO primary osteoblast differentiated for 0,5,10,15 and 20 days. Each 25µl reaction mix contained 5µl of 5X Green GoTaq® reaction buffer, dNTP at a final concentration of 0.2mM (10mM each dNTP stock), MgCl₂ at a final concentration of 1.5mM (25mM each stock) and GoTaq® DNA Polymerase 2.5units. Proportions for PCR mix are mentioned below along with the respective PCR conditions. PCR amplicons were visualized by electrophoresis in 1.5% Agarose gel (Sigma®) prepared in Tris-base-EDTA buffer and containing 0.5ug/ml ethidium bromide. Primer sequences used are detailed in table 5.1 below.

PCR reaction mix:

5X Green GoTaq® reaction buffer: 5µl
MgCl₂: 0.75µl
dNTP mix : 0.5µl
Forward Primer: 1.25µl
Reverse primer: 1.25µl
GoTaq® DNA Polymerase: 0.5µl
cDNA: 2µg
Nuclease free water: upto 25µl

Thermocycler conditions:

1) Hold 95°C Enter
2) 95°C – 1.30min
3) 95°C – 30sec
4) 59°C - 30 sec (for RAMP1) or
4) 60°C - 30 sec (for RAMP2) or
4) 50°C - 30 sec (for RAMP3)
5) 72°C - 45 sec (repeated 3-5, 35 cycles)
6) 72°C - 3min
7) Hold at 4°C

Table 5.1: RAMP1/2 and 3 primer sequences for end point PCR:

Primer ID	Primer Sequence	T _m	Position - mouse RAMP1/2/3 mRNA	Amplicon
<i>RAMP1f</i>	5' CACCATCTTTCATGGTCACTG 3'	60.3 ⁰ C	322	186bps
<i>RAMP1r</i>	3' CAATCGTGTGCGCCACGTGC 5'	63.5 ⁰ C	489	
<i>RAMP2f</i>	5' CATCCCACTGAGGACAGCCT 3'	61.4 ⁰ C	299	302bps
<i>RAMP2r</i>	3' GATCATGGCCAGGAGCACAT 5'	59.4 ⁰ C	591	
<i>RAMP3f</i>	5' AAAGCCTTCGCTGACATGAT 3'	55.3 ⁰ C	161	100bps
<i>RAMP3r</i>	3' CCATCTCGGTGCAGTTAGTG 5'	59.4 ⁰ C	244	

5.2.3 Real time PCR:

Real-time or quantitative PCR, is a technique use to simultaneously amplify and quantify the DNA sequence of a gene of interest. Traditionally quantification of the amplifying DNA sequence is carried out by two methods.

Non-specific quantification: This technique measures the incorporation of a double stranded DNA intercalating fluorogenic dye, like SYBR green that binds to newly amplified DNA.

Specific quantification: This technique measures the number of annealed DNA primers that are fluorescently probed. This quantification is sequence specific where primer sequences are probed with double dye probes like 6-carboxyfluorescein (FAM) and the probe is detected only when the primer sequence is hybridized with the newly synthesised complimentary DNA strand. This qPCR technique is commonly known as double dye probe qPCR or Taqman style qPCR. The double dye probe qPCR technique was used in our study.

5.2.3.i Gene of Interest:

Custom real-time PCR/ quantitative PCR (qPCR) assays with double dye probes – FAM labelled (Taqman style) were designed by Primerdesign® for each of the human and mouse RAMPs (1, 2 and 3) (Table 5.2). Primers were validated and a validated copy number positive control was provided for each qPCR assay. Each sample was run in triplicate per gene of interest, per reference gene per plate. The expression of each gene of interest was normalised to the expression of reference genes / house-keeping gene. The optimal number of reference genes needed and the most suitable reference genes were identified using the mouse geNorm™ kit by Primerdesign®. Primer sequences designed to detect individual RAMP expression are detailed below.

Table 5.2: Custom double dye probe primer sequences from Primerdesign®

<i>Primer ID</i>	<i>Primer Sequence</i>	<i>T_m</i>	<i>Position</i>	<i>Amplicon</i>
<i>RAMP1f</i>	5' ACCTGGGATTATAAGCCTGTTTA 3'	56.6 ⁰ C	1,727	85 bps
<i>RAMP1r</i>	3' CATTTCCTCTGTCTCTTCTTCAT 5'	56.4 ⁰ C	1,811	
<i>RAMP2f</i>	5' CCAACTGCTCCCTGGTGC 3'	58.1 ⁰ C	454	93 bps
<i>RAMP2r</i>	3' GGAAGGGGATGAGGCAGATG 5'	57.9 ⁰ C	546	
<i>RAMP3f</i>	5' CCAACTGCACCGAGATGGAG 3'	58.8 ⁰ C	270	98 bps
<i>RAMP3r</i>	3' GGAGAAGAACTGCCTGTGGAT 5'	58.0 ⁰ C	367	

5.2.3.ii Reference gene:

Accurate relative quantification, of the gene of interest expression depends on the normalisation value obtained from the expression of a robust house-keeping gene. There is increasing evidence that many traditionally used house-keeping genes are not as constant as suggested previously (Reddy et al 2013, Stephens et al 2011). This may be due to different tissue or disease origin or experimental parameters (Vandesompele et al 2002). Hence it is necessary to screen a range of standard house-keeping genes to identify the most robust reference gene that is stably expressed for a particular experimental set-up. Certain experiments may need more than one reference gene to validate the expression of genes of interest (Bustin et al 2009, Vandesompele et al 2002).

FAM labelled mouse geNorm™ reference gene selection kit with 6 reference genes: 18s ribosomal RNA, Beta-actin (ACTB), β_2 microglobulin (B2M), eukaryotic initiation factor-4A (eIF4A), Glyceraldehyde 3-phosphate dehydrogenase (GAPDH), 60S ribosomal protein L13a (RLP13A) were used to determine stable reference gene expression (Primerdesign®,UK). Reference genes stably expressed in both genotypes across all time points were identified by analysing geNorme CT values in qbase+ software by Biogazelle®. The qbase+ software evaluates two values: geNorm“M” and geNorm“V”.

The “M” value indicates the average expression stability value of a particular reference gene at each step of a stepwise exclusion of the least stable reference genes. geNorm“V” is known as the “pairwise variation”. The value “V” determines the optimal number of reference genes required in a particular experiment. If an optimal number of reference genes is not determined, then the three most stably expressing reference genes are chosen and run along with the gene of interest each time.

Each qPCR assays was setup in sterile MicroAmp® Optical 384-Well Reaction Plate (Life technologies™), in Scie-Plas UV sterilisation PCR cabinet (Topac, USA) on ice. All qPCR assays were run and analysed in Applied Biosystems™ 7900 Real Time PCR machine. Since all the primers were FAM labelled (absorbance maximum of 492 nm, emission maximum of 517 nm), FAM detectors were used to quantify amplification.

5.2.3.iii qPCR reaction mix (for all reference genes and genes of interest):

Resuspended primer mix:	1.0µl
<i>Precision</i> [™] 2x qPCR Mastermix:	10.0µl
RNAse/DNAse free water:	4.0µl
cDNA:	5.0µl (generated from 5ng RNA per reaction)

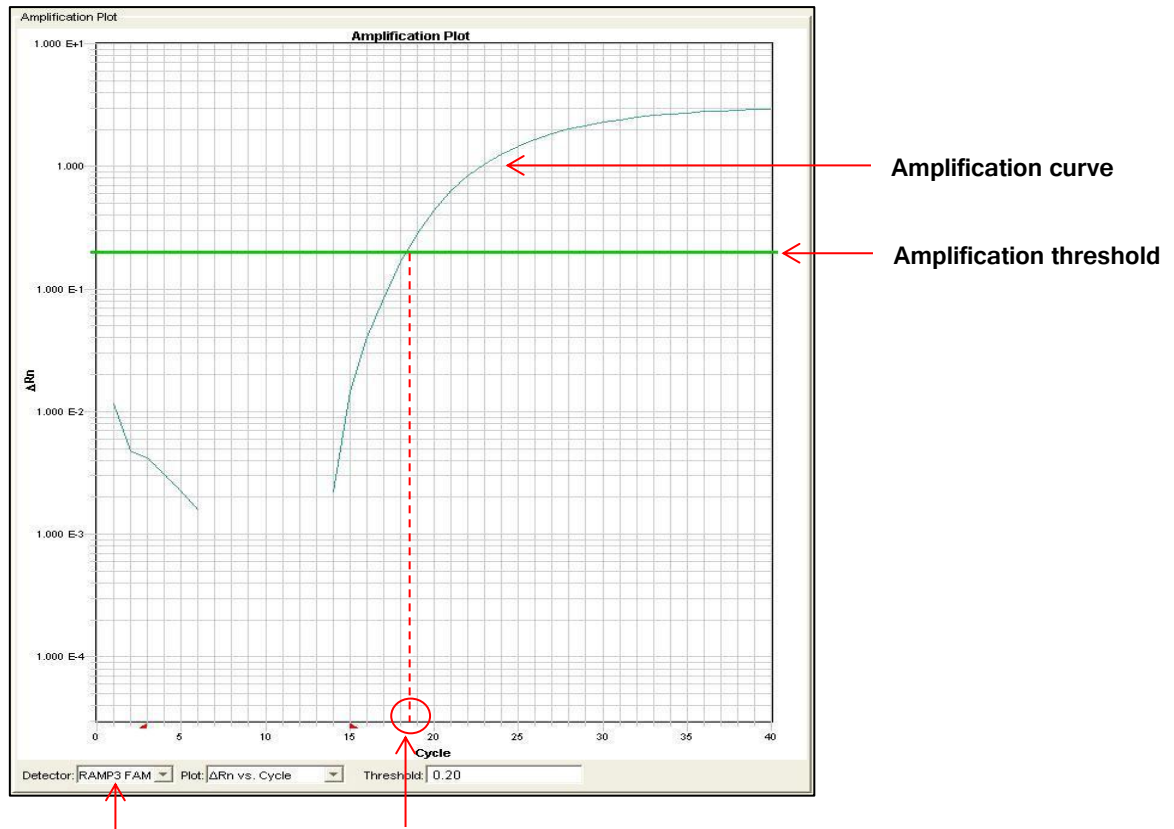
5.2.3.iv Thermocycler conditions used in Applied Biosystems[™] 7900 Real Time PCR machine:

- 1) Enzyme activation : 95°C – 10min
- 2) Denaturation: 95°C – 15sec
- 3) Data collection: 60°C – 60sec

Repeat step 2 and 3, 40 times.

5.2.3.v “CT value”

qPCR quantification is in terms of threshold cycle value - “CT value”. An amplification threshold for a certain gene is set for every experiment. Briefly, the number of PCR cycles required to reach the amplification threshold is the CT value. The CT value is inversely proportional to the expression of the gene. Hence higher the CT value, lower the expression of the gene. An example of an amplification plot generated by the qPCR machine is represented and annotated overleaf (Figure 5.1).



Gene of Interest & CT value ~18.7
fluorescent probe used

Fig 5.1: Amplification plot generated by the qPCR machine showing the amplification threshold, the gene of interest (RAMP3) and the fluorescent probe (FAM) detector used. The CT value can be calculated as the X value (~18.7) corresponding to the point at which the amplification curve intersects the threshold.

5.2.3.vi Calculating relative expression of a gene of Interest:

CT values are obtained for all the reference genes and the genes of interest. If multiple reference genes are used the mean CT value of all the reference genes is calculated.

1) The relative expression / normalised expression of a gene of interest is calculated as “Delta CT” (ΔCT):

$$\Delta CT = CT \text{ value (gene of interest)} - \text{mean CT value of all the reference genes.}$$

2) Fold change in expression and calculation of “Delta delta CT” ($\Delta\Delta CT$)

$$\Delta\Delta CT = \Delta CT \text{ value (one genotype/ timepoint)} - \Delta CT \text{ value (other genotype/ timepoint)}$$

$$\text{Fold change} = 2^{-\Delta\Delta CT}$$

5.2.3.vii Graphical representation and statistical analysis:

All graphical representations and statistical analysis were carried out in GraphPad Prism® 6. Two way ANOVA test and Bonferroni's post multiple comparison test were performed to determine the statistical significance of RAMP expression between genotypes and different differentiation time-points. P value ≤ 0.05 was considered significant.

5.3 Results

5.3.1 End point PCR to detect RAMP cDNA expression in primary osteoblasts:

5.3.1.i RAMP1

RAMP1 was expressed in all WT and RAMP3 KO primary osteoblast cDNA at all differentiation time points. Non reverse transcription (RT-) control of each sample was used as a genomic DNA control. None of the WT or RAMP3 KO RT- controls amplified a PCR product. RAMP1 cDNA was amplified in +ve control - mouse brain cDNA, but not in its RT- control (Fig. 5.2). All amplicons were confirmed to be RAMP1 cDNA sequences by sequencing.

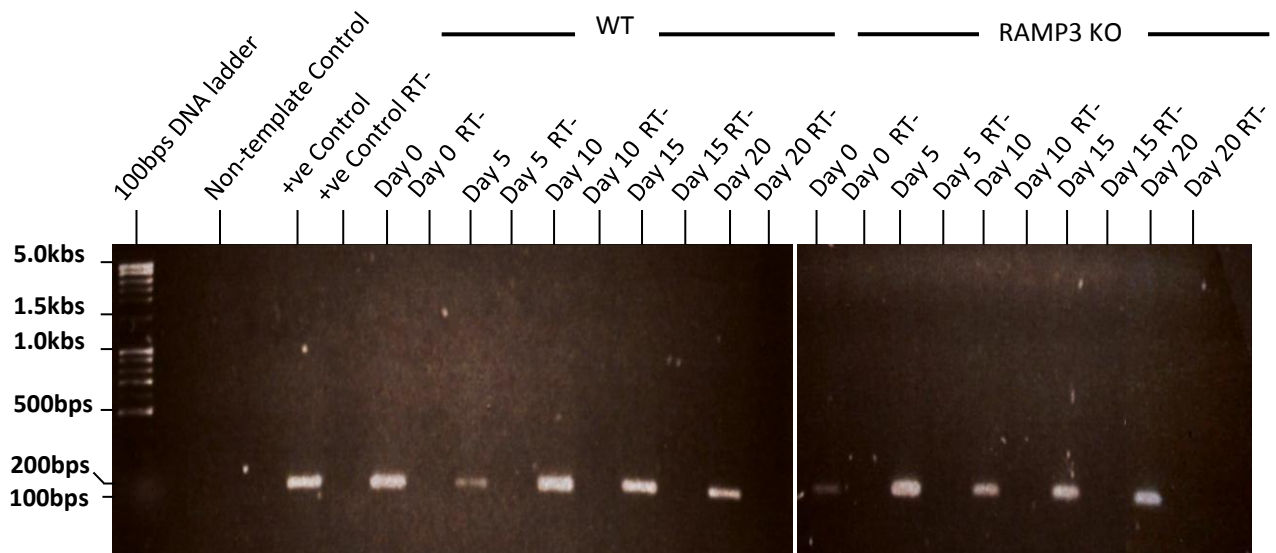


Fig 5.2 : Agarose gel electrophoresis (1.5%) for end point PCR to detect RAMP1 cDNA expression in WT and RAMP3 KO primary osteoblast cultures differentiated for 0, 5, 10, 15 and 20 days. 186bps cDNA amplicon was amplified in +ve control (mouse brain cDNA) and in both WT and RAMP3 KO primary osteoblast cDNA differentiated for 0,5,10,15 and 20 days. None of the RT- samples or controls amplified a product. Three experimental repeats of the entire sample set were carried out.

5.3.1.ii RAMP2:

Expression of RAMP2 was observed in all WT and RAMP3 KO primary osteoblast cDNA at all differentiation time points. Non reverse transcription (RT-) control of each sample was used as a genomic DNA control. RAMP2 cDNA was amplified in +ve control (mouse brain cDNA) but no product was amplified in the RT- control. Genomic RAMP2 amplification was observed in mouse brain RT- control. Genomic RAMP2 amplification was also observed in WT day 15, day15 RT-, day 20 RT- and brain RT- cDNA preparations (Fig. 5.3). All amplicons were confirmed to be RAMP2 cDNA sequences by sequencing.

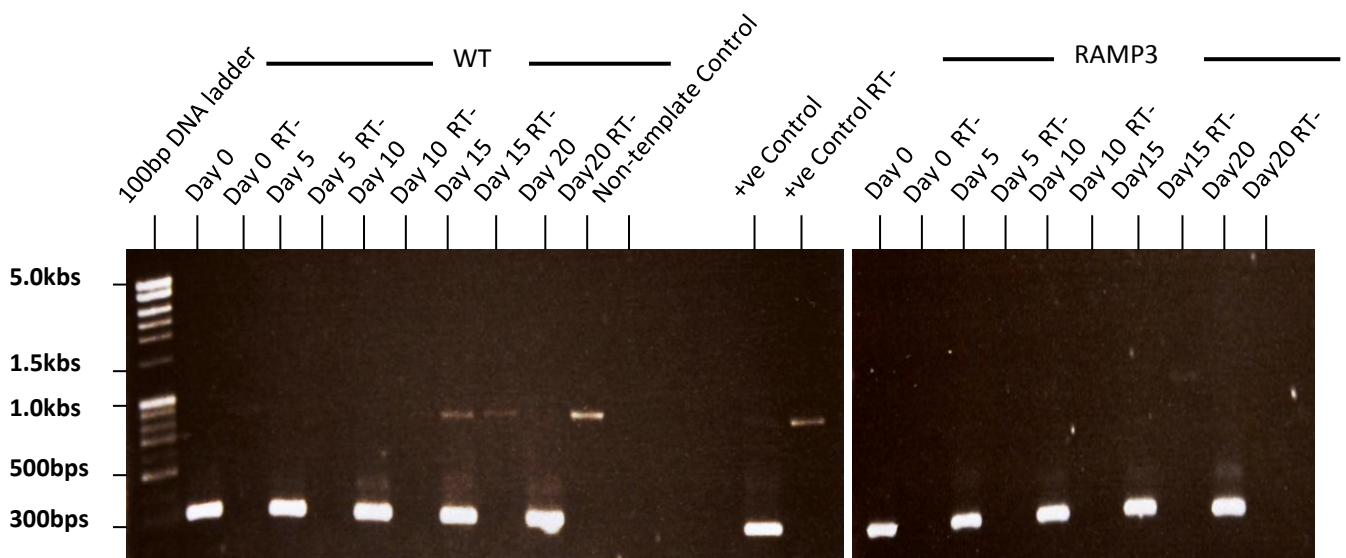


Fig 5.3: Agarose gel electrophoresis (1.5%) for end point PCR to detect RAMP2 cDNA expression in WT and RAMP3 KO primary osteoblast cultures differentiated for 0, 5, 1,15 and 20 days. 302bps cDNA amplicon was amplified in +ve control (mouse prostate cancer cell line BMA 178-2) and in both WT and RAMP3 KO primary osteoblast cDNA differentiated for 0,5,10,15 and 20 days. None of the RT- samples or controls amplified a product. Genomic RAMP2 amplification was observed in WT day 15, day15 RT-, day 20 RT- and +ve control RT- preparations. Three experimental repeats of the entire sample set were carried out.

5.3.1.iii RAMP3:

Expression of RAMP3 cDNA was only observed in all WT primary osteoblast cDNA at all differentiation time points but not in the RAMP3 KO samples as expected. Non reverse transcription (RT-) control of each sample was used as a genomic DNA control. None of the WT or RAMP3 KO RT- controls amplified products. RAMP3 cDNA was amplified in +ve control (mouse brain cDNA) but not in its RT- control (Fig. 5.4). All amplicons were confirmed to be RAMP3 cDNA sequences by sequencing.

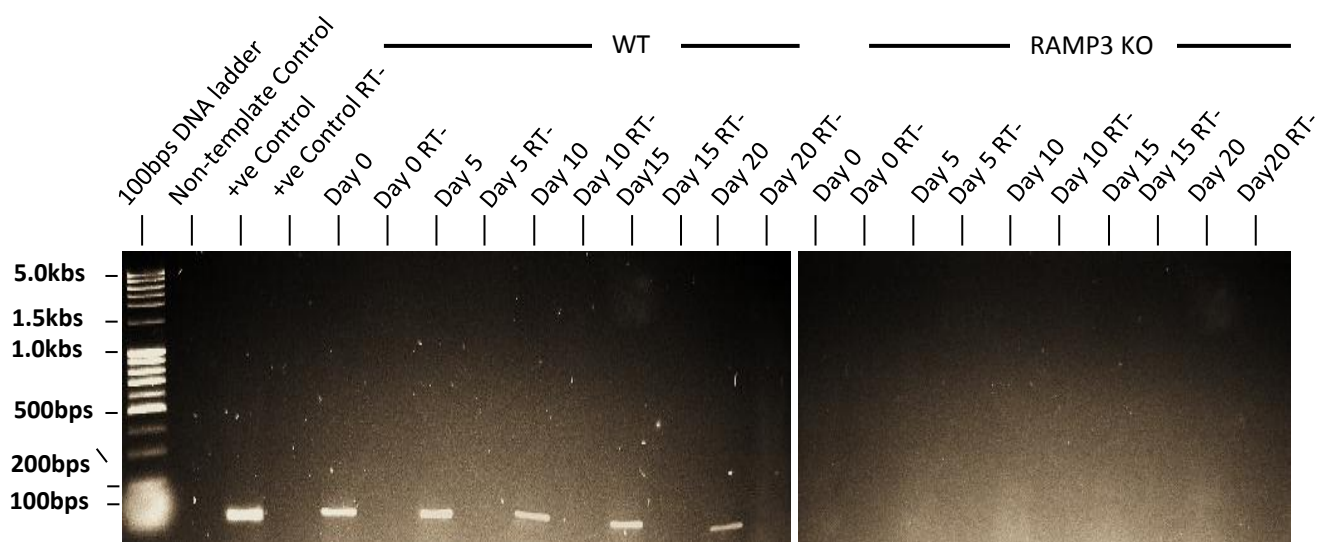


Fig 5.4: Agarose gel electrophoresis (1.5%) for end point PCR to detect RAMP3 cDNA expression in WT and RAMP3 KO primary osteoblast cultures differentiated for 0, 5, 1,15 and 20 days. 100bps cDNA amplicon was amplified in +ve control (mouse brain cDNA) and in WT primary osteoblast cDNA differentiated for 0,5,10,15 and 20 days. None of the RAMP3 KO primary osteoblast time-points expressed RAMP3 cDNA. Similarly none of the RT- samples or controls amplified products. Three experimental repeats of the entire sample set were carried out.

5.3.2 Quantitative PCR:

5.3.2.i Reference gene identification using geNorm™ kit:

The geNorm™ kit by Primerdesign® was used to determine the most stably expressing housekeeping genes in WT and RAMP3 KO primary osteoblasts and the number of reference genes required to validate the quantification of expression of genes of interest in these samples.

As mentioned earlier, the mouse geNorm™ reference gene selection kit consisted of 6 known reference genes 18s, ACTB, B2M, EIF4A2, GAPDH and RPL13A. The relative expression of these genes was determined in both WT and RAMP3 KO primary osteoblast cDNA at 5 time points during differentiation: day0, 5, 10, 15 and 20.

The CT values obtained for each of the reference genes was used to calculate the most stably expressing gene across (geNorm M) and the minimal number of reference genes needed for the experimental set up (geNorm V).

Figures 5.5 and 5.6 overleaf are graphical representations generated by the qBase+ software, showing relative expression of each reference gene at each time point in WT (Fig. 5.5) and in RAMP3 KO (Fig. 5.6).

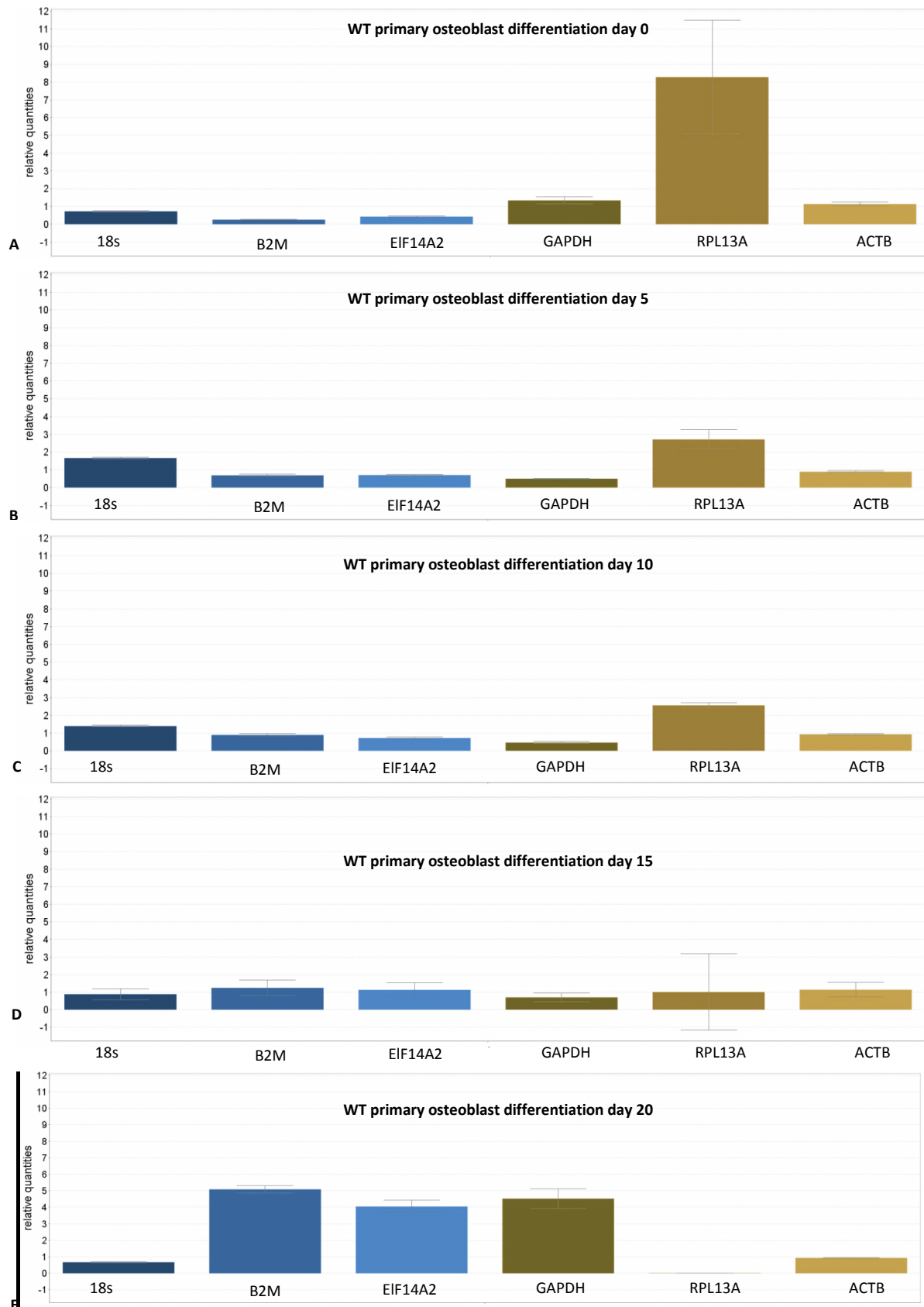


Fig 5.5: A graphical representation of relative cDNA expression of the reference genes (from left to right in each histogram): 18s, B2M, Elf14A2, GAPDH, RPL13A and ACTB, at each differentiation time point (top to bottom) day0 (A), day5 (B), day10 (C), day15 (D) and day20 (E) of WT primary osteoblast. Each sample was run in triplicate, per gene, and three independent experimental repeats were carried out ($n = 3$).

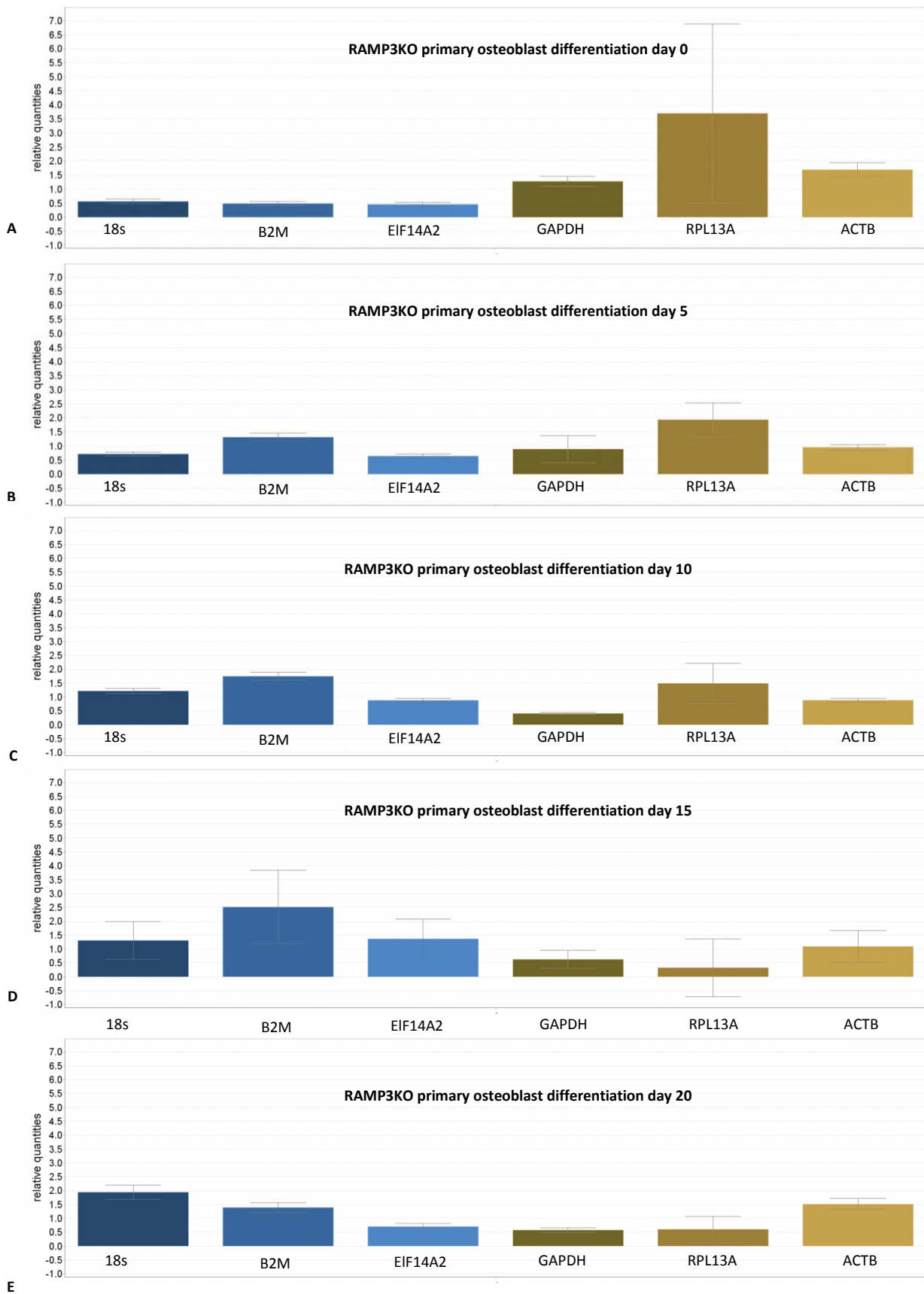


Fig 5.6: A graphical representation of relative cDNA expression of the reference genes (from left to right in each histogram): 18s, B2M, Elf14A2, GAPDH, RPL13A and ACTB, at each differentiation time point (top to bottom) day0 (A), day5 (B), day10 (C), day15 (D) and day20 (E) of RAMP3 KO primary osteoblast. Each sample was run in triplicate, per gene, and three independent experimental repeats were carried out ($n = 3$).

5.3.2.i.a geNorm M value:

The relative expressions were used to determine the average expression stability of each reference gene i.e. the geNorm “M” value.

The following graphs are generated by the qBase+ software representing the geNorm M value of WT (Fig. 5.7) and RAMP3 KO (Fig. 5.8) cultures. In each graph the genes are ranked according to their increasing stability. The values on the graph start with the least stable reference gene to the left and ends with the most stable reference gene to the right.

The determined “geNorm M” value suggests that the least stable reference gene in both WT and RAMP3KO primary osteoblasts, across all time points to be RPL13A. The genes ranked in the increasing order of stability in WT (Fig. 6.7) osteoblasts are: RPL13A, GAPDH, B2M, 18s, ACTB (β actin), and EIF14A2 (most stable). Likewise in RAMP3 KO, (Fig. 5.8) the order of genes in the increasing order of stability are: RPL13A (least stable), GAPDH, EIF14A2, B2M, ACTB (β actin), and 18s (most stable). This result is co-relates to the relative expression of individual reference gene represented in previous (Fig. 5.5 and 5.6).

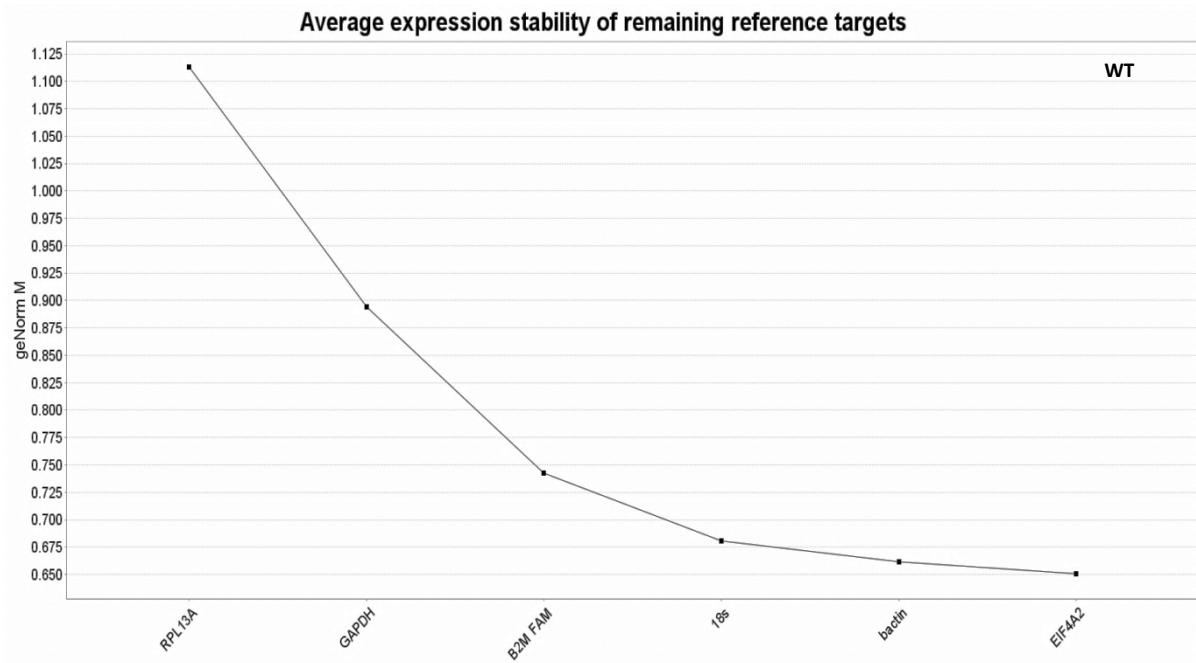


Fig 5.7: Graphical representation of average expression stability – “geNorm M” value” of reference genes in WT primary osteoblast cultures across all time points. . The values on the graph start with the least stable reference gene to the left and ends with the most stable reference gene to the right. Least stable gene expressed in WT across all time points is RPL13A. Whereas most stably expressing gene is EIF14A2.

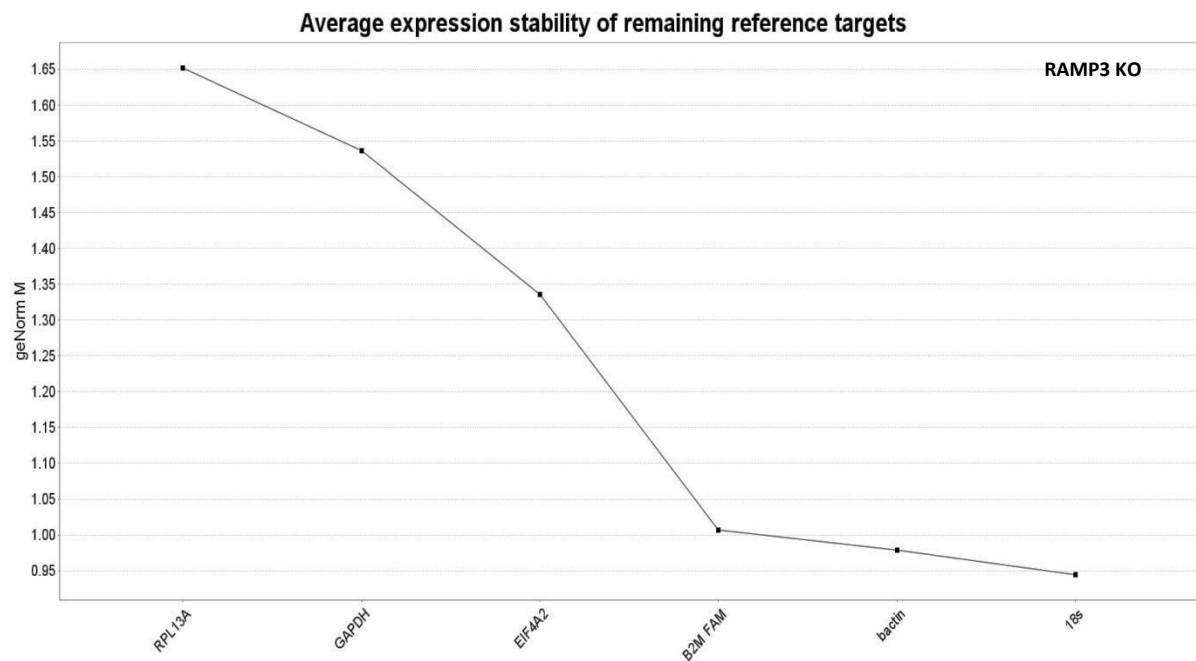


Fig 5.8: Graphical representation of average expression stability – “geNorm M value” of reference genes in RAMP3KO primary osteoblast cultures across all time points. The values on the graph start with the least stable reference gene to the left and ends with the most stable reference gene to the right. Least stably expressing reference gene in RAMP3 KO primary osteoblasts is RPL13A, and the most stably expressing gene is 18s.

5.3.2.i.b geNorm V value:

The final geNorm analysis is calculating the geNorm V value for different pairwise variations to determine the optimal number of reference genes for the particular experiment. Pairwise variation is “V (n/n+1)” where “n” is the number of reference genes considered. An optimal “n” i.e. the number of reference genes, is the one that results in a geNorm V value <0.15 (red line marking the threshold). The graphical output generated by qBase+ for WT and RAMP3 KO osteoblast with 5 time points each with respect to the geNorm M values determined for each gene is as follows (Fig. 5.9).

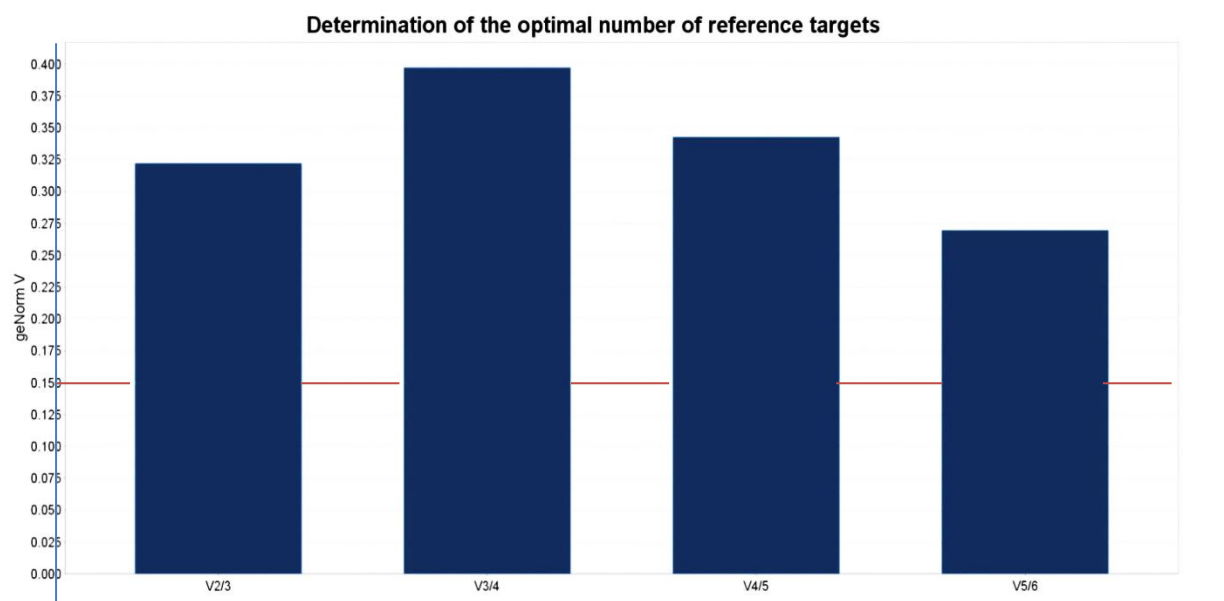


Fig 5.9: Graphical representation of “geNorm V value” to determine the optimal number of reference genes from the experiment. On Y-axis is the geNorm V value and on X-axis are the pairwise variations “V (n/n+1)” where n is equivalent to the number of reference genes considered. None of the “n” values (from left to right on X-axis: 2, 3, 4, 5) resulted in a geNorm V value below 0.15.

Since none of the “V (n/n+1)” result in a geNorm V value below 0.15 (red threshold line), the optimal number of reference target genes for the experiment remained undetermined. In instances when the optimal number of reference genes remains undetermined, qBase+ recommends minimal of three common (to both genotypes) and most stably expressing reference genes for that particular experiment. However the geNorm M graphs (Figs 5.7 and 5.8) suggested that only two common reference genes: 18s and ACTB were the most stably expressing in both WT and RAMP3 KO across all time points. Hence only two genes: 18s and ACTB were selected as reference genes to normalise the expression of all the genes of interest.

5.3.2.ii Genes of interest:

5.3.2.ii.a RAMP1

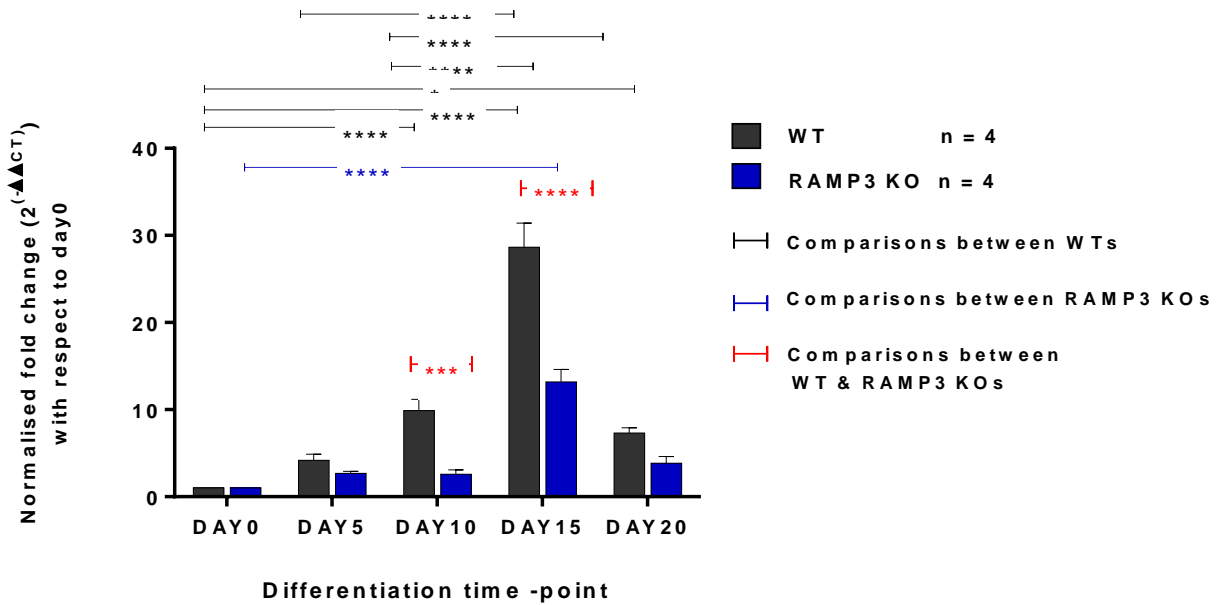
RAMP1 expression of a sample at a differentiation time-point was normalised to the mean expression of 18s and ACTB at the corresponding time point. As mentioned previously this value is $\Delta\text{CT RAMP1}$. Following this $\Delta\Delta\text{CT}$ values were calculated for the change in expression between day0 and each of the higher time-points. The fold change was calculated by the formula $2^{-\Delta\Delta\text{CT}}$. Each sample was run in triplicate and 4 independent experimental repeats were performed. Two-way ANOVA test and Bonferroni's post multiple comparison test were used to determine statistical differences in fold changes between day0 and each time-point of each genotypes. Statistical differences were also determined between WT and RAMP3 KO at each time-point. It was observed that there was a significant difference in the fold change between $\Delta\Delta\text{CT}$ values of day10 and 15 of RAMP3 KO and WTs. Statistical differences in fold change within each genotype in detailed below in table 5.3 and represented in Fig 5.10 overleaf. CT and ΔCT of individual experiments are summarised in the Appendix (section 9.1.4.i).

Table 5.3: Statistical analysis of RAMP1 mRNA expression in primary osteoblasts.

Bonferroni's multiple comparisons test	Mean Diff.	95% CI of diff.	Significant?	Summary	P Value
WT					
Day0 Vs. Day5	-4.200	-9.604 to 1.204	No	ns	0.2357
Day0 Vs. Day10	-9.893	-14.66 to -5.128	Yes	****	< 0.0001
Day0 Vs. Day15	-28.64	-33.40 to -23.87	Yes	****	< 0.0001
Day0 Vs. Day20	-7.325	-12.73 to -1.921	Yes	**	0.0037
Day5 Vs. Day10	-5.693	-11.39 to 0.002839	No	ns	0.0502
Day5 Vs. Day15	-24.44	-30.13 to -18.74	Yes	****	< 0.0001
Day5 Vs. Day20	-3.125	-9.365 to 3.115	No	ns	> 0.9999
Day10 Vs. Day15	-18.74	-23.84 to -13.65	Yes	****	< 0.0001
Day10 Vs. Day20	2.568	-3.128 to 8.265	No	ns	> 0.9999
Day15 Vs. Day20	21.31	15.62 to 27.01	Yes	****	< 0.0001
RAMP3 KO					
Day0 Vs. Day5	-2.670	-8.074 to 2.734	No	ns	> 0.9999
Day0 Vs. Day10	-2.590	-7.356 to 2.176	No	ns	> 0.9999
Day0 Vs. Day15	-13.20	-17.97 to -8.434	Yes	****	< 0.0001
Day0 Vs. Day20	-3.850	-8.262 to 0.5622	No	ns	0.1230
Day5 Vs. Day10	0.08000	-5.616 to 5.776	No	ns	> 0.9999
Day5 Vs. Day15	-10.53	-16.23 to -4.834	Yes	***	0.0001
Day5 Vs. Day20	-1.180	-6.584 to 4.224	No	ns	> 0.9999
Day10 Vs. Day15	-10.61	-15.70 to -5.515	Yes	****	< 0.0001
Day10 Vs. Day20	-1.260	-6.026 to 3.506	No	ns	> 0.9999
Day15 Vs. Day20	9.350	4.584 to 14.12	Yes	****	< 0.0001
WT vs RAMP3					
Day10	7.303	2.706 to 11.90	Yes	**	0.0010
Day 20	15.44	10.84 to 20.03	Yes	****	< 0.0001

CI: Confidence interval; Ns: Non significant

RAMP1 mRNA expression normalised to 18s and ACTB in differentiation primary osteoblasts



*Fig 5.10: Bar graph representing normalised expression as fold change of RAMP1 mRNA in WT (grey) and RAMP3 KO (blue) primary osteoblasts differentiated for 0, 5, 10, 15 and 20 days. n=4 each time-point each genotype. Two-way ANOVA test followed by Bonferroni's post multiple comparison correction test, was used for statistical analysis. P value ≤ 0.05 was considered significant. No significant difference in RAMP1 expression between WT and RAMP3KO primary osteoblasts. In WT osteoblasts, significant difference was observed between day 0 and day 10 (****), day 0 and day 15 (****) and day 0 and day 20 (**) of differentiation. In RAMP3 KO osteoblasts statistical difference was observed only between day0 and day15 (****). There was a significant difference between RAMP3KO and WT at day 10 and day 15.*

5.3.2.ii.b RAMP2

As with RAMP1, $\Delta\Delta\text{CT}$ RAMP2 values were determined for calculating the fold change between day0 and each time-point per genotype. Each sample was run in triplicate and 3 independent experimental repeats were carried out. Two-way ANOVA test and Bonferroni's post-test, showed no significant difference between WT and RAMP3 KO. Similar to RAMP1, a significant difference in RAMP2 expression between the differentiation time-points within each genotype was observed. RAMP2 expression was significantly increased in both the WT and RAMP3 osteoblasts from fifth day of differentiation. The CT and ΔCT values of individual experiments are summarised in the Appendix (section 9.1.4.i). The statistical analysis is summarised below in table 5.4 and represented in Fig 5.11 overleaf.

Table 5.4: Statistical analysis of RAMP2 mRNA expression in primary osteoblasts.

Bonferroni's Multiple Comparisons Test	Mean Diff.	95% CI Of Diff.	Significant?	Summary	P Value
WT					
Day 0 Vs. Day5	-99.18	-192.2 to -6.194	Yes	*	0.0319
Day 0 Vs. Day10	-177.4	-270.4 to -84.38	Yes	***	0.0002
Day 0 Vs. Day15	-212.1	-305.1 to -119.1	Yes	****	< 0.0001
Day 0 Vs. Day20	-80.41	-163.6 to 2.762	No	ns	0.0625
Day5 Vs. Day10	-78.19	-180.1 to 23.67	No	ns	0.2344
Day5 Vs. Day15	-112.9	-214.8 to -11.06	Yes	*	0.0240
Day5 Vs. Day20	18.77	-74.21 to 111.8	No	ns	> 0.9999
Day10 Vs. Day15	-34.74	-136.6 to 67.13	No	ns	> 0.9999
Day10 Vs. Day20	96.96	3.978 to 189.9	Yes	*	0.0375
Day15 Vs. Day20	131.7	38.71 to 224.7	Yes	**	0.0031
RAMP3 KO					
Day 0 Vs. Day5	-59.26	-142.4 to 23.91	No	ns	0.3342
Day 0 Vs. Day10	-206.6	-289.7 to -123.4	Yes	****	< 0.0001
Day 0 Vs. Day15	-212.7	-305.7 to -119.7	Yes	****	< 0.0001
Day 0 Vs. Day20	-117.1	-210.1 to -24.12	Yes	**	0.0088
Day5 Vs. Day10	-147.3	-230.5 to -64.14	Yes	***	0.0003
Day5 Vs. Day15	-153.5	-246.4 to -60.47	Yes	***	0.0007
Day5 Vs. Day20	-57.85	-150.8 to 35.14	No	ns	0.5890
Day10 Vs. Day15	-6.150	-99.14 to 86.84	No	ns	> 0.9999
Day10 Vs. Day20	89.46	-3.526 to 182.4	No	ns	0.0645
Day15 Vs. Day20	95.61	-6.251 to 197.5	No	ns	0.0755

CI: Confidence interval; Ns: Non significant

RAMP2 mRNA expression normalised to 18s and ACTB in differentiation primary osteoblasts

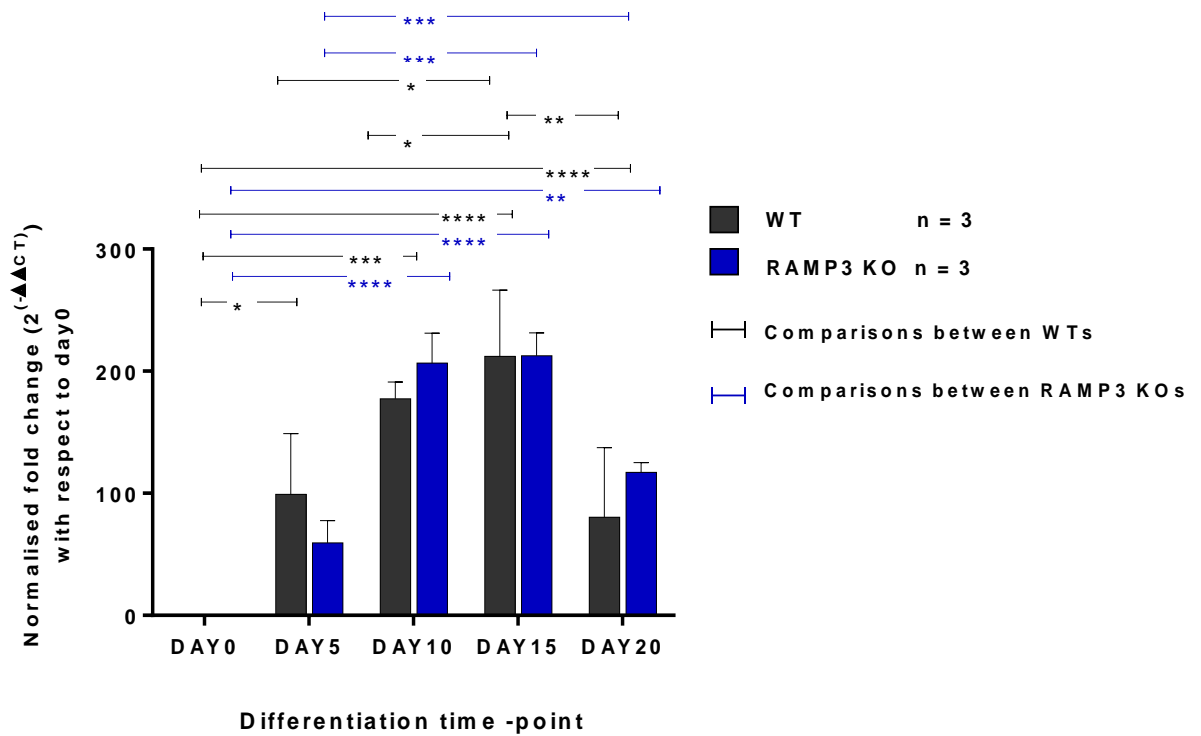


Fig 5.11: Bar graph representing normalised expression of RAMP2 cDNA in WT (grey) and RAMP3 KO (blue) primary osteoblasts differentiated for 0, 5, 10, 15 and 20 days. n=3 each time-point each genotype. Two-way ANOVA test followed by Bonferroni's post multiple comparison correction test, was used for statistical analysis. P value ≤ 0.05 was considered significant. No significant difference in RAMP2 expression between WT and RAMP3KO primary osteoblasts. In WT osteoblasts, significant difference was observed between day 0 and day 5 (*), day 0 and day 10 (***), day 0 and day 15 (****), day 0 and day 20 (****), day5 and day 10 (*), day5 and day 15 (*) and between day15 and day 20 of differentiation. Similarly in RAMP3 KO osteoblasts statistical difference was observed between day 0 and day 10 (****), day 0 and day 15 (****), day 0 and day 20 (***), day 5 and day 15 and day 5 and day 20 (***) of differentiation (**** < 0.0001)

5.3.2.ii.c RAMP3 :

The $\Delta\Delta\text{CT}$ RAMP3 values were only determined for WT osteoblasts as PCR products were not amplified in RAMP3 KO osteoblasts. Each sample was run in triplicate and 3 independent experimental repeats were carried out. Two-way ANOVA and Bonferroni's post-test showed a significant difference between the differentiation time-points within WTs osteoblasts. RAMP3 expression was significantly reduced in both the WT and RAMP3 osteoblasts from fifth day of differentiation. The CT and ΔCT of individual experiments are summarised in the Appendix (section 9.1.4.i). The statistical analysis is summarised below in table 5.5 and represented in Fig 5.12 overleaf.

Table 5.5: Statistical analysis of RAMP3 mRNA expression in primary osteoblasts.

Bonferroni's Multiple Comparisons Test	Mean Diff.	95% CI Of Diff.	Significant?	Summary	P Value
WT					
Day0 Vs. Day5	0.5828	0.2123 to 0.9533	Yes	***	0.0009
Day0 Vs. Day10	0.5701	0.1996 to 0.9406	Yes	**	0.0011
Day0 Vs. Day15	0.6418	0.2713 to 1.012	Yes	***	0.0003
Day0 Vs. Day20	0.8000	0.2761 to 1.324	Yes	**	0.0012
Day5 Vs. Day10	-0.01266	-0.3831 to 0.3578	No	ns	> 0.9999
Day5 Vs. Day15	0.05897	-0.3115 to 0.4295	No	ns	> 0.9999
Day5 Vs. Day20	0.2173	-0.3067 to 0.7412	No	ns	> 0.9999
Day10 Vs. Day15	0.07163	-0.2989 to 0.4421	No	ns	> 0.9999
Day10 Vs. Day20	0.2299	-0.2940 to 0.7539	No	ns	> 0.9999
Day15 Vs. Day20	0.1583	-0.3657 to 0.6822	No	ns	> 0.9999
RAMP3 KO					
Day0 Vs. Day5	0.0	-4.808 To 4.808	No	Ns	> 0.9999
Day0 Vs. Day10	0.0	-4.808 To 4.808	No	Ns	> 0.9999
Day0 Vs. Day15	0.0	-4.808 To 4.808	No	Ns	> 0.9999
Day0 Vs. Day20	0.0	-4.808 To 4.808	No	Ns	> 0.9999
Day5 Vs. Day10	0.0	-4.808 To 4.808	No	Ns	> 0.9999
Day5 Vs. Day15	0.0	-4.808 To 4.808	No	Ns	> 0.9999
Day5 Vs. Day20	0.0	-4.808 To 4.808	No	Ns	> 0.9999
Day10 Vs. Day15	0.0	-4.808 To 4.808	No	Ns	> 0.9999
Day10 Vs. Day20	0.0	-4.808 To 4.808	No	Ns	> 0.9999
Day15 Vs. Day20	0.0	-4.808 To 4.808	No	Ns	> 0.9999

CI: Confidence interval; Ns: Non significant

RAMP3 mRNA expression normalised to 18s and ACTB in differentiation primary osteoblasts

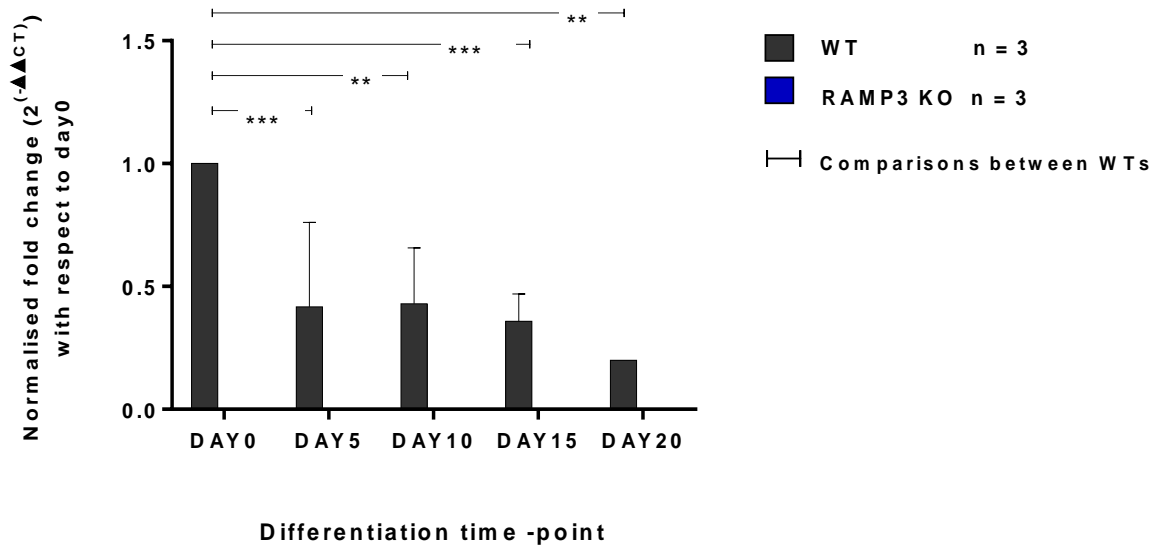


Fig 5.12: Bar graph representing normalised expression of RAMP3 cDNA in WT (grey) and RAMP3 KO (blue) primary osteoblasts differentiated for 0, 5, 10, 15 and 20 days. $n=3$ each time-point each genotype. Two-way ANOVA followed by Bonferroni's post multiple comparison correction test was used for statistical analysis. P value ≤ 0.05 was considered significant. No PCR product was detected in RAMP3KO osteoblast. In WT osteoblasts, significant difference was observed between day 0 and day 5 (***), day 0 and day 10 (**), day 0 and day 15 (***) and day 0 and day 20 (**) of differentiation.

5.4 Discussion

This study demonstrates an osteoblast-differentiation dependent expression of individual RAMPs. The end-point PCR showed that all the three RAMPs; 1, 2 and 3 are expressed by WT 129/SvEv primary osteoblasts and RAMP1 and 2 are expressed in the RAMP3 KO primary osteoblast as expected (See Figs. 5.2, 5.3 and 5.4). We observed that in WT primary osteoblast cultures, the expression of RAMP2 was the highest, followed by that of RAMP3 and that RAMP1 expression was the lowest however this could only be verified by qPCR (See Figs. 5.2, 5.3 and 5.4). The RAMP3 KO primary cultures did not amplify a product for RAMP3 cDNA as expected. However, similar to the WT primary osteoblast cDNA, RAMP3 KOs demonstrated a higher expression of RAMP2 than RAMP 1 during differentiation. Interestingly we also observed that in the WTs the expression of RAMP3 cDNA reduced with the progression of osteoblast differentiation which could again only be verified by qPCR (see Fig 5.4).

qPCR was performed using custom designed validated RAMP primers for the double-dye hydrolysis qPCR technique, more commonly known as the Taqman qPCR technique. Since the Taqman technique specifically quantifies the amplification of target sequence, we could be certain that the CT values generated reflected the target sequence amplification and not-specific random cDNA amplification. With increasing evidence that housekeeping gene expression varies with experimental conditions, transgenic manipulation amongst others, in same cell types, we intended to determine a stably expressed housekeeping/reference gene/s for our experiments. In accordance to the literature evidence, we observed in 6 reference genes that we selected to investigate, that their expression not only varied between genotypes, but also differs between the osteoblast differentiation time-points (see Fig. 5.5 and 5.6). Despite the variation in genotype and change in expression of reference genes during osteoblasts differentiation, we identified two stably expressing reference genes: 18s and β -actin (see Fig. 5.9), which were used in our subsequent experiments.

Despite strong RAMP amplicons observed in endpoint PCR, the CT values acquired by qPCR for all the RAMPs were above 25. CT value for RAMP1 throughout differentiation in both WT and RAMP3 ranged between 34 – 38, RAMP2 ranged between 25 – 38, RAMP3 CT values in WTs ranged between 26 – 38 and RAMP3 was not amplified in RAMP3KO primary osteoblast cDNA as expected (see Appendix 9.1.4.i). CT values higher than 37 were. The strong RAMP amplicons observed in endpoint PCR could have resulted from the higher concentrations of cDNA template

(2µg) compared to the low concentration of cDNA template used in qPCR reactions (5ng). The acceptance of expression level of a gene by qPCR technique with a CT value beyond 32 is debated. However in our qPCR reactions, if there was no amplification, (for example in case of non-template control reactions and the reactions of RAMP3 primer in RAMP3 KO primary osteoblast cDNA preparations) the qPCR machine did not generate an amplification plot and could not determine a CT value. Even with high CT values, an amplification plot was generated for the WT and RAMP3 primary osteoblasts. Therefore the higher CT values for RAMPs were not artifactual values resulting from nonspecific non-amplified reactions, but were robust quantifications that reflected the low concentrations of the RAMPs in primary osteoblasts. CT values higher than 37 were excluded. More over each reaction had a copy number control which validated the efficiency of the primers. The CT values for copy number positive control are detailed in the appendix 9.1.4.i.

In WT primary osteoblast cDNA, RAMP2 expression was more than that of RAMP3 which was in turn higher than RAMP1. In RAMP3 KO primary osteoblast cDNA, RAMP2 expression was higher than that of RAMP1. Since RAMP1 expression is the least amongst RAMPs and given the evidence that RAMP1 KO mice do not have a skeletal phenotype, it appears that RAMP1 does not play an important role in regulating the skeleton (as observed in data from our pilot study, Section 1.5) (Tsujikawa et al 2007).

There were no significant differences in 2 expressions between WT and RAMP3 KO primary osteoblast cDNA throughout differentiation; hence the expression of RAMP2 in osteoblasts is independent of RAMP3 expression. Interestingly, WT osteoblasts had significantly higher fold change in RAMP1 expression at day 10 and day15 compared to the RAMP3 KOs (see Fig 5.10). Furthermore, in both WTs and RAMP3 KOs, the expression of RAMP1 and 2 increased from day 5 of differentiation (see Fig. 5.10 and 5.11) and the expression of RAMP3 decreased from day 5 of differentiation (see Fig. 5.12). This can indicate that osteoblast maturation requires an increase in RAMP1 and 2 expressions and a decrease in RAMP3 expression. We can therefore propose that the effects of reduction in RAMP3 during osteoblast maturation are enhanced in the RAMP3 KO primary osteoblasts, due to the absence of RAMP3. We have also shown the RAMP3 KO primary osteoblasts have a different osteoblast differentiation profile in chapter 5. Since RAMP1 and RAMP2 expressions do not change in RAMP3 KOs, the differences in the osteoblast maturation are due to the absence of RAMP3. Coincidentally, maturation of osteoclasts into multinucleated cells also requires reduction in RAMP3 expression (Granholm et al 2008). Hence

in RAMP3 KO mice, both the osteoblasts and osteoclasts have enhanced development which could influence the bone remodelling process.

Bone remodelling process peaks at young age when the bones grow to form an adult skeleton to achieve a peak bone mass density by the age of 20. Since we see maximum advancement of the skeletal phenotype in the RAMP3 KO mice when they are neonates, we can suggest that the enhanced bone remodelling resulting from the improved osteoblast and osteoclast maturation could be responsible for the RAMP3 KO mice skeletal phenotype.

In conclusion, with osteoblast differentiation,

- RAMP1 and 2 mRNA expression increases, however RAMP1 expression levels are extremely low to begin with, and
- RAMP3 mRNA decreases.

Chapter 6: Effect of anabolic stimulations in WT and RAMP3 KO 129/SvEv primary osteoblasts.

6.1 Introduction

In this chapter we investigate the effects of various anabolic stimulations in WT and RAMP3 KO 129/SvEv primary osteoblasts.

6.1.1 Effect of Parathyroid hormone (PTH), Adrenomedullin (AM) and Amylin (AMY) stimulation:

The first half of this chapter focuses on the effect of PTH, AM and AMY stimulation on the expression of RAMPs. As discussed earlier, all the three peptides PTH, AM and AMY have an effect on osteoblasts differentiation and proliferation. Although the downstream cell signalling pathways following PTH, AM and AMY stimulation have been studied in depth by independent groups (Christopoulos et al 1999, Cornish et al 2001, Cornish et al 1995, Cornish et al 1997, Ishizuya et al 1997), currently there is no literature evidence that reflects the change in the endogenous expression of the receptors for these peptides.

All the four GPCRs- PTHR1/PTHR2, CLR and CTR form heterodimers with RAMPs 2 and 3 to form functional receptors for PTH, AM and AMY respectively. These accessory proteins ingeniously modulate the GPCR ligand specificity (Christopoulos et al 1999, Hay et al 2006, McLatchie et al 1998). RAMPs not only form functional receptors for these receptors, but also induce trafficking of partner GPCRs and chaperon them to the cell surface (McLatchie et al 1998, Parameswaran & Spielman 2006, Sexton et al 2001). Given the evidence that RAMPs form stable intracellular homodimers (Sexton et al 2001), it may be possible that on ligand activation, the homodimers in the cytoplasm dissociate to form heterodimers with partner GPCRs to enhance receptor presentation in response to the particular stimuli. Since alterations in RAMP2 and RAMP3 have shown to result in a skeletal phenotype, in transgenic mice, we were interested in investigating the change in the expression of these two receptors in WT and RAMP3 KO primary osteoblasts when stimulated with the aforementioned peptides. Furthermore we wanted to determine whether under stimulated conditions, RAMP2 protein compensated for the loss of RAMP3 in the RAMP3 KO osteoblasts.

6.1.2 The Wnt/ β -catenin and RAMP3 association:

The latter half of this chapter is focussed on the Wnt/ β -catenin pathway and RAMP3 association. One of the important regulatory pathways in the skeleton is the canonical Wnt pathway. Detailed review of the Wnt pathways is beyond the scope of this project. Briefly, in the canonical Wnt pathway, Wnt activates a heteromeric receptor complex that is made up Fizzled protein and LRP5 or 6 receptor (Bhanot et al 1996, Clevers & Nusse 2012, Wehrli et al 2000). Fizzled proteins are a family of seven transmembrane GPCRs and LRP5/6 are members of single transmembrane, low density lipoproteins. Activation of the Wnt receptor complex results in an increase in the phosphorylate β -catenin level in the cytoplasm which then translocates into the nucleus and activates targets genes (Rubinfeld et al 1993). DKK1 is a secreted protein that antagonises Wnt by binding to LRP5/6 (Bafico et al 2001, Semenov et al 2001, Semenov et al 2008). In bone, Wnt activation determines the fate of mesenchymal stem cells (MSCs) as it induces the MSCs to differentiate into osteoblasts.

There is recent evidence in the involvement of Wnt in regulation of RAMP3 expression. Many research groups have identified that RAMP3 is one of target genes of the Wnt pathway. In 2005 two independent groups Kenny et al and Ziegler et al reported down regulation of RAMP3 on phosphorylated β -catenin induction using northern blotting (Kenny et al 2005, Ziegler et al 2005). Following this, in 2009 Rohrs et al showed that RAMP3 expression is down regulated in the first 24 hours post Wnt3A stimulation (Rohrs et al 2009). Hence RAMP3 is one of the early response genes targeted by Wnt. Results from chapter 4 suggest that primary osteoblasts have an advanced differentiation pattern in the RAMP3 KO mice when compared to the WTs. Since the canonical Wnt pathway is one of the important regulatory pathways in osteoblast differentiation and since Wnt is proposed to reduce RAMP3 expression, we hypothesised, ***that the RAMP3 KO mice had enhanced Wnt / β -catenin pathway that could result in an advanced osteoblast differentiation.*** We aimed to investigate both, the endogenous Wnt regulated phosphorylated β -catenin levels in RAMP3 KO and the effect of external Wnt stimulation on the phosphorylated β -catenin levels in RAMP3 KOs in comparison to the WT primary osteoblasts.

6.2 Methods

6.2.1 Stimulation of primary osteoblast cultures:

Detailed calvarial primary culture protocol is described in Section 5.2.1. Independent WT and RAMP3 KO primary cultures were established for stimulation experiments. PTH, AM and AMY stimulated WT and RAMP3 KO osteoblasts were studied for expression of RAMP 2 and RAMP 3. Un-stimulated WT and RAMP3 KO primary osteoblasts were studied for expression of total β -catenin. And DKK1 and DKK1 + Wnt3A stimulated WT and RAMP KO primary osteoblasts were studied for the expression of phosphorylated β -catenin.

6.2.1.i Experimental set-up for RAMP2 and RAMP3 expression:

Three of each WT and RAMP3 KO primary osteoblasts were differentiated for 20 days in T25 culture flasks (Nunc™). Since concentration of 10^{-12} M and greater of PTH, AM, AMY have been reported to stimulate osteoblasts *in vitro*, we used 10^{-9} M concentration in our experiments (Matsumoto et al 1986, Cornish et al 1995, Cornish et al 1997). On the 20th day of differentiation, the osteogenic media was decanted and replaced with stimulation media containing 10nM/ml working concentration of one of full length peptides: PTH (Sigma®), AM(Sigma®), AMY (Sigma®) for 20 minutes. After stimulation, the stimulation media was decanted and cells were lysed. The whole cell lysates were used as protein sample. Protocol detailed in section 6.2.2.

6.2.1.ii Experimental set-up for total β -catenin expression:

Four of each WT and RAMP3 KO primary osteoblast cultures were differentiated for 10, 15 and 20 days in T25 culture flasks. On each of these time points, cells were harvested by the protocol detailed in section 7.2.2.

6.2.1.iii Experimental set-up for phosphorylated β -catenin expression:

Three of each WT and RAMP3 KO primary osteoblast cultures differentiated for 20 days in T25 culture flasks. Wnt3A at a concentration of 100ng/ml has been reported to give a potent β -catenin response *in vitro* (Hannoush 2008). One of the flasks, each culture was stimulated with media containing working concentration 100ng/ml of recombinant Wnt3A (R&D Systems™, Catalogue no: 1324-WN) for 20 mins. Cells were harvested from non-stimulated and Wnt3A stimulated flasks for each culture, each genotype by the protocol detailed in section 7.2.2.

6.2.1.iv Experimental set-up for endogenous phosphorylated β -catenin expression:

Three of each WT and RAMP3 KO primary osteoblast cultures were differentiated for 20 days in 6 well culture plates (Nunc™). A dose dependent decrease in phosphorylated- β -catenin has been reported with a dose range of: 0, 5ng, 50ng, 100ng, 200ng, 250ng/ml DKK1, hence these concentrations were used in our experimental setup (Qiang Ya-Wei et al 2007). The osteogenic media of each well was decanted and replaced with stimulation media containing one of the working concentrations (0, 5ng, 50ng, 100ng, 200ng, 250ng) of recombinant human DKK1 (R&D Systems™, Catalogue no: 5439-DK) . The stimulation media was decanted and cells were lysed and the whole cell lysate on each well was used as a protein sample. (Section 6.2.2)

6.2.1.v Experimental set-up for phosphorylated β -catenin expression on Wnt3A stimulation:

The WT and RAMP3 KO primary osteoblasts were differentiated for 20 days in 6 well culture plates (Nunc™). The osteogenic media of each well was decanted and replaced with stimulation media containing one of the working concentrations of recombinant human DKK1 (0, 5, 50, 100, 200, 250ng/ml). The stimulation media was decanted and replaced with stimulation media-2 containing 100ng/ml recombinant mouse Wnt3A (R&D Systems™, Catalogue no: 1324-WN) for 20 minutes. This stimulation media-2 was removed and cells were lysed, the details of which are in the following section 6.2.2.

6.2.2 Protein expression analysis:

6.2.2.i Total cell lysate protein from differentiating primary osteoblasts:

Cells were harvested from one T25 flask each culture (PTH, AM and AMY stimulation) or one well of the 6 well plate (DKK and Wnt stimulation) for each peptide stimulation concentration for each culture. First, the medium was removed and the cells were washed in PBS. 500µl (T25) or 200µl (one well of a 6 well plate) ice-cold NP40 lysis buffer (recipe in appendix) having fresh protease inhibitor cocktail 1X (PIC) was added to the cells and the cells were scraped and collected in 1.5ml tubes. This homogenate was then sonicated on ice at 10µm for 10 short pulses using a probe sonicator (Soniprep 150, Sanyo, Japan). The final supernatant was stored as aliquots at -20°C.

6.2.2.ii Total brain lysate protein-positive control:

Whole brain homogenates from previously snap frozen WT (SVEV/129) mice was prepared for Western blotting. The mouse brain (snap frozen tissue stored at -80°C) was weighed and allowed to soften at -20°C for an hour prior being chopped into small pieces. The chopped tissue was placed in a 7ml tissue grinder tube and 15 volumes of ice-cold 0.25 M Sucrose/Buffer A containing freshly prepared protease inhibitor cocktail 1X (PIC), was added. The tissue was first homogenized by 15 passes of the loose pestle and then by 15 passes of the tight pestle. This homogenate was centrifuged at 600 g for 5mins at 4°C and the supernatant was retained. The supernatant was then sonicated using a probe sonicator (Soniprep 150, Sanyo, Japan) by 10 brief pulses at 10µm before aliquoting and snap freezing it in liquid nitrogen. The samples were stored as aliquots at -20°C.

6.2.2.iii Sodium Dodecyl Sulphate-Polyacrylamide Gel Electrophoresis (SDS-PAGE)

Western blotting was carried out in 7% (CTR and CLR) and 15% (RAMP1/2/3) polyacrylamide gels. Biorad Mini-PROTEAN™ system was routinely used to carry out electrophoresis of proteins. The resolving and stacking (5%) gels were cast in 1.5 mm thickness plates. Once the samples were loaded in the gel, they were allowed to stack at 50 V for 50 mins after which the samples were resolved at 125 V for 2 hours.

6.2.2.iv Protein sample preparation for SDS - PAGE

For cell lines approx. 40-100µg and for mouse brain homogenate approximately 40 µg of proteins were loaded on to the gels. All protein samples were denatured in 2X and 4X Laemmli sample buffer, containing β-mercaptoethanol (Sigma®, Poole, UK), by boiling at 100°C for 5 minutes prior to electrophoresis (please refer appendix for working solution concentrations). Following denaturation, the samples were gently vortexed before being loaded into the wells. Additionally, 5 µl of biotinylated molecular weight standards (Cell signalling®, Massachusetts, USA) and 5 µl of prestained All Blue™ (Biorad®, California, USA) molecular weight standards were also loaded.

6.2.2.v Western Blotting:

Resolved proteins were electro-blotted on to Hybond™ nitrocellulose membrane (Amersham®, Massachusetts, USA). The Hybond™ membrane was pre-soaked in 100% methanol for 5 min then equilibrated in transfer buffer prior to use. The stacking gel of the polyacrylamide gel was excised and the orientation was noted. The sandwich for the electroblotting was prepared using two Teflon pads and 4 filter papers (3MM grade, Whatman® chromatography paper, Brenford, UK) per gel. The Teflon pads and the filter papers were also soaked in transfer buffer prior to blotting. The blotting arrangement comprised 2 3M Whatman filter papers and 1 Teflon pad on either side of the gel and membrane sandwich. Care was taken to avoid air bubbles between the different layers of the sandwich. The above arrangement was placed in a transfer cassette with the Hybond™ membrane positioned towards the cathode (white surface). The cassette was placed in the transfer tank containing ice-cold transfer buffer. The transfer tank itself was placed in an ice box and the transfer was allowed to occur at 50 V for 9 hours. Please refer appendix for working solution concentrations mentioned in this section.

6.2.2.vi Immuno-blotting

For each experiment, immune-blotting was carried out for the protein of interest and for a housekeeping protein, β-actin, used as a loading control. The membranes containing the transferred proteins were removed from the electro-blotting cassette and the lane containing the biotinylated marker was excised out with the aid of the prestained markers. Washing solutions used for immune-blotting were: PSB-tween (PBS with 0.25% Tween 20) for non- phosphorylated proteins and TBS-tween (TBS with 0.25% Tween 20) for phosphorylated proteins.

Membranes were first incubated for 1 hr at room temperature in the blocking solution i.e., either PBST containing 5% (w/v) dried skimmed milk or TBST containing 5% BSA on a roller mixer.

After giving the membranes two – 5 min washes in PBST/TBST, the membrane was incubated with primary antibodies dilution made up in blocking solution at 4°C overnight (See Table 7.1 for the dilutions used for each antibody), with gentle rotation on a roller . The membrane part containing the biotinylated marker was stored in PBST/TBST during this incubation. The primary antibody was washed out with three 5-min washes in PBST/TBST and the membrane was incubated with corresponding HRP-tagged secondary antibody made-up in blocking solution for 1 hour at room temperature. The biotinylated markers were incubated in PBST/TBST containing HRP-anti biotin for 1 hour at room temperature. Both pieces of the membranes were given two 5-min washes in PBST/TBST and were incubated in ECL Plus (Pierce®, Rockford Illinois, USA) chemiluminescence detection substrate that contained equal volumes of solution A and solution B premixed for 5 mins on a roller. The membranes were recovered from the chemiluminescence detection solution and were aligned together and placed in X-ray/photo film development cassette after removing excess chemiluminescence solution. The chemiluminescence was detected on Amersham Hyperfilm™ (Amersham®, Chalfont St Giles, UK) and multiple exposures were taken for each blot. The exposed photo films were developed manually in 1:10 diluted developer (AGFA- Gevaert N.V:G153-REF HT536 developer, Belgium) until bands of appropriate intensities appeared. The films were then briefly washed in water to remove excess developer and were fixed in fixer (AGFA-Gevaert N.V: G354 Rapid Fixer- REF 2828Q, Belgium) before being washed in water and left to dry. Please refer appendix for working solution concentrations mentioned in this section. Table 6.1 below summarises the details of all the antibodies and the dilutions at which they were used.

Table 6.1: Details of Antibodies used in Western blotting.

Primary antibody	Product details	Raised in	Dilution used	Secondary antibody	Dilution used	Dilutions made in
RAMP2	Abcam®, ab96546	Rabbit	1:200	Anti-rabbit-HRP DAKO®# P04498	1:1000	5% milk in PBST
RAMP3	Abcam®, ab123598	Rabbit	1:100	Anti-rabbit-HRP DAKO®# P04498	1:1000	5% milk in PBST
β-catenin	Abcam®, ab27798	Rabbit	1:300	Anti-rabbit-HRP DAKO®# P04498	1:5000	5% milk in PBST
Phosphorylated β-catenin (Ser33/37/Thr41)	Cell signaling®#9561	Rabbit	1:200	Anti-rabbit-HRP DAKO®# P04498	1:5000	5% BSA in TBST
β-actin	Abcam®, ab16039-500	Rabbit	1:5000	Anti-rabbit-HRP DAKO®# P04498	1:5000	5% milk in PBST

6.2.2.vii Quantification of protein expression:

Quantification of the expression of protein of interest on the immunoblots was performed by densitometry. GS-900™ Calibrated Densitometer (Bio-Rad™) was used to identify the peak band density. The peak band densities of the protein of interest were normalised to the peak band intensities of the house keeping protein used as a loading control. These normalised expression values were subjected to statistical analysis.

6.2.3 Statistical analysis:

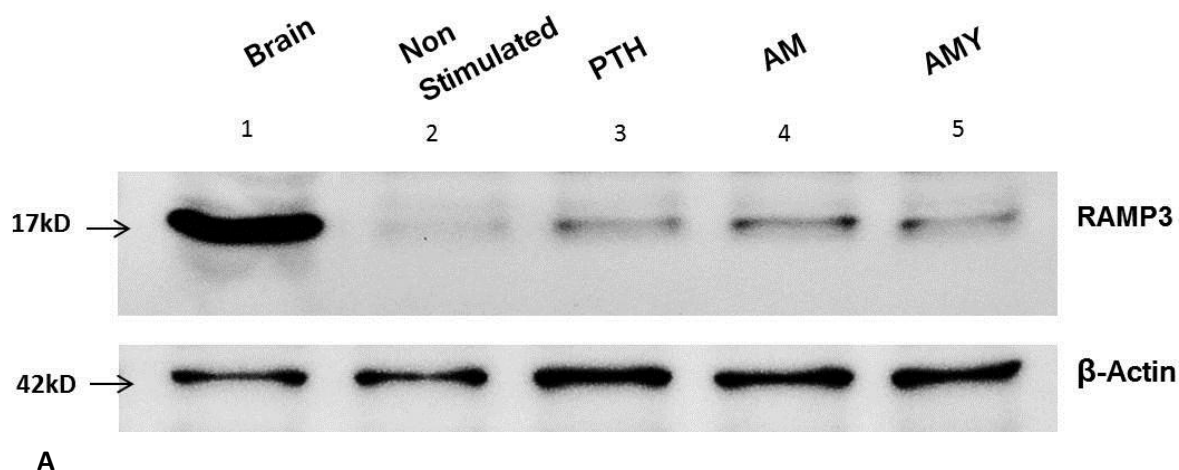
All the datasets were analysed using two way-ANOVA test in GraphPad Prism® 6 followed by Bonferroni's post multiple analysis correction test. P value ≤ 0.05 was considered significant. The statistical analysis was presented as bar graphs generated by the GraphPad Prism® 6.

6.3 Results

6.3.1 Parathyroid hormone (PTH), Adrenomedullin (AM) and Amylin (AMY) stimulation:

6.3.1.i RAMP3 expression on PTH, AM and AMY stimulation:

Expression levels of RAMP3 in differentiated WT primary calvarial osteoblasts were determined under basal and stimulated conditions. Twenty days differentiated WT 129/SvEv primary osteoblasts were stimulated with 10nM working concentration of full length PTH, AM and AMY peptides. 100µg protein was loaded in each well. Western blotting showed a significant increase in the expression of 17kDa RAMP3 monomer in PTH, AM and AMY stimulated WT primary osteoblasts, compared to basal/non-stimulate WT primary osteoblasts. Figure 6.1A overleaf is a representative Western blot showing the expression of RAMP3 and the loading control β-actin. Statistical analysis of the RAMP3 expression is presented in figure 6.1B.



RAMP3 expression in differentiated WT primary osteoblasts on PTH, AM and AMY stimulation

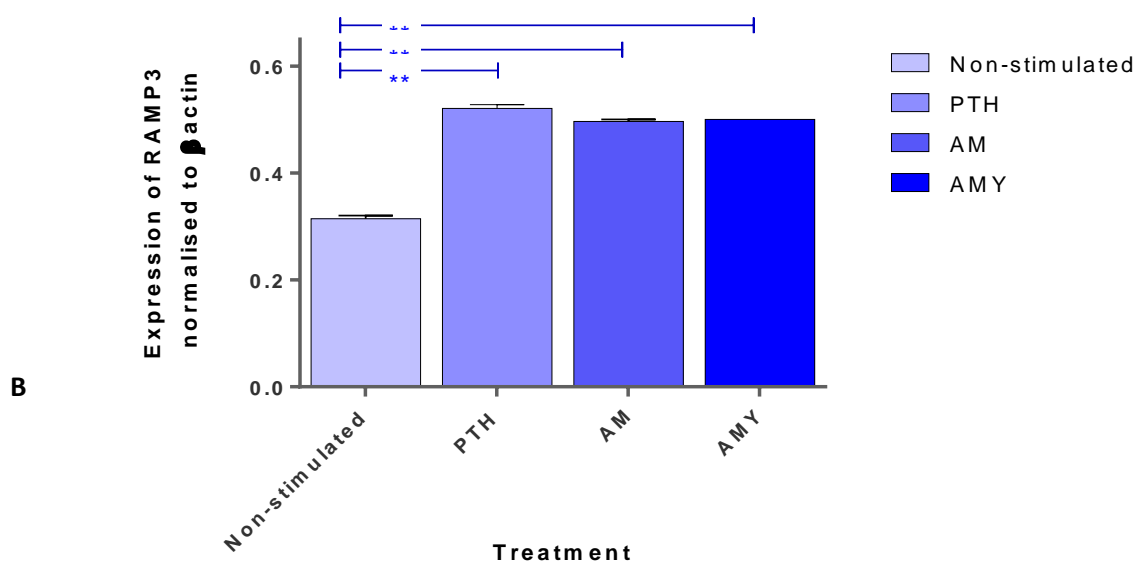


Fig 6.1: A) Representative Western blot showing expression of RAMP3 ~17kD (top) and β -actin (bottom) in differentiated WT primary calvarial osteoblasts cultures stimulated with PTH, AD and AMY. Stimulation with the CT family of peptides resulted in significant increase in RAMP3 expression in comparison to non-stimulated control cells. On day 20 of differentiation, osteoblasts were stimulated with 10nM concentration of full-length PTH, AM and AMY peptides for 20 mins prior being harvested for Western Blotting. Whole cell lysates were collected from three independent stimulated cultures (each genotype). Each independent culture was Western blotted twice. β -actin was the loading control. 100 μ g protein loaded in each well. Exposures were between 2-3 mins.

B) Quantification of levels of RAMP3 in peptide-stimulated differentiated WT osteoblasts, after normalizing to respective β -Actin levels. Levels of RAMP 3 were significantly higher osteoblasts stimulated with either PTH, AM or AMY in comparison to non-stimulated control cells. $n=3$ each genotype. Data was analysed using Two-way ANOVA test followed by post multiple comparison correction using Bonferroni's test.

Significance of p value: **** ≤ 0.0001 , *** ≤ 0.001 , ** ≤ 0.01 , * ≤ 0.005

6.3.1.ii RAMP2 expression in RAMP3 KO and WT 129/SvEv primary osteoblasts:

Levels of RAMP2 in response to the stimulation by 10nM working concentrations of full length PTH, AM and AMY peptides were investigated in WT and RAMP3 KO mice primary calvarial differentiated osteoblasts. 100µg protein was loaded in each well.

Western blotting for RAMP2 showed two distinct bands – one corresponding to the monomeric form of RAMP 2 (~13 kDa) and another higher molecular weight band (~55 kDa).

Similar to a response observed in the levels of RAMP3, both WT and RAMP3 KO osteoblasts showed significantly increased levels of RAMP2 upon stimulation with each PTH, AM and AMY full length peptides. However, the expression of RAMP2 did not vary between peptides. Furthermore, it was observed that stimulated WT primary osteoblasts had significantly higher levels of RAMP2 monomer than stimulated RAMP3 KO osteoblasts. It was even more interesting to observe that this was opposite with respect to the higher molecular weight band of RAMP 2 that is; there were significantly higher levels of this form of the 55kDa RAMP 2 in the stimulated RAMP3 KO osteoblasts compared to that of the WT cells. Hence in response to stimulation both WTs and RAMP3 KOs have increased RAMP2 on stimulation, but the RAMP3 KOs have less 13kDa RAMP2 and more 55kDa RAMP2 expression.

The expression levels of both these bands was normalised to the expression of housekeeping protein β -actin and statistically analysed using two-way ANOVA test followed by Bonferroni's post multiple comparison test. Figure 6.2 overleaf is a representative Western blot showing the expression of both monomer and higher molecular weight RAMP2 along with the loading control β -actin. Statistical analysis of both monomer and higher molecular weight RAMP2 expression is presented in Figure 6.3.

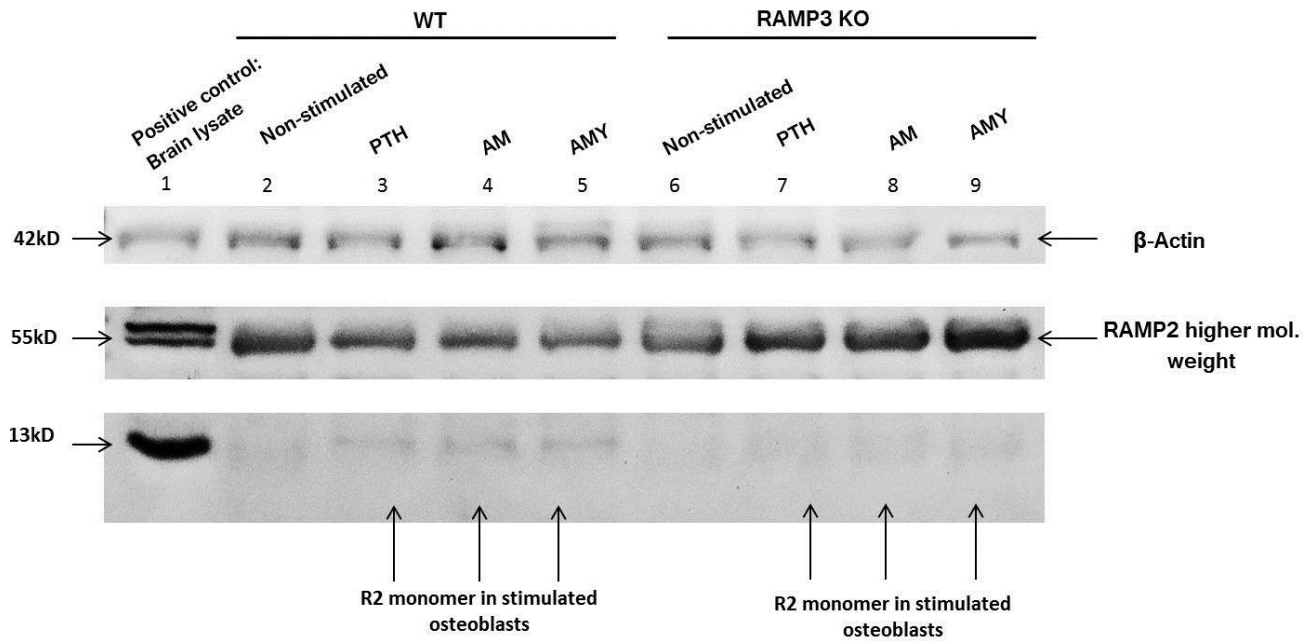


Fig 6.2: Representative Western Blot showing expression of RAMP2 in differentiated WT and RAMP3 KO primary calvarial osteoblasts cultures stimulated with PTH, AD and AMY. Stimulation with the CT family of peptides resulted in significant increase in RAMP2 expression in both WT and RAMP3 KO osteoblasts in comparison to non-stimulated control cells. Primary calvarial osteoblasts from WT animals were cultured in-vitro and were allowed to differentiate upto 20 days. On day 20 of differentiation, osteoblasts were stimulated with PTH, AM and AMY (0, 5, 50, 100, 200, 250ng/ml) for 20 mins prior being harvested for Western Blotting. Whole cell lysates were collected from three independent stimulated cultures (each genotype). Each independent culture was Western blotted twice. Western blotting for RAMP2 showed two significant bands (monomer at ~13 kDa and a higher molecular weight band at ~55 kDa), both of which were quantified. Mouse brain protein lysate was used as a positive control and β -actin was used as the loading control. 100 μ g protein loaded in each well. Exposures were between 2-3 mins.

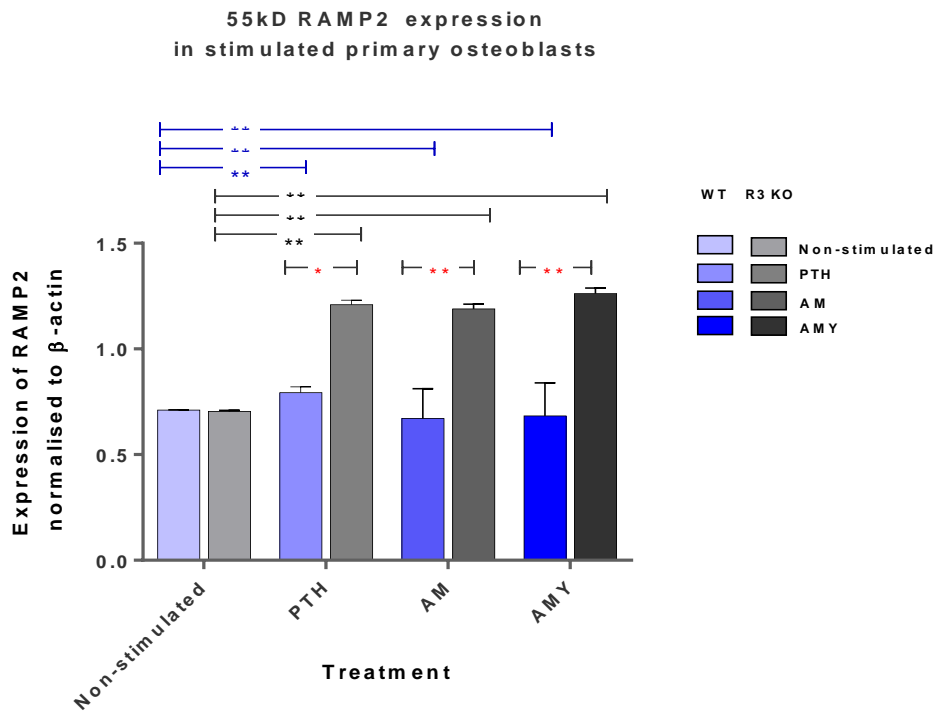
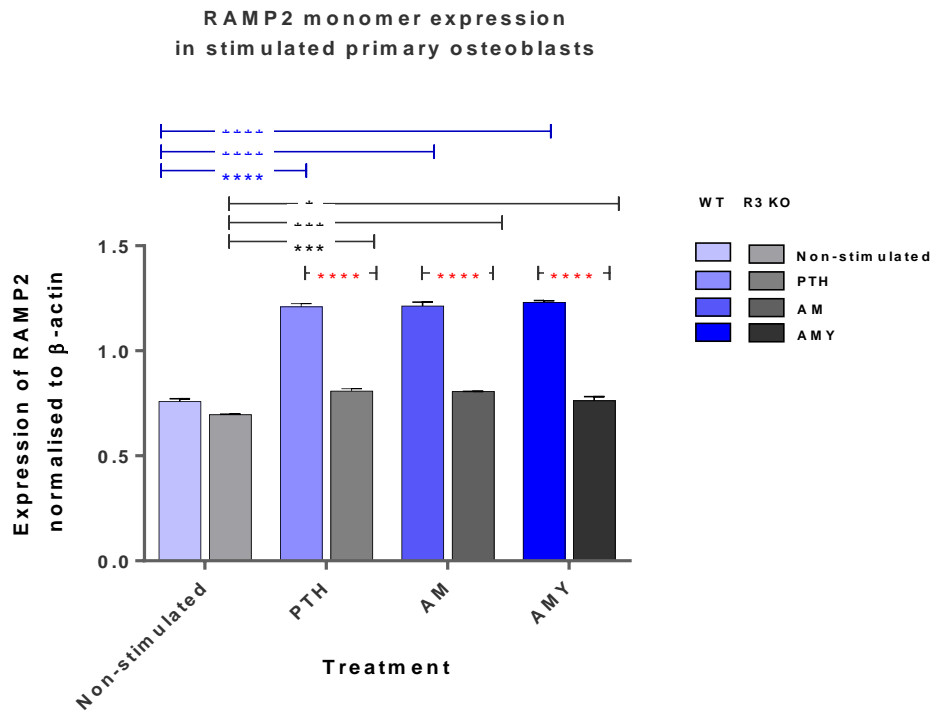


Fig 6.3: Quantification of levels of RAMP 2 in peptide-stimulated differentiated WT and RAMP 3 KO primary calvarial osteoblasts, after normalizing to respective β -Actin levels. Levels of RAMP 2 were significantly higher osteoblasts stimulated with either PTH, AM or AMY in comparison to non-stimulated control cells from both WT and RAMP3 KO mice. Additionally upon stimulation with each peptide, levels of high molecular band RAMP 2 were significantly higher in the RAMP 3 KO cells compared to the respective WT cells (control). However, levels of monomeric form of RAMP2 were observed significantly lower in the RAMP3 KO cells compared to the respective WT cells (control). $n=3$ each genotype. Data was analysed using Two-way ANOVA test followed by post multiple comparison correction using Bonferroni's test.

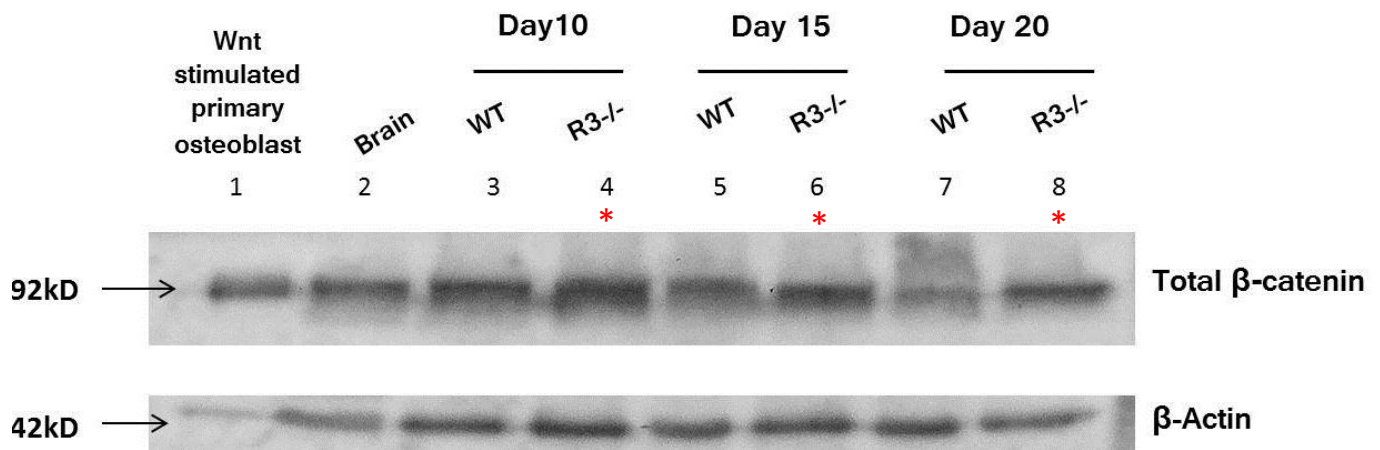
Significance of p value: **** ≤ 0.0001 , *** ≤ 0.001 , ** ≤ 0.01 , * ≤ 0.005

6.3.2 Wnt/ β -catenin pathway in RAMP3 KO primary osteoblasts

6.3.2.i Total β -catenin expression in WT and RAMP3 KO 129/SvEv primary osteoblasts:

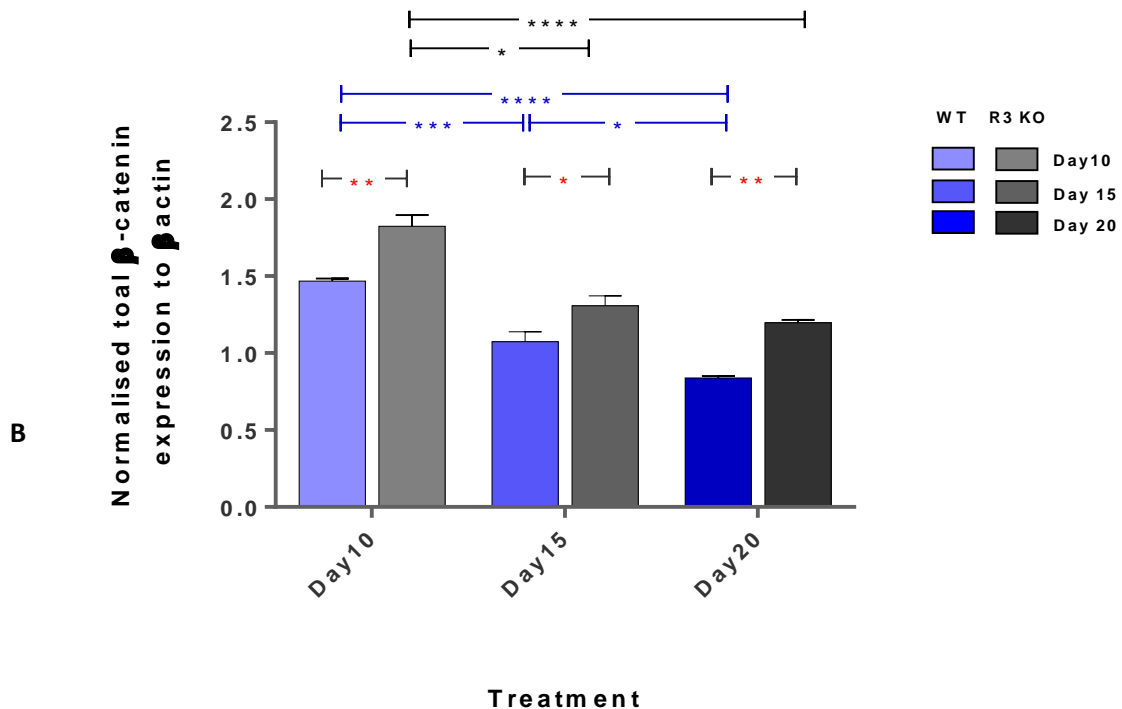
Expression levels of total β -catenin were determined in WT and RAMP3 KO primary osteoblasts at day 10, 15 and 20 of differentiation. It was observed that total β -catenin expression gradually decrease in both WT and RAMP3 KO primary osteoblast samples along with progression of the osteoblast differentiation. Both WT and RAMP3 KO osteoblasts had high levels of total β -catenin at day 10 of differentiations that were significantly reduced by day 20.

Despite a gradual decrease in the total β -catenin levels, it was interesting to observe that RAMP3 KO osteoblasts had consistently and significantly higher levels of total β -catenin throughout the differentiation process when compared to the WTs (day 10, 15 and 20). Fig 6.4A is a representative Western blot image showing the expression of total β -catenin and the loading control- β -actin, in both WT and RAMP3 KO primary osteoblasts. Figure 6.4B is a bar graph representing the statistical differences in the expression of total β -catenin normalised to β -actin.



A

Normalised total β -catenin expression in differentiating primary osteoblasts



B

Fig 6.4: A) Representative Western Blot showing increased expression of total β -catenin in RAMP3 KO differentiating osteoblasts in comparison to WT (*). Four independent primary calvarial osteoblasts from WT and RAMP 3 KO animals were cultured in-vitro and were allowed to differentiate in osteogenic medium for upto 20 days. Whole cell lysates were harvested from these four independent differentiation cultures (each genotype), at day 10, 15 and 20. Each independent culture was immuno-blotted twice for β -catenin expression. Wnt stimulated primary osteoblast and mouse brain tissue lysate were used as positive controls. Samples were immuno-blotted for β -actin as a loading control. 40 μ g protein loaded in each well. Exposures were between 2-3 mins.

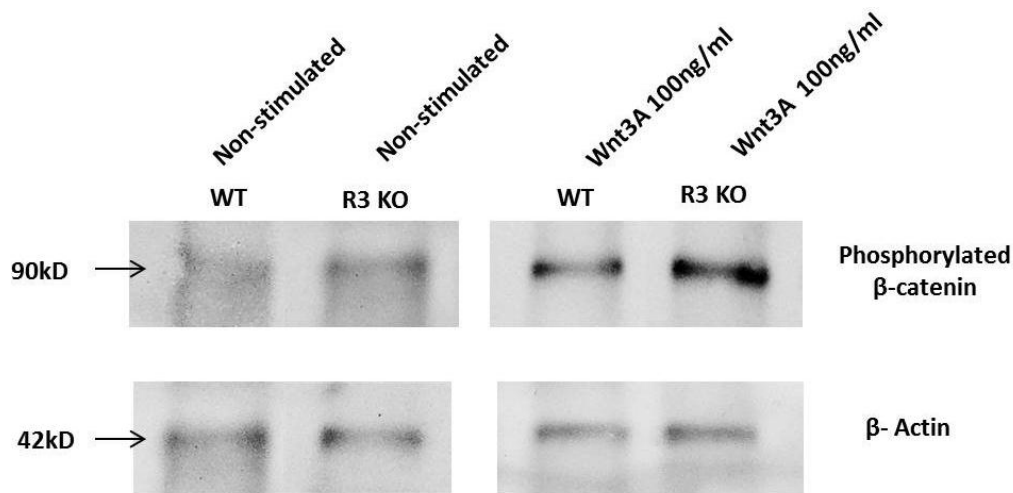
B) Quantification of levels of total β -catenin in WT and RAMP3 KO differentiating osteoblasts, after normalizing to respective β -actin levels. Levels of β -catenin were significantly increased in RAMP3 KO differentiating osteoblasts compared to WT at each time point. There was also differentiation dependent significant decrease in levels of β -catenin in both WT and RAMP3 KO osteoblasts. $n=8$ each genotype. Data was analysed using Two-way ANOVA test followed by post multiple comparison correction using Bonferroni's test.

Significance of p value: **** ≤ 0.0001 , *** ≤ 0.001 , ** ≤ 0.01 , * ≤ 0.05

6.3.2.ii Phosphorylated β -catenin expression in WT and RAMP3 KO 129/SvEv primary osteoblasts on Wnt3A stimulation:

To determine if the Wnt pathway is influenced by the increased total β -catenin levels in RAMP3 KO primary osteoblasts, we stimulated both WT and RAMP3 KO primary osteoblasts that were differentiated for 20 days with Wnt3A and determined the levels of phosphorylated β -catenin.

Western blots showed significantly increased levels of phosphorylated β -catenin in RAMP3 KO cultures, in both basal and in stimulated conditions in comparison to WT cultures. Expression levels of phosphorylated β -catenin were normalised to expression of β -actin. Figure 6.5A is a representative Western blot for phosphorylated β -catenin and β -actin in day 20 differentiated, non-stimulated and Wnt3A stimulated WT and RAMP3 KO primary osteoblasts. Figure 6.5B is a bar graph depicting the significant differences.



Phosho-β-catenin expression to Wnt stimulation

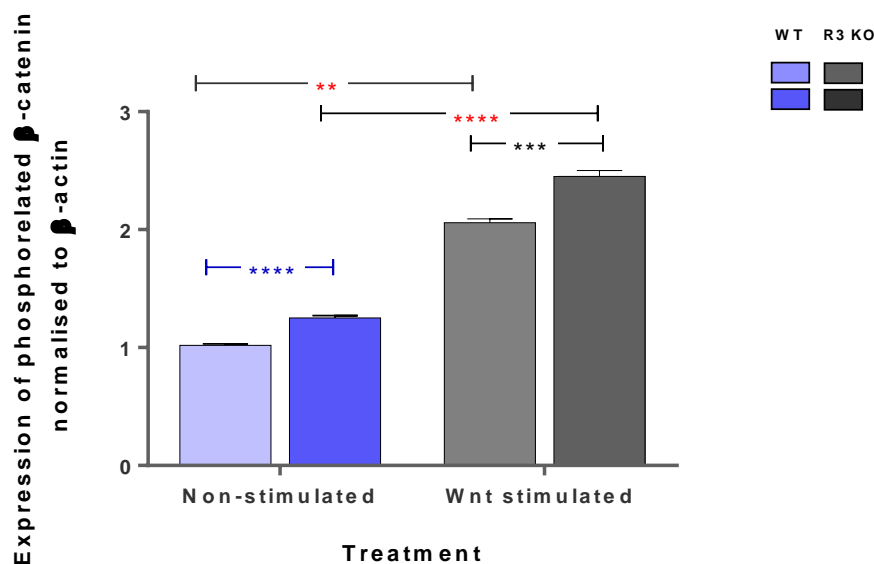


Fig 6.5: A) Representative Western Blot increased phosphorylated β -catenin levels in 20 days differentiated RAMP3KO primary calvarial osteoblast cultures compared to WT primary osteoblasts, under basal and Wnt stimulated conditions (top panel). Primary calvarial osteoblasts from WT and RAMP 3 KO animals were cultured in-vitro and were allowed to differentiate upto 20 days. On day 20 of differentiation, osteoblasts were stimulated with 100ng/ml working concentration of Wnt3A for 20 mins prior being harvested for Western Blotting. Whole cell lysates were collected from three independent stimulated cultures (each genotype). Each independent culture was Western blotted twice for phosphorylated β -catenin. β -actin was the loading control (bottom panel). 40 μ g protein loaded in each well. Exposures were between 2-3 mins.

B) Quantification of levels of phosphorylated β -catenin in WT and RAMP3 KO basal and Wnt stimulated, 20 days differentiated osteoblasts, after normalizing to respective β -Actin levels using two way-ANOVA test. RAMP3 KOs have significantly higher phospho- β -catenin at both non-stimulated ($p \leq 0.0001$) and Wnt stimulated ($p = 0.0002$) conditions. There is a significant increase in both Wnt stimulated WT and RAMP3 KO primary osteoblast cultures ($p \leq 0.0001$) compared to non-stimulated WT and RAMP3 KO primary osteoblast ($p \leq 0.0001$) respectively.

Significance of p value: **** ≤ 0.0001 , *** ≤ 0.001 , ** ≤ 0.01 , * ≤ 0.05

6.3.2.iii Effect of DKK1 stimulation on endogenous phosphorylated β -catenin expression in WT and RAMP3 KO 129/SvEv primary osteoblasts:

We next investigated whether the levels of phosphorylated β -catenin (active form) in RAMP3 KO osteoblasts responded to DKK1 stimulation as WT osteoblasts do. Given that activation of β -catenin is dependent upon Wnt activation, 20 days differentiated WT and RAMP3 KO osteoblasts were subjected to a range of working concentrations: 1,5ng/ml, 50ng/ml, 100ng/ml, 200ng/ml, 250ng/ml of recombinant human DKK1, a known Wnt antagonist. We were interested in determining a dose dependent alteration in levels of phospho- β -catenin in both RAMP3 and WT primary osteoblasts.

Western blotting for phosphorylated β -catenin in both WT and RAMP3 KO differentiated osteoblasts showed a highly significant dose-dependent decrease in levels of β -catenin with increase in DKK1 concentration. RAMP3 KO osteoblasts had significantly higher expression of phospho- β -catenin levels throughout compared to the WTs. The highest significance in the difference in the phospho- β -catenin levels of RAMP3 KO and WTs was observed at the DKK1 concentration of 100ng/ml when the expression of phospho- β -catenin starts dropping in both the cultures. This difference was obvious in the western blots. Figure 6.6 overleaf is a representative Western blot showing the expression of phospho- β -catenin and β -actin (loading control) in WT and RAMP3 KO primary osteoblasts stimulated with a range of DKK1 concentrations. Figure 6.7 is a graphical representation of the significant differences determined using two-way ANOVA test.

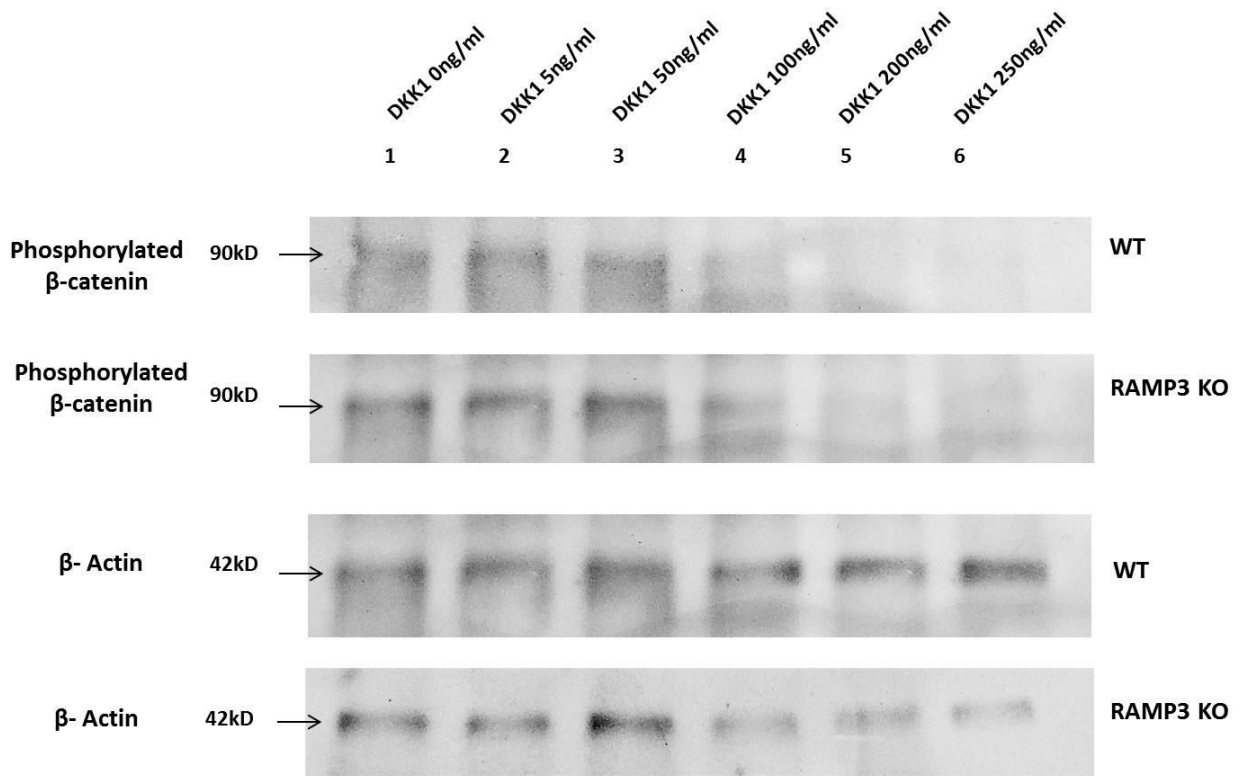


Fig 6.6: Representative Western Blot showing a dose dependent decrease in phosphorylated β -catenin (~90kD) levels in 20 day differentiation WT and RAMP3 KO primary calvarial osteoblasts cultures stimulated with different concentrations of DKK1. RAMP3 KO cultures had significantly higher expression of phosphorylated β -catenin compared to WT at each DKK stimulation concentration. Primary calvarial osteoblasts from WT and RAMP 3 KO animals were cultured in-vitro and were allowed to differentiate upto 20 days. On day 20 of differentiation, osteoblasts were stimulated with different concentrations of recombinant human DKK1 (0, 5, 50, 100, 200, 250ng/ml) for 20 mins prior being harvested for Western Blotting. Whole cell lysates were collected from three independent stimulated cultures (each genotype). Each independent culture was Western blotted once for phosphorylated β -catenin. β -actin (~42kD) was the loading control. 40 μ g protein loaded in each well. Exposures were between 5-7 mins.

Phospho- β -catenin in differentiated primary osteoblasts with Dkk stimulation

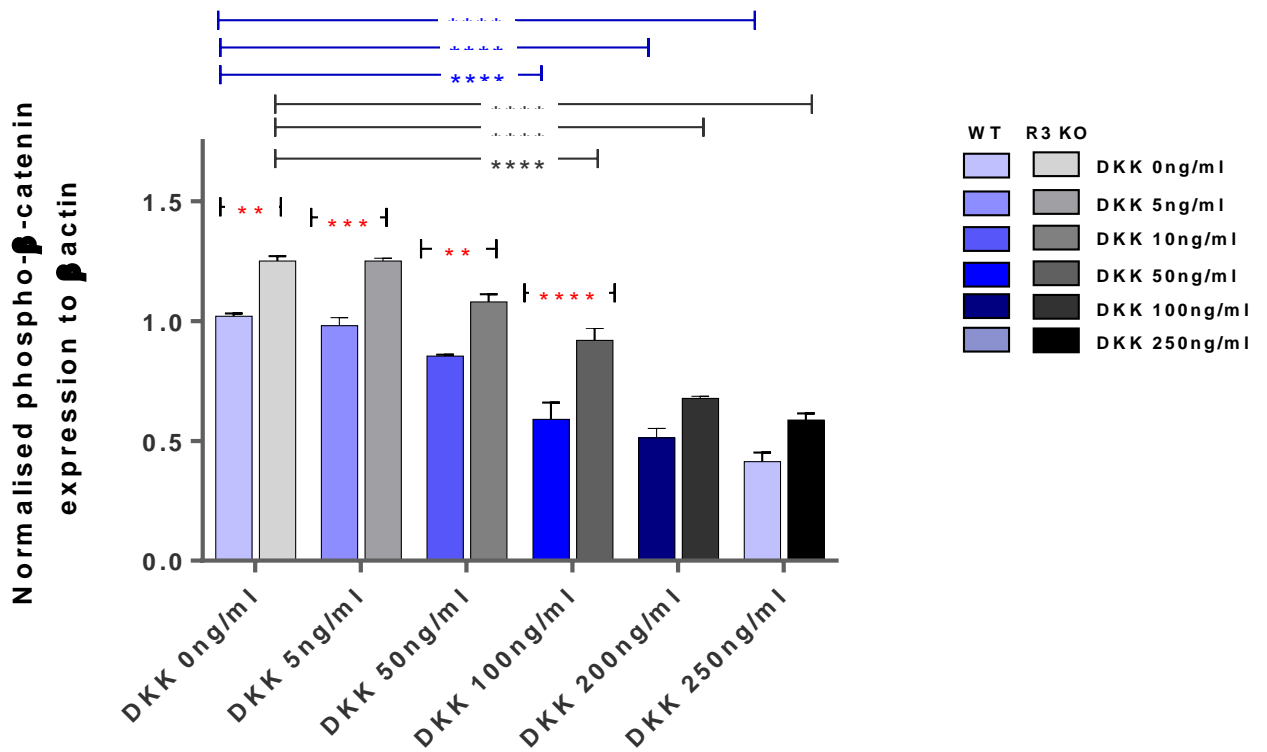


Fig 6.7: Quantification of levels of phosphorylated β -catenin on DKK1 stimulations, in WT and RAMP3 KO DKK stimulated differentiated osteoblasts, after normalizing to respective β -Actin levels Both WT and R3 KO differentiated osteoblasts showed a significant dose-dependent decrease in phosphorylated β -catenin levels with increase in DKK1 concentration. Levels of phosphorylated β -catenin were higher in RAMP3 KO osteoblasts than WT irrespective of DKK concentration. $n=3$ each genotype. Data was analysed using Two-way ANOVA test followed by post multiple comparison correction using Bonferroni's test.

Significance of p value: **** ≤ 0.0001 , *** ≤ 0.001 , ** ≤ 0.01 , * ≤ 0.05

6.3.2.iv Effect of DKK1 and Wnt3A stimulation on Phosphorylated β -catenin expression in WT and RAMP3 KO 129/SvEv primary osteoblast:

On determining the dose dependent response of phospho- β -catenin to DKK1 in both WT and RAMP3 KO mice we further wanted to determine the effect of exogenous Wnt3A stimulation post DKK1 stimulation. WT and RAMP3 KO primary osteoblast cultures were differentiated for 20 days and on the 20th day of differentiation they were first stimulated with a range of DKK1 concentrations (0, 5, 50, 100, 200, 250ng/ml) followed by a stimulation of Wnt3A (100ng/ml). Cells were harvested for protein after the Wnt3A stimulation. It should be noted that since the cultures were first stimulated with DKK1 and then by Wnt3A, what we are observing in this experiment is an increase in phospho- β -catenin concentrations after the DKK1 insult has reduced the endogenous phospho- β -catenin in the cells.

The increase in phospho- β -catenin in both WT and RAMP3KO following Wnt3A stimulation insignificant. However, interestingly the exogenous Wnt3A stimulation increase significantly more amount of phospho- β -catenin in RAMP3 KO primary osteoblasts in comparison to the WT primary osteoblasts. The increase in phospho- β -catenin in RAMP3 KOs begins with concentrations of the prior DKK1 stimulation as high as 200ng/ml. On contrary, the phospho- β -catenin of WT osteoblasts only increased when the previous DKK1 stimulation concentration is of 50ng/ml. Finally in accordance to what we have previously determined (Fig 6.5), when there is no prior DKK1 (0ng/ml) stimulation, RAMP3 KOs have the maximum and significantly higher levels of phospho- β -catenin expression when compared to the WTs. Figure 6.8 overleaf is a representative Western blot showing the expression of phospho- β -catenin in WT and RAMP3 KO primary osteoblasts stimulated with both DKK1 and Wnt3A. Figure 6.9 is a graphical representation of the significant differences determined using two-way ANOVA test.

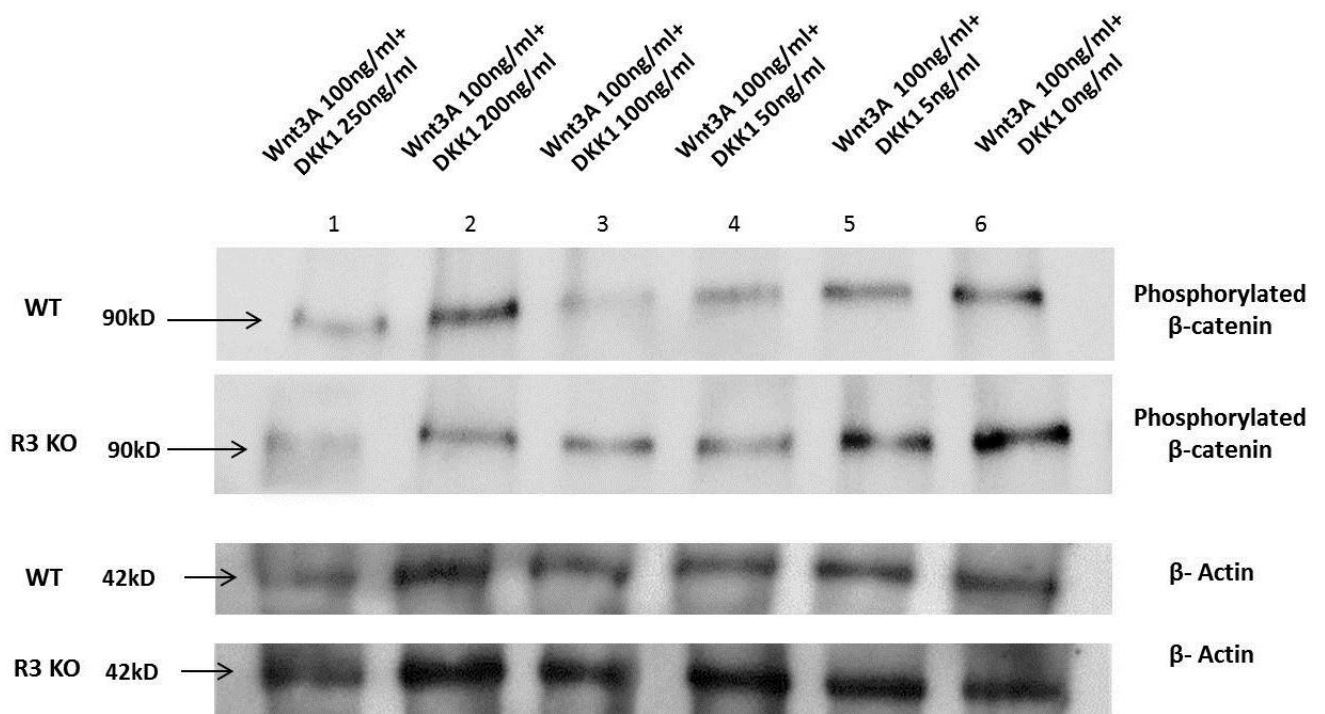


Fig 6.8: Representative Western Blot showing increase in phospho- β -catenin ($\sim 90\text{kD}$) levels in both WT and RAMP3KO osteoblasts on Wnt stimulation following DKK1 stimulation. It was observed that the expression of phospho- β -catenin levels is significantly higher in RAMP3KO s when compared to the WT. Maximum stimulation of phospho- β -catenin in both WT and RAMP3KOs is when the cells are not stimulated with DKK1. Primary calvarial osteoblasts from WT and RAMP 3 KO animals were cultured in-vitro and were allowed to differentiate upto 20 days. On day 20 of differentiation, osteoblasts were first stimulated with different concentrations of DKK (0, 5, 50, 100, 200, 250ng/ml) and were then subjected to Wnt stimulation for 20 mins prior being harvested for Western Blotting. Whole cell lysates were collected from three independent stimulated cultures (each genotype). Each independent culture was Western blotted once. β -actin was the loading control. $40\mu\text{g}$ protein loaded in each well. Exposures were between 2-3 mins.

Phospho- β -catenin in differentiated primary osteoblasts with Wnt and Dkk stimulation

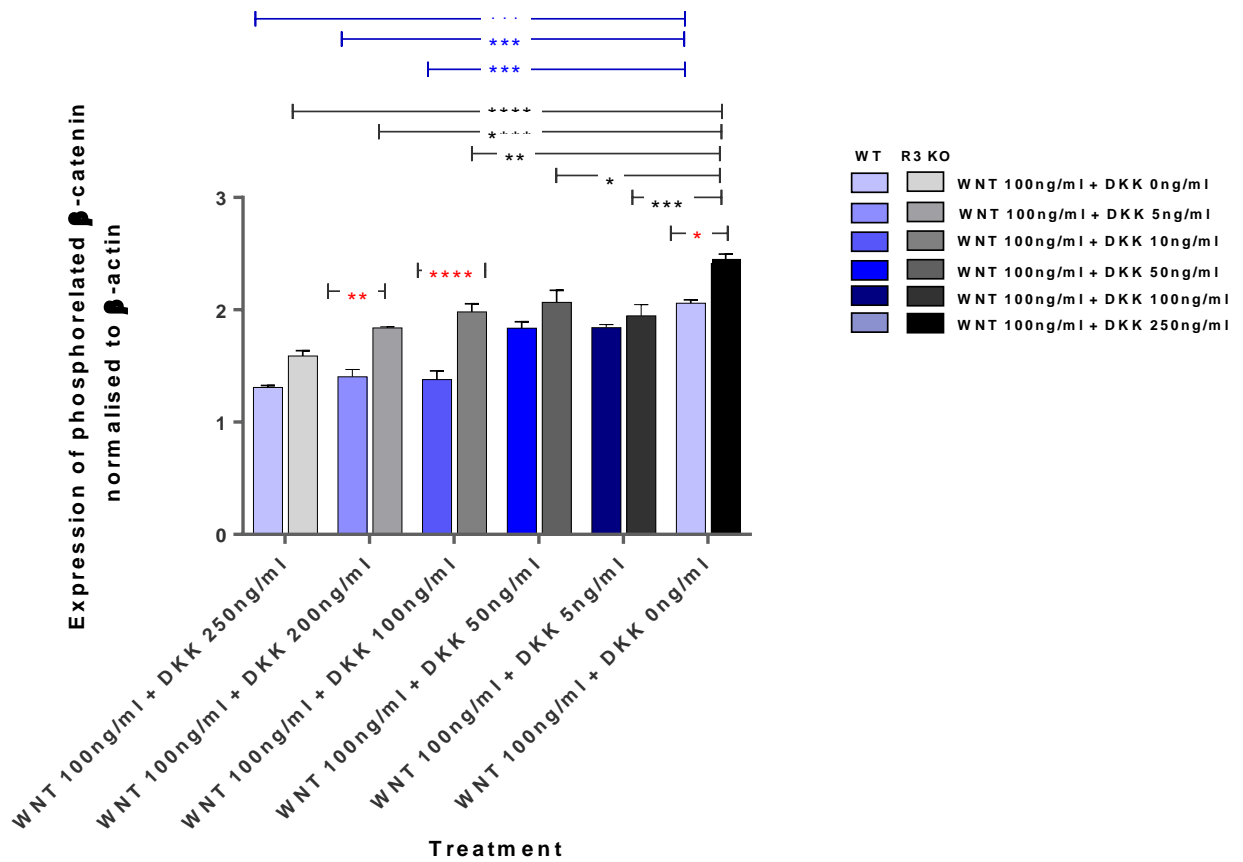


Fig 6.9: Quantification of levels of phosphorylated β -catenin in WT and RAMP3 KO DKK1 and Wnt3A stimulated differentiated osteoblasts, after normalizing to respective β -Actin levels. Wnt3A stimulation significantly increases the expression of phospho- β -catenin in both WTs and RAMP3 KOs. Levels of phosphorylated β -catenin were significantly higher in RAMP3 KO osteoblasts than WT osteoblasts when the prior DKK1 stimulation is of the concentration 200ng/ml (**), 100ng/ml (****) and 0ng/ml (*). Data was analysed using Two-way ANOVA test followed by post multiple comparison correction using Bonferroni's test.

Significance of p value: **** ≤ 0.0001 , *** ≤ 0.001 , ** ≤ 0.01 , * ≤ 0.05

6.4 Discussion

The principal objectives addressed in this body of work are investigating the effects of PTH, AM and AMY stimulation on RAMP2 and RAMP3 expression in WT 129/SvEv primary osteoblasts. Additionally we further determined the expression of total and phosphorylated β -catenin on Wnt3A and DKK1 stimulation in both WT and RAMP3 KO 129/SvEv primary osteoblasts using Western blotting.

Our work gives novel evidence to support of a functional association of RAMP3 and RAMP2 with PTH, AM and AMY peptides in primary osteoblasts. We have successfully demonstrated that stimulation of primary osteoblasts with these peptides results in an increase in the expression of RAMP3 monomer in WT 129/SvEv primary osteoblasts (see Fig 6.1). PTH receptor 1 (PTHR1) is known to be expressed by osteoblasts and plays an important role in regulating osteoblast differentiation by inducing ERK1/2 phosphorylation (Datta et al 2010, Fermor & Skerry 1995). In contrast, expression of PTHR2 in bone is not yet clearly demonstrated to date, although it is known to be highly expressed in brain (Takasu et al 1999). There is evidence supporting that RAMP2 forms a heterodimer with PTHR1 whereas RAMP3 forms a heterodimer with PTHR2 (Christopoulos et al 1999, Hay et al 2006). Since we have observed that RAMP3 expression is increased on PTH stimulation, it can be hypothesized that RAMP3 is also associated with PTHR1 that is yet to be identified or that RAMP2 mediated PTHR1 downsignalling results in an increase in RAMP3 expression. Furthermore, it is also plausible that the PTHR1/RAMP3 association could be responsible for the catabolic skeletal regulation given that RAMP3 KO mice with enhanced skeletal phenotype would lack this receptor mediated bone resorption. These mechanisms have yet to be clearly understood.

Stimulation with both AM and AMY also resulted in an increase in the expression of RAMP3 (Fig.6.1) suggesting that the primary WT 129/SvEv osteoblasts not only express a functional AM receptor 2: CLR/RAMP3 heterodimer but also express a functional AMY receptor 3: CTR/RAMP3 heterodimer in contradiction to previous reports that suggest CTR not being expressed in osteoblasts (Naot et al 2001, Naot & Cornish 2008).

In our experiments, we observed that RAMP2 was expressed in two forms. A monomeric form which was \sim 13kDa and a higher molecular weight form of \sim 55kDa (see Fig. 6.2 and 6.3). Interestingly on stimulation with PTH, AM and AMY, the WT primary osteoblasts expressed demonstrated a higher expression of both the 13kDa monomer and the 55kDa form in both WT

and RAMP3 KO osteoblasts compared to their non-stimulated controls. Additionally it was observed that levels of $\sim 13\text{kDa}$ monomer were significantly lower in stimulated the RAMP3 KO osteoblasts compared to stimulated WT osteoblasts. It was more interesting to observe that this was opposite in the case of the $\sim 55\text{kDa}$ form- that is., stimulated RAMP3 KO cells demonstrated significantly higher levels of $\sim 55\text{kDa}$ form in comparison to stimulated WT primary osteoblasts. In 2006, Nikitenko et al showed that only when co-transfected with RAMP3 or RAMP2, human CLR is expressed as a fully glycosylated 55kDa protein however CLR can have different glycosylation states that result in lower molecular weight of the protein (suplimentary figure 2 (Nikitenko et al 2006)). Since it is known that RAMPs are capable of changing the glycosylation state of their partner GPCR (Nag et al 2012, Parameswaran & Spielman 2006), the 55kDa protein can therefore possibly be a heteromer of non-glycosylated GPCR and RAMP2. If this is true, what we observe in the RAMP3 KO primary osteoblasts is that RAMP2 compensates for the absence of RAMP3 to form a heterodimer with GPCR, hence the expression of RAMP2 monomers is reduced as the more monomers are used for forming heterdimers with GPCR in the RAMP3 KOs when compared to the WTs. This hypothesis is schematically represented in figure 6.10 below.

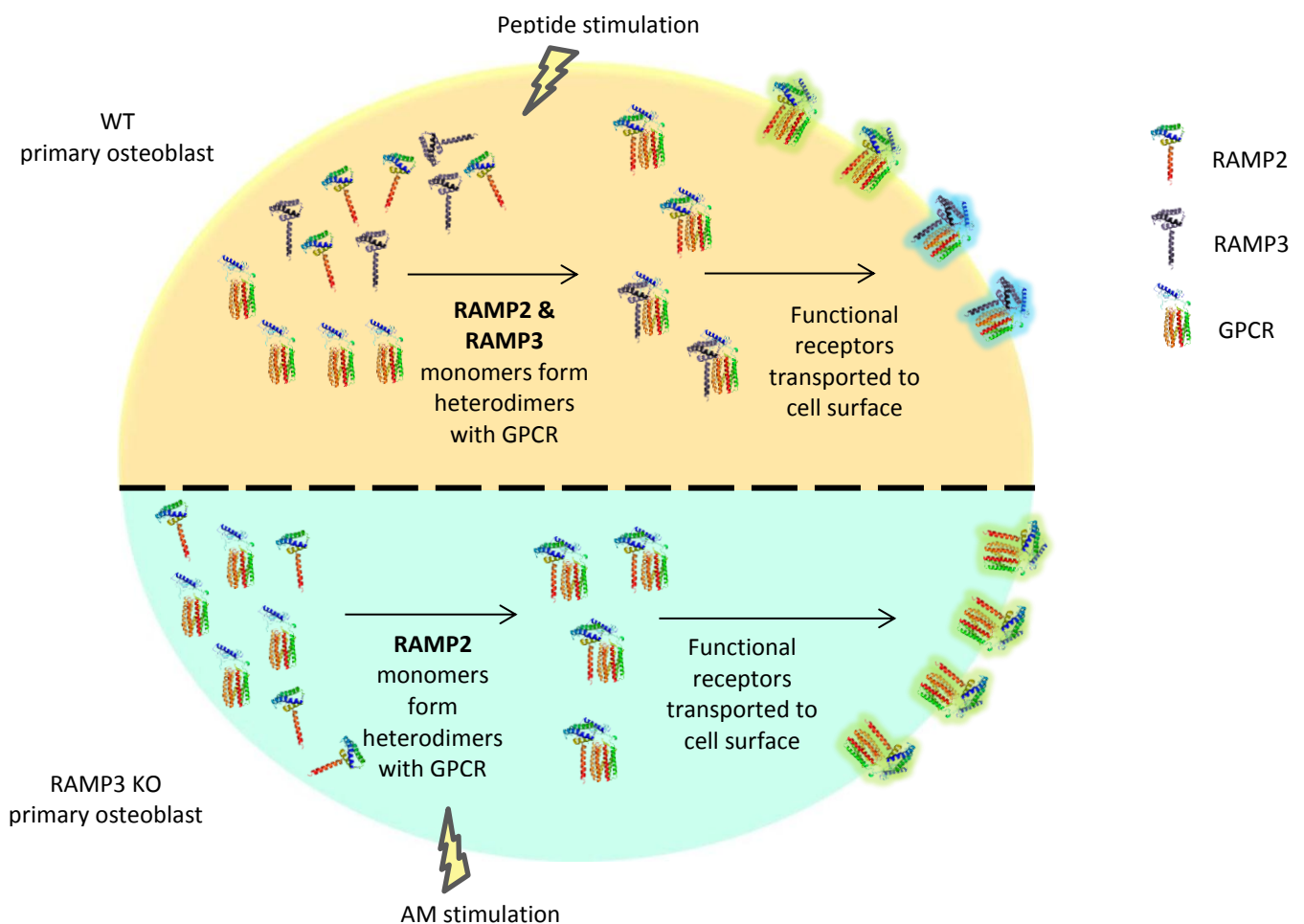


Fig 6.10: Schematic representation of the hypothesised compensatory mechanism between RAMP2 and RAMP3 in the RAMP3 KO primary osteoblasts.

It can also be proposed that RAMP2 forms stable multimeric complex that dissociates to form monomers which in turn form heterodimers with several GPCRs on stimulation by respective peptides. There is evidence that in pufferfish, RAMPs except for RAMP1 and RAMP3 can form stable multimers that are expressed on the plasma membrane (Nag et al 2012). We also know that RAMP1 and RAMP3 form stable homodimers in the cytoplasm but presence of cytoplasmic RAMP2 homodimers are not yet reported (Sexton et al 2001). In concordance to these reports, we did not observe RAMP2 dimers in 129/SvEv primary osteoblasts. It is plausible that the RAMP1 and 3 form homodimers whereas RAMP2 forms tetramers. From our data we can propose that in RAMP3 KO, there is an increased expression of RAMP2 tetramer to compensate for the absence of RAMP3 dimers in the cytoplasm so that RAMP2 monomers can further compensate for RAMP3 to form heterodimers with GPCRs.

It should be noted that with only 20min stimulation period of the peptides, the quantified expressions of RAMPs in this study only reflect the change in state of dimerization of RAMPs i.e. the change in hetero-dimer to monodimer state or vice versa but not the translational event. Increased duration of the stimulation or repeated stimulations for a longer period of time would not only enhance the effect of peptide stimulation on RAMP expression but also give a true reflection of the translation events post stimulation.

With an aim to investigate the association between Wnt and RAMP3, we have determined novel characteristics of the Wnt/ β -catenin pathway in the RAMP3 KO primary osteoblasts. We observed that the RAMP3 KO primary osteoblasts had a significantly higher expression of total β -catenin which was accounted for by increased levels of active/phosphorylated β -catenin (see Fig. 6.4 and 6.5). These findings are in concordance with previous reports of reduction of RAMP3 expression on Wnt3A stimulation (Rohrs et al 2009). Further, with increasing concentrations of DKK1, we observed that in comparison to the WT osteoblasts, RAMP3 KOs require higher DKK1 concentrations to reduce the amounts of endogenous phosphorylated β -catenin (Fig. 6.6 and 6.7). Additionally post DKK1 stimulation, an exogenous stimulation of 100ng/ml Wnt3A, resulted in significantly higher expression of phosphorylated β -catenin in the RAMP3 KO primary osteoblast compared to the WTs (Fig. 6.8 and 6.9). Given the evidence that Wnt signalling plays an important role in osteoblast differentiation (Glass et al 2005), we can suggest, that the RAMP3 KO mice have enhanced osteoblast differentiation which results from increased active phospho- β -catenin level acting through the Wnt3A pathway/s. This hypothesis is supported by our findings reported in chapters 2 and 4.

In conclusion, we have successfully shown that RAMP2 and RAMP3 both respond to PTH, AM and AMY stimulation and that RAMP2 possibly compensates for RAMP3 in the RAMP3 KO osteoblasts to form heterodimers with GPCRs. We have also provided novel evidence of increased Wnt signalling in the RAMP3 KO osteoblasts that could potentially be responsible for the enhanced osteoblast differentiation observed in RAMP3 KOs.

Chapter 7: Expression of calcitonin receptor (CTR) in primary osteoblasts.

7.1 Introduction

The Calcitonin family of peptides are known therapeutic targets for treating osteopenic skeletal disorders. The effects of CT family of peptides on osteoclasts and osteoblast have been studied for several decades. However, the research on expression of the receptors for CT family of peptides is limited. An in-depth review of the expression of receptors for CT peptides to date is discussed in Chapter 1. This chapter aims to address the conflicting literature evidence of expression of Amylin (AMY) receptor that comprises the Calcitonin receptor (CTR) and receptor activity modifying proteins (RAMPs), in osteoblasts.

Effects of administration of AMY on the skeleton are studied in a number of local and systemic mice and rat models. Systemic administration of AMY reduction on PTH mediates resorption in neonatal mice (Alam et al 1993, Pietschmann et al 1993). A daily subcutaneous local administration of AMY(1-8) over the hemicalveria of mice resulted in a reduction of local bone resorption, where as a systemic administration of both full length and AMY (1-8), reduced the bone resorption indices and increased histomorphometric indices, suggesting that AMY affects both osteoclasts and osteoblasts (Cornish et al 1995, Cornish et al 1998a).

In vitro effects of AMY on rat osteoclast cultures are reported to be due to the down regulation of osteoclast mobility (Alam *et al.* 1993). The expression of AMY receptors in osteoclasts is also well understood. The CTR is well established osteoclast marker (Hattersley & Chambers 1989). There is evidence of variable expression of CTR during osteoclastogenesis (Lerner 2006). In rat osteoblasts, Cornish *et. al.* reported that AMY induced proliferation at 10^{-11} M concentration is accompanied by increase in intracellular cAMP levels (Cornish et al 1995, Cornish et al 1999). Human osteoblast like cell proliferation is reported at concentrations between 10^{-9} M and 10^{-6} M along with increased osteocalcin expression on exposure to $1,25(\text{OH})_2\text{D}_3$ 10^{-8} M (Villa et al 1997). This indicated the presence of an AMY receptor in osteoblasts. It is known that a traditional AMY receptor comprises CTR and one of the RAMP isoforms.

The “CT receptor” was first identified in pig, in human and then rat (Albrandt et al 1993, Gorn et al 1992, Lin et al 1991, Martin et al 1995). The CTR transcription variants are classified as avian/teleost, artiodactyl and rat/human based on the biological and structural differences (Martin et al 1995). Human CTR transcript variants were cloned from BIN67 and T47D cells (Gorn et al 1992, Kuestner et al 1994). The shorter transcript variant expressed in T47D is predominantly expressed compared to the 16 amino acid longer variant is expressed in BIN67

cells (Gorn et al 1992, Kuestner et al 1994). The 16 amino acid insert resulted in ablation of intracellular calcium mobilization however there is no difference in affinity toward calcitonin between the two variants (Pondel 2000). When co-transfected with RAMP 1 and 3, CTR1 variant (16 aa insert minus) exhibited induced ^{125}I rat AMY binding, although RAMP1-AMY receptor had a higher affinity toward salmon AMY and less to human ^{125}I CT and rat ^{125}I AMY, RAMP3-AMY receptor did not show this difference in affinity (Christopoulos et al 1999). A similar binding data was reported by Chen *et al*, CTR1 variant had higher affinity towards salmon ^{125}I CT and less affinity towards human ^{125}I CT and rat ^{125}I AMY (Chen et al 1997b).

When identifying the CT receptor in rat, Sexton *et al* identified two CTR transcripts, the known CTR1a (478 amino acids) and a longer transcript CTR1b (515 amino acids), from rat hypothalamic cDNA library. Subsequently these variants were also reported to be expressed in LLC-PK1, a porcine kidney epithelial cell line (Zolnierowicz et al 1994). The additional 37 amino acids in CTR1b variant results in a change in the second extracellular domain of CTR which is expected to affect the ligand-receptor interaction (Sexton et al 1993). Salmon CTR (^{125}I -sCTR) shows a much higher affinity toward CTR1a compared to CTR1b and interestingly both rat and human CTR did not compete to bind to CTR1b even at as high concentration as 10^{-6}M (Houssami et al 1994, Martin et al 1995, Sexton et al 1993). It has been reported earlier that the CTR transcription variants expressed in rat are also expressed in mouse (Martin et al 1995). The tissue specific difference in expression in the variants may be targets for endogenous tissue specific isoforms of ligands (Martin et al 1995).

The CTR1b transcript is expressed predominantly in the brain (hypothalamus, nucleus accumbens, cerebral cortex and brain stem) while CTR1a is expressed by several peripheral tissues CTR (Sexton et al 1993). In kidney CTR1a and 1b are both expressed however it is observed that CTR1b expression is very low compared to that of CTR1a. In 1986, Nicholson et al demonstrated that osteoclasts abundantly expressed CTR, while no CTR expression could be detected in osteoblasts (Nicholson et al 1986). In rat osteoclast, both CTR1a and CTR1b variants are expressed, however CTR1a expression predominates CTR1b expression (Ikegame et al 1995). The rat osteosarcoma osteoblast like cell line UMR106-06 is reported to develop the ability to bind to salmon calcitonin only on prolonged maintenance, suggesting that this particular sub-clone of UMR106 cell line expresses CTR (Forrest et al 1985). It was reported that UMR106-06 expressed CTR1a transcript at mRNA level (Forrest et al 1985, Martin et al 1995). mRNA expression of CTR was also confirmed in the UMR106-06 cell line in a different study using RT-

PCR and Northern Blot, although CTR was not expressed at mRNA level in primary rat osteoblast cultures (Naot et al 2001). In 2003, using RT-PCR, expression of CTR mRNA in primary human osteoblast culture was reported for the first time by Villa *et. al.* however this study had a small sample group (n=2) (Villa et al 2003). In a much more extensive study on primary human osteoblast cultures (n=16) CTR mRNA was not detected by real time PCR (Naot & Cornish 2008).

RAMP2 but neither RAMP1 nor RAMP3, is expressed in pure osteoclast like cultures derived from mouse bone marrow co-culture and spleen (Nakamura et al 2005). This implies that the AMY activity in osteoclasts, is predominantly due to the receptor that comprises the CTR-RAMP2 heterodimer. High RAMP1, less RAMP2 and no RAMP3 mRNA expression in primary human osteoblast culture have been reported earlier (Villa et al 2003). RAMP2 mRNA was highly expressed in human bone marrow cultures which could account for the RAMP2 expression on osteoclast (Naot & Cornish 2008). Osteoblastic cell line MC3T3-E1 expresses all the three RAMPs however, the expression of RAMP1 and RAMP2 but not RAMP3 mRNA increases on dexamethasone treatment (Uzan et al 2004). RAMP1 is also expressed in human osteosarcoma cell line MG63 (Kawase et al 2003). A summary of CT peptide receptor expression in osteoclast and osteoblast is illustrated in Fig. 7.1 below.

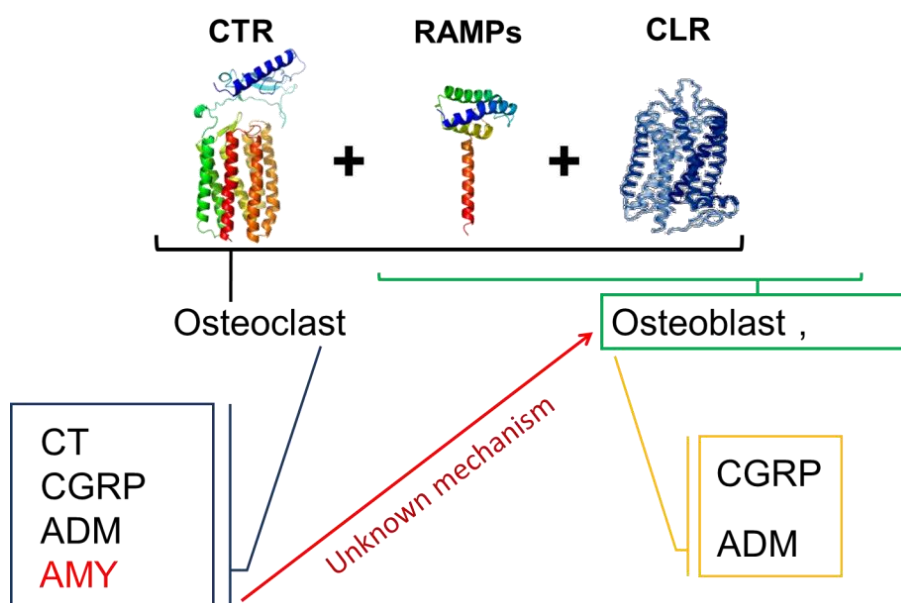


Fig 7.1: A schematic representation summarising the expression of CT family of peptide receptors in osteoclasts and osteoblast. Osteoclasts express CTR, CLR and RAMPs hence all the four CT peptides affect osteoclasts. However Osteoblasts express RAMPs and CLR hence should only be affected by CGRP and ADM only. AMY induces proliferation of osteoblast, but the mechanisms remain unknown.

Determining and characterising AMY receptors in osteoblasts is essential as the mechanism/s by which AMY induces proliferation of osteoblasts remain unknown. Moreover, CTR is a well-established osteoclast marker and is used in many studies. If CTR is expressed in osteoblasts, our fundamental understanding of the role of calcitonin and its receptor in the skeleton will be altered. The expression of RAMP isoforms in osteoblasts, during differentiation, is detailed in chapter 5. In this chapter we focus on the expression of the GPCR CTR in differentiating primary osteoblasts.

Since expression of CTR in osteoblast remains debated to date, we hypothesised that ***osteoblasts either express a novel AMY receptor that does not comprise CTR, or that the CTR in osteoblastic AMY receptor is a transcript variant of the known full length CTR.***

The objectives were:

- 1) To determine whether primary calvarial osteoblasts from WT 129/SvEv mice expressed CTR or CTR variants that formed an AMY receptor.
- 2) To compare the sequence of the CTR cDNA sequence to known CTR variants (if expressed).
- 3) To determine if both the WT and RAMP3 KO primary osteoblasts expresses known or novel CTR variant protein during differentiation
- 4) To determine if the CTR protein expression profile is different in WT and RAMP3 KO primary osteoblasts during differentiation.
- 5) To determine if a CTR variant expressed in WT and RAMP3 KO primary osteoblasts, does it respond to Amylin stimulation.

7.2 Methods and materials

7.2.1: Protein sample preparation

7.2.1.i Total cell lysate protein from differentiating primary osteoblasts:

Detailed calvarial primary culture protocol is described in Section 5.2. Total protein was collected from differentiating primary osteoblasts of WT (SVEV/129) and RAMP3 KO genotype on day 0, 5, 10, 15 and 20 of differentiation. One T25 flask each culture was harvested at every time point. The medium was removed and the cells were washed in PBS. 200µl ice-cold NP40 lysis buffer (recipe in appendix) having fresh protease inhibitor cocktail 1X (PIC) was added to the cells and the cells were scraped and collected in 1.5ml tubes. This homogenate was then sonicated on ice at 10µm for 10 short pulses using a probe sonicator (Soniprep 150, Sanyo, Japan). The final supernatant was stored as aliquots at -20°C.

7.2.1.ii Total cell lysate protein from basal and AMY stimulated primary osteoblasts:

Detailed protocol of harvesting protein from stimulated osteoblasts is described in section 6.2.1 and 6.2.2. Briefly, WT and RAMP3 KO primary osteoblasts were differentiated for 20 days and stimulated with 10nM working concentration of full length AMY peptide for 20 min prior to harvesting cells. Cell harvesting protocol is discussed in the above section 7.2.1.i.

7.2.1.iii Total brain lysate protein a positive control:

Whole brain homogenates from previously snap frozen WT (SVEV/129) mice was prepared for Western blotting. The mouse brain (snap frozen tissue stored at -80°C) was weighed and allowed to soften at -20°C for an hour prior being chopped into small pieces. The chopped tissue was placed in a 7ml tissue grinder tube and 15 volumes of ice-cold 0.25 M Sucrose/Buffer A containing freshly prepared protease inhibitor cocktail 1X (PIC), was added. The tissue was first homogenized by 15 passes of the loose pestle and then by 15 passes of the tight pestle. This homogenate was centrifuged at 600 g for 5mins at 4°C and the supernatant was retained. The supernatant was then sonicated using a probe sonicator (Soniprep 150, Sanyo, Japan) by 10 brief pulses at 10µm before aliquoting and snap freezing it in liquid nitrogen. The samples were stored as aliquots at -20°C.

7.2.2 Western Blotting for CTR:

Detailed protocol for SDS PAGE and immuno-blotting is described in Section 7.2.2. To determine CTR protein in WT (SVEV) and RAMP3 KO differentiating primary osteoblast cell lysate, SDS PAGE was carried out in 7% resolving gel with 50µg of protein was loaded in each well. Primary antibody - rabbit CTR antibody (Abcam®, Cambridge, UK) against 476-496 aa residues of rat CTR was used at 1:200 dilution and made up in PBST. This primary antibody recognised both CTR1a and CTR1b isoforms of CTR. Secondary antibody - goat antirabbit-HRP (Dako®, Aligent Technologies Company, Cambridge, UK) was used as a 1:3000 dilution made up in 5% blocking solution (skimmed milk in PBST w/v).

7.2.3 RNA sample preparation:

7.2.3.i Total RNA from differentiating primary osteoblasts:

Detailed calvarial primary culture protocol is described in Section 5.2. Total RNA was collected from differentiating calvarial primary osteoblasts of WT (SVEV/129) and RAMP3 KO genotype on day 20 of differentiation. One T25 flask each culture was harvested at every time point. The medium was removed and 500µl of TRIZOL® reagent was added to the cells. The cells were collected in 1.5 ml tubes by scraping. Total RNA was then extracted using the protocol provided by the manufacturer (Invitrogen™). RNA in each sample was quantified in NanoDrop® (Thermo Scientific, Wilmington, USA), a micro-volume UV-vis spectrophotometer, at A260 purity of preparation checked by determining the 260/280 ratio. Samples were then stored at -20°C.

7.2.3.ii Total RNA from mouse brain – positive control:

Total RNA was extracted from previously snap frozen WT (SVEV/129) mouse. The mouse brain (snap frozen tissue stored at -80°C) was weighed and allowed to soften at -20°C for an hour prior being chopped into small pieces. The 100mg chopped tissue was placed in a 7 ml tissue grinder tube and 1ml of ice-cold TRIZOL® reagent was added. The tissue was first homogenized by 15 passes of the loose pestle and then by 15 passes of the tight pestle. This homogenate was used to extract total RNA according to manufacturer's guidelines (Invitrogen™). RNA was quantified and stored similar to total RNA from cell cultures.

7.2.4 Reverse transcription to generate cDNA:

cDNA was generated from total RNA samples using ABI high capacity RNA – cDNA kit (Applied Biosciences, Life Technologies™, California, USA). For every 1µg of RNA a 20µl reaction mix was prepared by adding 10µl of 2X RT buffer mix, 1µl of 20X RT enzyme mix and Nuclease free water (up to 20µl) to the RNA sample. This mix was then set up in the following PCR reaction:

- 1) 37 °C – 1hr
- 2) 95 °C – 5 min
- 3) 4 °C – hold

cDNA (end product) was then stored at -20°C.

7.2.5 End point PCR:

GoTaq® DNA Polymerase kit (Promega Cooperation, Madison, USA) was used to detect CTR expression in osteoblast cDNA. Each 25µl reaction mix contained 5µl of 5X Green GoTaq® reaction buffer, dNTP at a final concentration of 0.2mM (10mM each dNTP stock), MgCl₂ at a final concentration of 1.5mM (25mM each stock) and GoTaq® DNA Polymerase 2.5units. Proportions for PCR mix mentioned below along with the PCR conditions. PCR amplicons were visualized by electrophoresis in 1.5% Agarose gel (Sigma®) prepared in Tris-base-EDTA buffer and containing 0.5ug/ml ethidium bromide.

PCR reaction mix:

5X Green GoTaq® reaction buffer: 5µl
MgCl₂: 0.75µl
dNTP mix : 0.5µl
Forward Primer: 1.25µl
Reverse primer: 1.25µl
GoTaq® DNA Polymerase: 0.5µl
cDNA: 1-2µg
Nuclease free water: upto 25µl

PCR conditions:

- 1) 95°C - 3min
- 2) 95°C - 30 sec
- 3) 55°C - 30 sec (for all CTR primer pairs)
- 4) 72°C - 30 sec (repeated 2-4, 35 cycles)
- 5) 72°C - 5min
- 6) Hold at 4°C

7.2.6 Determining expression and sequence of CTR cDNA in calvarial, primary osteoblasts:

The CTR gene comprises 16 exons. The protein coding region spans from the latter half of exon 3 to the first half of exon 16 (Fig. 7.2). Expression and sequence of full length CTR cDNA in WT osteoblast was determined using pairs of overlapping primers each of which resulted in an approximately 350bp amplicon. 17 primer pairs were designed such that each primer pair would re-amplify about 150bp of previous primer pair amplicon followed by a new leading 150bp stretch. Overlapping amplification helped confirm the cDNA sequences. A schematic representation of the use of overlapping primers is illustrated in figure below (Fig.7.2). Since all the primers amplified approximately 350bps of the cDNA, absence of amplicon or change in the sized of the expected amplicon indicated the change in the cDNA sequence of osteoblast. Primer sequence and amplification regions are detailed in Table 7.1 overleaf.

Schematic representation illustrating use of overlapping primers.

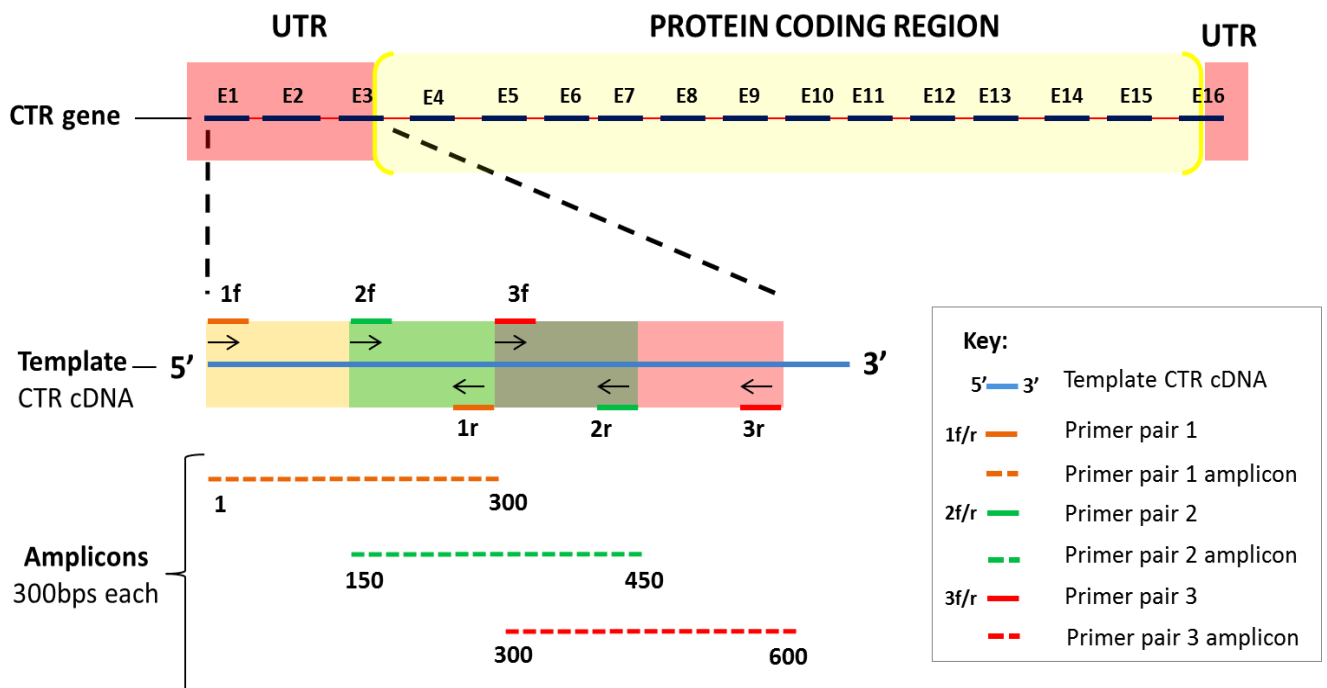


Fig 7.2: A schematic representation of the experimental design. Overlapping primers amplified overlapping regions which helped confirmed the cDNA sequence whilst amplification. In the above schematic example, Primer pair 1 f (forward) and r (reverse) amplifies the region 1 to 300, primer pair 2 f and r amplifies region 150 to 450 so on and so forth. In total 17 primer pairs were designed to facilitate sequencing of the full length CTR cDNA.

Table 7.1: Primer sequences for determining full-length mouse osteoblast CTR sequence.

<i>Primer ID</i>	<i>Primer Sequence</i>	<i>T_m</i>	<i>Position - mCalcr1b mRNA</i>	<i>Amplicon</i>
<i>mCTR1f</i>	5' GTCAGGAAAAGAAGTGCCCG 3'	59.12 °C	83 - 108	337bps
<i>mCTR1r</i>	3' CGCAGACTTCACTGGGCATC 5'	61.36 °C	360 - 341	
<i>mCTR2f</i>	5' GGCTTTCAGTGGAGAAGGGG 3'	60.32 °C	240 - 259	360bps
<i>mCTR2r</i>	3' TTTGCGGAGATTCCGCCTTT 5'	60.61 °C	599 - 580	
<i>mCTR3f</i>	5' CTGAGCTGTGCCCAGACAT 3'	59.70 °C	433 - 451	341bps
<i>mCTR3r</i>	3' CATAGCATTTGTA CTGAGCATCCA 5'	59.18 °C	774 - 751	
<i>mCTR4f</i>	5' GGTTCTTCTCGTGAACAGGT 3'	59.93 °C	610 - 630	350bps
<i>mCTR4r</i>	3' CCACTCTCCATTTTCATCACAGT 5'	58.67 °C	939 - 957	
<i>mCTR5f</i>	5' TTCCTGTACTTGGTTGGCCG 3'	60.25 °C	720 - 739	357bps
<i>mCTR5r</i>	3' GGAGTGACCCACAAGAGCC 5'	60.00 °C	1076 - 1058	
<i>mCTR6f</i>	5' GATGTGCTGGGACGACACTC 3'	60.74 °C	842 - 861	328bps
<i>mCTR6r</i>	3' GAACATGTGCTTGTGCAAGGT 5'	59.93 °C	1169 - 1149	
<i>mCTR7f</i>	5' TAGACACCCTGACAGCAACC 3'	59.31 °C	962 - 981	339bps
<i>mCTR7r</i>	3' TCCCACTGCATTGTCCACAT 5'	59.59 °C	1300 - 1281	
<i>mCTR8f</i>	5' TGGTTGCTTCCATGCTGATCT 3'	59.99 °C	1093 - 1113	343bps
<i>mCTR8r</i>	3' TCGCAGAGCATCCAGAAGTAG 5'	59.59 °C	1435 - 1415	
<i>mCTR9f</i>	5' TGAGGTTGTGCCCAATGGAG 3'	60.25 °C	1214 - 1233	346bps
<i>mCTR9r</i>	3' ACGAGTGATGGCGTGGATAA 5'	59.18 °C	1559 - 1540	
<i>mCTR10f</i>	5' GAGTGACACGAGGGAAAAGA 3'	59.97 °C	1322 - 1341	358bps
<i>mCTR10r</i>	3' GCGGACAATGTTGAGAAGAAAAGA 5'	59.50 °C	1679 - 1657	
<i>mCTR11f</i>	5' CATGGCTGTGTTTACCGACG 3'	59.56 °C	1463 - 1482	329bps
<i>mCTR11r</i>	3' ACACAACAACTGGATCCCCA 5'	59.78 °C	1791 - 1771	
<i>mCTR12f</i>	5' AGTGCAGAAACCCACTTGCT 3'	60.11 °C	1590 - 1609	323bps
<i>mCTR12r</i>	3' TGCACCTCATGGTTGCAGAA 5'	60.18 °C	1912 - 1893	
<i>mCTR13f</i>	5' AGATGAGGCAAACCCACGAG 3'	60.04 °C	1693 - 1712	344bps
<i>mCTR13r</i>	3' ATCTGGCTCAGCGAAGGCTA 5'	61.05 °C	2036 - 2017	
<i>mCTR14f</i>	5' TCCAACAAGGTGCTTGGGAA 3'	59.74 °C	1806 - 1825	345bps
<i>mCTR14r</i>	3' GGATGCGTCTTGCTGGATGA 5'	60.46 °C	2150 - 2133	
<i>mCTR15f</i>	5' CCAGTGGACGCAGTTCAAGA 3'	60.25 °C	1928 - 1947	322bps
<i>mCTR15r</i>	3' CCTGGGAGGATGGGAATCAC 5'	59.52 °C	2249 - 2230	
<i>mCTR16f</i>	5' CAGGAACCACGGAATCCTCC 3'	60.11 °C	2061 - 2080	336bps
<i>mCTR16r</i>	3' TCCAGGATGAATGATGGAGTTCA 5'	59.22 °C	2396 - 2374	
<i>mCTR17f</i>	5' AAGCCACCCCAAGCATTGT 3'	60.51 °C	2162 - 2180	350bps
<i>mCTR17r</i>	3' CTCAACGGTACAAATGGCTCAA 5'	59.19 °C	2511 - 2490	

7.2.7 Sequencing and in-silico analysis of osteoblast CTR cDNA:

PCR products from each primer pair was sequenced in Applied Biosystems' 3730 DNA Analyser using BigDye v3.1 by the Core Genomic Facility (University of Sheffield). Sequences were checked and corrected for misreads using the FinchTV™ (Geospiza Inc. Seattle, WA). Using the nucleotide query available at NCBI's basic local alignment search tool (BLAST), all the sequences were then checked for sequence similarity against mouse genomic and transcript database. Dissimilarities in the osteoblast CTR sequence, when compared to known full length CTR (Ensembl name Calcr-001) were identified using BLAST2n. Whole osteoblast CTR cDNA sequence was predicted by "stitching" together all the overlapping sequences *in silico*, using the overlapping regions as references. This whole osteoblast CTR cDNA sequence was aligned against two known protein coding CTR isoforms CTR1a (Ensembl name Calcr-001; Transcript ID ENSMUST00000075644) and CTR1b (Ensembl name Calcr-003; Transcript ID ENSMUST00000171613), using multiple sequence alignment tool CLUSTALW (EBM-EBI). Protein molecular weight of the known CTR isoforms and the osteoblast CTR isoform were predicted and compared online using 'Protein Molecular Weight' at www.bioinformatics.org.

7.3 Results

7.3.1 PCR using overlapping primer pairs:

Amplification for 17 overlapping regions across the full-length CTR cDNA was carried out in three independent WT primary osteoblast cultures. Primer pairs 1, 2, 3, 4, 5, 6, 8, 9, 11, 12, 13, 14, 15, 16 and 17 amplified expected CTR regions in all three WT cultures. Amplicons for primer pair 8 and 9 were smaller than expected amplicon size. Primer pairs 7 and 10 did not amplify cDNA in any of the cultures (Fig. 7.3).

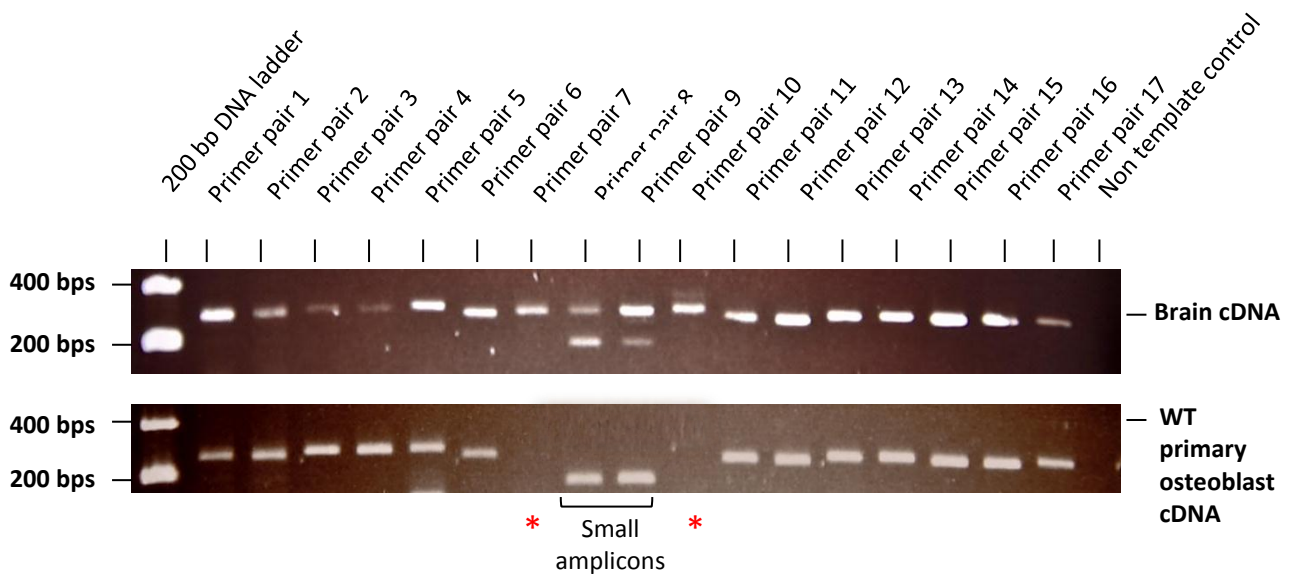


Fig 7.3: PCR amplicons for each primer pair (1-17) amplified in brain cDNA (top panel) and WT primary osteoblast cDNA (bottom panel). Lane 1 was loaded with 5 μ L of O'RangeRuler 200 bp DNA Ladder (Thermo Scientific™). Lanes 2 to lane 18 are loaded with PCR products of primer 1 to primer 17 respectively. Lane 19 is loaded with non-template control. Primer pairs 7 and 10 amplify cDNA in brain cDNA but not in primary osteoblast cDNA (red asterisks). Primer pairs 8 and 9 amplify ~200bps cDNA and ~340bps cDNA amplicons in brain however in primary osteoblast cDNA only the smaller ~200bps amplicons were amplified (marked on the image).

7.3.2 Sequencing:

Each of the amplicons was sequenced and the sequences were checked in software Finch TV™. Sequencing results, of a representative WT primary osteoblast cDNA for each amplicon are summarized in the appendix section 10.1.4.i.

7.3.3 Generating full length osteoblast CTR cDNA sequence in-silico from short overlapping PCR fragments and predicting protein sequence:

Example: Representative example of joining amplicon sequences: primer pairs 3,4 and 5:

Step 1: Identifying common sequences/regions to overlap (blue highlights):

Amplicon 3 sequence:

NNGGCATAAACTGAAAGGTGAGTGCTTATATAAGCATCGCTTATGGAAGGAGAAGAAACCGAGGGAGCAGGGCTA
CCACTTAGAGGATTTGAAAATGACTCCAAGGAGGTCCAGAGTGAAAAGGCGGAATCTCCGCAAACCGAAGATGAG
GTTTCCTTCTCGTGAAACAGGTTACCCCTGCTGCTCCTGCTCCTAGTGAGCCCAACTCCAGTTCCTCAGGCTCCTAC
CAATCTCACTGACTCCGGCCTTGATCAGGAGCCATTCTGTACTTGGTTGGCCGCAAGAAGCTGCTGGATGCTCA
GTACAAATGCTATGA

Amplicon 4 sequence:

GGGGCCCCGGCTCTAGTGAGCCACTCCAGTTCTTCAGGCTCCTACCAATCTCACTGACTCCGGCCTTGATCAGGA
GCCATTCTGTACTTGGTTGGCCGCAAGAAGCTGCTGGATGCTCAGTACAAATGCTATGACCGGATTCATCAGTT
GCCCTCTTATGAAGGAGAAGGTCTGTACTGCAACCGCACCTGGGATGGCTGGATGTGCTGGGACGACACTCCCGC
TGGAGCCACAGCCTATCAGCACTGCCCTGACTACTTCCCGGACTTTGACACAGCAGAAAAGTTTCAAATACTG
TGATGAAAAGGGAGAGTGG

Amplicon 5 sequence:

NNNNNGGTGGAAGGAAATGAAAATGACCCGATTCATCAGTTGCCCTCTTATGAAGGAGAAGGTCTGTACTGCCCT
TTTACCTGGGATGGCTGGATGTGCTGGGACGACACTCCCGCTGGAGCCACAGCCTATCAGCACTGCCCTGACTAC
TTCCCGGACTTTGACACAGCAGAAAAGGTTTCAAATACTGTGATGAAAATGGAGACTGGTTTAGACACCCTGAC
AGCAACCGAACCTGGTCCAACCTATACTCTGTGCAACGCTTTCACTTCTGAGAAACTGCAAAATGCGTACGTTCTT
TATTACCTGGCTCTTGTGGGTCACTCC



Step 2: Aligning the common overlapping regions:

NNGGCATAAACTGAAAGGTGAGTGCTTATATAAGCATCGCTTATGGAAGGAGAAGAAACCGAGGGAGCAGGGCTA
CCACTTAGAGGATTTGAAAATGACTCCAAGGAGGTCCAGAGTGAAAAGGCGGAATCTCCGCAAACCGAAGATGAG
GTTTCCTTCTCGTGAAACAGGTTACCCCTGCTGCTCCTGCTCCTAGTGAGCCCAACTCCAGTTCCTCAGGCTCCTAC
CAATCTCACTGACTCCGGCCTTGATCAGGAGCCATTCTGTACTTGGTTGGCCGCAAGAAGCTGCTGGATGCTCA
GTAC.....
.....GGATGCTCAGTACAAATG
CTATGACCGGATTCATCAGTTGCCCTCTTATGAAGGAGAAGGTCTGTACTGCAACCGCACCTGGGATGGCTGGAT
GTGCTGGGACGACACTCCCGCTGGAGCCACAGCCTATCAGCACTGCCCTGACTACTTCCCGGACTTTGACACAGC
AGAAAAGGTTTCAAATACTGTGATGAAAAGGGAGAGTGG.....
.....AAAATGGAGAGTGGTTTAGACACCCTGACAGCAACCGAACCTGGTC
CAACTATACTCTGTGCAACGCTTTCACTTCTGAGAAACTGCAAAATGCGTACGTTCTTTATTACCTGGCTCTTGT
GGGTCACTCC





Step 3: Joining the sequences to obtain a larger cDNA fragment sequence

NNGGCATAAACTGAAAAGG TGAGTGCTTATATAAGCATCGCTTATGGAAGGAGAAGAAACCGAGGGAGCAGGGCT
 ACC
 ACTTAGAGGATTTGAAAATGACTCCAAGGAGGTCCAGAGTGAAAAGGCGGAATCTCCGCAAACCGAAGATGAGGT
 TCCTTCTCGTGAACAGGTTACCCCTGCTGCTCCTGCTCCTAGTGAGCCCACTCCAGTTCTTCAGGCTCCTACCA
 ATCTCACTGACTCCGGCCTTGATCAGGAGCCATTCTGTACTTGGTTGGCCGCAAGAAGCTGCTGGATGCTCAGT
 ACAATGCTATGACCGGATTCATCAGTTGCCCTCTTATGAAGGAGAAGGTCTGTACTGCAACCGCACCTGGGATG
 GCTGGATGTGCTGGGACGACACTCCCCTGGAGCCACAGCCTATCAGCACTGCCCTGACTACTTCCCAGACTTTG
 ACACAGCAGAAAAGGTTTCAAATACTGTGATGAAAAGGAGAGTGTTTAGACACCCTGACAGCAACCGAACCT
 GGTCCAACCTATACTCTGTGCAACGCTTTCACCTCTGAGAACTGCAAAATGCGTACGTTCTTTATTACCTGGCTC
 TTGTGGGTCACTCC

All the short overlapping PCR fragments were stitched together and the whole osteoblast CTR variant sequence was predicted *in-silico*. This osteoblast CTR variant cDNA sequences had a 1491bp translating cDNA region, without exon 10 sequence. Start codon and stop codon were identified to determine the reading frame. The cDNA sequence in GenBank format is as follows:

Full length osteoblast CTR cDNA sequence:

	UTR		Start codon			
1	ACAGAGGATT	TGAAAATGAC	TCCAAGGAGG	TCCAGAGTGA	AAAGGCGGAA	TCTCCGCAAA
61	CCGAAGATGA	GGTTCCTTCT	CGTGAACAGG	TTCACCCTGC	TGCTCCTGCT	CCTAGTGAGC
121	CCAACTCCAG	TTCTTCAGGC	TCCTACCAAT	CTCACTGACT	CCGGCCTTGA	TCAGGAGCCA
181	TTCCTGTACT	TGGTTGGCCG	CAAGAAGCTG	CTGGATGCTC	AGTACAAATG	CTATGACCGG
241	ATTCATCAGT	TGCCCTCTTA	TGAAGGAGAA	GGTCTGTACT	GCAACCGCAC	CTGGGATGGC
301	TGGATGTGCT	GGGACGACAC	TCCCCTGGA	GCCACAGCCT	ATCAGCACTG	CCCTGACTAC
361	TTCCCGGACT	TTGACACAGC	AGAAAAGGTT	TCAAAATACT	GTGATGAAAA	TGGAGACTGG
421	TTTAGACACC	CTGACAGCAA	CCGAACCTGG	TCCAACTATA	CTCTGTGCAA	CGCTTTCACT
481	TCTGAGAAAC	TGCAAAATGC	GTACGTTCTT	TATTACCTGG	CTCTTGTGGG	TCACTCCTTG
541	TCGATTGCTG	C TTTGGTTGC	TTCCATGCTG	ATCTTCTGGA	TTTTCAAGAA	CCTTAGCTGC
601	CAGAGGGTGA	CCTTGCACAA	GCACATGTTT	CTTACTTATA	TTCTGAATTC	TATCATTTATC
661	ATCATCCACC	TGGTTGAGGT	TGTGCCCAAT	GGAGATCTGG	TGCGGCGGGA	TCCATAAAGT
721	TGCAAGGTTT	TACACTTTTT	ACATCAGTAC	ATGATGTCTT	GCAACTACTT	CTGGATGCTC
781	TGCGAGGGGA	TCTATCTTCA	TACTCTGATT	GTCATGGCTG	TGTTTACCGA	CGAGCAACGC
841	CTACGCTGGT	ACTATCTTCT	TGGCTGGGGG	TTCCCGATAG	TGCCAACCAT	TATCCACGCC
901	ATCACTCGTG	CCCTCTACTA	CAACGACAAC	TGCTGGCTGA	GTGCAGAAAC	CCACTTGCTT
961	TACATCATCC	ATGGACCCGG	TCATGGTGGC	TCTGGTGGTC	ACTTCTTCTT	TCTTCTCAAC
1021	ATTGTCCGCG	TGCTTGTGAC	CAAGATGAGG	CAAACCCACG	AGGCCGAGTC	CTACATGTAC
1081	CTGAAGGCTG	TGAAGGCCAC	CATGGTCCTT	GTGCCCTGC	TGGGGATCCA	GTTTGTGTG
1141	TTTCCCTGGA	GGCCCTCCAA	CAAGGTGCTT	GGGAAGATCT	ATGATTATCT	CATGCACTCT
1201	CTGATTCAAT	TCCAGGGATT	CTTTGTGGCG	ACTATCTACT	GCTTCTGCAA	CCATGAGGTG
1261	CAAGTCACCC	TGAAGCGCCA	GTGGACGCA	TTCAAGATCC	AGTGGAGCCA	ACGCTGGGGA
1321	AGGCAGCCGC	GCCCCACCA	CCGCGTAGT	AGTCTCTCTC	GGGCTGTAGC	CTTCGCTGAG
1381	CCAGATGGCC	TCCCCATTTA	CATCTGCCAT	CAGGAACCAC	GGAATCCTCC	AATCAGCAAC
1441	AACGAAGGCG	AGGAGAGTAC	TGAAATGATC	CCCATGAACG	TCATCCAGCA	AGACGCATCC
1501	GCTTGAATGT	GAAGCCACCC	CAAGCATTGT	GATCCACTGA	GCCTTCATTT	CCTGGGGAAA
			Stop codon		UTR	

No exon 10

Antibody binding region in the translated protein

This sequence was then aligned on NCBI using Basic logic alignment tool – BLAST and BLAST2n. First the osteoblast CTR cDNA sequence was aligned against the full length CTR variant, Calcr 001 sequence using BLAST2n (Zhang et al 2000). The alignment results showed a break in the alignment of the two sequences at the exon 10 sequence region. This was represented in the dot matrix plot. The graphical summary and the dot matrix plot for the alignment of the two sequences is presented in Figure 7.4. Apart from exon 10 region the two sequences showed 99% identities in their alignment (Table 7.2). For the detailed BLAST sequence alignment please ref appendix page 9.1.4.ii.

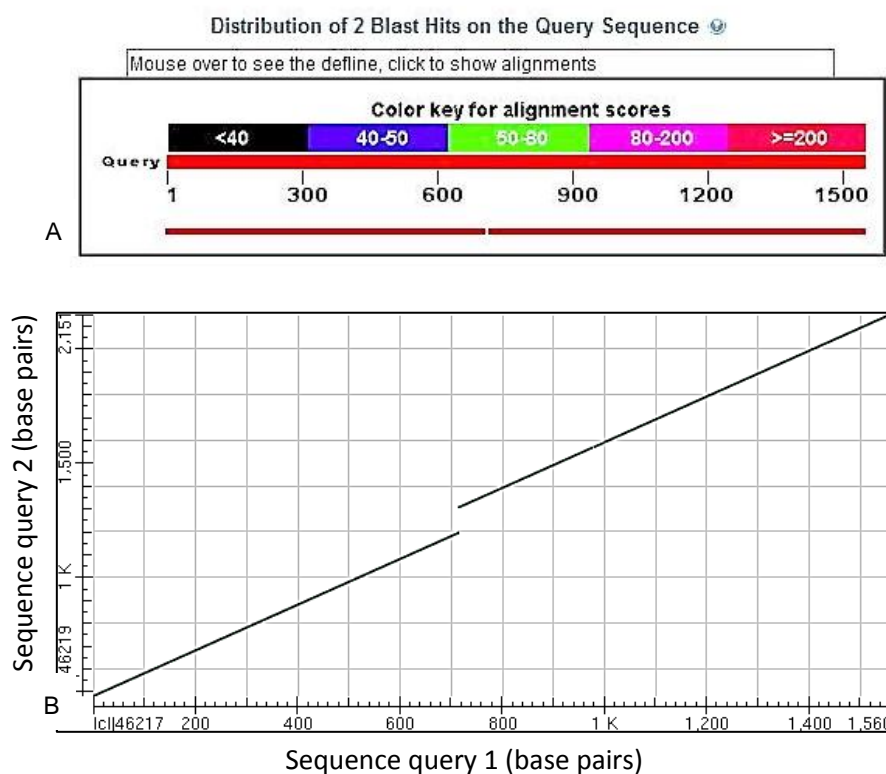


Fig 7.4: NCBI BLAST2n result. The predicted osteoblast CTR cDNA sequence is aligned against Calcr001 – full length CTR sequence. Image A, is screen shot of the graphical summary of the BLAST2n hits. Image B, is a screen shot of the dot matrix plot for the alignment between the two sequences.

Table 7.2: BLAST2n alignment result for osteoblast CTR and full length CTR variant Calcr001

BLAST2n of osteoblast CTR against :	Sequence ID	Length	Match	Score	Expect	Identities	Gaps
Full length Calcr 001 mouse variant.	lcl 46219 Range 1: 1306 to 2151	2460	2	1552 bits(840)	0.0	845/847(99%)	2/847(0%)
	Range 2: 481 to 1196			1323 bits(716)		0.0	716/716(100%)

The osteoblast CTR sequence was further aligned against the whole mouse genomic and transcript database. Four BLAST hits were obtained (Fig. 7.5). Two of which were against mouse transcript database; Mus musculus CTR variant 1a and 1b. The alignment results are briefly represented summarised in table 7.3. The detailed BLAST results are attached in the appendix section 9.1.6.ii (Morgulis et al 2008, Zhang et al 2000).

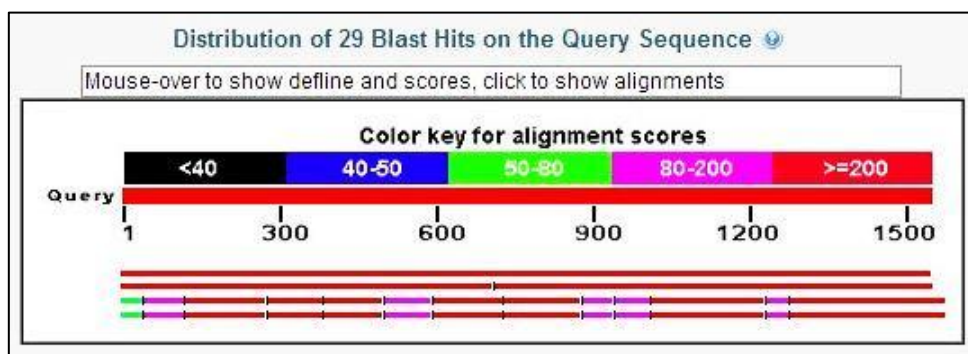


Fig 7.5: Screen shot of the graphical summary of NCBI BLAST alignment of osteoblast CTR cDNA sequence against mouse genomic and transcript database

Table 7.3 Osteoblast CTR cDNA sequence query, BLAST hits for mouse transcript database

BLAST hit Mouse transcripts	Sequence ID	Length	Match	Score	Expect	Identities	Gaps
Mus musculus calcitonin receptor (Calcr), transcript variant 1a, mRNA	ref NM_001042725.1 Range 1: 291 to 1850	3471	1	2870 bits(1554)	0.0	1559/1561 (99%)	2/1561 (0%)
Mus musculus calcitonin receptor (Calcr), transcript variant 1b, mRNA	ref NM_007588.2 Range 1: 1365 to 2210 Range 2: 540 to 1255	3831	2	1552 bits(840)	0.0	845/847 (99%)	2/847 (0%)
				1323 bits(716)	0.0	716/716 (100%)	0/716 (0%)

7.3.4 PCR for full length CTR:

Full length CTR expression was confirmed by a PCR with forward Primer 4 and reverse primer 7. Three independent WT osteoblast cDNA preparations, RAW 264 cell (generously provided by Dr. Grabowski, University of Sheffield) cDNA preparation and mouse brain cDNA preparation were tested for full length cDNA expression. It was observed that all the three WT osteoblast cDNA preparations expressed a product ~ 1700 bps. Raw 264 cell and mouse brain cDNA preparations both amplified 2 products, one ~ 1700 bps and other ~ 2200 bps (Fig. 7.6).

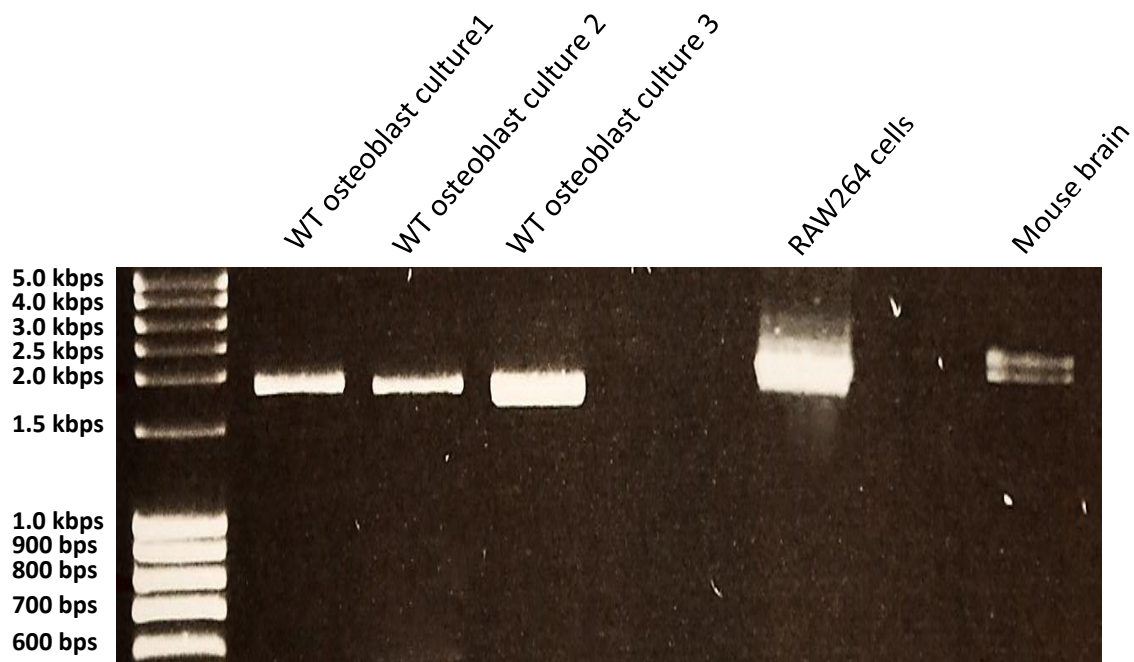


Fig 7.6: PCR amplicons for full length CTR amplicon amplified by forward primer 4 and reverse primer 17. Lane 1 was loaded with 1kbp DNA ladder Lanes 2, 3 and 4 are three independent WT osteoblast culture cDNA preps. Lane 6 is RAW264 cDNA and lane 8 is mouse brain cDNA. All the WT osteoblast expressed a ~ 1.7 kbp amplicon and both the RAW264 and mouse brain cDNA expressed two amplicons ~ 1.7 kbp and ~ 2.2 bps. In RAW264, the higher 2.2kbp band intensity is noticeably higher compared to the lower amplicon.

7.3.5 Predicting osteoblast CTR variant protein sequence:

The protein coding sequence determined using of the reading frame was used to predict the protein sequence of CTR expressed in osteoblast (see section 7.3.3). This osteoblast CTR variant was 496 amino acids long and 37 amino acids shorter than the full length CTR protein. The molecular weight was predicted to be 57.95 kDa using : The Sequence Manipulation Suite: Protein Molecular Weight (Stothard 2000).The osteoblast protein sequence in FASTA format is :

>MouseCTRosteoblast

```
MTPRRSRVKRRNLRKPKMRFLLVNRFTLLLLLLVSPTPVLQAPTNLTDSGLDQEPFLYL  
GRKKLLDAQYKCYDRIHQLPSEYEGGLYCNRTWDGWMCWDDTPAGATAYQHCPDYFPDFD  
TAEKVSKEYCDENGEWFRHPDSNRTWSNYTLCNAFTSEKLNAYVLYLALVGHSLSLIAAL  
VASMLIFWIFKNLSCQRVTLHKHMFLTYILNSIIIIHLVEVVPNGDLVRRDPI SCKVLH  
FLHQYMMSCNYFWMLCEGIYLHTLIVMAVFTDEQRLRWYLLGWGFPIVPTIIHAITRAL  
YYNDNCWLSAETHLLYIIHGPMVALVVNFFLLNIVRVLVTKMRQTHEAESYMYLKAVK  
ATMVLVPLLGIQFVVPWRPSNKVLGKIYDYLMSLIHFQGFVATIYCFNHEVQVTLK  
RQWTQFKIQWSQRWRRRRPTNRVVSAPRAVAFAEPDGLPIYICHQEPRNPPISNNEGEE  
STEMIPMNVIQQDASA
```

The osteoblast CTR protein sequence was aligned against the whole mouse CTR protein sequence, mouse CTR 1b protein sequence and mouse CTR1a protein sequence to determine the differences and similarities between all the registered CTR sequences on the mouse protein database. Multiple sequence alignment tool CLUSTALW 2.1 was used to perform stack alignment for all the 4 sequences (Higgins & Sharp 1988, Thompson et al 1994).

CLUSTALW output showed that the osteoblast CTR protein is identical to the traditional calcitonin receptor CTR1a, which is also 496 amino acids long and does not have exon 10 sequence in its cDNA, hence missing 37 amino acids. This missing 37 amino acids' region is clearly observed in the CLUSTAW output (Fig. 7.7). On the other hand CTR variant 1b is exactly similar to the full length CTR protein sequence and is 533 amino acids long.

Multiple sequence alignment, CLUSTALW output for mouse CTR protein sequences

```

CTRwholeMouse AAI19273.1      MTPRRSRVKRRNLRKPKMRFLLVNRFTLLLLLLVSPVLPVQAPTNLTDSS 50
CTR1aMouse NP_001036190.1   MTPRRSRVKRRNLRKPKMRFLLVNRFTLLLLLLVSPVLPVQAPTNLTDSS 50
CTRmouseosteoblast          MTPRRSRVKRRNLRKPKMRFLLVNRFTLLLLLLVSPVLPVQAPTNLTDSS 50
CTR1bMouse NP_031614.2      MTPRRSRVKRRNLRKPKMRFLLVNRFTLLLLLLVSPVLPVQAPTNLTDSS 50
*****

CTRwholeMouse AAI19273.1      LDQEPFLYLVGRKKLLDAQYKCYDRIHQLPSYEGEGLYCNRTWDGWMCWD 100
CTR1aMouse NP_001036190.1   LDQEPFLYLVGRKKLLDAQYKCYDRIHQLPSYEGEGLYCNRTWDGWMCWD 100
CTRmouseosteoblast          LDQEPFLYLVGRKKLLDAQYKCYDRIHQLPSYEGEGLYCNRTWDGWMCWD 100
CTR1bMouse NP_031614.2      LDQEPFLYLVGRKKLLDAQYKCYDRIHQLPSYEGEGLYCNRTWDGWMCWD 100
*****

CTRwholeMouse AAI19273.1      DTPAGATAYQHCPDYFPDFTAEKVSKYCDENGEWFRHPDSNRTWSNYTL 150
CTR1aMouse NP_001036190.1   DTPAGATAYQHCPDYFPDFTAEKVSKYCDENGEWFRHPDSNRTWSNYTL 150
CTRmouseosteoblast          DTPAGATAYQHCPDYFPDFTAEKVSKYCDENGEWFRHPDSNRTWSNYTL 150
CTR1bMouse NP_031614.2      DTPAGATAYQHCPDYFPDFTAEKVSKYCDENGEWFRHPDSNRTWSNYTL 150
*****

CTRwholeMouse AAI19273.1      CNAFTSEKLQNAYVLYYLALVGHSLSIAALVASMLIFWIFKNLSQCRVTL 200
CTR1aMouse NP_001036190.1   CNAFTSEKLQNAYVLYYLALVGHSLSIAALVASMLIFWIFKNLSQCRVTL 200
CTRmouseosteoblast          CNAFTSEKLQNAYVLYYLALVGHSLSIAALVASMLIFWIFKNLSQCRVTL 200
CTR1bMouse NP_031614.2      CNAFTSEKLQNAYVLYYLALVGHSLSIAALVASMLIFWIFKNLSQCRVTL 200
*****

CTRwholeMouse AAI19273.1      HKHMFLTYILNSIIIIHLVEVVPNGDLVRRDPMHIFHHNTHMWTMQWEL 250
CTR1aMouse NP_001036190.1   HKHMFLTYILNSIIIIHLVEVVPNGDLVRRDP----- 233
CTRmouseosteoblast          HKHMFLTYILNSIIIIHLVEVVPNGDLVRRDP----- 233
CTR1bMouse NP_031614.2      HKHMFLTYILNSIIIIHLVEVVPNGDLVRRDPMHIFHHNTHMWTMQWEL 250
*****

CTRwholeMouse AAI19273.1      SPPLPLSAHEGKMDPHASEVISCKVLHFLHQYMMSCNYFWMLCEGIYLHT 300
CTR1aMouse NP_001036190.1   -----ISCKVLHFLHQYMMSCNYFWMLCEGIYLHT 263
CTRmouseosteoblast          -----ISCKVLHFLHQYMMSCNYFWMLCEGIYLHT 263
CTR1bMouse NP_031614.2      SPPLPLSAHEGKMDPHASEVISCKVLHFLHQYMMSCNYFWMLCEGIYLHT 300
*****

CTRwholeMouse AAI19273.1      LIVMAVFTDEQRLRWYLLGWGFPIVPTIIHAITRALYNDNCWLSAETH 350
CTR1aMouse NP_001036190.1   LIVMAVFTDEQRLRWYLLGWGFPIVPTIIHAITRALYNDNCWLSAETH 313
CTRmouseosteoblast          LIVMAVFTDEQRLRWYLLGWGFPIVPTIIHAITRALYNDNCWLSAETH 313
CTR1bMouse NP_031614.2      LIVMAVFTDEQRLRWYLLGWGFPIVPTIIHAITRALYNDNCWLSAETH 350
*****

CTRwholeMouse AAI19273.1      LLYIIHGPMVALVNVNFFFLNIVRVLVTKMRQTHEAESYMLKAVKATM 400
CTR1aMouse NP_001036190.1   LLYIIHGPMVALVNVNFFFLNIVRVLVTKMRQTHEAESYMLKAVKATM 363
CTRmouseosteoblast          LLYIIHGPMVALVNVNFFFLNIVRVLVTKMRQTHEAESYMLKAVKATM 363
CTR1bMouse NP_031614.2      LLYIIHGPMVALVNVNFFFLNIVRVLVTKMRQTHEAESYMLKAVKATM 400
*****

CTRwholeMouse AAI19273.1      VLVPLLGIQFVVFPWRPSNKVLGKIYDYLMSLIHFQGFVATIYCFCNH 450
CTR1aMouse NP_001036190.1   VLVPLLGIQFVVFPWRPSNKVLGKIYDYLMSLIHFQGFVATIYCFCNH 413
CTRmouseosteoblast          VLVPLLGIQFVVFPWRPSNKVLGKIYDYLMSLIHFQGFVATIYCFCNH 413
CTR1bMouse NP_031614.2      VLVPLLGIQFVVFPWRPSNKVLGKIYDYLMSLIHFQGFVATIYCFCNH 450
*****

CTRwholeMouse AAI19273.1      EVQVTLKRQWTQFKIQWSQRWGRRRRPTNRVVSAPRAVAFAEPDGLPIYI 500
CTR1aMouse NP_001036190.1   EVQVTLKRQWTQFKIQWSQRWGRRRRPTNRVVSAPRAVAFAEPDGLPIYI 463
CTRmouseosteoblast          EVQVTLKRQWTQFKIQWSQRWGRRRRPTNRVVSAPRAVAFAEPDGLPIYI 463
CTR1bMouse NP_031614.2      EVQVTLKRQWTQFKIQWSQRWGRRRRPTNRVVSAPRAVAFAEPDGLPIYI 500
*****

CTRwholeMouse AAI19273.1      CHQEPRNPPISNNEGEESTEMIPMNVIQQDASA 533
CTR1aMouse NP_001036190.1   CHQEPRNPPISNNEGEESTEMIPMNVIQQDASA 496
CTRmouseosteoblast          CHQEPRNPPISNNEGEESTEMIPMNVIQQDASA 496
CTR1bMouse NP_031614.2      CHQEPRNPPISNNEGEESTEMIPMNVIQQDASA 533
*****

```

Fig 7.7: Multiple sequence alignment tool - CLUSTALW output. Colourful alphabets represent amino acids. "*" represents highly conserved sequences. The black box highlights the region that determines the differences in the sequences.

7.3.6 CTR protein expression in differentiating primary osteoblast lysates:

CTR protein expression was determined in both WT (129/SvEv) and RAMP3 KO differentiating primary osteoblast cell lysates. Total cell lysate of primary osteoblasts containing 50µg of protein was loaded in each well. Mouse brain lysate was used as a positive control. Beta-actin was used as loading control and brain tissue lysate was used as a positive control for CTR expression. In both the WT and RAMP3 KO osteoblast culture lysates, ~58kDa band was observed. In the positive control there were two bands a higher band ~62kD and a lower band ~58kDa.

In WT cultures, it was observed that CTR expression increases with osteoblast differentiation. Significantly highest expression of CTR was at day 20 of differentiation. With similar amounts of total protein lysates, RAMP3 KO osteoblasts exhibited a different pattern of CTR expression. CTR expression was observed to be minimal at day 5 and 15, moderate at day 10 and maximum and equivalent to WT expression at day 20 of differentiation. The difference between the CTR expression on day 20 compared to all the other time points was significant in RAMP3 KOs. The expression of CTR was quantified by densitometry and normalised to β-Actin expression. Figure 7.8 overleaf shows a representative blot and the graphical representation of densitometry quantification.

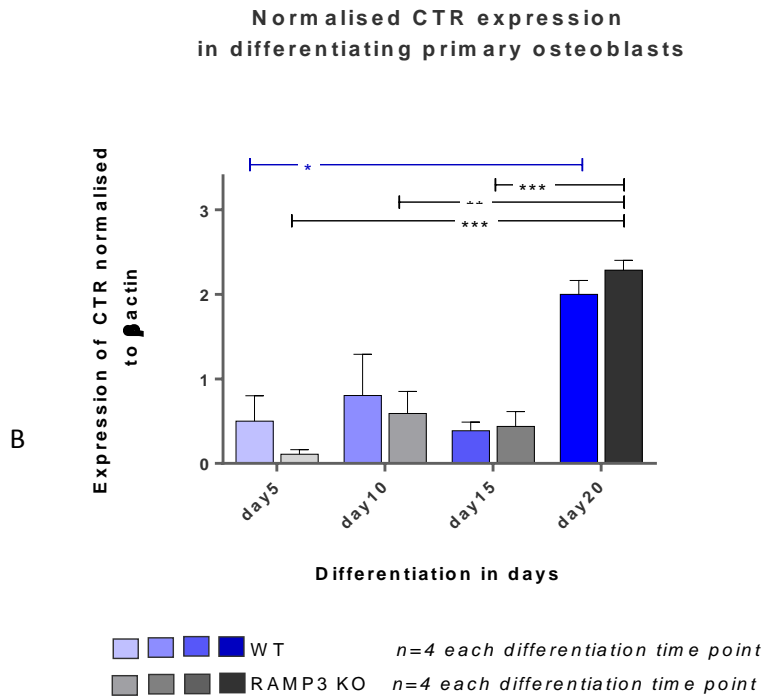
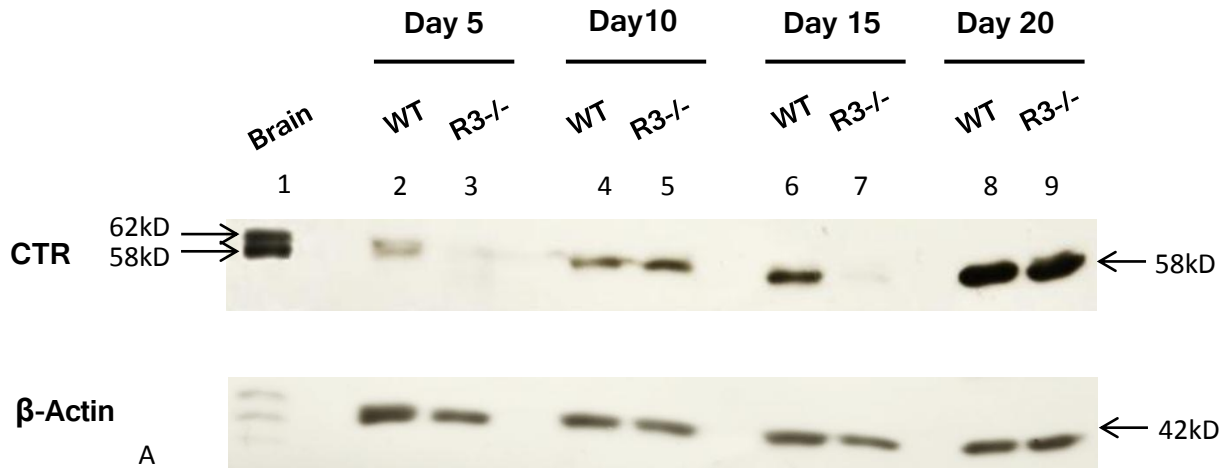


Fig 7.8: Representative Western blot from four independent cultures, immuno-blotted in duplicate, to determine CTR expression in WT and RAMP3 KO (R3 -/-) osteoblast cultures (A) and densitometry quantification of CTR expression normalised to β -Actin (B). The top panel in a Western blot is for CTR (2 min exposure) and bottom panel is for loading control - β -Actin (2 min exposure) of the same. 50 μ g of each protein lysate sample was loaded. Lanes 2, 4, 6 and 8 are WT cell lysates whereas, lanes 3, 5, 7 and 9 are RAMP3 KO lysates. Brain tissue lysate (lane 1) was used as a positive control for CTR expression which showed 2 bands corresponding to approximately 62kD and 58kD size. Differentiation time points day 5, 10, 15 and 20 for each WT and RAMP3 KO preparations are indicated on top. ~58kD CTR protein was observed in both WT and RAMP3 KO cultures however, the expression pattern was different to each genotype. β -Actin was expressed at 42kD. Fig B is a bar graph showing the quantification (mean \pm SEM) of CTR expression normalised to β -Actin in four independent experiments. The increase in CTR expression at day 20 of differentiation was significant in both WT and RAMP3 KO primary cultures, in comparison to other time point in the respective cultures.

Significance of p value: **** ≤ 0.0001 , *** ≤ 0.001 , ** ≤ 0.01 , * ≤ 0.05

7.3.7: Expression of CTR in WT and RAMP3 KO primary osteoblasts in response to PTH, AM and AMY stimulation:

We further intended to verify if the CTR variant expressed in the WT and RAMP3 KO primary osteoblasts is functional. To test this we investigated the change in CTR expression in both WT and RAMP3 KO primary osteoblasts upon Amylin stimulation. Differentiated (20 day) WT and RAMP3 KO primary osteoblasts were stimulated with 10nM working concentration of full length Amylin (AMY). Protocol is detailed earlier section 6.2.1 and 6.2.2. Since Western blotting was performed on two AMY stimulated and non-stimulated WT and RAMP3 KO primary osteoblast cultures, statistical analysis was not performed.

The immune-blot for CTR showed increased expression of CTR of ~58kDa in the AMY stimulated WT and RAMP3 KOs compared to respective non-stimulated preparations. Whole brain lysate was used as a positive control showed only a higher molecular weight CTR ~65kDa. Figure 7.9 below is a representative blot showing CTR expression in AMY stimulated WT and RAMP3 KO primary cultures.

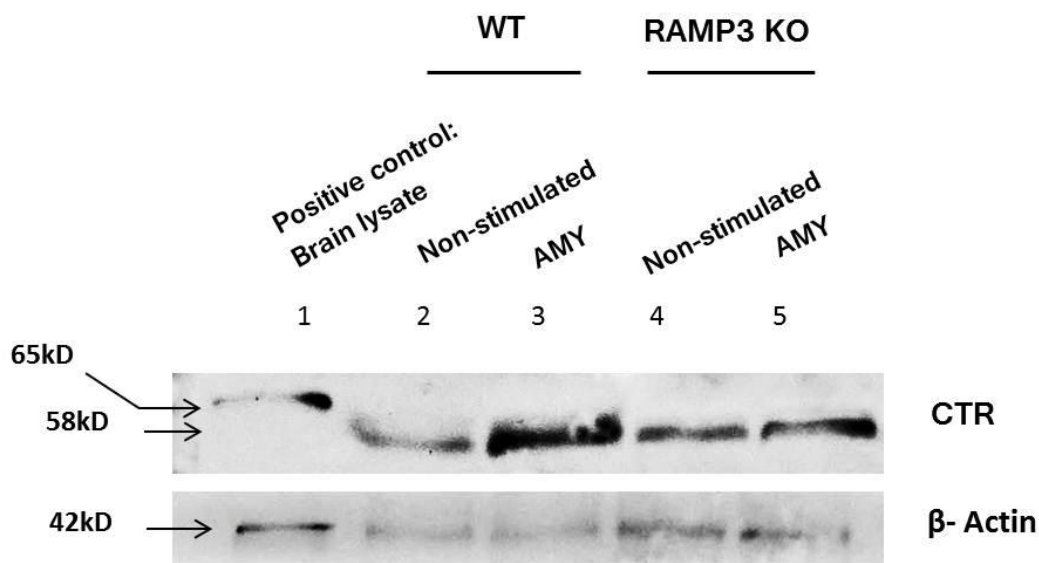


Fig 7.9: Representative Western Blot showing expression of CTR in 20 days differentiated WT and RAMP 3 KO primary calvarial osteoblasts cultures stimulated with 10nM full length AMY. Stimulation with the CT family of peptides resulted in increased expression of CTR ~58kDa in comparison to non-stimulated control cells. The CTR protein in whole brain lysate had a higher molecular weight ~65kDa. β-actin was used as the loading control. Exposures were between 2-3 mins.

7.4 Discussion

The mechanisms by which AMY induces osteoblast proliferation are not yet clearly understood, we therefore aimed to determine the expression of AMY receptor in differentiating WT primary calvarial osteoblast cultures derived from 129/SvEv mice. We hypothesised that osteoblasts either express a novel AMY receptor that does not comprise CTR, or that the CTR in an osteoblast AMY receptor is a transcript variant of the known full length CTR. The chief objective was to determine whether both CTR mRNA and protein were expressed in primary differentiating osteoblasts and if so to determine the complete sequence of this CTR variant.

Using overlapping primers and Western blotting, we successfully demonstrated that 129/SvEv mouse derived primary calvarial osteoblasts express a CTR transcriptional variant throughout differentiation. Overlapping primer sequences proved to be an efficient technique to determine and map a complete cDNA sequence of a formerly unknown CTR variant. Not only did we determine the complete sequence of the CTR transcript, but also determined the exact difference in transcript compared to the full length CTR. *In-silico* analysis then confirmed that the CTR transcript we determined in the WT 129/SvEv cDNA was similar to the known CTR1a transcript, which is a 37 amino acids shorter variant than the full length CTR1b transcript. As discussed earlier, the additional 37 amino acids in CTR1b variant result in a change in the second extracellular domain of CTR which is expected to affect the ligand-receptor interaction (Sexton et al 1993). Figure 7.10 below highlights this domain.

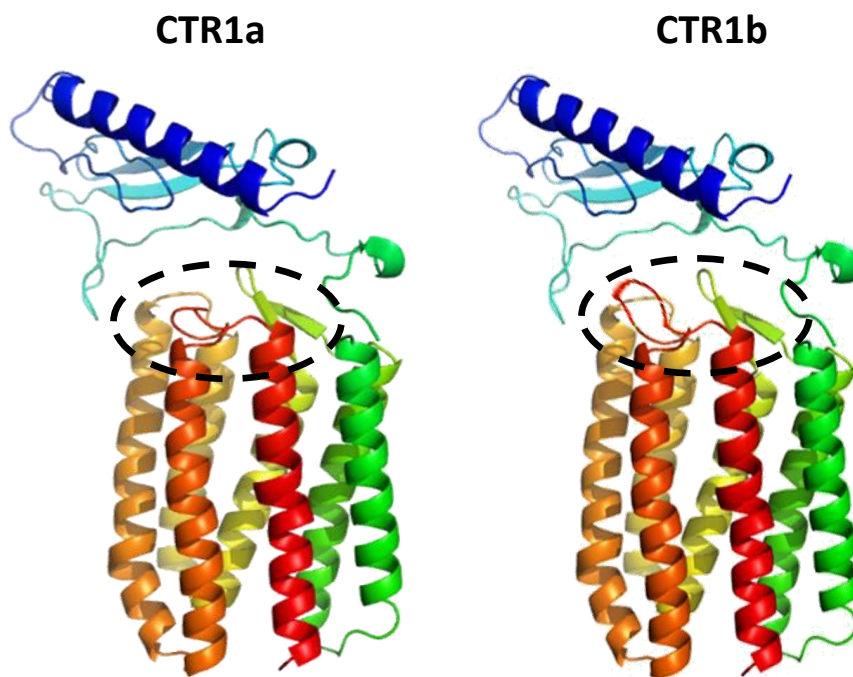


Fig 7.10: Representative 3D ribbon protein models of CTR transcripts 1a (left) and 1b (right). The additional 37 amino acids in CTR1b result in the change in the extracellular domain marked by black dashed-circle. Figure generated from (CLR- GPCR) ribbon model created by Prof. P. Artymiuk, University of Sheffield.

The positive controls used in the study: differentiated RAW264 cDNA (mRNA) and mouse brain cDNA (mRNA and protein) show expression of both the CTR variants at mRNA as seen in figure 7.6 and protein level 7.8 consistent with earlier findings by Sexton *et al* and Ikegame *et al* (Ikegame et al 1995, Sexton et al 1993). In WT primary osteoblasts only CTR1a was expressed at both mRNA and protein level. To date only 'O6' sub clone of the UMR106-cells have shown robust expression of CTR1a, but not CTR1b on prolonged maintenance. This indicates that CTR1a may be the only CTR variant expressed in osteoblasts. Since CTR1a is has a higher affinity toward both CT and AMY compared to CTR1b, it is certain that even with just CTR1a expression, the 129/SvEv osteoblasts could have potent CT and AMY receptors. Although osteoclasts, express both CTR1a and CTR1b, unlike in brain, expression of CTR1a is higher than CTR1b. This indicates that the expression of CTR1a could be a tissue (bone) specific expression. The expression of different CTR variants in brain osteoclasts and osteoblasts is summarised in table 7.4 below.

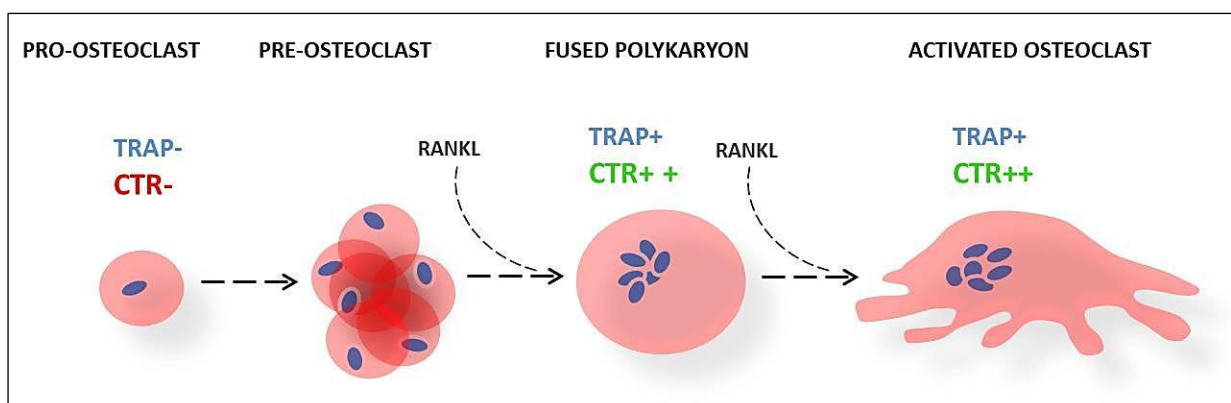
Table 7.4: CTR expression in brain, osteoclasts and osteoblasts

	Brain	Osteoclasts	Osteoblasts
CTR1a	↑↑	↑↑↑↑	↑↑
CTR1b	↑↑↑↑	↑↑	Not expressed

CTR protein expression was observed to be different at each time point during differentiation in the WT primary osteoblasts; it is therefore clear that the expression of CTR in osteoblasts is dependent on osteoblast differentiation and osteogenic environment (Fig 7.8). WT primary osteoblasts have maximum expression of CTR when they are completely differentiated. However, CTR expression in osteoclasts increases during early osteoclast differentiation stage when the hematopoietic stem cells (HSCs) proliferate and start differentiating into early osteoclast precursors. (N. Surangika Soysa et al. 2012). This reflects the cell specific regulatory function of CTR. In RAMP3 KOs, it was observed that RAMP3 KO osteoblast cultures had lower CTR expression compared to WTs until day 20 of differentiation. On the day 20 of differentiation the CTR expression in RAMP3 KOs increases and is similar to that of WTs. Since the cytoplasmic tail of RAMP3 interacts with the N-ethylmaleimide-sensitive factor (NSF) via the PDZ motif that recycles GPCR-RAMP3 complexes (Parameswaran et al., 2006), the reduction in CTR expression in the RAMP3 KO primary osteoblasts in early osteoblast differentiation stages could

due to reduced CTR in the cell cytoplasm which results from the loss of this recycling within the RAMP3 KO primary osteoblasts. Nevertheless the increase in the CTR expression in both WT and RAMP3 KOs at day 20 of differentiation could be due to a dynamic increase in mRNA and protein translation events induced at the late osteoblast differentiation stage in the absence of RAMP3. This up-regulation of CTR could result in an increase in CTR expression (saturated protein levels) at magnitudes that render the difference in circulating CTR levels in WT and RAMP3 KOs insignificant. Figure 7.11 below summarises this hypothesis.

Up-regulation of CTR at early differentiation stage in Osteoclasts



Up-regulation of CTR at late differentiation stage in Osteoblasts

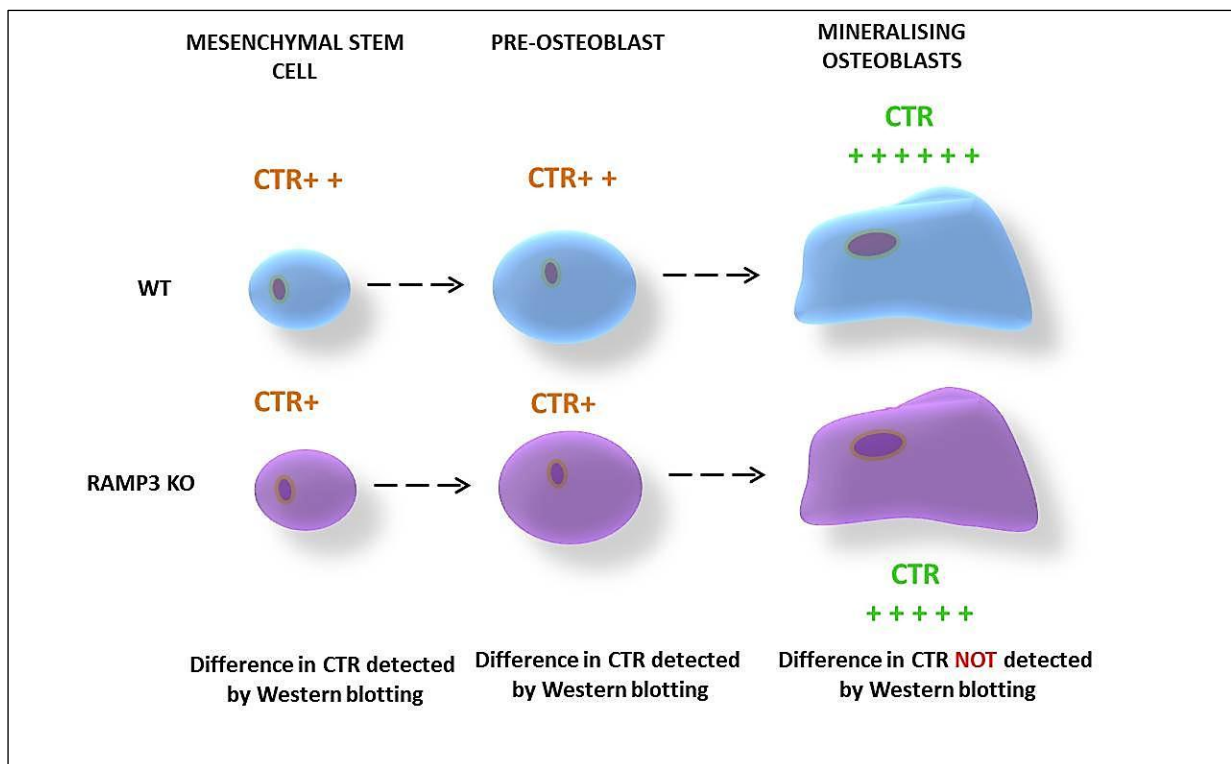


Fig 7.11: Schematic representation of the regulation of osteoclasts and osteoblast differentiation by Calcitonin receptor (CTR).

The current study gives novel evidence of expression of a CTR variant similar to the known CTR1a and all the three RAMPs in WT primary osteoblasts during differentiation (chapter 6). We have successfully shown that the CTR variant responds to Amylin stimulation in both WTs and RAMP3 KO primary osteoblasts (Fig 7.8). Hence it is plausible that these primary osteoblasts have the traditional AMY receptor components that form receptors which can certainly be targeted by tissue specific ligand isoforms (Sexton et al 1993). Furthermore, since the osteoblast CTR resembles the dominant CT receptor isoform CTR1a in structure, it is expected that on activation, the osteoblast CTR is as potent as the CTR1a.

This work can be taken further by investigating the functional aspects of the receptor in osteoblasts. For example, ligand binding assays can be used to determine if CT peptides compete to bind to the 'CTR1a+RAMP1/2/3' receptor in primary osteoblasts. Downstream signalling can be elucidated by determining the effect of different antagonists on cAMP activation. The receptor-ligand interactions and downstream G-protein activation can be investigated using FRET analysis in differentiating primary osteoblast cell membrane preparations. To visualise the receptor-ligand interaction and to determine whether the 'CTR1a+ RAMP 1/2/3' receptor in osteoblasts is expressed at the osteoblast cell membrane, primary osteoblasts can be stimulated with different tagged ligands (Biotinylated-AMY/CT) and studied using confocal microscopy.

This novel data shall certainly enhance our understanding of skeletal regulation mediated by the CT family of peptides.

Chapter 8: Discussion

8.1 Summary and discussion

The current study provides us novel insights into the role of RAMP3 as a regulator of bone mass. We have successfully filled in few gaps in literature with respect to the current understanding of RAMPs as accessory proteins. In this section we shall focus on the significant findings and the implications of our work.

8.1.1 RAMP3 KO mice have an age dependent anabolic skeletal phenotype:

This work provides novel evidence to RAMP3 mediated skeletal regulation. RAMP3 KO mice have accelerated skeletal development at birth which results in protection against age related bone loss. It was observed that at neonatal age, RAMP3 KO mice have a gross skeletal enhancement however with age; the enhancement is confined to trabecular bone of long bones and the significance of difference is higher in females. It can be debated that the technical limitations of microCT could be responsible for the inefficiency in detecting the gross differences in adult mice.

Histological evidence suggests that the enhanced skeletal development in the adult RAMP3 KO mice is an anabolic effect. It was observed that the number of osteoblasts in the trabecular bone was significantly higher than the number of osteoblasts in WT, and that the RAMP3 KO osteoblasts covered a larger surface of the trabecular bone compared to WT osteoblasts. We determined no differences in osteoclast numbers. Interestingly the adult RAMP3 KO mice also showed a difference in the growth plate in comparison to the WT. The length of the chondrocyte columns in RAMP3 KO mice was significantly more in comparison to the chondrocyte columns in WT and was suggestive of enhanced differentiation of the proliferative cells into hypertrophic cells and that RAMP3 KO had enhanced endochondral ossification. This is a novel evidence of the involvement of RAMP3 in endochondral ossification. The increased osteoblast numbers in the trabecular bone and the enhanced differentiation of the proliferative cells to form hypertrophic cells that get mineralised at the growth plate again supported the hypothesis that the skeletal phenotype of the RAMP3 KO was an anabolic phenomenon.

Further investigation of the differentiation pattern of the primary osteoblasts of both WT and RAMP3 KO mice revealed that RAMP3 KO primary osteoblasts had an altered differentiation pattern. We observed a prolonged ALP activity in the RAMP3 KO osteoblasts that could be responsible for enhanced differentiation of the pre-osteoblasts into mature osteoblasts in the RAMP3 KO mice. RAMP3 KO mice also had fewer but larger colony forming units (CFUs). The

CFUs mineralised equal amount of matrix in both RAMP3 KO and WT cultures despite there being significantly fewer CFUs in RAMP3 KOs. However collagen formation in RAMP3 KOs was significantly reduced. This could suggest that more MSCs differentiated into osteoblasts compared to the number of MSCs that differentiation into chondrocytes. The differences in primary osteoblast differentiation pattern provoked the investigation of Wnt/ β -catenin pathway in RAMP3 KO mice, as the canonical Wnt pathway defines osteoblast differentiation and given the evidence the RAMP3 is an early response gene of the Wnt/ β -catenin pathway and that RAMP3 expression decreases with increased expression of Wnt (Kenny et al 2005, Rohrs et al 2009, Ziegler et al 2005). We successfully demonstrated that the RAMP3 KO primary osteoblasts had significantly more total and phosphorylated β -catenin and that the RAMP3 KOs required more DKK1 to reduce the endogenous phosphorylated- β -catenin levels when compared to the WT primary osteoblast. We also showed that an exogenous Wnt3A stimulation induced significantly more amount of phosphorylated β -catenin in RAMP3 KO osteoblasts compared to the WTs. These findings along with the differences observed in the growth plates of RAMP3 KOs and the difference in the differentiation patterns of primary osteoblasts suggest the RAMP3 KO mice have enhanced differentiation of osteoblasts that result in increased skeletal development.

Additionally Wnt plays an important role in mouse embryogenesis (C. R. Kemp 2007). We can propose that in WTs, the increase in Wnt during embryogenesis results in reduction of RAMP3. This could imply that reduction in RAMP3 but not RAMP2 expression is characteristic during embryogenesis, hence the RAMP3 KO mice are viable as RAMP3 expression is dispensable, but RAMP2 KO mice are embryonically lethal as RAMP2 expression is indispensable during embryogenesis (C. R. Kemp 2007, Dackor et al 2007, Kenny et al 2005, Ziegler et al 2005). We can also propose that the acceleration in the development of the gross skeleton in RAMP3 KOs at early age is regulated by the Wnt signalling that regulates embryogenesis. Whereas in adults, Wnt signalling pathway that regulates the wear and tare of the bone, could be responsible for the enhanced trabecular bone in adult RAMP3 KOs.

8.1.2 RAMP2 protein compensates for RAMP3 protein in an event of stimulation:

Investigating RAMP expressions during primary osteoblast differentiation gave novel insight into the regulation of RAMPs in osteoblast differentiation. We observed that in WTs with the advancement of osteoblast differentiation, there is an increase in RAMP1 and RAMP2 expression and a decrease in RAMP3 expression. The decrease in RAMP3 expression in mature osteoblasts

escalated the notion that RAMP3 KO mice have enhancement in osteoblast differentiation. Interestingly there was no significant difference in the mRNA expression of RAMP1 and RAMP3 in RAMP3 KO and WT at any time-point during osteoblasts differentiation. Therefore, there is no compensation between RAMPs at mRNA level. This is in concordance with the reports by Dackor et al and Kadmiel et al (Dackor et al 2007, Kadmiel et al 2012).

Although there is no compensation between RAMP2 and RAMP3 at mRNA level, it is possible that RAMPs compensate each other at a protein level. We can hypothesize that RAMPs form stable multimers that are maintained in compartments in the cytoplasm and these multimers dissociate to form monomers which can form complexes with GPCRs on appropriate stimulation (Sexton et al 2001). The current study gives novel evidence of up-regulation of RAMP3 monomer in WT and RAMP2 monomers in both WT and RAMP3 KO osteoblasts on PTH, AM and AMY stimulation when compared to their non-stimulated controls. Interestingly we observed that two forms of RAMP2: monomer ~13kDa and a multimer ~55kDa were expressed in the mouse brain lysate that was used as a positive control, WT primary osteoblasts and RAMP3 KO primary osteoblasts. On stimulation with the peptides PTH, AM and AMY, RAMP3 KO primary osteoblasts express significantly more amounts of the higher molecular weight RAMP2 compared to WT primary osteoblasts, suggesting that multimeric form of RAMP2 can compensate for the absence of RAMP3 in the RAMP3 KO osteoblasts. This compensatory mechanism if existent is independent of the mRNA expressions as the compensation would be between circulating levels of RAMP proteins in the cytoplasm. Moreover, we know that dimerization is a prerequisite for CLR (McLatchie et al 1998). If we hypothesize that RAMP2 and RAMP3 compete to form heterodimer with CLR to form a functional receptor for AM, an alteration in the expression of either RAMP2 or RAMP3 may cause a shift in the interaction (Figure 8.1).

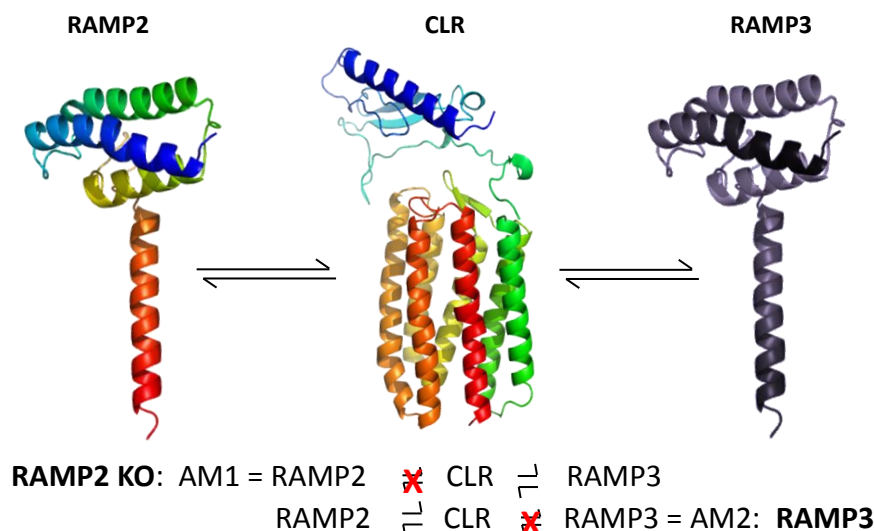


Fig 8.1: Schematic representation of the competitive heterodimerisation between RAMP2 and RAMP3 with CLR.

If there is a compensatory mechanism or competitive heterodimerisation between RAMP2 and RAMP3, we can also postulate that the skeletal phenotype of the RAMP3 KO could be a result of overexpression of RAMP2. Apart from RAMP2/ CLR, this phenomenon could result in enhanced activation of other the receptor complexes like RAMP2/PTHr1 and RAMP2/CTR in the RAMP3 KOs (Hay et al 2003, McLatchie et al 1998, Parameswaran & Spielman 2006). This would in turn result in an increase in bone formation through the activity of the peptides PTH, AM and AMY respectively.

8.1.3 RAMP2 and RAMP3, differences and preferences:

Both RAMP2 and RAMP3 are involved in forming functional receptors for Adrenomedullin and Amylin. However, interestingly knockout animals of RAMP2 and RAMP3 have completely different phenotypes. As mentioned earlier, RAMP2 gene silencing results in embryonic lethality, which is also seen in AM KO mice (Dackor et al 2007). On the other hand RAMP3 KO mice are viable and do not put on weight with age (Dackor et al 2007). This suggests that RAMP2 has a more profound physiological function during the developmental stages and that it brings about the basal effect of GPCR signalling. Whereas, RAMP3 plays a role in maintaining normal physiology during adulthood and that it may be induced only in times of physiological stress (Dackor et al 2007). Another evidence to support this concept is that the cytoplasmic tail of RAMP3 interacts with the N-ethylmaleimide-sensitive factor (NSF) via the PDZ motif, and enhances recycling and rapid re-sensitizing of CLR/RAMP3 complex to plasma membrane (Parameswaran & Spielman 2006) i.e., RAMP3 has the ability to traffic and recycle partner GPCRs, which would be useful in challenged physiological conditions.

However, reasons for such different phenotypes are not yet clearly understood. One of the possible explanations other than the Wnt theory proposed earlier would be a difference in affinity between RAMP2 and RAMP3 towards CLR and CTR, to form heterodimer complexes. i.e., given a choice, RAMP2 could prefer heterodimerisation with CLR (to form AM receptor), over CTR (to form receptor for AMY), whereas RAMP3 could prefer CTR over CLR. RAMP2 and AM association is evident from KO studies. It is known that the N-terminal of AM is involved in vasodilation whereas a short peptide region 27-52 is implicated to induce mitogenic effect in osteoblasts via MAPK activation (Cornish et al 2003). Since embryonically lethal RAMP2 KO mice show pericardial effusion signifying the importance of RAMP2 in vascular development, it can be suggested that RAMP2 interaction with AM is related to the vasodilation activity of AM

(Dackor et al 2007, Dackor et al 2006). On the other hand, the association of RAMP3 and AMY is evident for the fact that RAMP3 KO mice strikingly share the skeletal phenotype with the AMY KO mice. Both RAMP3 KO and AMY KO adult mice have increased growth plate thickness and increase in the trabecular thickness with no change in net trabecular bone volume (Davey et al 2006).

8.1.4 Calcitonin receptor in osteoblasts:

Apart from investigating the role of RAMP3 in regulating skeletal development, this work also investigated the expression of CTR in osteoblasts. Our work provides novel evidence of expression of the traditional CTR receptor by both WT and RAMP3 KO 129/SvEv primary osteoblasts. The CTR expressed by the primary osteoblasts resembles the known CTR1a in sequence and structure. We have successfully shown that this receptor responds to AMY stimulation, hence suggesting the CTR in the osteoblasts resembles CTR1a in function too. Further, we have given evidence that CTR expression increases significantly when the osteoblasts are fully matured and form mineralised matrix suggesting that CTR plays an important role late osteoblast differentiation in contrast to its role in regulating early osteoclast differentiation (Soysa et al 2012). It could be possible that the previous reports of CTR not being expressed in the osteoblasts were not carried out in mature mineralising osteoblasts. However, our findings could be specific to the 129/SvEv background mouse strain.

8.2. Technical limitations

One of the major technical limitations of this study was the resolution available for bone microCT analysis. It was observed that the resolution of 17.5µm was insufficient to detect the differences between the WT and RAMP3 KO whole bones despite there being differences at microscopic levels. Another major difficulty was mimicking the effects of ovariectomy in the 129/SvEv mice. WT 129/SvEv mice did not develop classical ovariectomy induced bone loss phenotype; hence this intervention could not produce reliable comparisons between the two genotypes. As discussed earlier this could be due to the breeding of the WT 129/SvEv animals. Hence pure WT 129/SvEv animals should be used as controls for any future skeletal analysis.

Histological analysis was limited by the quality of the sections. Due to the inconsistency of the sections, analyses of results from experiments from such as dual calcein labels in the trabecular bone were not comparable. The use of slide scanner however helped overcome the inconsistency in H&E and TRAP stained sections as measurements could be confined to a consistent area electronically on the Aperio® software. Nevertheless, since the slide scanner available in the University of Sheffield was not equipped for fluorescent microscopy, calcein labelled sections could not be analysed electronically.

It was difficult to yield satisfactory amounts of protein from differentiated primary osteoblast cultures. It was evident that RAMPs were expressed in very low concentrations, and hence analyses of comparable RAMP protein levels could not be performed on basal (non - stimulated) primary osteoblasts. Detectable RAMP protein bands were observed only after loading upto ~100µg of protein in our stimulation experiments. Given that the expression of RAMPs were very low, a considerable time was used for optimizing the Western Blotting protocols. Furthermore, we had to test several commercial RAMP 1/2 and 3 antibodies before selecting the RAMP2 and RAMP3 antibody for this study as commercially available antibodies are not efficient. It was disappointing that the production of the mouse anti-RAMP1 antibody that was very efficient was discontinued by Abcam®. RAMP1 Western blotting protocol was previously optimised on osteoblast like cell lines. However due to the unavailability of the antibody at a later stage, the expression of RAMP1 protein was not determined.

8.3 Future work

In the time available for this project it was not possible to investigate all the skeletal aspects of the RAMP3 KO 129/SvEv mice. Future investigations would aim to first address the limitations that were incurred during this project. WT 129/SvEv pure breeding line should be established and protocols for ovariectomy should be optimised in the WTs before comparing the skeletal phenotypes of RAMP3 KO and the WTs in the event of this intervention. Given the evidence that RAMP2 plays an important role in embryogenesis, it would be worth monitoring the gestation period of the RAMP3 KO mice to determine if the skeletal development in the RAMP3 KO mice is due to increased gestation. Furthermore, samples sections for histology should be consistent and comparable if similar investigations are conducted again in future.

This work can be taken ahead by investigating the skeletal phenotype of double tissue specific KOs of RAMPs and the partner GPCRs. Since both RAMP3 KOs and AMY KO have similar skeletal phenotypes, it will certainly be useful to study the skeletal phenotype of a tissue specific RAMP3/CTR KOs. Additionally the effect of RAMP3 antibody on skeleton of WT, fracture models and osteoporotic models could be elucidated. The effect of RAMP3 antibody can further be investigated with other therapies like PTH (1-34) treatment or anti-DKK1 therapy to determine if blocking RAMP3 enhances effect of these treatments.

To investigate the compensatory mechanisms between RAMP2 and RAMP3, the protein concentrations of individual RAMPs could be determined in the cytoplasm and the cell membranes of WT and RAMP3 KO primary osteoblasts under basal and stimulated conditions. Compensation of RAMPs on the cell membrane could also be studied by immunocytochemistry with different probes for different RAMPs.

With the limited time of this project we could only identify the CTR variant in the primary osteoblasts of the 129/SvEv mice, future investigations would aim in determining the functional aspects of the CTR in the primary osteoblasts in a differentiation dependent experimental set-up. The functional aspects of the osteoblast CTR variant in native WT and RAMP3 KO cell membrane preparations can be studied using Fluorescence Resonance Energy Transfer (FRET) technique. This technique would help us determine the pattern of G-protein activation for the osteoblast CTR variant.

8.4 Conclusion

In conclusion we have successfully demonstrated that RAMP3 is a potential anabolic therapeutic target for age dependent skeletal disorders.

The association of Wnt/ β -catenin pathway and RAMP3 signalling could make this target even more promising. Ideally, the proposed therapy would involve RAMP3 antibody treatment coupled with other anabolic therapies like anti-DKK1 treatment or PTH (1-34). Moreover, we have successfully provided novel evidence to the expression of Calcitonin receptor (CTR) identical to CTR1a variant in primary osteoblasts.

The outcomes of this study shall help us further understand the subtle modulations of GPCR activations through RAMPs in both healthy and disease state physiology.

Chapter 9: Appendix

9.1 Appendix

9.1.1 Chapter 2: Advanced skeletal phenotype of RAMP3 KO mice

Skeletal Stains

Alcian Blue solution (always freshly prepared):

20 mg Alcian Blue (8GX grade)

22ml D/W

160 ml 100% Ethanol

40 ml Glacial Acetic Acid (increase or reduce proportionately as required)

Alizarin Red S Solution (always freshly prepared):

100 ml 1% KOH solution (freshly prepared - 1% (w/v) KOH in water).

1 mg Alizarin Red

9.1.2 Chapter 3: Skeletal response of RAMP3KO mice to ovariectomy:

9.1.2.i Statistical analysis of microCT analysis of baseline, sham and OVX WT and RAMP3 KO

mice

Table 9.1: Statistical analysis microCT analysis to study response to OVX

Bonferroni's Multiple Comparisons Test	Mean Diff.	95% CI Of Diff.	Significant?	Summary	P Value
Whole Femur BV					
WT					
Baseline Vs. Sham	0.5107	-1.814 to 2.835	No	NS	> 0.9999
Baseline Vs. OVX	0.03765	-2.287 to 2.362	No	NS	> 0.9999
Sham Vs OVX	-0.4730	-2.797 to 1.851	No	NS	> 0.9999
RAMP3 KO					
Baseline Vs. Sham	-0.0425	-2.367 to 2.282	No	NS	> 0.9999
Baseline Vs. OVX	0.02402	-2.300 to 2.348	No	NS	> 0.9999
Sham Vs OVX	0.06651	-2.258 to 2.391	No	NS	> 0.9999
WT Vs. RAMP3KO					
Baseline Vs Baseline	-0.0001	-2.324 to 2.324	No	NS	> 0.9999
Sham Vs Sham	-0.5533	-2.878 to 1.771	No	NS	> 0.9999
OVX Vs OVX	-0.0137	-2.338 to 2.311	No	NS	> 0.9999
WHOLE TIBIA BV					
WT					
Baseline Vs. Sham	0.3697	-1.639 to 2.378	No	NS	> 0.9999
Baseline Vs. OVX	-0.6057	-2.614 to 1.403	No	NS	> 0.9999
Sham Vs OVX	-0.9754	-2.984 to 1.033	No	NS	> 0.9999
RAMP3 KO					
Baseline Vs. Sham	-0.5564	-2.565 to 1.452	No	NS	> 0.9999
Baseline Vs. OVX	-0.3499	-2.358 to 1.658	No	NS	> 0.9999
Sham Vs OVX	0.2065	-1.802 to 2.215	No	NS	> 0.9999
WT Vs. RAMP3KO					
Baseline Vs Baseline	0.2705	-1.738 to 2.279	No	NS	> 0.9999
Sham Vs Sham	-0.6556	-2.664 to 1.353	No	NS	> 0.9999
OVX Vs OVX	0.5262	-1.482 to 2.535	No	NS	> 0.9999
FEMUR CORTICAL BV					
WT					
Baseline Vs. Sham	0.07057	-0.1082 to 0.2493	No	NS	> 0.9999
Baseline Vs. OVX	-0.0981	-0.2878 to 0.09149	No	NS	> 0.9999
Sham Vs OVX	-0.1687	-0.3583 to 0.02092	No	NS	0.1176
RAMP3 KO					
Baseline Vs. Sham	0.001026	-0.1778 to 0.1798	No	NS	> 0.9999
Baseline Vs. OVX	0.1203	-0.05847 to 0.2991	No	NS	0.5681
Sham Vs OVX	0.1193	-0.05950 to 0.2981	No	NS	0.5908
WT Vs. RAMP3KO					
Baseline Vs Baseline	-0.04631	-0.2251 to 0.1325	No	NS	> 0.9999
Sham Vs Sham	-0.1158	-0.2946 to 0.06293	No	NS	0.6732
OVX Vs OVX	0.1721	-0.01748 to 0.3618	No	NS	0.1024

Bonferroni's Multiple Comparisons Test	Mean Diff.	95% CI Of Diff.	Significant?	Summary	P Value
FEMUR CORTICAL THICKNESS					
WT					
Baseline Vs. Sham	-0.00806	-0.03343 to 0.01731	No	NS	> 0.9999
Baseline Vs. OVX	-0.00896	-0.03587 to 0.01795	No	NS	> 0.9999
Sham Vs OVX	-0.00090	-0.02781 to 0.02601	No	NS	> 0.9999
RAMP3 KO					
Baseline Vs. Sham	0.00100	-0.02437 to 0.02637	No	NS	> 0.9999
Baseline Vs. OVX	0.01176	-0.01361 to 0.03713	No	NS	> 0.9999
Sham Vs OVX	0.01076	-0.01461 to 0.03613	No	NS	> 0.9999
WT Vs. RAMP3KO					
Baseline Vs Baseline	-0.01073	-0.03610 to 0.01464	No	NS	> 0.9999
Sham Vs Sham	-0.00167	-0.02704 to 0.02370	No	NS	> 0.9999
OVX Vs OVX	0.00999	-0.01693 to 0.03690	No	NS	> 0.9999
FEMUR TRABECULAR BONE VOLUME					
WT					
Baseline Vs. Sham	0.01131	-0.08108 to 0.1037	No	NS	> 0.9999
Baseline Vs. OVX	0.03514	-0.06285 to 0.1331	No	NS	> 0.9999
Sham Vs OVX	0.02383	-0.07416 to 0.1218	No	NS	> 0.9999
RAMP3 KO					
Baseline Vs. Sham	-0.02136	-0.1137 to 0.07103	No	NS	> 0.9999
Baseline Vs. OVX	0.04185	-0.05614 to 0.1398	No	NS	> 0.9999
Sham Vs OVX	0.06321	-0.03478 to 0.1612	No	NS	0.6790
WT Vs. RAMP3KO					
Baseline Vs Baseline	0.02588	-0.06651 to 0.1183	No	NS	> 0.9999
Sham Vs Sham	-0.00679	-0.09917 to 0.08560	No	NS	> 0.9999
OVX Vs OVX	0.03259	-0.07070 to 0.1359	No	NS	> 0.9999
FEMUR TRABECULAR BONE VOLUME/ TISSUE VOLUME BV/TV					
WT					
Baseline Vs. Sham	0.3381	-1.897 to 2.573	No	NS	> 0.9999
Baseline Vs. OVX	1.534	-0.8364 to 3.905	No	NS	0.6611
Sham Vs OVX	1.196	-1.175 to 3.567	No	NS	> 0.9999
RAMP3 KO					
Baseline Vs. Sham	-0.1111	-2.482 to 2.260	No	NS	> 0.9999
Baseline Vs. OVX	1.366	-1.004 to 3.737	No	NS	> 0.9999
Sham Vs OVX	1.478	-1.021 to 3.976	No	NS	0.9567
WT Vs. RAMP3KO					
Baseline Vs Baseline	0.4712	-1.764 to 2.706	No	NS	> 0.9999
Sham Vs Sham	0.02200	-2.349 to 2.393	No	NS	> 0.9999
OVX Vs OVX	0.3034	-2.196 to 2.802	No	NS	> 0.9999
FEMUR TRABECULAR THICKNESS					
WT					
Baseline Vs. Sham	0.001238	-0.00426 to 0.0067	No	NS	> 0.9999
Baseline Vs. OVX	0.002925	-0.00290 to 0.0088	No	NS	> 0.9999
Sham Vs OVX	0.001687	-0.0041 to 0.0075	No	NS	> 0.9999
RAMP3 KO					
Baseline Vs. Sham	-0.00123	-0.0067 to 0.00426	No	NS	> 0.9999
Baseline Vs. OVX	0.00180	-0.0040 to 0.00763	No	NS	> 0.9999
Sham Vs OVX	0.00303	-0.0028 to 0.00886	No	NS	> 0.9999
WT Vs. RAMP3KO					
Baseline Vs Baseline	-0.00070	-0.0062 to 0.0048	No	NS	> 0.9999
Sham Vs Sham	-0.00317	-0.0087 to 0.0023	No	NS	> 0.9999
OVX Vs OVX	-0.00182	-0.0079 to 0.0043	No	NS	> 0.9999

Bonferroni's Multiple Comparisons Test	Mean Diff.	95% CI Of Diff.	Significant?	Summary	P Value
FEMUR TRABECULAR SEPARATION					
WT					
Baseline Vs. Sham	-0.00234	-0.03985 to 0.03514	No	NS	> 0.9999
Baseline Vs. OVX	-0.01241	-0.05218 to 0.02736	No	NS	> 0.9999
Sham Vs OVX	-0.01006	-0.04983 to 0.02971	No	NS	> 0.9999
RAMP3 KO					
Baseline Vs. Sham	-0.00075	-0.03825 to 0.03675	No	NS	> 0.9999
Baseline Vs. OVX	-0.02431	-0.06408 to 0.01546	No	NS	0.8494
Sham Vs OVX	-0.02356	-0.06333 to 0.01621	No	NS	0.9607
WT Vs. RAMP3KO					
Baseline Vs Baseline	-0.00201	-0.03951 to 0.03548	No	NS	> 0.9999
Sham Vs Sham	-0.00040	-0.03790 to 0.03709	No	NS	> 0.9999
OVX Vs OVX	-0.01391	-0.05583 to 0.02801	No	NS	> 0.9999
FEMUR TRABECULAR NUMBER					
WT					
Baseline Vs. Sham	0.03158	-0.3657 to 0.4288	No	NS	> 0.9999
Baseline Vs. OVX	0.2575	-0.1639 to 0.6788	No	NS	0.8406
Sham Vs OVX	0.2259	-0.1955 to 0.6473	No	NS	> 0.9999
RAMP3 KO					
Baseline Vs. Sham	-0.00918	-0.4305 to 0.4122	No	NS	> 0.9999
Baseline Vs. OVX	0.2522	-0.1691 to 0.6736	No	NS	0.9122
Sham Vs OVX	0.2614	-0.1827 to 0.7055	No	NS	0.9736
WT Vs. RAMP3KO					
Baseline Vs Baseline	0.1294	-0.2678 to 0.5267	No	NS	> 0.9999
Sham Vs Sham	0.08866	-0.3327 to 0.5100	No	NS	> 0.9999
OVX Vs.OVX	0.1242	-0.3200 to 0.5683	No	NS	> 0.9999
FEMUR TRABECULAR PATTERN FACTOR					
WT					
Baseline Vs. Sham	2.794	-5.932 to 11.52	No	NS	> 0.9999
Baseline Vs. OVX	-4.188	-13.44 to 5.068	No	NS	> 0.9999
Sham Vs OVX	-6.983	-16.24 to 2.273	No	NS	0.3173
RAMP3 KO					
Baseline Vs. Sham	-0.5119	-9.238 to 8.214	No	NS	> 0.9999
Baseline Vs. OVX	-1.935	-11.19 to 7.320	No	NS	> 0.9999
Sham Vs OVX	-1.423	-10.68 to 7.832	No	NS	> 0.9999
WT Vs. RAMP3KO					
Baseline Vs Baseline	-0.8172	-9.544 to 7.909	No	NS	> 0.9999
Sham Vs Sham	-4.124	-12.85 to 4.603	No	NS	> 0.9999
OVX Vs.OVX	1.436	-8.321 to 11.19	No	NS	> 0.9999
TIBIA CORTICAL BONE VOLUME					
WT					
Baseline Vs. Sham	-0.04029	-0.1766 to 0.09604	No	NS	> 0.9999
Baseline Vs. OVX	-0.1901	-0.3264 to -0.05374	Yes	**	0.0020
Sham Vs OVX	-0.1498	-0.2861 to -0.01345	Yes	*	0.0227
RAMP3 KO					
Baseline Vs. Sham	-0.08672	-0.2230 to 0.04961	No	NS	0.7367
Baseline Vs. OVX	-0.02630	-0.1626 to 0.1100	No	NS	> 0.9999
Sham Vs OVX	-0.02978	-0.1661 to 0.1066	No	NS	> 0.9999
WT Vs. RAMP3KO					
Baseline Vs Baseline	-0.07358	-0.2099 to 0.06275	No	NS	> 0.9999
Sham Vs Sham	-0.1200	-0.2563 to 0.01633	No	NS	0.1271
OVX Vs.OVX	0.09019	-0.04614 to 0.2265	No	NS	0.6203

Bonferroni's Multiple Comparisons Test	Mean Diff.	95% CI Of Diff.	Significant?	Summary	P Value
TIBIA CORTICAL THICKNESS					
WT					
Baseline Vs. Sham	0.01433	-0.00158 to 0.0302	No	NS	0.1089
Baseline Vs. OVX	0.00913	-0.00678 to 0.0250	No	NS	> 0.9999
Sham Vs OVX	-0.00519	-0.0211 to 0.0107	No	NS	> 0.9999
RAMP3 KO					
Baseline Vs. Sham	0.02734	0.01143 to 0.04326	Yes	***	0.0001
Baseline Vs. OVX	0.00401	-0.01190 to 0.01993	No	NS	> 0.9999
Sham Vs OVX	-0.00961	-0.0255 to 0.00630	No	NS	0.9106
WT Vs. RAMP3KO					
Baseline Vs Baseline	-0.00859	-0.02451 to 0.0073	No	NS	> 0.9999
Sham Vs Sham	0.00442	-0.0115 to 0.02034	No	NS	> 0.9999
OVX Vs.OVX	-0.01372	-0.0296 to 0.00219	No	NS	0.1458
TIBIA TRABECULAR BONE VOLUME					
WT					
Baseline Vs. Sham	0.01446	-0.02864 to 0.05757	No	ns	> 0.9999
Baseline Vs. OVX	0.02640	-0.01424 to 0.06703	No	ns	0.6588
Sham Vs OVX	0.01193	-0.03117 to 0.05504	No	ns	> 0.9999
RAMP3 KO					
Baseline Vs. Sham	-0.02187	-0.06498 to 0.02123	No	ns	> 0.9999
Baseline Vs. OVX	0.03910	-0.00154 to 0.07974	No	ns	0.0671
Sham Vs OVX	0.06098	0.01787 to 0.1041	Yes	**	0.0018
WT Vs. RAMP3KO					
Baseline Vs Baseline	0.009008	-0.03163 to 0.04965	No	ns	> 0.9999
Sham Vs Sham	-0.02733	-0.07277 to 0.01811	No	ns	0.9061
OVX Vs OVX	0.02171	-0.01892 to 0.06235	No	ns	> 0.9999
TIBIA TREABECULAR BV/TV					
WT					
Baseline Vs. Sham	0.6249	-0.7808 to 2.031	No	ns	> 0.9999
Baseline Vs. OVX	1.318	-0.08815 to 2.723	No	ns	0.0816
Sham Vs OVX	0.6927	-0.7131 to 2.098	No	ns	> 0.9999
RAMP3 KO					
Baseline Vs. Sham	-0.1951	-1.686 to 1.296	No	ns	> 0.9999
Baseline Vs. OVX	1.853	0.4473 to 3.259	Yes	**	0.0038
Sham Vs OVX	2.048	0.5571 to 3.539	Yes	**	0.0024
WT Vs. RAMP3KO					
Baseline Vs Baseline	-0.4701	-1.876 to 0.9357	No	ns	> 0.9999
Sham Vs Sham	-1.290	-2.781 to 0.2009	No	ns	0.1415
OVX Vs OVX	0.0653	-1.340 to 1.471	No	ns	> 0.9999
TIBIA TRABECULAR THICKNESS					
WT					
Baseline Vs. Sham	0.00413	-0.00036 to 0.00862	No	ns	0.0933
Baseline Vs. OVX	0.00535	0.00086 to 0.00985	Yes	*	0.0108
Sham Vs OVX	0.00122	-0.00327 to 0.00571	No	ns	> 0.9999
RAMP3 KO					
Baseline Vs. Sham	-0.00122	-0.00598 to 0.00355	No	ns	> 0.9999
Baseline Vs. OVX	0.00292	-0.00157 to 0.00742	No	ns	0.6614
Sham Vs OVX	0.00414	-0.00061 to 0.00891	No	ns	0.1383
WT Vs. RAMP3KO					
Baseline Vs Baseline	-0.00089	-0.00539 to 0.00360	No	ns	> 0.9999
Sham Vs Sham	-0.00624	-0.01101 to -0.0014	Yes	**	0.0041
OVX Vs OVX	-0.00332	-0.0078 to 0.00117	No	ns	0.3575

Bonferroni's Multiple Comparisons Test	Mean Diff.	95% CI Of Diff.	Significant?	Summary	P Value
TIBIA TRABECULAR SEPARATION					
WT					
Baseline Vs. Sham	0.03403	-0.1108 to 0.1788	No	ns	> 0.9999
Baseline Vs. OVX	0.00898	-0.1358 to 0.1538	No	ns	> 0.9999
Sham Vs OVX	-0.02505	-0.1699 to 0.1198	No	ns	> 0.9999
RAMP3 KO					
Baseline Vs. Sham	0.02326	-0.1303 to 0.1769	No	ns	> 0.9999
Baseline Vs. OVX	-0.04003	-0.1848 to 0.1048	No	ns	> 0.9999
Sham Vs OVX	-0.06330	-0.2169 to 0.09030	No	ns	> 0.9999
WT Vs. RAMP3KO					
Baseline Vs Baseline	0.06574	-0.07907 to 0.2106	No	ns	> 0.9999
Sham Vs Sham	0.05497	-0.09863 to 0.2086	No	ns	> 0.9999
OVX Vs OVX	0.01673	-0.1281 to 0.1615	No	ns	> 0.9999
TIBIA TRABECULAR NUMBER					
WT					
Baseline Vs. Sham	0.06817	-0.2010 to 0.3373	No	ns	> 0.9999
Baseline Vs. OVX	0.2055	-0.06363 to 0.4747	No	ns	0.3000
Sham Vs OVX	0.1374	-0.1318 to 0.4065	No	ns	> 0.9999
RAMP3 KO					
Baseline Vs. Sham	-0.09717	-0.3827 to 0.1883	No	ns	> 0.9999
Baseline Vs. OVX	0.3457	0.07656 to 0.6149	Yes	**	0.0051
Sham Vs OVX	0.3587	0.07324 to 0.6442	Yes	**	0.0064
WT Vs. RAMP3KO					
Baseline Vs Baseline	-0.08417	-0.3533 to 0.1850	No	ns	> 0.9999
Sham Vs Sham	-0.1653	-0.4508 to 0.1201	No	ns	> 0.9999
OVX Vs OVX	0.05602	-0.2131 to 0.3252	No	ns	> 0.9999
TIBIA TRABECULAR PATTERN FACTOR					
WT					
Baseline Vs. Sham	-42.90	-62.10 to -23.71	Yes	****	< 0.0001
Baseline Vs. OVX	-45.56	-64.75 to -26.36	Yes	****	< 0.0001
Sham Vs OVX	-2.653	-21.85 to 16.54	No	ns	> 0.9999
RAMP3 KO					
Baseline Vs. Sham	-60.72	-81.08 to -40.36	Yes	****	< 0.0001
Baseline Vs. OVX	-63.23	-82.42 to -44.04	Yes	****	< 0.0001
Sham Vs OVX	-2.512	-22.87 to 17.85	No	ns	> 0.9999
WT Vs. RAMP3KO					
Baseline Vs Baseline	-1.461	-20.65 to 17.73	No	ns	> 0.9999
Sham Vs Sham	-19.27	-39.63 to 1.084	No	ns	0.0758
OVX Vs OVX	-19.13	-38.33 to 0.06053	No	ns	0.0513

9.1.3 Chapter 4: Characterising RAMP3 KO osteoblasts

9.1.3.i Primary Osteoblast culture buffers and solutions:

- 1) Hanks with calcium and magnesium (without phenol red) (Lonza®)
- 2) Phosphate buffered saline (Sigma®)
- 3) Penicillin-Streptomycin solution (Sigma®)
- 4) Collagenase 1A (Sigma®) (stock solution:10mg/ml in Hank's stored as 1ml aliquots at -20°C)
- 5) 4mM tetrasodium EDTA in PBS
- 6) Trypsin-EDTA solution (Gibco®)
- 7) Non - differentiation media : Alpha minimum essential media (MEM) (Gibco®) with 10% heat inactivated fetal calf serum (FCS) (Sigma®), 0.5% penicillin-streptomycin solution
- 8) Osteoblast differentiation media: Alpha MEM, 10%FCS, 0.5% penicillin-streptomycin solution 5mM/l β -Glycerophosphate (Sigma®) (stock solution: 0.5M in alpha MEM), 10nM dexamethasone (stock: 1mM in 100% methanol) and 100 μ g/ml Ascorbic acid (Sigma®)

9.1.4 Chapter 5: Expression of RAMPs in differentiating primary osteoblasts

9.1.4.i CT and Delta CT values of RAMP1, 2 and 3 in WT and RAMP3 osteoblasts:

RAMP1									
		n=1		n=2		n=3		n=4	
	Time-point	avg.CT	Delta CT						
WT	DAY 0	38.23	21.43	39.55	20.96	39.05	22.29	38.16	21.00
	DAY 5	36.92	19.14	38.41	19.15	-	-	34.97	16.89
	DAY 10	35.88	18.25	36.52	17.33	37.25	19.25	37.55	19.68
	DAY 15	34.88	16.86	34.53	16.11	34.82	17.23	35.12	17.79
	DAY 20	35.97	18.68	36.24	17.97	37.63	16.24	37.01	15.29
RAMP3 KO	DAY 0	38.91	20.30	37.20	19.32	38.92	21.76	38.38	21.36
	DAY 5	39.06	18.76	36.47	18.04	36.55	18.82	36.19	18.66
	DAY 10	37.79	16.92	36.80	18.10	37.76	19.93	38.43	20.45
	DAY 15	37.76	16.82	35.94	15.67	36.76	19.20	35.15	17.37
	DAY 20	38.69	18.13	36.78	17.23	38.69	21.10	36.92	19.02
	NTC	Undetermined		Undetermined		Undetermined		Undetermined	
	CNC	17.49		20.27					

NTC: Non Template Control; **CNC:** Copy Number Control; **avg CT** = average of three CT values.

RAMP2									
		n=1		n=2		n=3		n=4	
	Time-point	avg.CT	Delta CT						
WT	DAY 0	35.35	18.16	33.53	14.94	38.68	21.40	32.77	15.61
	DAY 5	28.62	11.09	28.41	9.15	36.60	18.99	25.96	7.88
	DAY 10	26.95	9.32	26.58	7.39	27.98	10.33	27.49	9.61
	DAY 15	26.23	8.25	25.39	6.97	26.54	7.33	25.50	8.17
	DAY 20	29.13	11.83	28.65	10.39	29.03	7.84	27.05	5.34
RAMP3 KO	DAY 0	35.95	17.34	34.12	16.24	34.81	17.38	37.01	19.99
	DAY 5	29.33	9.03	29.48	11.05	29.40	11.77	29.31	11.78
	DAY 10	27.24	6.36	26.32	7.62	27.23	9.57	27.88	9.90
	DAY 15	26.44	5.50	28.72	8.45	26.94	9.56	27.52	9.74
	DAY 20	27.50	6.95	26.93	7.39	27.99	10.44	28.48	10.58
	NTC	Undetermined		Undetermined		Undetermined		Undetermined	
	CNC	20.44		20.87					

RAMP3							
		n=1		n=2		n=3	
	Time-point	avg.CT	Delta CT	avg.CT	Delta CT	avg.CT	Delta CT
WT	DAY 0	35.35	18.16	33.53	14.94	38.68	21.40
	DAY 5	28.62	11.09	28.41	9.15	36.60	18.99
	DAY 10	26.95	9.32	26.58	7.39	27.98	10.33
	DAY 15	26.23	8.25	25.39	6.97	26.54	7.33
	DAY 20	29.13	11.83	28.65	10.39	29.03	7.84
RAMP3 KO	DAY 0	No PCR product amplified (undetermined)					
	DAY 5						
	DAY 10						
	DAY 15						
	DAY 20						
	NTC	Undetermined		Undetermined		Undetermined	
	CNC	18.27		18.30		18.02	

NTC: Non Template Control; **CNC:** Copy Number Control; **avg CT** = average of three CT values.

9.1.5. Chapter 6: Expression of RAMPs in response to stimulation.

9.1.5.i Western Blotting Reagents

1) Sample buffer

1X Laemmli Sample Buffer (LSB):
 62.5 mM Tris-HCl (pH 6.8),
 2% (w/v) SDS, 10% Glycerol,
 5% (v/v) Beta mercaptoethanol (2-ME)
 0.001% (w/v) Bromophenol blue (Laemmli, 1970).

2) 5X Running Buffer

72g glycine 1M
 15.5g Tris base 130mM
 25ml 20%SDS
 975ml D/W

3) Transfer Buffer

3g Tris base 25mM
 14.4g glycine 200mM
 200ml Methanol 20% (v/v)
 800ml D/w
 TBS 10X
 80g NaCl
 2g KCl
 30g Tris base
 800ml Water
 pH to 7.4 and make up to 1L

4) Resolving gel	12%	15%	17%
ddH ₂ O	7.9ml	3.7ml	3.2ml
30% Acrylamide	3.73ml	8ml	11.3ml
1.5M Tris 8.8	4.0ml	4ml	5ml
10% SDS	160µl	160µl	200µl
10% APS	160µl	160µl	200µl
TEMED	16 µl	16 µl	20 µl
Total volume for 2 gels	16ml	16ml	20ml

5) Stacking gel	6%
ddH ₂ O	5.3ml
30% Acrylamide	2ml
0.5M Tris 6.8	2.5ml
10% SDS	100µl
10% APS	100µl
TEMED	10 µl
Total volume for 2 gels	10ml

6) Blocking solution	5%	5%
Milk	2.5gms	0.5gms
PBST	50 ml	10ml
Total vol	50	10ml

7) Washing solutions		
PBST	0.25%	0.25%
Tween 20	2.5gms	1.25gms
PBS	1L	500ml
TBST	0.25%	0.25%
Tween 20	2.5gms	1.25gms
TBS	1L	500ml

8) Cell Harvesting

Buffer A:

20 mM HEPES (pH 7.4),
10 mM KCl, 1.5 mM MgCl₂,
1 mM dithiothreitol (DTT),
250 mM sucrose.
Protease inhibitor cocktail -1X

NP40 lysis buffer

50mM Tris-HCl pH 8.0
150mM NaCl
1% NP-40
Protease inhibitor cocktail 1X
*100mM PMSF for phosphorylated proteins

0.25M Sucrose/Buffer A:

50 mM triethanolamine (TEA) (pH 7.5),
25 mM KCl, 5 mM MgCl₂,
0.5 mM DTT, 0.5 mM phenylmethanesulfonyl fluoride (PMSF),
250 mM sucrose
Protease inhibitor cocktail -1X
PMSF stock solution
100 mM PMSF solution was prepared in 100% ethanol solution and stored at 4°C.

9.1.6 Chapter 7: Expression of CTR in differentiating primary osteoblasts:

9.1.6.i Sequencing results: Sequences of the amplicons of all individual overlapping primer pairs: Sequences of PCR products amplified by each primer pair. cDNA prepared from three independent WT (SVEV) primary osteoblast cultures differentiated for 20 days, was amplified against each primer (n=3 for each primer pair).

Table 9.2: Sequences of amplicons of each overlapping primer pairs:

Primer pairs	Produce size	Product sequencing result
<i>mCTR3 f/r</i>	315	NNGGCATAAACTGAAAAGGTGAGTGCTTATATAAGCATCGCTTATGGAAGG AGAAGAAAACCGAGGGAGCAGGGCTACCACTTAGAGGATTTGAAAATGACT CCAAGGAGGTCCAGAGTGAAAAGGCGGAATCTCCGCAAACCGAAGATGAG GTTCCCTTCTCGTGAACAGGTTACCCCTGCTGCTCCTGCTCCTAGTGAGCC CAACTCCAGTTCTTCAGGCTCCTACCAATCTCACTGACTCCGGCCCTTGAT CAGGAGCCATTCCCTGTACTTGGTTGGCCGCAAGAAGCTGCTGGATGCTCA GTACAAAATGCTATGA
<i>mCTR4 f/r</i>	319	GGGGCCCCGGCTCTAGTGAGCCACTCCAGTTCTTCAGGCTCCTACCAATC TCACTGACTCCGGCCTTGATCAGGAGCCATTCCCTGTACTTGGTTGGCCGC AAGAAGCTGCTGGATGCTCAGTACAAAATGCTATGACCGGATTCATCAGTT GCCCTCTTATGAAGGAGAAGGTCTGTACTGCAACCGCACCTGGGATGGCT GGATGTGCTGGGACGACACTCCCCTGGAGCCACAGCCTATCAGCACTGC CCTGACTACTTCCCGACTTTGACACAGCAGAAAAGGTTTCAAATACTG TGATGAAAAGGGAGAGTGG
<i>mCTR5 f/r</i>	327	NNNNNGGTGGAAGGAAATGAAAATGACCGGATTCATCAGTTGCCCTCTTA TGAAGGAGAAGGTCTGTACTGCCCTTTTACCTGGGATGGCTGGATGTGCT GGGACGACACTCCCCTGGAGCCACAGCCTATCAGCACTGCCCTGACTAC TTCCCGGACTTTGACACAGCAGAAAAGGTTTCAAATACTGTGATGAAAA TGGAGAGTGGTTTACACACCCCTGACAGCAACCGAACCTGGTCCAACATA CTCTGTGCAACGCTTTCACCTCTGAGAAACTGCAAAAATGCGTACGTTCTT TATTACCTGGCTCTTGTGGGTCACTCC
<i>mCTR6 f/r</i>	303	NNNNNCGGCCAAATCAGCACTGACCTGACTACTTCCCGACTTTGACACA GCAGAAAAGGTTTCAAATACTGTGATGAAAATGGAGAGTGGTTTACACA CCCTGACAGCAACCGAACCTGGTCCAACATACTCTGTGCAACGCTTTCA CTTCTGAGAAACTGCAAAAATGCGTACGTTCTTTATTACCTGGCTCTTGTG GGTCACTCCTTGTGCGATTGCTGCTTTGGTTGCTTCCATGCTGATCTTCTG GATTTTCAAGAACCTTAGCTGCCAGAGGGTGACCTTGACACAAGCACATGT TCA
<i>mCTR8 f/r</i>	209	NNNNNNNNNAACCTGCTTCAGGGTGACCTTGACACAAGCACATGTTCCCTT ACTTATATTCTGAATTCTATCATTATCATCATCCACCTGGTTGAGGTTGT GCCCAATGGAGATCTGGTGC GGCGGGATCCTATAAGTTGCAAGGTTCTAC ACTTTTTACATCAGTACATGATGTCTTGCAACTACTTCTGGATGCTCTGC GAA

<i>mCTR9 f/r</i>	212	NNNNNNNNNGGACTATATTTGCAAGGTTCTACACTTTTTTACATCACGTAC ATGATGTCTTGCAACTACTTCTGGATCCTTTGCGAGGGGATCTATCTTCA TACTCTGATTGTCATGGCTGTGTTTACCGACGAGCAACGCCTACGCTGGT ACTATCTTCTTGGCTGGGGGTTCCCGATAGTGCCAACCATTATCCACGCC ATCACTCGTAAA
<i>mCTR11 f/r</i>	295	NNNNNNNNNTTCNTGGCTGGGGGTTCCCGATAGTGCCAACCATTATCCA CGCCATCACTCGTGCCCTCTACTACAACGACAACCTGCTGGCTGAGTGCAG AAACCCACTTGCTTTACATCATCCATGGACCCGTCATGGTGGCTCTGGTG GTCAACTTCTTCTTTCTTCTCAACATTGTCCGCGTCTTGTGACCAAGAT GAGGCAAACCCACGAGGCCGAGTCCACATGTACCTGAAGGCTGTGAAGG CCACCATGGTCCCTTGTGCCCTGCTGGGGATCCGTTTTTGTGTGTGT
<i>mCTR12 f/r</i>	293	NGGGACCCGGTCATGGTGGCTCTGGTGGTCACTTCTTCTTTCTTCTCAAC ATTGTCCGCGTGCTTGTGACCAAGATGAGGCAAACCCACGAGGCCGAGTC CTACATGTACCTGAAGGCTGTGAAGGCCACCATGGTCCCTTGTGCCCTGC TGGGGATCCAGTTTGTGTGTGTTTCCCTGGAGGCCCTCCAACAAGGTGCTT GGGAAGATCTATGATTATCTCATGCACTCTCTGATTCAATTTCCAGGGATT CTTGTGGCGACTATCTACTGCTTCTGCAACCATGAGGTGCAA
<i>mCTR13 f/r</i>	316	NNNNNATGTA CTGAGGCTGTGAGGCCACCATGGTCCCTTGTGCCCTGCTG GGGATCCAGTTTGTGTGTGTTTCCCTGGAGGCCCTCCAACAAGGTGCTTGG GAAGATCTATGATTATCTCATGCACTCTCTGATTCAATTTCCAGGGATTCT TTGTGGCGACTATCTACTGCTTCTGCAACCATGAGGTGCAAGTCACCCCTG AAGCGCCAGTGGACGCAGTTCAAGATCCAGTGGAGCCAACGCTGGGGAAG GCGCCGCCGCCCCACCAACCGCGTAGTTAGTGCTCCTCGGGCTGTAGCCT TCGCGTAGCCAGATAA
<i>mCTR14 f/r</i>	310	NNNNNNNNNTCTCTGATTCTTTCCAGGGATTCTTTGTGGCGACTATCTAC TGCTTCTGCAACCATGAGGTGCAAGTCACCCGTAAGCGCCAGTGGACGCA GTTCAAGATCCAGTGGAGCCAACGCTGGGGAAGGCGCCGCCGCCCCACCA ACCGCGTAGTTAGTGCTCCTCGGGCTGTAGCCTTTCGCTGAGCCAGATGGC CTCCCCATTTACATCTGCCATCAGGAACCACGGAATCCTCCAATCAGCAA CAACGAAGGCGAGGAGAGTACTGAAATGATCCCCATGAACGTCATCCAGC AGAACGCATC
<i>mCTR15 f/r</i>	297	NNNNNAGGCGGGGGAAGGGCGCCGCCGCCCCACCAACCGCGTAGTTAGTG CTCCTCGGGCTGTAGCCTTCGCTGAGCCAGATGGCCTCCCCATTTACATC TGCCATCAGGAACCACGGAATCCTCCAATCAGCAACAACGAAGGCGAGGA GAGTACTGAAATGATCCCCATGAACGTCATCCAGCAAGACGCATCCGCTT GAATGTGAAGCCACCCCAAGCATTGTGATCCACTGAGCCTTCATTTCCCTG GGGAAAAGACAGACCATGTGTTTCAAGTGATTCCATCCCTCCAGTAA
<i>mCTR16 f/r</i>	302	NGGCCGAGAGAGTACTGAATGATCCCCATGAACGTCATCCAGCAAGACGC ATCCGCTTGAATGTGAAGCCACCCCAAGCATTGTGATCCACTGAGCCTTC ATTTCTTGGGAAAGACAGACCATGTGTTTCAAGTGATTCCCATCCTCCC AGGAGCTGACCATAATCTTTGTGAAGAAGTGTAAAGTGAATTTGTCCATA GTGAATTTGAAGAAAGTGATTCTTGGTACTATTGCTTTGGGAGTCAGTCT AGGAATAGAGTCTCCCATTTGCAACTTGTGAACCTCCATCTTCATCCTGGAA AA
<i>mCTR17 f/r</i>	205	NNNNNTTCTGGGGAAGAAGACCATGTGTTTTCAAGTGATTCCCATCCTCCC AGGAGCTGACCATATCATTTGTGAAGAAGTGTAAAGTGAATTTGTCCATA GTGAATTTGAAGAAAGTGATTCTTGGTACTATTGCTTTGGGAGTCAGTCT AGGAATAGAGTCTCCCATTTGCAACTTGTGAACCTCCATCATTCATCCTGGA CTGAGATGACTGTGTTTCGTAGGAAAGCAGGCAAGGTGTTCAAAGATGTC

9.1.6.ii NCBI BLAST results:

9.1.6.ii.a NCBI BLAST2n result for osteoblast CTR cDNA and full length CTR variant

Calcr001:

Sequence alignments: Sequence ID: lcl|46219 Length: 2460, Number of Matches: 2

1) Range 1: 1306 to 2151

Score	Expect	Identities	Gaps	Strand
1552 bits(840)	0.0	845/847(99%)	2/847(0%)	Plus/Plus
Query 715	ATAAGTTGCAAGGTTCTACACTTTTACATCAGTACATGATGTCTTGCAACTACTTCTGG	774		
Sbjct 1306	ATAAGTTGCAAGGTTCTACACTTTTACATCAGTACATGATGTCTTGCAACTACTTCTGG	1365		
Query 775	ATGCTCTGCGAGGGGATCTATCTTCACTACTCTGATTGTCATGGCTGTGTTTACCGACGAG	834		
Sbjct 1366	ATGCTCTGCGAGGGGATCTATCTTCACTACTCTGATTGTCATGGCTGTGTTTACCGACGAG	1425		
Query 835	CAACGCCTACGCTGGTACTATCTTCTTGGCTGGGGTTCCCGATAGTGCCAACCATATC	894		
Sbjct 1426	CAACGCCTACGCTGGTACTATCTTCTTGGCTGGGGTTCCCGATAGTGCCAACCATATC	1485		
Query 895	CACGCCATCACTCGTGCCCTCTACTACAACGACAACCTGCTGGCTGAGTGAGAAACCCAC	954		
Sbjct 1486	CACGCCATCACTCGTGCCCTCTACTACAACGACAACCTGCTGGCTGAGTGAGAAACCCAC	1545		
Query 955	TTGCTTTACATCATCCATGGACCCGGTCATGGTGGCTCTGGTGGTC-ACTTCTTCTTCT	1013		
Sbjct 1546	TTGCTTTACATCATCCATGGACCC-GTCATGGTGGCTCTGGTGGTCAACTTCTTCTTCT	1604		
Query 1014	TCTCAACATTGTCCGCGTGTGTGACCAAGATGAGGCAAACCCACGAGGCCGAGTCCTA	1073		
Sbjct 1605	TCTCAACATTGTCCGCGTGTGTGACCAAGATGAGGCAAACCCACGAGGCCGAGTCCTA	1664		
Query 1074	CATGTACCTGAAGGCTGTGAAGGCCACCATGGTCCCTTGTGCCCTGTGGGATCCAGTT	1133		
Sbjct 1665	CATGTACCTGAAGGCTGTGAAGGCCACCATGGTCCCTTGTGCCCTGTGGGATCCAGTT	1724		
Query 1134	TGTTGTGTTTTCCCTGGAGGCCCTCCAACAAGGTGCTTGGGAAGATCTATGATTATCTCAT	1193		
Sbjct 1725	TGTTGTGTTTTCCCTGGAGGCCCTCCAACAAGGTGCTTGGGAAGATCTATGATTATCTCAT	1784		
Query 1194	GCACTCTCTGATTCAATTTCCAGGGATTCTTTGTGGCGACTATCTACTGCTTCTGCAACCA	1253		
Sbjct 1785	GCACTCTCTGATTCAATTTCCAGGGATTCTTTGTGGCGACTATCTACTGCTTCTGCAACCA	1844		
Query 1254	TGAGGTGCAAGTCACCCCTGAAGCGCCAGTGGACGAGTCAAGATCCAGTGGAGCCAACG	1313		
Sbjct 1845	TGAGGTGCAAGTCACCCCTGAAGCGCCAGTGGACGAGTCAAGATCCAGTGGAGCCAACG	1904		
Query 1314	CTGGGAAGGCGCCGCGCCCAACCAACCGCGTAGTTAGTGCTCCTCGGGCTGTAGCCTT	1373		
Sbjct 1905	CTGGGAAGGCGCCGCGCCCAACCAACCGCGTAGTTAGTGCTCCTCGGGCTGTAGCCTT	1964		
Query 1374	CGCTGAGCCAGATGGCCTCCCCATTTACATCTGCCATCAGGAACACGGAATCCTCCAAT	1433		
Sbjct 1965	CGCTGAGCCAGATGGCCTCCCCATTTACATCTGCCATCAGGAACACGGAATCCTCCAAT	2024		
Query 1434	CAGCAACAACGAAGGCGAGGAGAGTACTGAAATGATCCCCATGAACGTCATCCAGCAAGA	1493		
Sbjct 2025	CAGCAACAACGAAGGCGAGGAGAGTACTGAAATGATCCCCATGAACGTCATCCAGCAAGA	2084		
Query 1494	CGCATCCGCTTGAATGTGAAGCCACCCCAAGCATTGTGATCCACTGAGCCTTCATTTCT	1553		
Sbjct 2085	CGCATCCGCTTGAATGTGAAGCCACCCCAAGCATTGTGATCCACTGAGCCTTCATTTCT	2144		
Query 1554	GGGGAAA 1560			
Sbjct 2145	GGGGAAA 2151			

2) Range 2: 481 to 1196

Score	Expect	Identities	Gaps	Strand
1323 bits(716)	0.0	716/716(100%)	0/716(0%)	Plus/Plus

```

Query 1 ACAGAGGATTTGAAAATGACTCCAAGGAGGTCCAGAGTGAAAAGGCGGAATCTCCGCAA 60
      |||
Sbjct 481 ACAGAGGATTTGAAAATGACTCCAAGGAGGTCCAGAGTGAAAAGGCGGAATCTCCGCAA 540

Query 61 CCGAAGATGAGGTTCCCTTCTCGTGAACAGGTTACCCTGCTGCTCCTGCTCCTAGTGAGC 120
      |||
Sbjct 541 CCGAAGATGAGGTTCCCTTCTCGTGAACAGGTTACCCTGCTGCTCCTGCTCCTAGTGAGC 600

Query 121 CCAACTCCAGTTCTTCAGGCTCTACCAATCTCACTGACTCCGGCCTTGATCAGGAGCCA 180
      |||
Sbjct 601 CCAACTCCAGTTCTTCAGGCTCTACCAATCTCACTGACTCCGGCCTTGATCAGGAGCCA 660

Query 181 TTCCTGTACTTGGTTGGCCGCAAGAAGCTGCTGGATGCTCAGTACAAATGCTATGACCGG 240
      |||
Sbjct 661 TTCCTGTACTTGGTTGGCCGCAAGAAGCTGCTGGATGCTCAGTACAAATGCTATGACCGG 720

Query 241 ATTCAATCAGTTGCCCTCTTATGAAGGAGAAGGTCTGTACTGCAACCGCACCTGGGATGGC 300
      |||
Sbjct 721 ATTCAATCAGTTGCCCTCTTATGAAGGAGAAGGTCTGTACTGCAACCGCACCTGGGATGGC 780

Query 301 TGGATGTGCTGGGACGACACTCCCGCTGGAGCCACAGCCTATCAGCACTGCCCTGACTAC 360
      |||
Sbjct 781 TGGATGTGCTGGGACGACACTCCCGCTGGAGCCACAGCCTATCAGCACTGCCCTGACTAC 840

Query 361 TTCCCGACTTTGACACAGCAGAAAAGGTTTCAAAATACTGTGATGAAAATGGAGAGTGG 420
      |||
Sbjct 841 TTCCCGACTTTGACACAGCAGAAAAGGTTTCAAAATACTGTGATGAAAATGGAGAGTGG 900

Query 421 TTTAGACACCTGACAGCAACCGAACCTGGTCCAACATACTCTGTGCAACGCTTTCCTACT 480
      |||
Sbjct 901 TTTAGACACCTGACAGCAACCGAACCTGGTCCAACATACTCTGTGCAACGCTTTCCTACT 960

Query 481 TCTGAGAACTGCAAAATGCGTACGTTCTTTATTACCTGGCTCTTGTGGGTCCTCCTTG 540
      |||
Sbjct 961 TCTGAGAACTGCAAAATGCGTACGTTCTTTATTACCTGGCTCTTGTGGGTCCTCCTTG 1020

Query 541 TCGATTGCTGCTTTGGTTGCTTCCATGCTGATCTTCTGGATTTTCAAGAACCTTAGCTGC 600
      |||
Sbjct 1021 TCGATTGCTGCTTTGGTTGCTTCCATGCTGATCTTCTGGATTTTCAAGAACCTTAGCTGC 1080

Query 601 CAGAGGGTGACCTTGACACAAGCACATGTTCCCTTACTTATATCTGAATTCATCATTATC 660
      |||
Sbjct 1081 CAGAGGGTGACCTTGACACAAGCACATGTTCCCTTACTTATATCTGAATTCATCATTATC 1140

Query 661 ATCATCCACCTGGTTGAGGTTGTGCCCAATGGAGATCTGGTGCGGCGGGATCCTAT 716
      |||
Sbjct 1141 ATCATCCACCTGGTTGAGGTTGTGCCCAATGGAGATCTGGTGCGGCGGGATCCTAT 1196

```

9.1.4.ii.b NCBI BLAST result for osteoblast CTR cDNA sequence:

Sequence alignments:

1) Mus musculus calcitonin receptor (Calcr), transcript variant 1a, mRNA

Sequence ID: [ref|NM_001042725.1](#) Length: 3471 Number of Matches: 1

Range 1: 291 to 1850

Score	Expect	Identities	Gaps	Strand
2870 bits(1554)	0.0	1559/1561(99%)	2/1561(0%)	Plus/Plus

```

Query 1 ACACAGGATTGAAAATGACTCCAAGGAGGTCCAGAGTGAAAAGGCGGAATCTCCGCAA 60
      |||
Sbjct 291 ACACAGGATTGAAAATGACTCCAAGGAGGTCCAGAGTGAAAAGGCGGAATCTCCGCAA 350

Query 61 CCGAAGATGAGGTTTCCTTCTCGTGAAACAGGTTCAACCCTGCTGCTCCTAGTGAGC 120
      |||
Sbjct 351 CCGAAGATGAGGTTTCCTTCTCGTGAAACAGGTTCAACCCTGCTGCTCCTAGTGAGC 410

Query 121 CCAACTCCAGTTCTTCAGGCTCCTACCAATCTCACTGACTCCGGCCTTGATCAGGAGCCA 180
      |||
Sbjct 411 CCAACTCCAGTTCTTCAGGCTCCTACCAATCTCACTGACTCCGGCCTTGATCAGGAGCCA 470

Query 181 TTCCTGACTTGGTTGGCCGCAAGAAGCTGCTGGATGCTCAGTACAAATGCTATGACCGG 240
      |||
Sbjct 471 TTCCTGACTTGGTTGGCCGCAAGAAGCTGCTGGATGCTCAGTACAAATGCTATGACCGG 530

Query 241 ATTCATCAGTTGCCCTCTTATGAAGGAGAAGGTCTGTACTGCAACCGCACCTGGGATGGC 300
      |||
Sbjct 531 ATTCATCAGTTGCCCTCTTATGAAGGAGAAGGTCTGTACTGCAACCGCACCTGGGATGGC 590

Query 301 TGGATGTGCTGGGACGACACTCCCGCTGGAGCCACAGCCTATCAGCACTGCCCTGACTAC 360
      |||
Sbjct 591 TGGATGTGCTGGGACGACACTCCCGCTGGAGCCACAGCCTATCAGCACTGCCCTGACTAC 650

Query 361 TTCCCGGACTTTGACACAGCAGAAAAGGTTTCAAATACTGTGATGAAAATGGAGAGTGG 420
      |||
Sbjct 651 TTCCCGGACTTTGACACAGCAGAAAAGGTTTCAAATACTGTGATGAAAATGGAGAGTGG 710

Query 421 TTTAGACACCTGACAGCAACCGAACCTGGTCCAACATACTCTGTGCAACGCTTTCACT 480
      |||
Sbjct 711 TTTAGACACCTGACAGCAACCGAACCTGGTCCAACATACTCTGTGCAACGCTTTCACT 770

Query 481 TCTGAGAAATGCAAAATGCGTACGTTCTTTATTACCTGGCTCTGTGGGTCACTCCTTG 540
      |||
Sbjct 771 TCTGAGAAATGCAAAATGCGTACGTTCTTTATTACCTGGCTCTGTGGGTCACTCCTTG 830

Query 541 TCGATTGCTGCTTTGGTTGCTTCCATGCTGATCTTCTGGATTTTCAAGAACCTTAGCTGC 600
      |||
Sbjct 831 TCGATTGCTGCTTTGGTTGCTTCCATGCTGATCTTCTGGATTTTCAAGAACCTTAGCTGC 890

Query 601 CAGAGGGTGACCTTGACACAAGCACATGTTCCCTACTTATATTTGAATTCATCATTATC 660
      |||
Sbjct 891 CAGAGGGTGACCTTGACACAAGCACATGTTCCCTACTTATATTTGAATTCATCATTATC 950

Query 661 ATCATCCACCTGGTTGAGGTTGTGCCCAATGGAGATCTGGTGCGGCGGGATCCTATAAGT 720
      |||
Sbjct 951 ATCATCCACCTGGTTGAGGTTGTGCCCAATGGAGATCTGGTGCGGCGGGATCCTATAAGT 1010

Query 721 TGCAAGGTTCTACACTTTTTACATCAGTACATGATGCTTTGCAACTACTTCTGGATGCTC 780
      |||
Sbjct 1011 TGCAAGGTTCTACACTTTTTACATCAGTACATGATGCTTTGCAACTACTTCTGGATGCTC 1070

Query 781 TCGGAGGGGATCTATCTTCATACTCTGATTGTCATGGCTGTGTTTACCGACGAGCAACGC 840
      |||
Sbjct 1071 TCGGAGGGGATCTATCTTCATACTCTGATTGTCATGGCTGTGTTTACCGACGAGCAACGC 1130

Query 841 CTACGCTGGTACTATCTTCTTGCTGGGGTTCCCGATAGTGCCAACCATATCCACGCC 900
      |||
Sbjct 1131 CTACGCTGGTACTATCTTCTTGCTGGGGTTCCCGATAGTGCCAACCATATCCACGCC 1190

Query 901 ATCACTCGTCCCTCTACTACAACGACAACCTGCTGGCTGAGTGCAGAAACCCACTTGCTT 960
      |||
Sbjct 1191 ATCACTCGTCCCTCTACTACAACGACAACCTGCTGGCTGAGTGCAGAAACCCACTTGCTT 1250
    
```

```

Query 961 TACATCATCCATGGACCCGGTCATGGTGGCTCTGGTGGTC-ACFTCTCTTTCTTCTCAA 1019
          |||
Sbjct 1251 TACATCATCCATGGACCC-GTCATGGTGGCTCTGGTGGTCAACTCTTCTTCTTCTCAA 1309

Query 1020 CATTGTCCGCGTGTGTGACCAAGATGAGGCAAACCCACGAGGCCGAGTCTACATGTA 1079
          |||
Sbjct 1310 CATTGTCCGCGTGTGTGACCAAGATGAGGCAAACCCACGAGGCCGAGTCTACATGTA 1369

Query 1080 CCTGAAGGCTGTGAAGGCCACCATGGTCTTGTGCCCTGCTGGGGATCCAGTTTGTGTG 1139
          |||
Sbjct 1370 CCTGAAGGCTGTGAAGGCCACCATGGTCTTGTGCCCTGCTGGGGATCCAGTTTGTGTG 1429

Query 1140 GTTTCCTCGGAGGCCCTCCAACAAGGTGCTGGGAAGATCTATGATTATCTCATGCACTC 1199
          |||
Sbjct 1430 GTTTCCTCGGAGGCCCTCCAACAAGGTGCTGGGAAGATCTATGATTATCTCATGCACTC 1489

Query 1200 TCTGATTCATTTCCAGGATTCTTTGTGGCGACTATCTACTGCTTCTGCAACCATGAGGT 1259
          |||
Sbjct 1490 TCTGATTCATTTCCAGGATTCTTTGTGGCGACTATCTACTGCTTCTGCAACCATGAGGT 1549

Query 1260 GCAAGTCACCCTGAAGCGCCAGTGGACGCAGTTCAAGATCCAGTGGAGCCAACGCTGGGG 1319
          |||
Sbjct 1550 GCAAGTCACCCTGAAGCGCCAGTGGACGCAGTTCAAGATCCAGTGGAGCCAACGCTGGGG 1609

Query 1320 AAGGCGCCGCGCCCAACACCGCGTAGTTAGTGCTCCTCGGGCTGTAGCCTTCGCTGA 1379
          |||
Sbjct 1610 AAGGCGCCGCGCCCAACACCGCGTAGTTAGTGCTCCTCGGGCTGTAGCCTTCGCTGA 1669

Query 1380 GCCAGATGGCCTCCCATTTACATCTGCCATCAGGAACACGGAATCCTCCAATCAGCAA 1439
          |||
Sbjct 1670 GCCAGATGGCCTCCCATTTACATCTGCCATCAGGAACACGGAATCCTCCAATCAGCAA 1729

Query 1440 CAACGAAGGCGAGGAGAGTACTGAAATGATCCCATGAACGTATCCAGCAAGACGCATC 1499
          |||
Sbjct 1730 CAACGAAGGCGAGGAGAGTACTGAAATGATCCCATGAACGTATCCAGCAAGACGCATC 1789

Query 1500 CGCTTGAATGTGAAGCCACCCCAAGCATTGTGATCCACTGAGCCTTCATTTCTGGGGAA 1559
          |||
Sbjct 1790 CGCTTGAATGTGAAGCCACCCCAAGCATTGTGATCCACTGAGCCTTCATTTCTGGGGAA 1849

Query 1560 A 1560
          |
Sbjct 1850 A 1850

```

2) Mus musculus calcitonin receptor (Calcr), transcript variant 1b, mRNA

Sequence ID: [ref|NM_007588.2|](#) Length: 3831 Number of Matches: 2

1) Range 1: 1365 to 2210

Score	Expect	Identities	Gaps	Strand
1552 bits(840)	0.0	845/847(99%)	2/847(0%)	Plus/Plus

```

Query 715 ATAAGTTGCAAGGTTCTACACTTTTTACATCAGTACATGATGTCTTGCAACTACTTCTGG 774
          |||
Sbjct 1365 ATAAGTTGCAAGGTTCTACACTTTTTACATCAGTACATGATGTCTTGCAACTACTTCTGG 1424

Query 775 ATGCTCTGCGAGGGGATCTATCTTCACTCTGATTGTCATGGCTGTGTTTACCGACGAG 834
          |||
Sbjct 1425 ATGCTCTGCGAGGGGATCTATCTTCACTCTGATTGTCATGGCTGTGTTTACCGACGAG 1484

Query 835 CAACGCCTACGCTGGTACTATCTTCTTGGCTGGGGTTCCCGATAGTGCCAACCATTATC 894
          |||
Sbjct 1485 CAACGCCTACGCTGGTACTATCTTCTTGGCTGGGGTTCCCGATAGTGCCAACCATTATC 1544

Query 895 CACGCCATCACTCGTGCCCTCTACTACAACGACAACCTGCTGGCTGAGTGCAGAAACCCAC 954
          |||
Sbjct 1545 CACGCCATCACTCGTGCCCTCTACTACAACGACAACCTGCTGGCTGAGTGCAGAAACCCAC 1604

Query 955 TTGCTTTACATCATCCATGGACCCGGTCATGGTGGCTCTGGTGGTC-ACFTCTCTTTCT 1013
          |||
Sbjct 1605 TTGCTTTACATCATCCATGGACCC-GTCATGGTGGCTCTGGTGGTCAACTTCTTCTTTCT 1663

Query 1014 TCTCAACATGTGTCGCGTGTGTGACCAAGATGAGGCAAACCCACGAGGCCGAGTCTTA 1073
          |||
Sbjct 1664 TCTCAACATGTGTCGCGTGTGTGACCAAGATGAGGCAAACCCACGAGGCCGAGTCTTA 1723

```

```

Query 1074 CATGTACCTGAAGGCTGTGAAGGCCACCATGGTCCTTGTGCCCTGCTGGGGATCCAGTT 1133
          |||
Sbjct 1724 CATGTACCTGAAGGCTGTGAAGGCCACCATGGTCCTTGTGCCCTGCTGGGGATCCAGTT 1783

Query 1134 TGTGTGTTTTCCCTGGAGGCCCTCCAACAAGGTGCTTGGGAAGATCTATGATTATCTCAT 1193
          |||
Sbjct 1784 TGTGTGTTTTCCCTGGAGGCCCTCCAACAAGGTGCTTGGGAAGATCTATGATTATCTCAT 1843

Query 1194 GCACTCTCTGATTCAATTTCCAGGGATTCTTTGTGGCGACTATCTACTGCTTCTGCAACCA 1253
          |||
Sbjct 1844 GCACTCTCTGATTCAATTTCCAGGGATTCTTTGTGGCGACTATCTACTGCTTCTGCAACCA 1903

Query 1254 TGAGGTGCAAGTCACCTGAAGCGCCAGTGGACGCGAGTTCAAGATCCAGTGGAGCCAACG 1313
          |||
Sbjct 1904 TGAGGTGCAAGTCACCTGAAGCGCCAGTGGACGCGAGTTCAAGATCCAGTGGAGCCAACG 1963

Query 1314 CTGGGAAGGCGCGCGCCGCCACCAACCGCGTAGTTAGTGCTCCTCGGGCTGTAGCCTT 1373
          |||
Sbjct 1964 CTGGGAAGGCGCGCGCCGCCACCAACCGCGTAGTTAGTGCTCCTCGGGCTGTAGCCTT 2023

Query 1374 CGCTGAGCCAGATGGCCTCCCCATTTACATCTGCCATCAGGAACCACGGAATCCTCCAAT 1433
          |||
Sbjct 2024 CGCTGAGCCAGATGGCCTCCCCATTTACATCTGCCATCAGGAACCACGGAATCCTCCAAT 2083

Query 1434 CAGCAACAACGAAGGCGAGGAGAGTACTGAAATGATCCCCATGAACGTCATCCAGCAAGA 1493
          |||
Sbjct 2084 CAGCAACAACGAAGGCGAGGAGAGTACTGAAATGATCCCCATGAACGTCATCCAGCAAGA 2143

Query 1494 CGCATCCGCTTGAATGTGAAGCCACCCCAAGCATTGTGATCCACTGAGCCTTCATTTCCCT 1553
          |||
Sbjct 2144 CGCATCCGCTTGAATGTGAAGCCACCCCAAGCATTGTGATCCACTGAGCCTTCATTTCCCT 2203

Query 1554 GGGGAAA 1560
          |||
Sbjct 2204 GGGGAAA 2210

```

2) Range 2: 540 to 1255

Score	Expect	Identities	Gaps	Strand
1323 bits(716)	0.0	716/716(100%)	0/716(0%)	Plus/Plus

```

Query 1 ACAGAGGATTTGAAAATGACTCCAAGGAGGTCCAGAGTGAAAAGGCGGAATCTCCGCAA 60
          |||
Sbjct 540 ACAGAGGATTTGAAAATGACTCCAAGGAGGTCCAGAGTGAAAAGGCGGAATCTCCGCAA 599

Query 61 CCGAAGATGAGGTTCCCTTCTCGTGAACAGGTTACCCCTGCTGCTCCTAGTGAGC 120
          |||
Sbjct 600 CCGAAGATGAGGTTCCCTTCTCGTGAACAGGTTACCCCTGCTGCTCCTAGTGAGC 659

Query 121 CCAACTCCAGTTCTTTCAGGCTCTACCAATCTCACTGACTCCGGCCTTGATCAGGAGCCA 180
          |||
Sbjct 660 CCAACTCCAGTTCTTTCAGGCTCTACCAATCTCACTGACTCCGGCCTTGATCAGGAGCCA 719

Query 181 TTCCTGTACTTGGTTGGCCGCAAGAAGCTGCTGGATGCTCAGTACAAATGCTATGACCGG 240
          |||
Sbjct 720 TTCCTGTACTTGGTTGGCCGCAAGAAGCTGCTGGATGCTCAGTACAAATGCTATGACCGG 779

Query 241 ATTATCAGTTGCCCTCTTATGAAGGAGAAGGTCTGTACTGCAACCGCACCTGGGATGGC 300
          |||
Sbjct 780 ATTATCAGTTGCCCTCTTATGAAGGAGAAGGTCTGTACTGCAACCGCACCTGGGATGGC 839

Query 301 TGGATGTGCTGGGACGACACTCCCGCTGGAGCCACAGCCTATCAGCACTGCCCTGACTAC 360
          |||
Sbjct 840 TGGATGTGCTGGGACGACACTCCCGCTGGAGCCACAGCCTATCAGCACTGCCCTGACTAC 899

Query 361 TTCCCGGACTTTGACACAGCAGAAAAGGTTTCAAATACTGTGATGAAAATGGAGAGTGG 420
          |||
Sbjct 900 TTCCCGGACTTTGACACAGCAGAAAAGGTTTCAAATACTGTGATGAAAATGGAGAGTGG 959

Query 421 TTTAGACACCCTGACAGCAACCGAACCTGGTCCAATACTCTGTGCAACGCTTTCACT 480
          |||
Sbjct 960 TTTAGACACCCTGACAGCAACCGAACCTGGTCCAATACTCTGTGCAACGCTTTCACT 1019

Query 481 TCTGAGAAACTGCAAAATGCGTACGTTCTTTATTACCTGGCTCTTGTGGGTCACTCCTTG 540
          |||
Sbjct 1020 TCTGAGAAACTGCAAAATGCGTACGTTCTTTATTACCTGGCTCTTGTGGGTCACTCCTTG 1079

```

```

Query 541   TCGATTGCTGCTTTGGTTGCTTCCATGCTGATCTTCTGGATTTCAAGAACCTTAGCTGC 600
           |||
Sbjct 1080   TCGATTGCTGCTTTGGTTGCTTCCATGCTGATCTTCTGGATTTCAAGAACCTTAGCTGC 1139

Query 601   CAGAGGGTGACCTTGCACAAGCACATGTTCCCTTACTTATATCTGAATTCTATCATTATC 660
           |||
Sbjct 1140   CAGAGGGTGACCTTGCACAAGCACATGTTCCCTTACTTATATCTGAATTCTATCATTATC 1199

Query 661   ATCATCCACCTGGTTGAGGTTGTGCCCAATGGAGATCTGGTGCGGCGGGATCCTAT 716
           |||
Sbjct 1200   ATCATCCACCTGGTTGAGGTTGTGCCCAATGGAGATCTGGTGCGGCGGGATCCTAT 1255

```

Bibliography

- Ajubi NE, Klein-Nulend J, Alblas MJ, Burger EH, Nijweide PJ. 1999. Signal transduction pathways involved in fluid flow-induced PGE2 production by cultured osteocytes. *Am J Physiol* 276: E171-8
- Akiyama H, Chaboissier MC, Martin JF, Schedl A, de Crombrughe B. 2002. The transcription factor Sox9 has essential roles in successive steps of the chondrocyte differentiation pathway and is required for expression of Sox5 and Sox6. *Genes & development* 16: 2813-28
- Alam AS, Moonga BS, Bevis PJ, Huang CL, Zaidi M. 1993. Amylin inhibits bone resorption by a direct effect on the motility of rat osteoclasts. *Exp Physiol* 78: 183-96
- Albrandt K, Brady EM, Moore CX, Mull E, Sierzega ME, Beaumont K. 1995. Molecular cloning and functional expression of a third isoform of the human calcitonin receptor and partial characterization of the calcitonin receptor gene. *Endocrinology* 136: 5377-84
- Albrandt K, Mull E, Brady EM, Herich J, Moore CX, Beaumont K. 1993. Molecular cloning of two receptors from rat brain with high affinity for salmon calcitonin. *FEBS Lett* 325: 225-32
- Amara SG, Evans RM, Rosenfeld MG. 1984. Calcitonin/calcitonin gene-related peptide transcription unit: tissue-specific expression involves selective use of alternative polyadenylation sites. *Mol Cell Biol* 4: 2151-60
- Amara SG, Jonas V, Rosenfeld MG, Ong ES, Evans RM. 1982. Alternative RNA processing in calcitonin gene expression generates mRNAs encoding different polypeptide products. *Nature* 298: 240-4
- Asai J, Nakazato M, Miyazato M, Kangawa K, Matsuo H, Matsukura S. 1990. Regional distribution and molecular forms of rat islet amyloid polypeptide. *Biochem Biophys Res Commun* 169: 788-95
- Auerbach W, Dunmore JH, Fairchild-Huntress V, Fang Q, Auerbach AB, et al. 2000. Establishment and chimera analysis of 129/SvEv- and C57BL/6-derived mouse embryonic stem cell lines. *BioTechniques* 29: 1024-8, 30, 32
- Auriola S, Frith J, Rogers MJ, Koivuniemi A, Monkkonen J. 1997. Identification of adenine nucleotide-containing metabolites of bisphosphonate drugs using ion-pair liquid chromatography-electrospray mass spectrometry. *Journal of chromatography. B, Biomedical sciences and applications* 704: 187-95

- Bafico A, Liu G, Yaniv A, Gazit A, Aaronson SA. 2001. Novel mechanism of Wnt signalling inhibition mediated by Dickkopf-1 interaction with LRP6/Arrow. *Nature cell biology* 3: 683-6
- Bagi CM, Mecham M, Weiss J, Miller SC. 1993. Comparative morphometric changes in rat cortical bone following ovariectomy and/or immobilization. *Bone* 14: 877-83
- Balcerzak M, Hamade E, Zhang L, Pikula S, Azzar G, et al. 2003. The roles of annexins and alkaline phosphatase in mineralization process. *Acta biochimica Polonica* 50: 1019-38
- Ballica R, Valentijn K, Khachatryan A, Guerder S, Kapadia S, et al. 1999. Targeted expression of calcitonin gene-related peptide to osteoblasts increases bone density in mice. *J Bone Miner Res* 14: 1067-74
- Baron R, Hesse E. 2012. Update on bone anabolics in osteoporosis treatment: rationale, current status, and perspectives. *The Journal of clinical endocrinology and metabolism* 97: 311-25
- Baud CA. 1968. [Structure and functions of osteocytes in normal conditions and under the influence of parathyroid extract]. *Schweizerische medizinische Wochenschrift* 98: 717-20
- Bean AJ, Zhang X, Hokfelt T. 1994. Peptide secretion: what do we know? *FASEB J* 8: 630-8
- Beaumont K, Pittner RA, Moore CX, Wolfe-Lopez D, Prickett KS, et al. 1995. Regulation of muscle glycogen metabolism by CGRP and amylin: CGRP receptors not involved. *Br J Pharmacol* 115: 713-5
- Becker KL NE, Choen R, Silva OL, Snider RH. 1996. Calcitonin: Structure, Molecular Biology, and Actions In *"Principles of Bone Biology"* pp. 471-94.: Academic Press.
- Becker L NE, Choen R, Silva OL, Snider RH. 1995. Calcitonin gene family of peptides. In *"Principles and Practice of Endocrinology and Metabolism"* pp. 474-83. Philadelphia.: JP Lippincott Co.
- Bell D, McDermott BJ. 2008. Intermedin (adrenomedullin-2): a novel counter-regulatory peptide in the cardiovascular and renal systems. *Br J Pharmacol* 153 Suppl 1: S247-62
- Bhanot P, Brink M, Samos CH, Hsieh JC, Wang Y, et al. 1996. A new member of the frizzled family from Drosophila functions as a Wntless receptor. *Nature* 382: 225-30
- Blair HC, Teitelbaum SL, Ghiselli R, Gluck S. 1989. Osteoclastic bone resorption by a polarized vacuolar proton pump. *Science* 245: 855-7
- Bomberger JM, Spielman WS, Hall CS, Weinman EJ, Parameswaran N. 2005. Receptor activity-modifying protein (RAMP) isoform-specific regulation of adrenomedullin receptor trafficking by NHERF-1. *J Biol Chem* 280: 23926-35

- Bonewald LF. 2011. The amazing osteocyte. *J Bone Miner Res* 26: 229-38
- Bouschet T, Martin S, Henley JM. 2005. Receptor-activity-modifying proteins are required for forward trafficking of the calcium-sensing receptor to the plasma membrane. *J Cell Sci* 118: 4709-20
- Bouxsein ML, Myers KS, Shultz KL, Donahue LR, Rosen CJ, Beamer WG. 2005. Ovariectomy-induced bone loss varies among inbred strains of mice. *J Bone Miner Res* 20: 1085-92
- Boyle WJ, Simonet WS, Lacey DL. 2003. Osteoclast differentiation and activation. *Nature* 423: 337-42
- Brain SD, Williams TJ, Tippins JR, Morris HR, MacIntyre I. 1985. Calcitonin gene-related peptide is a potent vasodilator. *Nature* 313: 54-6
- Bronsky J, Prusa R, Nevorol J. 2006. The role of amylin and related peptides in osteoporosis. *Clin Chim Acta* 373: 9-16
- Buckley RR. 2002. *CONTRIBUTIONS OF THE 3' HOX GENES, HOXA1, HOXB1, AND HOXB2, TO PATTERNING OF THE AXIAL SKELETON DURING DEVELOPMENT*. University of Kansas, Kansas
- Bustin SA, Benes V, Garson JA, Hellemans J, Huggett J, et al. 2009. The MIQE guidelines: minimum information for publication of quantitative real-time PCR experiments. *Clinical chemistry* 55: 611-22
- C. R. Kemp MH, E. Willems, D. Wawrzak, M. Metioui, L. Leyns. 2007. The Roles of Wnt Signaling in Early Mouse Development and Embryonic Stem Cells. *Functional Development and Embryology* 1: 1-13
- Calvi LM, Sims NA, Hunzelman JL, Knight MC, Giovannetti A, et al. 2001. Activated parathyroid hormone/parathyroid hormone-related protein receptor in osteoblastic cells differentially affects cortical and trabecular bone. *J Clin Invest* 107: 277-86
- Cameron VA, Fleming AM. 1998. Novel sites of adrenomedullin gene expression in mouse and rat tissues. *Endocrinology* 139: 2253-64
- Canalis E. 1983. Effect of hormones and growth factors on alkaline phosphatase activity and collagen synthesis in cultured rat calvariae. *Metabolism: clinical and experimental* 32: 14-20
- Caron KM, Smithies O. 2001. Extreme hydrops fetalis and cardiovascular abnormalities in mice lacking a functional Adrenomedullin gene. *Proc Natl Acad Sci U S A* 98: 615-9

- Castle AL, Kuo CH, Ivy JL. 1998. Amylin influences insulin-stimulated glucose metabolism by two independent mechanisms. *Am J Physiol* 274: E6-12
- Chambers TJ, Magnus CJ. 1982. Calcitonin alters behaviour of isolated osteoclasts. *J Pathol* 136: 27-39
- Chan YF, O WS, Tang F. 2008a. Adrenomedullin in the rat testis. I: Its production, actions on testosterone secretion, regulation by human chorionic gonadotropin, and its interaction with endothelin 1 in the leydig cell. *Biol Reprod* 78: 773-9
- Chan YF, Tang F, O WS. 2008b. Adrenomedullin in the rat testis. II: Its production, actions on inhibin secretion, regulation by follicle-stimulating hormone, and its interaction with endothelin 1 in the Sertoli cell. *Biol Reprod* 78: 780-5
- Chang W, Tu C, Chen TH, Bikle D, Shoback D. 2008. The extracellular calcium-sensing receptor (CaSR) is a critical modulator of skeletal development. *Science signaling* 1: ra1
- Chen D, Harris MA, Rossini G, Dunstan CR, Dallas SL, et al. 1997a. Bone morphogenetic protein 2 (BMP-2) enhances BMP-3, BMP-4, and bone cell differentiation marker gene expression during the induction of mineralized bone matrix formation in cultures of fetal rat calvarial osteoblasts. *Calcif Tissue Int* 60: 283-90
- Chen G, Deng C, Li YP. 2012. TGF-beta and BMP signaling in osteoblast differentiation and bone formation. *International journal of biological sciences* 8: 272-88
- Chen WJ, Armour S, Way J, Chen G, Watson C, et al. 1997b. Expression cloning and receptor pharmacology of human calcitonin receptors from MCF-7 cells and their relationship to amylin receptors. *Mol Pharmacol* 52: 1164-75
- Christiansen C. 1990. Hormonal prevention and treatment of osteoporosis--state of the art 1990. *The Journal of steroid biochemistry and molecular biology* 37: 447-9
- Christopoulos A, Christopoulos G, Morfis M, Udawela M, Laburthe M, et al. 2003. Novel receptor partners and function of receptor activity-modifying proteins. *J Biol Chem* 278: 3293-7
- Christopoulos G, Perry KJ, Morfis M, Tilakaratne N, Gao Y, et al. 1999. Multiple amylin receptors arise from receptor activity-modifying protein interaction with the calcitonin receptor gene product. *Molecular pharmacology* 56: 235-42
- Clausen T. 2000. Effects of amylin and other peptide hormones on Na⁺-K⁺ transport and contractility in rat skeletal muscle. *J Physiol* 527 Pt 1: 121-30
- Clementi G, Caruso A, Cutuli VM, de Bernardis E, Prato A, Amico-Roxas M. 1996. Amylin given by central or peripheral routes decreases gastric emptying and intestinal transit in the rat. *Experientia* 52: 677-9

- Clevers H, Nusse R. 2012. Wnt/beta-catenin signaling and disease. *Cell* 149: 1192-205
- Cockcroft JR, Noon JP, Gardner-Medwin J, Bennett T. 1997. Haemodynamic effects of adrenomedullin in human resistance and capacitance vessels. *Br J Clin Pharmacol* 44: 57-60
- Compston J. 2011. Pathophysiology of atypical femoral fractures and osteonecrosis of the jaw. *Osteoporosis international : a journal established as result of cooperation between the European Foundation for Osteoporosis and the National Osteoporosis Foundation of the USA* 22: 2951-61
- Confavreux CB, Fontana A, Guastalla JP, Munoz F, Brun J, Delmas PD. 2007. Estrogen-dependent increase in bone turnover and bone loss in postmenopausal women with breast cancer treated with anastrozole. Prevention with bisphosphonates. *Bone* 41: 346-52
- Cooper GJ, Willis AC, Clark A, Turner RC, Sim RB, Reid KB. 1987. Purification and characterization of a peptide from amyloid-rich pancreases of type 2 diabetic patients. *Proc Natl Acad Sci U S A* 84: 8628-32
- Copp DH, Cheney B. 1962. Calcitonin-a hormone from the parathyroid which lowers the calcium-level of the blood. *Nature* 193: 381-2
- Cornish J, Callon KE, Bava U, Coy DH, Mulvey TB, et al. 2001. Systemic administration of adrenomedullin(27-52) increases bone volume and strength in male mice. *J Endocrinol* 170: 251-7
- Cornish J, Callon KE, Cooper GJ, Reid IR. 1995. Amylin stimulates osteoblast proliferation and increases mineralized bone volume in adult mice. *Biochem Biophys Res Commun* 207: 133-9
- Cornish J, Callon KE, Coy DH, Jiang NY, Xiao L, et al. 1997. Adrenomedullin is a potent stimulator of osteoblastic activity in vitro and in vivo. *Am J Physiol* 273: E1113-20
- Cornish J, Callon KE, Gasser JA, Bava U, Gardiner EM, et al. 2000. Systemic administration of a novel octapeptide, amylin-(1---8), increases bone volume in male mice. *Am J Physiol Endocrinol Metab* 279: E730-5
- Cornish J, Callon KE, King AR, Cooper GJ, Reid IR. 1998a. Systemic administration of amylin increases bone mass, linear growth, and adiposity in adult male mice. *The American journal of physiology* 275: E694-9
- Cornish J, Callon KE, Lin CQ, Xiao CL, Gamble GD, et al. 1999. Comparison of the effects of calcitonin gene-related peptide and amylin on osteoblasts. *J Bone Miner Res* 14: 1302-9

- Cornish J, Callon KE, Lin CQ, Xiao CL, Mulvey TB, et al. 1998b. Dissociation of the effects of amylin on osteoblast proliferation and bone resorption. *Am J Physiol* 274: E827-33
- Cornish J, Grey A, Callon KE, Naot D, Hill BL, et al. 2004. Shared pathways of osteoblast mitogenesis induced by amylin, adrenomedullin, and IGF-1. *Biochem Biophys Res Commun* 318: 240-6
- Cornish J, Naot D, Reid IR. 2003. Adrenomedullin--a regulator of bone formation. *Regul Pept* 112: 79-86
- Cornish J, Reid IR. 2001. Effects of amylin and adrenomedullin on the skeleton. *J Musculoskelet Neuronal Interact* 2: 15-24
- Dackor R, Fritz-Six K, Smithies O, Caron K. 2007. Receptor activity-modifying proteins 2 and 3 have distinct physiological functions from embryogenesis to old age. *The Journal of biological chemistry* 282: 18094-9
- Dackor RT, Fritz-Six K, Dunworth WP, Gibbons CL, Smithies O, Caron KM. 2006. Hydrops fetalis, cardiovascular defects, and embryonic lethality in mice lacking the calcitonin receptor-like receptor gene. *Mol Cell Biol* 26: 2511-8
- Dacquin R, Davey RA, Laplace C, Levasseur R, Morris HA, et al. 2004. Amylin inhibits bone resorption while the calcitonin receptor controls bone formation in vivo. *J Cell Biol* 164: 509-14
- Datta NS, Samra TA, Mahalingam CD, Datta T, Abou-Samra AB. 2010. Role of PTH1R internalization in osteoblasts and bone mass using a phosphorylation-deficient knock-in mouse model. *J Endocrinol* 207: 355-65
- Davey RA, Moore AJ, Chiu MW, Notini AJ, Morris HA, Zajac JD. 2006. Effects of amylin deficiency on trabecular bone in young mice are sex-dependent. *Calcif Tissue Int* 78: 398-403
- Davey RA, Turner AG, McManus JF, Chiu WS, Tjahjono F, et al. 2008. Calcitonin receptor plays a physiological role to protect against hypercalcemia in mice. *J Bone Miner Res* 23: 1182-93
- Day TF, Guo X, Garrett-Beal L, Yang Y. 2005. Wnt/beta-catenin signaling in mesenchymal progenitors controls osteoblast and chondrocyte differentiation during vertebrate skeletogenesis. *Developmental cell* 8: 739-50
- de Koning EJ, Morris ER, Hofhuis FM, Posthuma G, Hoppener JW, et al. 1994. Intra- and extracellular amyloid fibrils are formed in cultured pancreatic islets of transgenic mice expressing human islet amyloid polypeptide. *Proc Natl Acad Sci U S A* 91: 8467-71

- Deal C, Gideon J. 2003. Recombinant human PTH 1-34 (Forteo): an anabolic drug for osteoporosis. *Cleveland Clinic journal of medicine* 70: 585-6, 89-90, 92-4 passim
- Deems RO, Deacon RW, Young DA. 1991. Amylin activates glycogen phosphorylase and inactivates glycogen synthase via a cAMP-independent mechanism. *Biochem Biophys Res Commun* 174: 716-20
- Delmas PD, Demiaux B, Malaval L, Chapuy MC, Meunier PJ. 1986. [Osteocalcin (or bone gla-protein), a new biological marker for studying bone pathology]. *Presse medicale* 15: 643-6
- Dempster DW, Cosman F, Parisien M, Shen V, Lindsay R. 1993. Anabolic actions of parathyroid hormone on bone. *Endocr Rev* 14: 690-709
- Dequeker J, Geusens P. 1989. Osteoporosis: a modern disease. *Acta clinica Belgica* 44: 215-20
- Ducy P, Schinke T, Karsenty G. 2000. The osteoblast: a sophisticated fibroblast under central surveillance. *Science* 289: 1501-4
- Ducy P, Zhang R, Geoffroy V, Ridall AL, Karsenty G. 1997. Osf2/Cbfa1: a transcriptional activator of osteoblast differentiation. *Cell* 89: 747-54
- Ellegaard M, Thorkildsen C, Petersen S, Petersen JS, Jorgensen NR, et al. 2010. Amylin(1-8) is devoid of anabolic activity in bone. *Calcif Tissue Int* 86: 249-60
- Enlow D. 1962. Function of the Haversian System
- Eriksen EF, Colvard DS, Berg NJ, Graham ML, Mann KG, et al. 1988. Evidence of estrogen receptors in normal human osteoblast-like cells. *Science* 241: 84-6
- Ettinger B, Pressman A, Schein J. 1998. Clinic visits and hospital admissions for care of acid-related upper gastrointestinal disorders in women using alendronate for osteoporosis. *The American journal of managed care* 4: 1377-82
- European-Medicines-Agency. 20 July 2012. European Medicines Agency recommends limiting long term used of calcitonin medicines
- Evans RM, Amara S, Rosenfeld MG. 1983. Molecular events in developmental regulation of neuroendocrine genes: characterization of the novel neuropeptide CGRP. *Cold Spring Harb Symp Quant Biol* 48 Pt 1: 413-7
- Farnum CE, Wilsman NJ. 1993. Determination of proliferative characteristics of growth plate chondrocytes by labeling with bromodeoxyuridine. *Calcif Tissue Int* 52: 110-9
- Fermor B, Skerry TM. 1995. PTH/PTHrP receptor expression on osteoblasts and osteocytes but not resorbing bone surfaces in growing rats. *J Bone Miner Res* 10: 1935-43

- Ferrier GJ, Pierson AM, Jones PM, Bloom SR, Girgis SI, Legon S. 1989. Expression of the rat amylin (IAPP/DAP) gene. *J Mol Endocrinol* 3: R1-4
- Findlay DM, Sexton PM. 2004. Calcitonin. *Growth Factors* 22: 217-24
- Fink JS, Verhave M, Kasper S, Tsukada T, Mandel G, Goodman RH. 1988. The CGTCA sequence motif is essential for biological activity of the vasoactive intestinal peptide gene cAMP-regulated enhancer. *Proc Natl Acad Sci U S A* 85: 6662-6
- Flahaut M, Pfister C, Rossier BC, Firsov D. 2003. N-Glycosylation and conserved cysteine residues in RAMP3 play a critical role for the functional expression of CRLR/RAMP3 adrenomedullin receptor. *Biochemistry* 42: 10333-41
- Fletcher S, Jones RG, Rayner HC, Harnden P, Hordon LD, et al. 1997. Assessment of renal osteodystrophy in dialysis patients: use of bone alkaline phosphatase, bone mineral density and parathyroid ultrasound in comparison with bone histology. *Nephron* 75: 412-9
- Fluhmann B, Muff R, Hunziker W, Fischer JA, Born W. 1995. A human orphan calcitonin receptor-like structure. *Biochem Biophys Res Commun* 206: 341-7
- Foord SM, Topp SD, Abramo M, Holbrook JD. 2005. New methods for researching accessory proteins. *J Mol Neurosci* 26: 265-76
- Forrest SM, Ng KW, Findlay DM, Michelangeli VP, Livesey SA, et al. 1985. Characterization of an osteoblast-like clonal cell line which responds to both parathyroid hormone and calcitonin. *Calcif Tissue Int* 37: 51-6
- Franz-Odenaal TA, Hall BK, Witten PE. 2006. Buried alive: how osteoblasts become osteocytes. *Developmental dynamics : an official publication of the American Association of Anatomists* 235: 176-90
- Franzoso G, Carlson L, Xing L, Poljak L, Shores EW, et al. 1997. Requirement for NF-kappaB in osteoclast and B-cell development. *Genes & development* 11: 3482-96
- Fraser NJ, Wise A, Brown J, McLatchie LM, Main MJ, Foord SM. 1999. The amino terminus of receptor activity modifying proteins is a critical determinant of glycosylation state and ligand binding of calcitonin receptor-like receptor. *Mol Pharmacol* 55: 1054-9
- Frost HM. 1991. Some ABC's of skeletal pathophysiology. 7. Tissue mechanisms controlling bone mass. *Calcif Tissue Int* 49: 303-4
- Gagel RF, Hoff AO, Huang SE, GJ C. 2007. Deletion of Calcitonin/CGRP gene causes a profound cortical resorption phenotype in mice. *J Bone Miner Res* 22: S1:S35

- Gebre-Medhin S, Mulder H, Pekny M, Westermark G, Tornell J, et al. 1998. Increased insulin secretion and glucose tolerance in mice lacking islet amyloid polypeptide (amylin). *Biochem Biophys Res Commun* 250: 271-7
- German MS, Moss LG, Wang J, Rutter WJ. 1992. The insulin and islet amyloid polypeptide genes contain similar cell-specific promoter elements that bind identical beta-cell nuclear complexes. *Mol Cell Biol* 12: 1777-88
- Ghatei MA, Gu J, Mulderry PK, Blank MA, Allen JM, et al. 1985. Calcitonin gene-related peptide (CGRP) in the female rat urogenital tract. *Peptides* 6: 809-15
- Glass DA, 2nd, Bialek P, Ahn JD, Starbuck M, Patel MS, et al. 2005. Canonical Wnt signaling in differentiated osteoblasts controls osteoclast differentiation. *Developmental cell* 8: 751-64
- Gorn AH, Lin HY, Yamin M, Auron PE, Flannery MR, et al. 1992. Cloning, characterization, and expression of a human calcitonin receptor from an ovarian carcinoma cell line. *The Journal of clinical investigation* 90: 1726-35
- Gothlin G, Ericsson JL. 1976. The osteoclast: review of ultrastructure, origin, and structure-function relationship. *Clin Orthop Relat Res*: 201-31
- Granholm S, Lundberg P, Lerner UH. 2008. Expression of the calcitonin receptor, calcitonin receptor-like receptor, and receptor activity modifying proteins during osteoclast differentiation. *J Cell Biochem* 104: 920-33
- Green J, Goldsbury C, Mini T, Sunderji S, Frey P, et al. 2003. Full-length rat amylin forms fibrils following substitution of single residues from human amylin. *J Mol Biol* 326: 1147-56
- Grigoriadis AE, Wang ZQ, Cecchini MG, Hofstetter W, Felix R, et al. 1994. c-Fos: a key regulator of osteoclast-macrophage lineage determination and bone remodeling. *Science* 266: 443-8
- Hakeda Y, Nakatani Y, Hiramatsu M, Kurihara N, Tsunoi M, et al. 1985. Inductive effects of prostaglandins on alkaline phosphatase in osteoblastic cells, clone MC3T3-E1. *Journal of biochemistry* 97: 97-104
- Harmar AJ. 2001. Family-B G-protein-coupled receptors. *Genome Biol* 2: REVIEWS3013
- Hattersley G, Chambers TJ. 1989. Calcitonin receptors as markers for osteoclastic differentiation: correlation between generation of bone-resorptive cells and cells that express calcitonin receptors in mouse bone marrow cultures. *Endocrinology* 125: 1606-12
- Hauschka PV. 1986. Osteocalcin: the vitamin K-dependent Ca²⁺-binding protein of bone matrix. *Haemostasis* 16: 258-72

- Hay DL, Christopoulos G, Christopoulos A, Sexton PM. 2006. Determinants of 1-piperidinecarboxamide, N-[2-[[5-amino-1-[[4-(4-pyridinyl)-1-piperazinyl]carbonyl]pentyl]amino]-1-[(3,5-dibromo-4-hydroxyphenyl)methyl]-2-oxoethyl]-4-(1,4-dihydro-2-oxo-3(2H)-quinazoliny 1) (BIBN4096BS) affinity for calcitonin gene-related peptide and amylin receptors--the role of receptor activity modifying protein 1. *Mol Pharmacol* 70: 1984-91
- Hay DL, Howitt SG, Conner AC, Schindler M, Smith DM, Poyner DR. 2003. CL/RAMP2 and CL/RAMP3 produce pharmacologically distinct adrenomedullin receptors: a comparison of effects of adrenomedullin22-52, CGRP8-37 and BIBN4096BS. *Br J Pharmacol* 140: 477-86
- Hertwig P. 1942. Neue Mutationen und Kopplungsgruppen bei der Hausmaus. *z. Indukt. Abstammungs- und Vererbungslehre* 80: 220-46
- Hewitt SC, Collins J, Grissom S, Deroo B, Korach KS. 2005. Global uterine genomics in vivo: microarray evaluation of the estrogen receptor alpha-growth factor cross-talk mechanism. *Mol Endocrinol* 19: 657-68
- Higgins DG, Sharp PM. 1988. CLUSTAL: a package for performing multiple sequence alignment on a microcomputer. *Gene* 73: 237-44
- Hilairt S, Belanger C, Bertrand J, Laperriere A, Foord SM, Bouvier M. 2001a. Agonist-promoted internalization of a ternary complex between calcitonin receptor-like receptor, receptor activity-modifying protein 1 (RAMP1), and beta-arrestin. *J Biol Chem* 276: 42182-90
- Hilairt S, Foord SM, Marshall FH, Bouvier M. 2001b. Protein-protein interaction and not glycosylation determines the binding selectivity of heterodimers between the calcitonin receptor-like receptor and the receptor activity-modifying proteins. *J Biol Chem* 276: 29575-81
- Hill PA. 1998. Bone remodelling. *British journal of orthodontics* 25: 101-7
- Hinson JP, Kapas S, Smith DM. 2000. Adrenomedullin, a multifunctional regulatory peptide. *Endocr Rev* 21: 138-67
- Hirata Y, Hayakawa H, Suzuki Y, Suzuki E, Ikenouchi H, et al. 1995. Mechanisms of adrenomedullin-induced vasodilation in the rat kidney. *Hypertension* 25: 790-5
- Hoff AO, Catala-Lehnen P, Thomas PM, Priemel M, Rueger JM, et al. 2002. Increased bone mass is an unexpected phenotype associated with deletion of the calcitonin gene. *J Clin Invest* 110: 1849-57

- Horcajada-Molteni MN, Davicco MJ, Lebecque P, Coxam V, Young AA, Barlet JP. 2000. Amylin inhibits ovariectomy-induced bone loss in rats. *J Endocrinol* 165: 663-8
- Hori M, Uzawa T, Morita K, Noda T, Takahashi H, Inoue J. 1988. Effect of human parathyroid hormone (PTH(1-34)) on experimental osteopenia of rats induced by ovariectomy. *Bone and mineral* 3: 193-9
- Horton WA, Machado MM. 1988. Extracellular matrix alterations during endochondral ossification in humans. *Journal of orthopaedic research : official publication of the Orthopaedic Research Society* 6: 793-803
- Houssami S, Findlay DM, Brady CL, Myers DE, Martin TJ, Sexton PM. 1994. Isoforms of the rat calcitonin receptor: consequences for ligand binding and signal transduction. *Endocrinology* 135: 183-90
- Ichikawa-Shindo Y, Sakurai T, Kamiyoshi A, Kawate H, Inuma N, et al. 2008. The GPCR modulator protein RAMP2 is essential for angiogenesis and vascular integrity. *J Clin Invest* 118: 29-39
- Iida-Klein A, Yee DC, Brandli DW, Mirikitani EJ, Hahn TJ. 1992. Effects of calcitonin on 3',5'-cyclic adenosine monophosphate and calcium second messenger generation and osteoblast function in UMR 106-06 osteoblast-like cells. *Endocrinology* 130: 381-8
- Ikegame M, Rakopoulos M, Zhou H, Houssami S, Martin TJ, et al. 1995. Calcitonin receptor isoforms in mouse and rat osteoclasts. *J Bone Miner Res* 10: 59-65
- Iozzo RV. 1998. Matrix proteoglycans: from molecular design to cellular function. *Annual review of biochemistry* 67: 609-52
- Ishizuya T, Yokose S, Hori M, Noda T, Suda T, et al. 1997. Parathyroid hormone exerts disparate effects on osteoblast differentiation depending on exposure time in rat osteoblastic cells. *J Clin Invest* 99: 2961-70
- Jones CD, Jevnikar MG, Pike AJ, Peters MK, Black LJ, et al. 1984. Antiestrogens. 2. Structure-activity studies in a series of 3-aryl-2-arylbenzo[b]thiophene derivatives leading to [6-hydroxy-2-(4-hydroxyphenyl)benzo[b]thien-3-yl] [4-[2-(1-piperidinyl)ethoxy]-phenyl]methanone hydrochloride (LY156758), a remarkably effective estrogen antagonist with only minimal intrinsic estrogenicity. *Journal of medicinal chemistry* 27: 1057-66
- Jonsson KB, Frost A, Nilsson O, Ljunghall S, Ljunggren O. 1999. Three isolation techniques for primary culture of human osteoblast-like cells: a comparison. *Acta orthopaedica Scandinavica* 70: 365-73

- Kadmiel M, Fritz-Six K, Pacharne S, Richards GO, Li M, et al. 2011. Research resource: Haploinsufficiency of receptor activity-modifying protein-2 (RAMP2) causes reduced fertility, hyperprolactinemia, skeletal abnormalities, and endocrine dysfunction in mice. *Mol Endocrinol* 25: 1244-53
- Kadmiel M, Fritz-Six KL, Caron KM. 2012. Understanding RAMPs through genetically engineered mouse models. *Advances in experimental medicine and biology* 744: 49-60
- Kaji H, Sugimoto T, Kanatani M, Nasu M, Chihara K. 1996. Estrogen blocks parathyroid hormone (PTH)-stimulated osteoclast-like cell formation by selectively affecting PTH-responsive cyclic adenosine monophosphate pathway. *Endocrinology* 137: 2217-24
- Kanatsuka A, Makino H, Ohsawa H, Tokuyama Y, Yamaguchi T, et al. 1989. Secretion of islet amyloid polypeptide in response to glucose. *FEBS Lett* 259: 199-201
- Kano H, Kohno M, Yasunari K, Yokokawa K, Horio T, et al. 1996. Adrenomedullin as a novel antiproliferative factor of vascular smooth muscle cells. *J Hypertens* 14: 209-13
- Kapas S, Catt KJ, Clark AJ. 1995. Cloning and expression of cDNA encoding a rat adrenomedullin receptor. *J Biol Chem* 270: 25344-7
- Karsenty G, Ferron M. 2012. The contribution of bone to whole-organism physiology. *Nature* 481: 314-20
- Kawase T, Okuda K, Burns DM. 2003. Immature human osteoblastic MG63 cells predominantly express a subtype 1-like CGRP receptor that inactivates extracellular signal response kinase by a cAMP-dependent mechanism. *European journal of pharmacology* 470: 125-37
- Kenny PA, Enver T, Ashworth A. 2005. Receptor and secreted targets of Wnt-1/beta-catenin signalling in mouse mammary epithelial cells. *BMC cancer* 5: 3
- Khosla S, Melton LJ, 3rd, Riggs BL. 1999. Osteoporosis: gender differences and similarities. *Lupus* 8: 393-6
- Kitamura K, Kangawa K, Eto T. 2002. Adrenomedullin and PAMP: discovery, structures, and cardiovascular functions. *Microsc Res Tech* 57: 3-13
- Kitamura K, Kangawa K, Ishiyama Y, Washimine H, Ichiki Y, et al. 1994. Identification and hypotensive activity of proadrenomedullin N-terminal 20 peptide (PAMP). *FEBS Lett* 351: 35-7
- Kitamura K, Kangawa K, Kawamoto M, Ichiki Y, Nakamura S, et al. 1993a. Adrenomedullin: a novel hypotensive peptide isolated from human pheochromocytoma. *Biochem Biophys Res Commun* 192: 553-60

- Kitamura K, Sakata J, Kangawa K, Kojima M, Matsuo H, Eto T. 1993b. Cloning and characterization of cDNA encoding a precursor for human adrenomedullin. *Biochem Biophys Res Commun* 194: 720-5
- Kleerekoper M, Villanueva AR, Stanciu J, Rao DS, Parfitt AM. 1985. The role of three-dimensional trabecular microstructure in the pathogenesis of vertebral compression fractures. *Calcified tissue international* 37: 594-7
- Klein-Nulens Ba. 2003. *Bone Research Protocols*. pp. 19-28. Humana Press.
- Klibanski. 2001. NIH Consensus Development Panel on Osteoporosis. *JAMA* 285: 785-95
- Knothe Tate ML, Adamson JR, Tami AE, Bauer TW. 2004. The osteocyte. *The international journal of biochemistry & cell biology* 36: 1-8
- Komori T. 2006. Regulation of osteoblast differentiation by transcription factors. *J Cell Biochem* 99: 1233-9
- Kornenberg H. 2005. How PTHrP controls growth plate chondrocytes. *IBMS BoneKEy* 2: 7-15
- Kraenzlin ME, Ch'ng JL, Mulderry PK, Ghatei MA, Bloom SR. 1985. Infusion of a novel peptide, calcitonin gene-related peptide (CGRP) in man. Pharmacokinetics and effects on gastric acid secretion and on gastrointestinal hormones. *Regul Pept* 10: 189-97
- Kuestner RE, Elrod RD, Grant FJ, Hagen FS, Kuijper JL, et al. 1994. Cloning and characterization of an abundant subtype of the human calcitonin receptor. *Mol Pharmacol* 46: 246-55
- Kung AW. 2003. Androgen and bone mass in men. *Asian journal of andrology* 5: 148-54
- Kutz WE, Gong Y, Warman ML. 2005. WISP3, the gene responsible for the human skeletal disease progressive pseudorheumatoid dysplasia, is not essential for skeletal function in mice. *Mol Cell Biol* 25: 414-21
- Lacey DL, Timms E, Tan HL, Kelley MJ, Dunstan CR, et al. 1998. Osteoprotegerin ligand is a cytokine that regulates osteoclast differentiation and activation. *Cell* 93: 165-76
- Lane NE, Kelman A. 2003. A review of anabolic therapies for osteoporosis. *Arthritis research & therapy* 5: 214-22
- Leffert JD, Newgard CB, Okamoto H, Milburn JL, Luskey KL. 1989. Rat amylin: cloning and tissue-specific expression in pancreatic islets. *Proc Natl Acad Sci U S A* 86: 3127-30
- Leighton B, Foot E. 1990. The effects of amylin on carbohydrate metabolism in skeletal muscle in vitro and in vivo. *Biochem J* 269: 19-23
- Lerner UH. 2006. Deletions of genes encoding calcitonin/alpha-CGRP, amylin and calcitonin receptor have given new and unexpected insights into the function of calcitonin receptors and calcitonin receptor-like receptors in bone. *J Musculoskelet Neuronal Interact* 6: 87-95

- Levasseur R, Kato M.,Patel M.S.,Chan L., Karsenty G. . 2001. Low bone mass, low body weight and abnormal eye vascularization in mice in LRP5, the gene mutaed in human osteoporosis pseudoglioma syndrome. *J Bone Miner Res* 16: s152
- Lewiecki EM. 2004. Management of osteoporosis. *Clinical and molecular allergy : CMA* 2: 9
- Li L, Tang F, O WS. 2010. Coexpression of adrenomedullin and its receptor component proteins in the reproductive system of the rat during gestation. *Reprod Biol Endocrinol* 8: 130
- Li YY, Li L, Hwang IS, Tang F, O WS. 2008. Coexpression of adrenomedullin and its receptors in the reproductive system of the rat: effects on steroid secretion in rat ovary. *Biol Reprod* 79: 200-8
- Lin HY, Harris TL, Flannery MS, Aruffo A, Kaji EH, et al. 1991. Expression cloning and characterization of a porcine renal calcitonin receptor. *Transactions of the Association of American Physicians* 104: 265-72
- Lindsay R, Hart DM, Aitken JM, MacDonald EB, Anderson JB, Clarke AC. 1976. Long-term prevention of postmenopausal osteoporosis by oestrogen. Evidence for an increased bone mass after delayed onset of oestrogen treatment. *Lancet* 1: 1038-41
- Love RR, Mazess RB, Barden HS, Epstein S, Newcomb PA, et al. 1992. Effects of tamoxifen on bone mineral density in postmenopausal women with breast cancer. *The New England journal of medicine* 326: 852-6
- Luckman SP, Hughes DE, Coxon FP, Graham R, Russell G, Rogers MJ. 1998. Nitrogen-containing bisphosphonates inhibit the mevalonate pathway and prevent post-translational prenylation of GTP-binding proteins, including Ras. *J Bone Miner Res* 13: 581-9
- Lufkin EG. 1992. Therapeutic alternatives for postmenopausal osteoporosis. *Comprehensive therapy* 18: 14-7
- Lufkin EG, Wahner HW, O'Fallon WM, Hodgson SF, Kotowicz MA, et al. 1992. Treatment of postmenopausal osteoporosis with transdermal estrogen. *Annals of internal medicine* 117: 1-9
- Lukert BP. 1992. Glucocorticoid-induced osteoporosis. *Southern medical journal* 85: 2S48-51
- Lukert BP, Johnson BE, Robinson RG. 1992. Estrogen and progesterone replacement therapy reduces glucocorticoid-induced bone loss. *J Bone Miner Res* 7: 1063-9
- Lukinius A, Wilander E, Westermark GT, Engstrom U, Westermark P. 1989. Co-localization of islet amyloid polypeptide and insulin in the B cell secretory granules of the human pancreatic islets. *Diabetologia* 32: 240-4

- Lutz TA, Del Prete E, Scharrer E. 1994. Reduction of food intake in rats by intraperitoneal injection of low doses of amylin. *Physiol Behav* 55: 891-5
- Mackie EJ. 2003. Osteoblasts: novel roles in orchestration of skeletal architecture. *The international journal of biochemistry & cell biology* 35: 1301-5
- Manolagas SC. 2000. Birth and death of bone cells: basic regulatory mechanisms and implications for the pathogenesis and treatment of osteoporosis. *Endocr Rev* 21: 115-37
- Marie PJ. 2003. Fibroblast growth factor signaling controlling osteoblast differentiation. *Gene* 316: 23-32
- Marie PJ, Hott M, Modrowski D, De Pollak C, Guillemain J, et al. 1993. An uncoupling agent containing strontium prevents bone loss by depressing bone resorption and maintaining bone formation in estrogen-deficient rats. *J Bone Miner Res* 8: 607-15
- Marotti G, Zallone AZ, Ledda M. 1976. Number, size and arrangement of osteoblasts in osteons at different stages of formation. *Calcified tissue research* 21 Suppl: 96-101
- Martin TJ, Findlay DM, Houssami S, Ikegame M, Rakopoulos M, et al. 1995. Heterogeneity of the calcitonin receptor: functional aspects in osteoclasts and other sites. *The Journal of nutrition* 125: 2009S-14S
- Mayahara H, Ito T, Nagai H, Miyajima H, Tsukuda R, et al. 1993. In vivo stimulation of endosteal bone formation by basic fibroblast growth factor in rats. *Growth Factors* 9: 73-80
- Mazzuoli G, Minisola S, Bianchi G, Pacitti MT, Rosso R, et al. 1990a. The effects of oophorectomy on skeletal metabolism. *The Journal of steroid biochemistry and molecular biology* 37: 457-9
- Mazzuoli GF, Tabolli S, Bigi F, Valtorta C, Minisola S, et al. 1990b. Effects of salmon calcitonin on the bone loss induced by ovariectomy. *Calcified tissue international* 47: 209-14
- McLatchie LM, Fraser NJ, Main MJ, Wise A, Brown J, et al. 1998. RAMPs regulate the transport and ligand specificity of the calcitonin-receptor-like receptor. *Nature* 393: 333-9
- Melton LJ, 3rd, Wahner HW, Richelson LS, O'Fallon WM, Riggs BL. 1986. Osteoporosis and the risk of hip fracture. *American journal of epidemiology* 124: 254-61
- Meunier PJ. 2004. [Strontium ranelate: new therapeutic agent for postmenopausal osteoporosis]. *Medecine sciences : M/S* 20: 631-3
- Meunier PJ, Roux C, Seeman E, Ortolani S, Badurski JE, et al. 2004. The effects of strontium ranelate on the risk of vertebral fracture in women with postmenopausal osteoporosis. *The New England journal of medicine* 350: 459-68

- Michelangeli VP, Fletcher AE, Allan EH, Nicholson GC, Martin TJ. 1989. Effects of calcitonin gene-related peptide on cyclic AMP formation in chicken, rat, and mouse bone cells. *J Bone Miner Res* 4: 269-72
- Millet I, Vignery A. 1997. The neuropeptide calcitonin gene-related peptide inhibits TNF-alpha but poorly induces IL-6 production by fetal rat osteoblasts. *Cytokine* 9: 999-1007
- Mohan S, Baylink DJ. 1991. Bone growth factors. *Clin Orthop Relat Res*: 30-48
- Morgulis A, Coulouris G, Raytselis Y, Madden TL, Agarwala R, Schaffer AA. 2008. Database indexing for production MegaBLAST searches. *Bioinformatics* 24: 1757-64
- Muff R, Buhlmann N, Fischer JA, Born W. 1999. An amylin receptor is revealed following co-transfection of a calcitonin receptor with receptor activity modifying proteins-1 or -3. *Endocrinology* 140: 2924-7
- Mulder H. 1993. Calcitonin-testosterone interrelationship. A classic feedback system? *Neth J Med* 42: 209-11
- Mulderry PK, Ghatei MA, Bishop AE, Allen YS, Polak JM, Bloom SR. 1985. Distribution and chromatographic characterisation of CGRP-like immunoreactivity in the brain and gut of the rat. *Regul Pept* 12: 133-43
- Nag K, Sultana N, Hirose S. 2012. Calcitonin receptor-like receptor (CLR) influences posttranslational events of receptor activity-modifying proteins (RAMPs). *Biochem Biophys Res Commun* 418: 824-9
- Nagasaki M, Doi A, Matsuno H, Miyano S. 2004. A versatile petri net based architecture for modeling and simulation of complex biological processes. *Genome Inform* 15: 180-97
- Nakagawa N, Kinoshita M, Yamaguchi K, Shima N, Yasuda H, et al. 1998. RANK is the essential signaling receptor for osteoclast differentiation factor in osteoclastogenesis. *Biochem Biophys Res Commun* 253: 395-400
- Nakamura M, Morimoto S, Yang Q, Hisamatsu T, Hanai N, et al. 2005. Osteoclast-like cells express receptor activity modifying protein 2: application of laser capture microdissection. *J Mol Endocrinol* 34: 257-61
- Naot D, Callon KE, Grey A, Cooper GJ, Reid IR, Cornish J. 2001. A potential role for adrenomedullin as a local regulator of bone growth. *Endocrinology* 142: 1849-57
- Naot D, Cornish J. 2008. The role of peptides and receptors of the calcitonin family in the regulation of bone metabolism. *Bone* 43: 813-8
- Neher R, Riniker B, Rittel W, Zuber H. 1968. [Human calcitonin. Structure of calcitonin M and D]. *Helv Chim Acta* 51: 1900-5

- Nesbitt SA, Horton MA. 1997. Trafficking of matrix collagens through bone-resorbing osteoclasts. *Science* 276: 266-9
- Nicholson GC, Moseley JM, Sexton PM, Mendelsohn FA, Martin TJ. 1986. Abundant calcitonin receptors in isolated rat osteoclasts. Biochemical and autoradiographic characterization. *J Clin Invest* 78: 355-60
- Nikitenko LL, Blucher N, Fox SB, Bicknell R, Smith DM, Rees MC. 2006. Adrenomedullin and CGRP interact with endogenous calcitonin-receptor-like receptor in endothelial cells and induce its desensitisation by different mechanisms. *J Cell Sci* 119: 910-22
- O'Connell JP, Kelly SM, Raleigh DP, Hubbard JA, Price NC, et al. 1993. On the role of the C-terminus of alpha-calcitonin-gene-related peptide (alpha CGRP). The structure of des-phenylalaninamide³⁷-alpha CGRP and its interaction with the CGRP receptor. *Biochem J* 291 (Pt 1): 205-10
- Odvina CV, Zerwekh JE, Rao DS, Maalouf N, Gottschalk FA, Pak CY. 2005. Severely suppressed bone turnover: a potential complication of alendronate therapy. *The Journal of clinical endocrinology and metabolism* 90: 1294-301
- Okazaki T, Ogawa Y, Tamura N, Mori K, Isse N, et al. 1996. Genomic organization, expression, and chromosomal mapping of the mouse adrenomedullin gene. *Genomics* 37: 395-9
- Pacharne S. 2008. *RAMPs potential role in regulation of bone mass and skeletal disorders*. University of Sheffield, Sheffield,UK
- Parameswaran N, Spielman WS. 2006. RAMPs: The past, present and future. *Trends Biochem Sci* 31: 631-8
- Parfitt AM, Drezner MK, Glorieux FH, Kanis JA, Malluche H, et al. 1987. Bone histomorphometry: standardization of nomenclature, symbols, and units. Report of the ASBMR Histomorphometry Nomenclature Committee. *J Bone Miner Res* 2: 595-610
- Parfitt AM, Mathews CH, Villanueva AR, Kleerekoper M, Frame B, Rao DS. 1983. Relationships between surface, volume, and thickness of iliac trabecular bone in aging and in osteoporosis. Implications for the microanatomic and cellular mechanisms of bone loss. *The Journal of clinical investigation* 72: 1396-409
- Patil SM, Xu S, Sheftic SR, Alexandrescu AT. 2009. Dynamic alpha-helix structure of micelle-bound human amylin. *J Biol Chem* 284: 11982-91
- Paz-Filho G, Mastronardi C, Franco CB, Wang KB, Wong ML, Licinio J. 2012. Leptin: molecular mechanisms, systemic pro-inflammatory effects, and clinical implications. *Arquivos brasileiros de endocrinologia e metabologia* 56: 597-607

- Pieber TR, Stein DT, Ogawa A, Alam T, Ohneda M, et al. 1993. Amylin-insulin relationships in insulin resistance with and without diabetic hyperglycemia. *Am J Physiol* 265: E446-53
- Pietschmann P, Farsoudi KH, Hoffmann O, Klaushofer K, Horandner H, Peterlik M. 1993. Inhibitory effect of amylin on basal and parathyroid hormone-stimulated bone resorption in cultured neonatal mouse calvaria. *Bone* 14: 167-72
- Pittner R, Beaumont K, Young A, Rink T. 1995. Dose-dependent elevation of cyclic AMP, activation of glycogen phosphorylase, and release of lactate by amylin in rat skeletal muscle. *Biochim Biophys Acta* 1267: 75-82
- Pittner RA, Albrandt K, Beaumont K, Gaeta LS, Koda JE, et al. 1994. Molecular physiology of amylin. *J Cell Biochem* 55 Suppl: 19-28
- Plummer NW, Spicher K, Malphurs J, Akiyama H, Abramowitz J, et al. 2012. Development of the mammalian axial skeleton requires signaling through the Galpha(i) subfamily of heterotrimeric G proteins. *Proc Natl Acad Sci U S A* 109: 21366-71
- Pondel M. 2000. Calcitonin and calcitonin receptors: bone and beyond. *International journal of experimental pathology* 81: 405-22
- Reddy DS, Bhatnagar-Mathur P, Cindhuri KS, Sharma KK. 2013. Evaluation and validation of reference genes for normalization of quantitative real-time PCR based gene expression studies in peanut. *PloS one* 8: e78555
- Redlich K, Smolen JS. 2012. Inflammatory bone loss: pathogenesis and therapeutic intervention. *Nature reviews. Drug discovery* 11: 234-50
- Riggs BL, Melton LJ, 3rd. 1986. Involutional osteoporosis. *The New England journal of medicine* 314: 1676-86
- Riggs BL, Melton LJ, 3rd. 1992. The prevention and treatment of osteoporosis. *The New England journal of medicine* 327: 620-7
- Riggs BL, Wahner HW, Seeman E, Offord KP, Dunn WL, et al. 1982. Changes in bone mineral density of the proximal femur and spine with aging. Differences between the postmenopausal and senile osteoporosis syndromes. *The Journal of clinical investigation* 70: 716-23
- Rodrigo J, Polak JM, Terenghi G, Cervantes C, Ghatei MA, et al. 1985. Calcitonin gene-related peptide (CGRP)-immunoreactive sensory and motor nerves of the mammalian palate. *Histochemistry* 82: 67-74
- Rogers MJ, Frith JC, Luckman SP, Coxon FP, Benford HL, et al. 1999. Molecular mechanisms of action of bisphosphonates. *Bone* 24: 73S-79S

- Rogers MJ, Ji X, Russell RG, Blackburn GM, Williamson MP, et al. 1994. Incorporation of bisphosphonates into adenine nucleotides by amoebae of the cellular slime mould *Dictyostelium discoideum*. *Biochem J* 303 (Pt 1): 303-11
- Rohrs S, Kutzner N, Vlad A, Grunwald T, Ziegler S, Muller O. 2009. Chronological expression of Wnt target genes *Ccnd1*, *Myc*, *Cdkn1a*, *Tfrc*, *Plf1* and *Ramp3*. *Cell biology international* 33: 501-8
- Rosenfeld MG, Mermod JJ, Amara SG, Swanson LW, Sawchenko PE, et al. 1983. Production of a novel neuropeptide encoded by the calcitonin gene via tissue-specific RNA processing. *Nature* 304: 129-35
- Ross GR, Chauhan M, Gangula PR, Reed L, Thota C, Yallampalli C. 2006. Female sex steroids increase adrenomedullin-induced vasodilation by increasing the expression of adrenomedullin2 receptor components in rat mesenteric artery. *Endocrinology* 147: 389-96
- Ross GR, Yallampalli U, Gangula PR, Reed L, Sathishkumar K, et al. 2010. Adrenomedullin relaxes rat uterine artery: mechanisms and influence of pregnancy and estradiol. *Endocrinology* 151: 4485-93
- Rubinfeld B, Souza B, Albert I, Muller O, Chamberlain SH, et al. 1993. Association of the APC gene product with beta-catenin. *Science* 262: 1731-4
- Russell RG, Rogers MJ. 1999. Bisphosphonates: from the laboratory to the clinic and back again. *Bone* 25: 97-106
- Saita M, Shimokawa A, Kunitake T, Kato K, Hanamori T, et al. 1998. Central actions of adrenomedullin on cardiovascular parameters and sympathetic outflow in conscious rats. *Am J Physiol* 274: R979-84
- Sakagami Y, Girasole G, Yu XP, Boswell HS, Manolagas SC. 1993. Stimulation of interleukin-6 production by either calcitonin gene-related peptide or parathyroid hormone in two phenotypically distinct bone marrow-derived murine stromal cell lines. *J Bone Miner Res* 8: 811-6
- Scheijen B, Bronk M, van der Meer T, Bernards R. 2003. Constitutive E2F1 overexpression delays endochondral bone formation by inhibiting chondrocyte differentiation. *Mol Cell Biol* 23: 3656-68
- Scutt A. RL, Scutt N., Still K. 2003. Bone Research Protocols. pp. 29-39: Humana Press
- Semenov MV, Tamai K, Brott BK, Kuhl M, Sokol S, He X. 2001. Head inducer Dickkopf-1 is a ligand for Wnt coreceptor LRP6. *Current biology : CB* 11: 951-61

- Semenov MV, Zhang X, He X. 2008. DKK1 antagonizes Wnt signaling without promotion of LRP6 internalization and degradation. *J Biol Chem* 283: 21427-32
- Sexton PM, Albiston A, Morfis M, Tilakaratne N. 2001. Receptor activity modifying proteins. *Cell Signal* 13: 73-83
- Sexton PM, Findlay DM, Martin TJ. 1999. Calcitonin. *Curr Med Chem* 6: 1067-93
- Sexton PM, Houssami S, Hilton JM, O'Keeffe LM, Center RJ, et al. 1993. Identification of brain isoforms of the rat calcitonin receptor. *Molecular endocrinology* 7: 815-21
- Shih C, Bernard GW. 1997. Calcitonin gene related peptide enhances bone colony development in vitro. *Clin Orthop Relat Res*: 335-44
- Shimekake Y, Nagata K, Ohta S, Kambayashi Y, Teraoka H, et al. 1995. Adrenomedullin stimulates two signal transduction pathways, cAMP accumulation and Ca²⁺ mobilization, in bovine aortic endothelial cells. *J Biol Chem* 270: 4412-7
- Shinki T, Ueno Y, DeLuca HF, Suda T. 1999. Calcitonin is a major regulator for the expression of renal 25-hydroxyvitamin D₃-1 α -hydroxylase gene in normocalcemic rats. *Proc Natl Acad Sci U S A* 96: 8253-8
- Simpson EM, Linder CC, Sargent EE, Davisson MT, Mobraaten LE, Sharp JJ. 1997. Genetic variation among 129 substrains and its importance for targeted mutagenesis in mice. *Nature genetics* 16: 19-27
- Sooy K, Sabbagh Y, Demay MB. 2005. Osteoblasts lacking the vitamin D receptor display enhanced osteogenic potential in vitro. *J Cell Biochem* 94: 81-7
- Soysa NS, Alles N, Aoki K, Ohya K. 2012. Osteoclast formation and differentiation: An overview. *Journal of medical and dental sciences* 59: 65-74
- St-Jacques B, Hammerschmidt M, McMahon AP. 1999. Indian hedgehog signaling regulates proliferation and differentiation of chondrocytes and is essential for bone formation. *Genes & development* 13: 2072-86
- Steenbergh PH, Hoppener JW, Zandberg J, Lips CJ, Jansz HS. 1985. A second human calcitonin/CGRP gene. *FEBS Lett* 183: 403-7
- Stein GS, Lian JB, van Wijnen AJ, Stein JL, Montecino M, et al. 2004. Runx2 control of organization, assembly and activity of the regulatory machinery for skeletal gene expression. *Oncogene* 23: 4315-29
- Stein LJBaGS. 1999. *Cells of Bone in Principles of Bone and Cartilage Metabolism*. pp. 165-185. San Diego: Academic Press.

- Steiner S, Born W, Fischer JA, Muff R. 2003. The function of conserved cysteine residues in the extracellular domain of human receptor-activity-modifying protein. *FEBS Lett* 555: 285-90
- Stephens AS, Stephens SR, Morrison NA. 2011. Internal control genes for quantitative RT-PCR expression analysis in mouse osteoblasts, osteoclasts and macrophages. *BMC research notes* 4: 410
- Storm T, Thamsborg G, Steiniche T, Genant HK, Sorensen OH. 1990. Effect of intermittent cyclical etidronate therapy on bone mass and fracture rate in women with postmenopausal osteoporosis. *The New England journal of medicine* 322: 1265-71
- Stothard P. 2000. The sequence manipulation suite: JavaScript programs for analyzing and formatting protein and DNA sequences. *BioTechniques* 28: 1102, 04
- Taichman RS, Emerson SG. 1994. Human osteoblasts support hematopoiesis through the production of granulocyte colony-stimulating factor. *The Journal of experimental medicine* 179: 1677-82
- Takahashi N, Yamana H, Yoshiki S, Roodman GD, Mundy GR, et al. 1988. Osteoclast-like cell formation and its regulation by osteotropic hormones in mouse bone marrow cultures. *Endocrinology* 122: 1373-82
- Takasu H, Gardella TJ, Luck MD, Potts JT, Jr., Bringhurst FR. 1999. Amino-terminal modifications of human parathyroid hormone (PTH) selectively alter phospholipase C signaling via the type 1 PTH receptor: implications for design of signal-specific PTH ligands. *Biochemistry* 38: 13453-60
- Tam CW, Husmann K, Clark NC, Clark JE, Lazar Z, et al. 2006. Enhanced vascular responses to adrenomedullin in mice overexpressing receptor-activity-modifying protein 2. *Circ Res* 98: 262-70
- Teti DV, Cavallaro A, Valenti A, Santarpia G, Sofo V, Misefari A. 1989. Effect of prostaglandin E2 on pokeweed mitogen-activated human lymphocyte cultures. *Immunopharmacology and immunotoxicology* 11: 687-700
- Thompson JD, Higgins DG, Gibson TJ. 1994. CLUSTAL W: improving the sensitivity of progressive multiple sequence alignment through sequence weighting, position-specific gap penalties and weight matrix choice. *Nucleic acids research* 22: 4673-80
- Tippins JR, Morris HR, Panico M, Etienne T, Bevis P, et al. 1984. The myotropic and plasma-calcium modulating effects of calcitonin gene-related peptide (CGRP). *Neuropeptides* 4: 425-34

- Tondravi MM, McKercher SR, Anderson K, Erdmann JM, Quiroz M, et al. 1997. Osteopetrosis in mice lacking haematopoietic transcription factor PU.1. *Nature* 386: 81-4
- Tsai JN, Uihlein AV, Lee H, Kumbhani R, Siwila-Sackman E, et al. 2013. Teriparatide and denosumab, alone or combined, in women with postmenopausal osteoporosis: the DATA study randomised trial. *Lancet* 382: 50-6
- Tschopp FA, Henke H, Petermann JB, Tobler PH, Janzer R, et al. 1985. Calcitonin gene-related peptide and its binding sites in the human central nervous system and pituitary. *Proc Natl Acad Sci U S A* 82: 248-52
- Tsujikawa K, Yayama K, Hayashi T, Matsushita H, Yamaguchi T, et al. 2007. Hypertension and dysregulated proinflammatory cytokine production in receptor activity-modifying protein 1-deficient mice. *Proc Natl Acad Sci U S A* 104: 16702-7
- Udagawa N, Takahashi N, Akatsu T, Tanaka H, Sasaki T, et al. 1990. Origin of osteoclasts: mature monocytes and macrophages are capable of differentiating into osteoclasts under a suitable microenvironment prepared by bone marrow-derived stromal cells. *Proceedings of the National Academy of Sciences of the United States of America* 87: 7260-4
- Une Y, Sato Y, Alam S, Nagabuchi E, Hata Y, Uchino J. 1993. [Effect of radio-immunochemotherapy-using antiferritin antibody combined with anthracycline drugs on hepatocellular carcinoma cell]. *Gan to kagaku ryoho. Cancer & chemotherapy* 20: 161-3
- Upton PD, Austin C, Taylor GM, Nandha KA, Clark AJ, et al. 1997. Expression of adrenomedullin (ADM) and its binding sites in the rat uterus: increased number of binding sites and ADM messenger ribonucleic acid in 20-day pregnant rats compared with nonpregnant rats. *Endocrinology* 138: 2508-14
- Uzan B, de Vernejoul MC, Cressent M. 2004. RAMPs and CRLR expressions in osteoblastic cells after dexamethasone treatment. *Biochemical and biophysical research communications* 321: 802-8
- Valentijn K, Gutow AP, Troiano N, Gundberg C, Gilligan JP, Vignery A. 1997. Effects of calcitonin gene-related peptide on bone turnover in ovariectomized rats. *Bone* 21: 269-74
- van Beek ER, Cohen LH, Leroy IM, Ebetino FH, Lowik CW, Papapoulos SE. 2003. Differentiating the mechanisms of antiresorptive action of nitrogen containing bisphosphonates. *Bone* 33: 805-11
- van Wijnen AJ, Stein GS, Gergen JP, Groner Y, Hiebert SW, et al. 2004. Nomenclature for Runt-related (RUNX) proteins. *Oncogene* 23: 4209-10

- Vandesompele J, De Preter K, Pattyn F, Poppe B, Van Roy N, et al. 2002. Accurate normalization of real-time quantitative RT-PCR data by geometric averaging of multiple internal control genes. *Genome Biol* 3: RESEARCH0034
- Vejlens L. 1971. Glycosaminoglycans of human bone tissue. I. Pattern of compact bone in relation to age. *Calcified tissue research* 7: 175-90
- Vignery A, Baron R. 1980. Dynamic histomorphometry of alveolar bone remodeling in the adult rat. *Anat Rec* 196: 191-200
- Villa I, Dal Fiume C, Maestroni A, Rubinacci A, Ravasi F, Guidobono F. 2003. Human osteoblast-like cell proliferation induced by calcitonin-related peptides involves PKC activity. *Am J Physiol Endocrinol Metab* 284: E627-33
- Villa I, Rubinacci A, Ravasi F, Ferrara AF, Guidobono F. 1997. Effects of amylin on human osteoblast-like cells. *Peptides* 18: 537-40
- Vine W, Smith P, LaChappell R, Blase E, Young A. 1998. Effects of rat amylin on renal function in the rat. *Horm Metab Res* 30: 518-22
- Wallach S, Rousseau G, Martin L, Azria M. 1999. Effects of calcitonin on animal and in vitro models of skeletal metabolism. *Bone* 25: 509-16
- Wang X, Nakamura M, Mori I, Takeda K, Nakamura Y, et al. 2004. Calcitonin receptor gene and breast cancer: quantitative analysis with laser capture microdissection. *Breast Cancer Res Treat* 83: 109-17
- Watanabe H, Takahashi E, Kobayashi M, Goto M, Krust A, et al. 2006. The estrogen-responsive adrenomedullin and receptor-modifying protein 3 gene identified by DNA microarray analysis are directly regulated by estrogen receptor. *J Mol Endocrinol* 36: 81-9
- Wehrli M, Dougan ST, Caldwell K, O'Keefe L, Schwartz S, et al. 2000. arrow encodes an LDL-receptor-related protein essential for Wingless signalling. *Nature* 407: 527-30
- Wendel M, Sommarin Y, Heinegard D. 1998. Bone matrix proteins: isolation and characterization of a novel cell-binding keratan sulfate proteoglycan (osteoaderin) from bovine bone. *J Cell Biol* 141: 839-47
- Yang BC, Lippton H, Gumusel B, Hyman A, Mehta JL. 1996. Adrenomedullin dilates rat pulmonary artery rings during hypoxia: role of nitric oxide and vasodilator prostaglandins. *J Cardiovasc Pharmacol* 28: 458-62
- Yasuda H, Shima N, Nakagawa N, Mochizuki SI, Yano K, et al. 1998. Identity of osteoclastogenesis inhibitory factor (OCIF) and osteoprotegerin (OPG): a mechanism by which OPG/OCIF inhibits osteoclastogenesis in vitro. *Endocrinology* 139: 1329-37

- Zaidi M, Moonga BS, Abe E. 2002. Calcitonin and bone formation: a knockout full of surprises. *J Clin Invest* 110: 1769-71
- Zaidi M, Shankar VS, Adebajo OA, Lai FA, Pazianas M, et al. 1996. Regulation of extracellular calcium sensing in rat osteoclasts by femtomolar calcitonin concentrations. *Am J Physiol* 271: F637-44
- Zhang Z, Schwartz S, Wagner L, Miller W. 2000. A greedy algorithm for aligning DNA sequences. *Journal of computational biology : a journal of computational molecular cell biology* 7: 203-14
- Ziegler S, Rohrs S, Tickenbrock L, Moroy T, Klein-Hitpass L, et al. 2005. Novel target genes of the Wnt pathway and statistical insights into Wnt target promoter regulation. *The FEBS journal* 272: 1600-15
- Zolnierowicz S, Cron P, Solinas-Toldo S, Fries R, Lin HY, Hemmings BA. 1994. Isolation, characterization, and chromosomal localization of the porcine calcitonin receptor gene. Identification of two variants of the receptor generated by alternative splicing. *J Biol Chem* 269: 19530-8